LBL-30373

Lawrence Berkeley Laboratory
UNIVERSITY OF CALIFORNIA

EARTH SCIENCES DIVISION

Crystal Attenuation and Velocity Structure at the San Andreas Fault Zone in Central California

Jonathan Edward Schein
(Ph.D. Thesis)

July 1987

U. C. Lawrence Berkeley Laboratory
Library, Berkeley

FOR REFERENCE

Not to be taken from this room

LBL-30373
Copy 1
Bldg. 50 Library.

Prepared for the U.S. Department of Energy under Contract Number DE-AC03-76SF00098

DISCLAIMER

This document was prepared as an account of work sponsored by the United States Government. While this document is believed to contain correct information, neither the United States Government nor any agency thereof, nor the Regents of the University of California, nor any of their employees, makes any warranty, express or implied, or assumes any legal responsibility for the accuracy, completeness, or usefulness of any information, apparatus, product, or process disclosed, or represents that its use would not infringe privately owned rights. Reference herein to any specific commercial product, process, or service by its trade name, trademark, manufacturer, or otherwise, does not necessarily constitute or imply its endorsement, recommendation, or favoring by the United States Government or any agency thereof, or the Regents of the University of California. The views and opinions of authors expressed herein do not necessarily state or reflect those of the United States Government or any agency thereof or the Regents of the University of California.

LBL-30373

Crustal Attenuation and Velocity Structure at the San Andreas Fault Zone in Central California

Jonathan Edward Scheiner

(Ph.D. Thesis)

Department of Geology and Geophysics
University of California

and

Center for Computational Seismology
Earth Sciences Division
Lawrence Berkeley Laboratory
University of California
Berkeley, California 94720

July 1987

This work was supported by the U.S. Department of Energy under Contract No. DE-AC03-76SF00098.

Crustal Attenuation and Velocity Structure at the San Andreas Fault Zone in Central California

Jonathan Edward Scheiner

Abstract

Detailed analysis of an 18 km seismic reflection profile across a creeping segment of the San Andreas fault zone indicates that, consistent with the results of numerous other studies of earthquake data, the fault zone may be represented as a low velocity zone situated between a largely granitic crustal block to the west and a crustal block composed of Franciscan material to the east. A weak scattering model of wave propagation has been applied to study the attenuation properties of the fault zone and the bounding crustal blocks. This approach was motivated by the marked contrast in crustal reflectivity observed between the two crustal blocks in the stacked reflection section. The attenuation was parameterized by an apparent Q operator which included the combined effects of elastic scattering and intrinsic dissipation. The apparent Qs average about 115 in the western crust and about 70 in the eastern crust with a Q of 40 in the fault zone. The coda method (Sato, 1977) employed here has not been applied previously to reflection data. The technique depends on the observation of spatially coherent reflectivity; thus, regions characterized by considerable lateral heterogeneity, such as the fault zone, were difficult to model. The values of Q for these unfiltered data are consistent with those of a similar analysis of the S-wave coda from a microearthquake data set in the region.

The frequency dependence of the Q parameter has been determined based on analyses of the filtered reflection and microearthquake data. In all cases the apparent Q is proportional to frequency, this proportionality being uniformly greater within the Franciscan crust than within

the granitic western crust; this result is consistent with an emerging worldwide observation which suggests that the degree of frequency dependence of Q is greater in tectonically active regions than in stable or quiescent regions.

Finally, these velocity and Q results are incorporated into a forward modeling scheme which shows that the laminated crust-mantle contact observed in the western portion of the reflection section requires laminae spanning over 3.5 kilometers with reflection coefficients of about 0.067.

In memory of my poppie

Bernard (Ben) Gittelsohn (1902-1987),

a man of poetry, wit and a whole lotta love

Acknowledgements

This work could not have been completed without the support and guidance of many people to whom I am greatly indebted. The initial impetus as well as the ongoing support, enthusiam and guidance must be credited to my adviser, Dr. Thomas V. McEvilly; my success in graduate school may never have been realized without his confidence, patience and support. I am also thankful to Dr. Lane Johnson for his scholarly and compassionate example, and to Dr. Frank Morrison for his most careful and insightful reading of this manuscript.

Several of my colleagues at U. C. Berkeley have provided important contributions: Many useful theoretical discussions with Phil Cummins, Don Vasco and Keith McLaughlin were most helpful in setting the initial stage for the scattering attenuation analysis. I wish to thank Dan O'Connell for his assistance in much of the spectral computations and graphics work as well as for blazing a trail in the manuscript formatting procedures necessary for the actual output of this thesis. I am grateful to John Peterson for his graphics support and to Dave Tralli for his input in the forward modeling study. Mario Pardo helped at the very early stages of the diffusion study. I especially appreciate the guidance of Dr. Richard Lee and Gerald D'Spain at the beginning of my graduate school experience as well as the advice of Dr. Oliver Johns of San Francisco State University. Data processing of the reflection profile was aided by Mike Wilkens of Digicon, Inc. and Sam Blakeslee. Also helpful in data processing was Dr. Ernie Majer of the Center for Computational Seismology at Lawrence Berkeley Laboratory whose general assistance throughout my tenure at U. C. Berkeley has made the experience that much more comfortable and rewarding. The association of Michael Leonard, Yaolin Shi, Lee Hirsch, and countless others is most appreciated. All of these aforementioned contributions were made in a spirit of cooperation and genuine comraderie that has made it all worthwhile.

The help of these colleagues and professors was crucial to my success in this endeavor; but

the basic educational foundation as well as the ongoing support, patience and love of my mother and father has really been the key to my educational achievement. They provided me with the basic education, knowledge, and values that have enabled me to realize my aspirations. Their steadfast confidence and love as well as that of my entire family has been with me each step of the way.

Finally, I wish to thank mi novia, Caroline, whose sincere devotion and patience I shall forever appreciate.

Table of Contents

Dedication i

Acknowledgements ii

Chapter 1 Introduction 1

Chapter 2 Geology and Tectonics 12

2.1 Introduction 12

2.2 Geology 15

2.2.1 Field Observations 15

2.2.2 Franciscan Eugeosynclinal Core Complex 19

2.2.3 Salinian Plutonic Block 24

2.3 Tectonics 26

2.3.1 Overview 26

2.3.2 Mesozoic Subduction and Formation of the Franciscan Complex 28

2.3.3 Origin and Emplacement of the Salinian Block 30

2.3.4 Recent History 35

2.4 Discussion 36

References 42

Chapter 3 Velocity and Attenuation 45

3.1 Introduction 45

3.2 Data 49

3.2.1 1978 CGG Reflection Profile 49

3.2.2 Microearthquake Array 50

3.3 Velocity Analysis and Structural Interpretation 64

3.4 Attenuation Analyses 87

3.4.1 Overview 87

3.4.2 Early Studies: CDP Reflection Data and Absorption Models 89

3.4.3 Weak Scattering Approach: Theoretical Development 104

3.4.4 Weak Scattering Approach: Method 109

3.4.5 Scattering Analysis Results: Unfiltered Data 115

3.4.6 Scattering Analysis Results: Filtered Data 126

3.4.7 Mean Free Path 132

3.5 Summary and Discussion 135

Tables 140

Appendix 145

References 156

Chapter 4 Forward Modeling 162

4.1 Introduction 162

4.2 Model Descriptions 164

4.3 Method 173

4.4 Results 177

4.5 Summary and Discussion 185

References 188

Chapter 5 Summary and Conclusions 190

Chapter 1

Introduction

The San Andreas fault zone is a prominent feature in virtually every geophysical sense in addition to its physiographic manifestations. As a transform fault separating the North American and Pacific lithospheric plates in California it represents both a natural danger and a unique opportunity for the study of plate motion and its attendant seismicity. Of specific interest in this study is a section of the fault zone and its bounding crusts along the Bickmore Canyon/Bear Valley region of central California; the marked contrast in geology across the fault motivates many questions regarding the general geotectonic development of western North America, including the subduction of indigenous and/or allochthonous material (e.g. Franciscan formation) and the lateral translation of entire mountain ranges (e.g. Salinian Block).

This section of the San Andreas fault in San Benito County is bound to the east and west by the Diablo and Gabilan Ranges, respectively. Detailed geologic mapping of the region indicates that, beneath a veneer of Quaternary deposits, the composition of the upper crust east of the fault consists predominantly of the eugeosynclinal subduction complex known as the Franciscan melange; the upper crust west of the San Andreas fault consists of the granitic plutonic mass known as the Salinian Block. A summary of the geology of the region is given in Chapter 2 as well as a description of the tectonic history of the development of western North America. It is in this context that a study of the geophysical features of the crust must proceed, especially for such a structurally complex and active region.

Models of the composition of the lower Diablo crust have been obtained based on laboratory analyses under the appropriate pressures and temperatures of the basement rocks exposed at the surface. Lin and Wang (1980) favor an olivine gabbro and/or a hornblende gabbro composition based on studies of the acoustic velocities of such samples at pressures up to 1 GPa and temperatures up to 400° C, and subsequent comparison of these data with published seismic field studies. In a similar study Stewart and Peselnick (1978) find consistent results with those of Lin

and Wang (1980), however, they indicate that a more abrupt change in petrology or chemistry from the upper Franciscan crust to a more basic rock may be evidence of subducted oceanic material.

Unlike the Diablo crust, there is seismic evidence of a somewhat abrupt transition at mid-crustal depth (e.g. $\approx$ 10 km) within the Gabilan crust. Based on analysis of refraction data Stewart (1968) inferred that a low velocity material exists below the Gabilan batholith at this depth and suggested that it may be of Franciscan composition. Dickinson (1981) made the same suggestion on geotectonic grounds. However Walter and Mooney (1982) have re-examined the refraction data and, in conjunction with the results of numerous other seismological and geological data, have favored a gneissic composition for the lower Gabilan crust. This conclusion was also reached by Lin and Wang (1980) based on their laboratory study of various granites obtained in the field.

Given the complex and controversial geotectonic models for the formation of the Salinian Block and its subsequent northwestward translation, as well as that of the subduction environment in which the Franciscan melange was formed, there is considerable motivation to understand the nature of the crusts bounding this major transform fault. Of perhaps more immediate concern is the understanding of several seismological manifestations of both the general contrast in crustal composition across the San Andrea fault and the structure of the fault zone itself; a refined understanding of the structure of this region is required to explain several important observations pertaining to earthquake data: The observed distortions in radiation patterns from local earthquakes recorded at the many stations of the U.S. Geological Survey (USGS) and U.C. Berkeley (UCB) networks, travel time anomalies within the same local networks, and hypocenter location problems using a laterally homogeneous velocity model all emphasize the need for a more refined model of the velocity structure.

These seismological manifestations of the contrast in crustal properties across the fault are in many ways consistent with other geophysical observations in this region of the San Andreas fault zone: Elongate zones of anomalously high magnetic susceptibility with axes trending

approximately along the major structural trend have been reported (Wang, 1984). The Bouguer gravity maps of the California coast (e.g. Bishop and Chapman, 1967) show a narrow, elongated gravity low roughly along the main trace of the San Andreas; although some of this latter effect is surely due to the low density sedimentary basins along the valley as well as the two kilometer-wide gouge zone, detailed modeling of these gravity anomalies seem to require the presence of an additional low density slab more than one kilometer wide extending into the seismogenic zone (Pavoni, 1973; Wang et al., 1986). Mazzella (1977) and Phillips and Kuckes (1983) note that the fault zone itself in this region is characterized as an anomalously low resistivity zone. The electromagnetic induction experiment of Phillips and Kuckes (1983) indicates a significant contrast between the relatively low resistivity Franciscan crust (e.g. 20 Ω–m) and the higher resistivity Gabilan crust (e.g. 1000 Ω–m). Their two-layer model also suggested that a transition to a lower resistivity material at mid-crustal depth west of the fault may be evidence of a wedge of fault gouge extending westward or, alternatively, of subducted oceanic crust that may have been serpentinized. The depth and structure of this low resistivity material are consistent with both the low density pocket proposed by Pavoni (1973) from analysis of gravity data and the low velocity wedge proposed by Feng and McEvilly (1983) from analysis of seismic reflection data. As Phillips and Kuckes (1983) point out, the presence of oceanic (mafic) crust that is highly serpentinized beneath the granitic batholith would explain the resistivity data, but would probably correlate with a high velocity and perhaps higher density material and would thus be inconsistent with the aforementioned studies; the suggestion that fault gouge is indicated by these data is also supported by more recent analysis of gravity data by Wang, et al. (1986). In their investigation of a gravity survey along the same profile as that of the reflection survey analyzed by Feng and McEvilly (1983) and constrained by their velocity model, Wang, et al. (1986) suggested that a funnel-shaped low velocity wedge within the fault zone was probably composed of fault gouge; laboratory studies of clay-rich gouge obtained in this same region show significantly low resistivity only when saturated with aqueous saline fluids (Wang, 1984), suggesting that a saturated (clayey) fault gouge would satisfy both the density data and the

resistivity data for the fault zone. Whether or not such an explanation is satisfactory for the resistivity and velocity observations for the lower Gabilan crust is not clear.

In contrast with the aforementioned geophysical expressions, there is no local thermal anomaly at the main fault trace although a broad band of high heat flow extends across a 100 km wide region encompassing essentially the entire Coast Range province (Lachenbruch and Sass, 1973; 1980); conjecture has been offerred to explain this broad anomaly in terms of the underthrusting of very young hot oceanic lithosphere beneath the Coast Ranges (Lachenbruch and Sass, 1973). Although there is no observed heat flow anomaly across these major lithospheric plates, variations in heat flow along the strike of the San Andreas fault zone have been observed, and attempts have been made to correlate these variations with seismicity. The Bickmore Canyon/Bear Valley region is located within a section of the San Andreas fault that is characterized by significant seismicity as well as steady aseismic creep; earthquakes of low to moderate magnitude are common, however large earthquakes are rare (Wesson, et al., 1973; Bakun and McLaren, 1984). In contrast, the regions northwest and southeast of here are characterized by much lower levels of seismicity, no aseismic creep and infrequent but great earthquakes (e.g. in 1906 and 1857, respectively). These 'locked' regions to the northwest and southeast are also *colder*: average heat flow values are about 1.7 HFU (71 mW/m^2), in contrast to an average heat flow of about 2.1 HFU (88 mW/m^2) over the active creeping segment (Sibson, 1982). Furthermore, there are indications that the transition depth from the brittle regime to a ductile regime may increase about 2 to 3 km in passing, along strike, from the *hotter*, creeping segment to the *colder*, locked segment (Sibson, 1982). If this 'frictional/quasi-plastic' transition depth represents the base of the seismogenic zone, and if larger ($M > 5.5$) earthquakes characteristically nucleate towards the base of the seismogenic zone (i.e. in regions capable of accumulating the highest strain energy concentrations) as proposed by Sibson (1982), then these and other variations in geophysical parameters along the fault may provide a means of mapping fault structure and shear strength.

In this study of a creeping section of the San Andreas fault an attempt is made to refine our understanding of the compressional velocity structure of the fault zone as well as that of the bounding crusts. In addition to a parameterization in terms of the velocity, it is believed that an understanding of the attenuation characteristics of the media will enable further illumination of any structural or compositional detail. Due to the inherent difficulties associated with the imaging of the laterally inhomogeneous fault zone itself, determination of the velocity and attenuation structure of the bounding crusts was emphasized. The attenuation structure was parameterized in terms of an apparent Q operator, and was determined by the coda decay technique of Aki and Chouet (1975) and Sato (1977; 1978). An initial goal of this attenuation study was to decompose the total apparent attenuation into its elastic scattering and intrinsic dissipation components. Because of the inherent non-linearity of the problem given the weak scattering model of wave propagation, it was not possible to accurately partition the total attenuation according to these two components. The attenuation study was motivated by observation of the significant contrast in reflectivity between the bounding crusts of the San Andreas fault as indicated by the stacked reflection section (see Figure 3-6). The scattering model was adopted to explain this marked contrast based on an assumed difference in heterogeneity structure for these two crustal blocks. However, the resulting Q_P values from the analysis of the reflection data do not provide an entirely adequate explanation; that is, the apparent Qs are not significantly different across the fault, as anticipated. This may well be due to the different partitioning of intrinsic versus scattering loss mechanisms between the two crustal blocks. Such a difference would not necessarily be manifested in these resulting values of the apparent Q. On the other hand, some of the assumptions of the weak scattering model, particularly as applied to seismic reflection data may be too broad. The determination of the dissipation properties of the crust at depth is a most difficult task and would seem to require a multi-faceted approach including several techniques and types of data as well as a comparison with laboratory results.

The primary data set examined was that of an 18 km seismic reflection line bisected by the main trace of the San Andreas fault; this data set was used in the determination of the P-

wave velocity structure by conventional reflection processing methods. The apparent 'Q_P' structure determined by the analysis of this data was complemented by a determination of the 'Q_S' structure using shear wave coda from a microearthquake data set. This latter data set was recorded by two portable arrays on either side of the fault, deployed in a separate polarization study of coda waves in 1982 (McLaughlin, 1982; Vasco et al., 1983). Both of these data sets are described in detail in Chapter 3 as are the analyses for velocity and attenuation based largely on these data.

Velocity analysis of the reflection data by conventional processing methods indicates that the fault zone represents a prominent low velocity zone (see Figures 3-20, 3-21). This final model is consistent with the trend of numerous studies representing over two decades of refinement in our understanding of the P-wave velocity structure in this active region (see Figure 3-22). Although not inconsistent with the model of Feng and McEvilly (1983) the final model given here is somewhat coarser; in particular, evidence for a low velocity wedge extending westward from the fault zone at mid-crustal depth as suggested by their investigation of the same data set was not resolvable by these conventional reflection processing techniques (e.g. constant velocity analysis (CVA) and coherency methods). There is, in general, more structural detail observed within the Gabilan media than within the Franciscan crust to the east; this is due entirely to the paucity of spatially coherent reflection energy from this latter medium. Such a lack of coherent energy return is probably due to the more heterogeneous nature of the Franciscan melange. Hence, the attenuation structure of the media is investigated by the coda decay technique in which a weak scattering environment is assumed.

One persistent effect noted in the study of these reflection data is that of a laminated Moho reflection west of the fault at about 7 - 8 seconds (two-way) reflection time (see Figure 3-6). (It is not clear what the seismic signature of the Moho is east of the fault due to the markedly lower level of reflection energy return through the Franciscan medium.) This laminated appearance has been widely reported in many different tectonic regimes (Clowes and Kanasewich, 1970; Lynn et al., 1981; Hale and Thompson, 1982). In this data set the Moho

appears over a depth range of two to three seconds (two-way time) and, as is shown in forward modeling studies (see Chapter 4), is probably due to a cyclic series of layers spanning at least 3 kilometers in thickness and having reflection coefficients as high as 0.067. Any plausible geologic models offerred to explain such fine structure would have to be capable of incorporating the widespread nature of this observation.

The apparent attenuation structure was determined as an average over a mid-crustal depth range ($6 < z < 17$ km) by analysis of the amplitude decay of horizontally stacked CDP seismograms; the peak amplitude of a given window of data occurred at the (two-way) arrival time of a given spatially coherent reflector as noted on the stacked section. These apparent Qs include the combined effects of elastic scattering as well that of intrinsic dissipation; separation of these effects was not feasible in this investigation. The apparent Qs determined from this study of the CDP reflection data average about 115 in the western crust and about 70 in the eastern crust with a Q of 40 for the fault zone itself. Those Q values obtained by the investigation of the microearthquake data from the portable arrays are generally consistent with these Qs, however the average values (i.e. Q_S) for the western and eastern crusts were 92 and 114, respectively. While such a difference in trend between the results for the two data sets may be due to different mechanisms for compressional and shear waves, this may be a premature explanation, especially given the relatively small amount of microearthquake data studied here. Significant variations in coda intensity were observed at neighboring receiver sites for a common microearthquake source. The rather strong averaging process involved in the study of the reflection data was not applicable to the microearthquake data. In summary, the use of the coda decay technique to study crustal attenuation would seem to require a relatively large (microearthquake or earthquake) data set; the attendant averaging afforded by such a large data set may help to smooth these local variations and thus to aid in the determination of an unambiguous profile of the average crustal attenuation. In any case, it is interesting to note that these aforementioned Q values are consistent with those obtained by Aki and Chouet (1975) from a similar analysis of microearthquake data in the same region.

In contrast to the ambiguity regarding the absolute values of the apparent Q parameter, analysis of the filtered data for each data set reveals a consistent difference in the degree of frequency dependence of the apparent Q between the bounding crusts of the fault. (Results within the fault zone itself are relatively lacking owing primarily to the lack of discernible structure in this portion of the stacked reflection section.) Consistent with numerous other studies of body waves at frequencies above about 0.5 Hz (see text–section 3.4.6 for a summary of published results) the apparent Qs were found in all cases to increase with frequency; of perhaps greater significance is the trend toward greater frequency dependence in the 'Franciscan' data relative to the 'granitic' data (P and S-waves). This may be part of an emerging pattern for body wave data; whereas several studies have detailed the relation between the degree of frequency dependence of Q and the degree of heterogeneity or tectonic activity, very few studies have sought to determine the fine structure associated with the comparison of this frequency dependence over a small regional area (Chen et al., 1984; Rhea, 1984). The results of these studies are, in general, consistent with the emerging pattern suggesting that there is a greater degree of frequency dependence for heterogeneous and/or tectonically active regions than for more homogeneous and/or quiescent regions.

Since it was not possible to determine the partitioning of the attenuation process according to its intrinsic and elastic scattering components, it remains unclear to what extent the observed frequency dependence is dominated by either process. Given that most laboratory measurements of attenuation suggest that the intrinsic Q is independent of frequency it seems reasonable that the observed frequency dependence is dominated by some scattering process. However this conclusion cannot be drawn definitively, especially considering the generally high (e.g. ultrasonic) frequencies over which these laboratory measurements are carried out relative to seismic frequencies. The partitioning of the apparent attenuation according to these basic processes is a significant problem that must be addressed, although no particular method is suggested by this study. The weak scattering model may be used for such a partitioning (see Section 3.4.3) however because of its inherent non-linearity, the solution to the problem involves *a priori*

knowledge of both the overall level of apparent attenuation and the degree of partitioning of the two components. As such this technique remains wholly inadequate to address the partitioning problem.

References: Chapter 1

Aki, K. and B. Chouet, 1975. Origin of coda waves: source, attenuation, and scattering effects, *J. of Geophys. Res.*, **80**, 3322-3342.

Bishop, C. C. and R. H. Chapman, 1967. Bouguer gravity map of California, Santa Cruz sheet, *Calif. Div. Mines and Geol.*

Bakun, William H. and Marcia McLaren, 1984. Microearthquakes and the nature of the creeping-to-locked transition of the San Andreas fault zone near San Juan Bautista, California, *Bull. Seism. Soc. Am.*, **74**, 235-254.

Chen, Peishan, Otto W. Nuttli, Wenhua Ye and Jiazheng Qin, 1984. Estimates of short-period Q values and seismic moments from coda waves for earthquakes of the Beijing and Yunnan regions of China, *Bull. Seism. Soc. Am.*, **74**, 1189-1207.

Clowes, R. M. and E. R. Kanasewich, 1970. Seismic attenuation and the nature of reflecting horizons within the crust, *J. Geophys. Res.*, **75**, 6693-6705.

Dickinson, W. R., 1981. Plate tectonics and the continental margin of California, in *The Geotectonic Development of California*, W. G. Ernst, Editor, Prentice-Hall, New York, 1-28.

Feng, R. and T. V. McEvilly, 1983. Interpretation of seismic reflection data for the structure of the San Andreas fault zone, *Bull. Seism. Soc. Am.*, **73**, 1701-1720.

Hale, L. D. and G. A. Thompson, 1982. The seismic reflection character of the continental Mohorovicic discontinuity, *J. Geophys. Res.* **87**, 4625-4635.

Lachenbruch, A. H. and J. H. Sass, Thermo-mechanical aspects of the San Andreas fault system, in *Proc. Conf. Geol. Problems of San Andreas Fault System, Stanford Univ. Publ. Geol. Sci.*, **13**, 192-205.

Lachenbruch, A. H. and J. H. Sass, 1980. Heat flow and energetics of the San Andreas fault zone, *J. Geophys. Res.*, **85**, 6185-6222.

Lin, Wunan and Chi-Yuen Wang, 1980. P-wave velocities in rocks at high pressure and temperature and the constitution of the central California crust, *Geophys. J. R. Astr. Soc.*, **61**, 379-400.

Lynn, Heloise B., Laura D. Hale and George A. Thompson, 1981. Seismic reflections from the basal contacts of batholiths, *J. Geophys. Res.*, **86**, 10633-10638.

Mazzella, A. T., 1977. *Resistivity study across the San Andreas fault zone*, PhD thesis, University of California, Berkeley.

McLaughlin, K. L., 1982. *Spatial coherency of seismic waveforms*, PhD thesis, University of California, Berkeley.

Pavoni, N., 1973. A structural model for the San Andreas fault zone along the northeast side of

the Gabilan Range, in *Proc. Conf. Geol. Problems of San Andreas Fault System, Stanford Univ. Publ. Geol. Sci.*, **13**, 259-267.

Phillips, Wayne J. and Arthur F. Kuckes, 1983. Electrical conductivity structure of the San Andreas fault in central California, *J. Geophys. Res.*, **88**, 7467-7474.

Rhea, Susan, 1984. Q determined from local earthquakes in the South Carolina coastal plain, *Bull. Seism. Soc. Am.*, **74**, 2257-2268.

Sato, H., 1977. Energy propagation including scattering effects: single isotropic scattering approximation, *J. Phys. Earth*, **25**, 27-41.

Sato, H., 1978. Mean free path of S-waves under the Kanto district of Japan, *J. Phys. Earth*, **26**, 185-198.

Stewart, R. and L. Peselnick, 1978. Systematic behavior of compressional velocity in Franciscan rocks at high pressure and temperature, *J. Geophys. Res.*, **83**, 831-839.

Stewart, Samuel W., 1968. Preliminary comparison of seismic traveltimes and inferred crustal structure adjacent to the San Andreas fault in the Diablo and Gabilan Ranges of central California, *Proc. Conf. Geol. Problems of San Andreas Fault System, Stanford Univ. Publ. Geol. Sci.*, **11**, 218-230.

Sibson, Richard, 1982. Seismic style in relation to heat flow along the San Andreas fault system, in *Issues in Rock Mechanics, 23rd Symposium on Rock Mechanics*, Port City Press Inc., Baltimore, Maryland, 361-371.

Vasco, Don W., McEvilly, T. V. and John E. Peterson, 1983. Polarization analysis and the effect of lithology on the coda of two earthquakes in the San Andreas fault zone, central California, *Earthquake Notes*, **54**, 35.

Walter, A. W. and W. D. Mooney, 1982. Crustal structure of the Diablo and Gabilan Ranges, central California: A reinterpretation, *Bull. Seism. Soc. Am.*, **72**, 1567-1590.

Wang, Chi-Yuen, 1984. On the constitution of the San Andreas fault zone in central California, *J. Geophys. Res.*, **89**, 5858-5866.

Wang, Chi-Yuen, Feng Rui, Yao Zhengsheng and Shi Xingjue, 1986. Gravity anomaly and density structure of the San Andreas fault zone, *Pageoph*, **124**, 127-140.

Wesson, Robert L., R. O. Burford and William L. Ellsworth, 1973. Relationship between seismicity, fault creep, and crustal loading along the central San Andreas fault, in *Proc. Conf. Geol. Problems of San Andreas Fault System, Stanford Univ. Publ. Geol. Sci.*, **13**, 303-321.

Chapter 2

Geology and Tectonics

2.1 *INTRODUCTION*

The San Andreas fault represents the boundary between the North American and Pacific lithospheric plates. Detailed geologic mapping throughout California has, in the light of the plate tectonic model, helped to provide a working knowledge of the complex history of plate interactions in western North America. This knowledge is useful in understanding various structural features evident in the stacked section of the 1978 seismic "Bickmore Canyon" reflection survey discussed at length in Chapter 3. Furthermore, there are many other pertinent questions raised by the results of other geophysical studies upon which the geologic information has important bearing.

The particular section of the San Andreas fault that is of interest here is in San Benito County in central California (Figure 2-1). Here the main trace of the San Andreas fault separates the Gabilan Range and Gabilan Mesa area of the Salinian plutonic block to the west and southwest from the Diablo Range area to the northeast. The Franciscan basement of the Diablo Range is overlain by a thick sedimentary cover of Mesozoic and Cenozoic assemblages. This entire unit is intensely folded and compressed with fold axes roughly parallel to the San Andreas fault. In contrast, the granitic plutonic mass to the west is largely undeformed with but a thin sedimentary veneer, although where this sedimentary cover thickens (along the eastern margin of the Gabilan Range and Mesa toward the San Andreas fault) there is progressively more deformation (Dibblee, 1980). The deformation of the rocks to the east is due to clockwise shear movement of the relatively pliable and weak Franciscan basement against the comparatively rigid Salinian Block along the San Andreas fault system (Dibblee, 1980).

This section of the San Andreas fault between San Juan Bautista and Parkfield is characterized by a high level of shallow (2 to 12 km) seismicity in addition to steady creep; it is bounded to the northwest and southeast by locked portions of the fault where several large earthquakes have occurred in historical time (Bakun and McLaren, 1984).

The Bickmore Canyon/Bear Valley reflection survey has provided the impetus for many investigations as to the nature of the upper and lower crusts as well as that of the crust-mantle boundary: Probably the most obvious feature of the stacked section is the marked contrast in reflectivity between the eastern (Franciscan) and western (granitic) crustal blocks including the reflection from the base of the crust. This general feature has inspired several studies of the attenuation and scattering properties of the media (Scheiner, 1983; Scheiner and McEvilly, 1984). The Moho reflection itself has motivated a number of analyses to determine the nature of its apparently laminated character (Lynn et al., 1981; Hale and Thompson, 1982) and its dip (McEvilly and Clymer, 1975; Feng and McEvilly, 1983). In addition, the shallow structure indicated at reflection times of about 3 to 4 seconds may represent the base of the granitic batholith (Stewart, 1968; Lynn et al., 1981; Page, 1981). Feng and McEvilly (1983) have also indicated that this feature may represent, in part, a low velocity wedge extending westward from the fault zone; on the basis of a gravity study as well as the available laboratory data, Wang et al., (1986) have suggested that this low velocity wedge could be fault gouge. Finally, there is seismological evidence suggesting that Franciscan metasediments exist beneath the Gabilan batholith and that these reflections at about 3 seconds represent the transition from a granitic upper crust to a Franciscan lower crust (Stewart, 1968). Although this hypothesis is disputed (Walter and Mooney, 1982) a tectonic model has been suggested based on the available geologic and tectonic data that would seem to support such a lower crustal composition (Dickinson, 1981). Specifically, a combination of the pre-Tertiary position of the Salinian Block and an apparent change during the Cretaceous to a more shallow subduction environment lends credence to the hypothesis that during this period significant underthrusting of Franciscan material beneath the Sierran plutonic mass occurred.

These and many other important questions are raised by the Bickmore data as well as by other geophysical studies; answers to these questions have far-reaching consequences for the tectonic history of the continental margin. It is thus important that a comprehensive geotectonic model be offered that will plausibly complement the geophysical data in such a way as to refine our understanding of the crust in this seismically active region. Furthermore, in order to understand the general contrast in spatially coherent reflectivity observed between the two bounding crusts of this section of the fault in terms of the attenuation characteristics and/or in terms of the scattering efficiency of the two media (and the fault zone), it is necessary to incorporate all the available knowledge about the geology and related material properties of the media. In addition to the geologic data, any such tectonic model must be consistent with the data from plate motion studies (Atwater, 1970; Atwater and Molnar, 1973; Minster and Jordan, 1978). The following is a brief description of the geologic and tectonic knowledge that exists which bears upon the aforementioned structural features manifested in the Bickmore data.

2.2 GEOLOGY

2.2.1 *FIELD OBSERVATIONS*

On the eastern part of the Diablo Range the upper Jurassic Franciscan basement is structurally overlain by the Butts Ranch syncline consisting of thick assemblages of Cretaceous, middle and upper Eocene, and middle Miocene sediments (Figures 2-2, 2-3 and 2-4). Between the Butts Ranch syncline and the San Andreas fault zone is the San Benito River area; here the Franciscan is overlain by upper Miocene and Pliocene sediments (Wilson, 1942). To the west of the San Andreas, the Gabilan Range has a granitic basement underlying middle and upper Miocene sediments and volcanics. Pliocene and Pleistocene non-marine sediments overlap various parts of the entire region east and west of the main fault trace.

The style of deformation of the Gabilan is chiefly by block faulting whereas the dominant style of deformation in the Diablo Range is folding and thrust faulting with some strong overturning. The Pinnacles fault, a north-south trending normal fault, and the Chalone Creek fault, another normal fault trending N 30° W are the dominant normal faults in the Gabilans (see Figure 2-3). In addition, the Vergeles fault west of Hollister is believed to be a former strand of the San Andreas, probably active in the early Miocene time, with uplift of the granitic basement to the south (Dibblee, 1980). The Pinnacles fault is a steeply dipping fault (60° to 70° to the east) with Miocene volcanics and sediments downdropped on the east and granite upthrown on the west; Wilson (1942) mapped it for about 10 km within the San Benito quadrangle. The Chalone Creek fault is of undetermined dip and is characterized by Monterey sediments on the east downdropped against older Miocene volcanics on the west. East of these two faults and within a kilometer west of the San Andreas is the "Bear Valley" fault (Figure 2-4), however its existence has not been corroborated by later mapping; Dibblee (1980) interprets this *contact* to be "a northeast-dipping unconformity at the base of the valley sediments that includes [*sic*] Franciscan rocks as local landslide masses at the base" (p. 10 of Dibblee, 1980),

(see Figure 2-5D). In the southwestern portion of the quadrangle the granite is cut by a series of middle Miocene rhyolite dikes which have been emplaced along fractures that trend roughly N 30° W and dip 55°– 65° to the northeast. In addition there are some small dikes that trend somewhat differently; the longest continuous dikes are about 3 km (Wilson, 1942). Wilson (1942) assumes that the fractures along which these dikes are emplaced were normal faults. (The dikes of the Pinnacles National Monument just south of Bickmore Canyon/Bear Valley, which are dated radiometrically at 23.5 m.y., have been correlated with the Neenach volcanics of the Mojave east of the San Andreas (Mathews, 1973); this correlation is one of several pieces of evidence that about 300 km of right-lateral displacement has occurred along the San Andreas fault in the last 24 m.y.)

East of the San Andreas in the Diablo Range there are several active faults, which splay from the main trace of the San Andreas. The Calaveras fault, an active, probably vertical, (right) strike-slip fault, has been extensively studied with refraction seismic methods (Walter and Mooney, 1982; Blumling and Prodehl, 1983; Blumling et al., 1985; Mooney and Colburn, 1985; and others) following a $M_L = 5.7$ earthquake on 6, August 1979 near Coyote Lake. The Calaveras, Sargent and Zayante-Vergeles faults are characterized by vertical offsets of basement rocks and shallow low velocity zones (Mooney and Colburn, 1985). Northeast of the Calaveras fault, synclinally folded Cretaceous stata of the Great Valley Sequence are juxtaposed against Franciscan rocks to the southwest; here, the Calaveras forms the western boundary of the Diablo Range. Southeast of Hollister the Calaveras merges into the Paicines fault which continues parallel to the San Andreas before breaking up into the Pine Rock fault and several other minor faults (e.g. Hernandez, Clear Creek, Waltham Canyon, Castle Mountain, and others) near the location of the Bickmore Canyon/Bear Valley reflection profile (Dibblee, 1980). These faults nearly merge in the southeastward direction and die out in the intensely folded Pliocene strata south of Hollister. The Pine Rock fault, located within 4 km of the main trace of the San Andreas appears to be the continuation of the Paicines fault as indicated in Figure (2-3). Movement on most of these faults is probably oblique right slip, although locally some of them

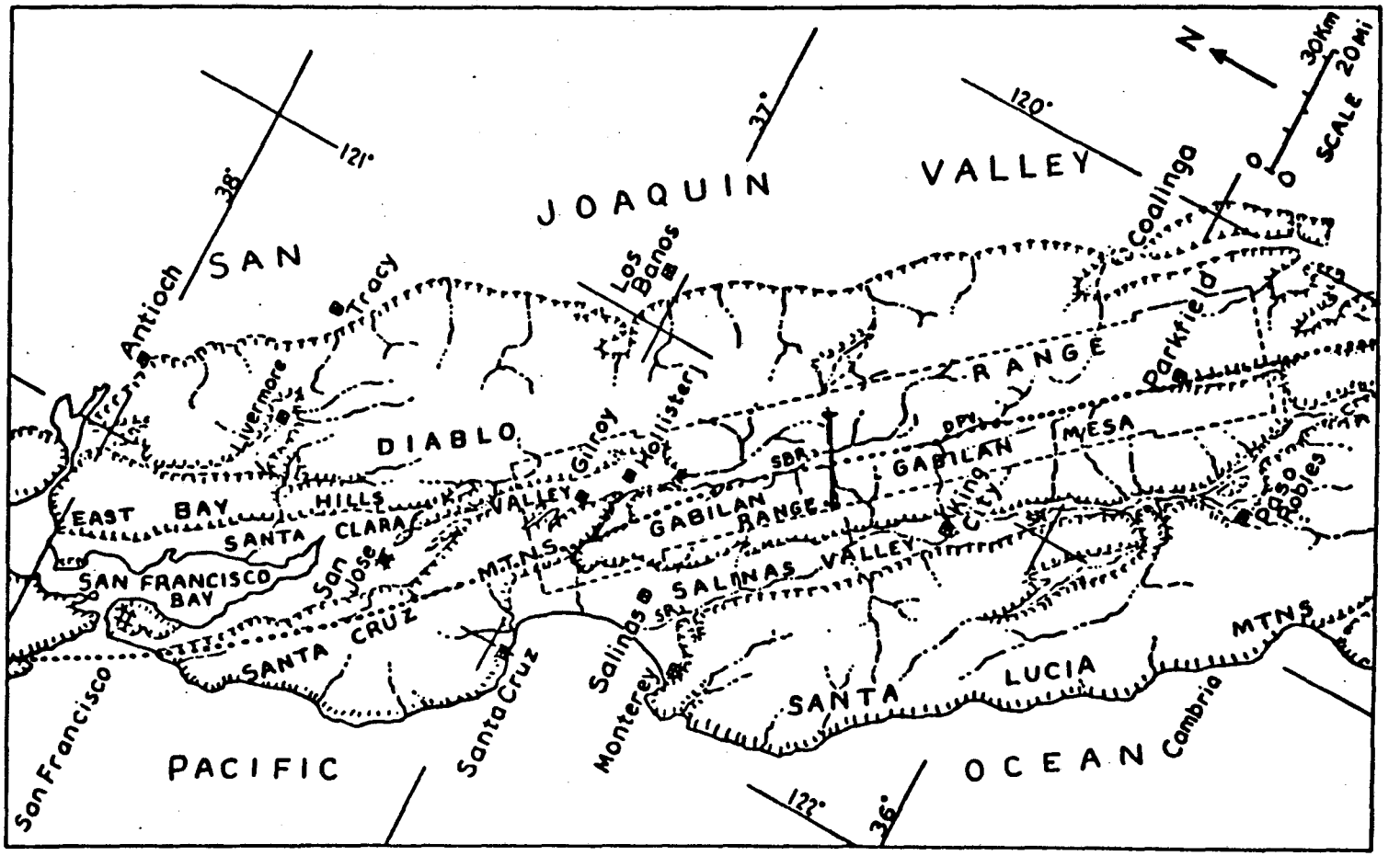

Figure 2-1) Physiographic map of San Benito County showing the San Andreas fault through the Gabilan (west) and Diablo (east) Ranges; after Dibblee (1980). The 1978 'Bickmore Canyon' seismic reflection profile is indicated by the bar near the center of the dashed rectangle along the San Andreas fault.

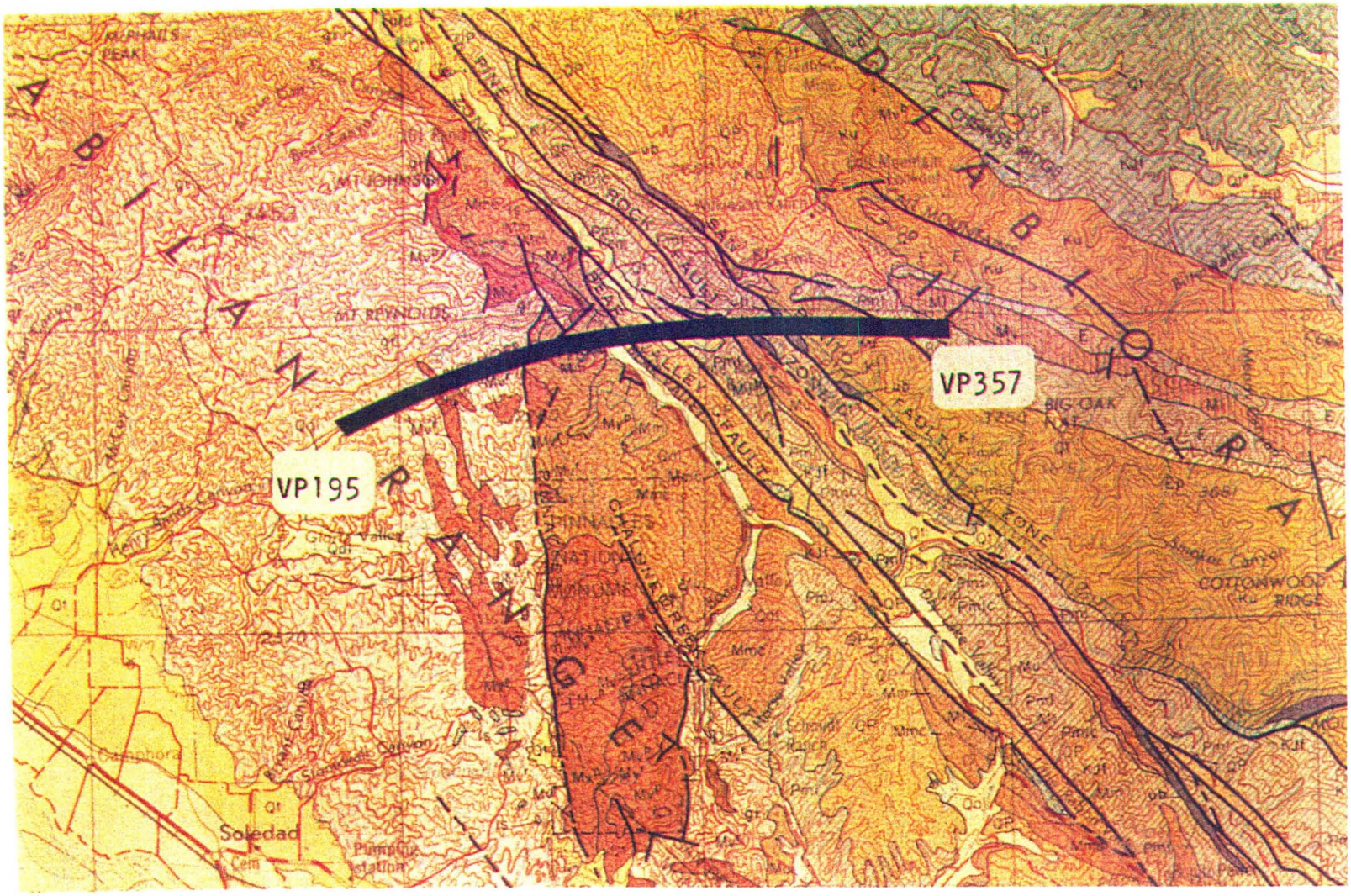

Figure 2-2) Geologic map of San Benito County in the vicinity of the 1978 seismic reflection profile; adapted from the Santa Cruz sheet of the Geological Atlas of California (C. W. Jennings and R. G. Strand, 1958); source positions of the profile are indicated by VP numbers, increasing eastward.

appear to be thrust faults (Dibblee, 1980). Continuing to the southeast these steep faults are within the Miocene and Pliocene terrane that unconformably overlies the Franciscan Complex and serpentinite.

The Quien Sabe fault appears to splay east-southeastward from the Calaveras fault and is mapped locally near the base of the Diablo Range near Hollister as low scarps in alluvial deposits (Dibblee, 1980). Part of the Diablo Range may have been elevated along this and other related faults. The Bradley fault, believed to be inactive, may have formed the contact between the Franciscan Complex and the Panoche Formation (Dibblee 1980); this fault is located about 7 km east of the San Andreas roughly midway between Hollister and Bear Valley.

As indicated above, there are some differences in geologic interpretation between the studies of Wilson (1942) and Dibblee (1980). The differences are minor, especially considering the tectonic complexity of the region. These differences are clearly manifested in the two geologic cross-sections of the region of interest of the San Andreas fault zone (see Figures 2-6 and 2-5, respectively). Besides the Bear Valley fault mentioned previously, there is the question of the Paicines fault and the name(s) given to its southerly extensions. For Wilson (1942) its extension to the south is the San Benito fault, whereas for Dibblee (1980) the picture is more complex: the 'Calaveras-Paicines' fault system splays into a number of other minor faults. There is no San Benito fault in Dibblee's model. (The fact that different field geologists over many decades give different names to minor faults is not uncommon.) The onset of this splaying of the Calaveras-Paicines fault system occurs near the eastern extension of the Bickmore Canyon/Bear Valley reflection profile. For practical purposes in the interpretation of this reflection data, the San Benito fault is considered to be the southerly extension of the Paicines fault.

The only other significant difference between the two cross-sections concerns the structural feature called the "Vallecitos syncline" by Dibblee; it is a prominent and deep-rooted syncline within the Diablo Range and extends about 10 km to the east of the Paicines fault. As can be inferred from these cross-sections of Wilson and Dibblee, (i.e. Figures 2-6 and 2-5) of the San Andreas fault zone,

the depth extent of the two studies is quite different and it may well be that Dibblee's model shows the Vallecitos syncline because he is willing to extend his surface information to a greater depth. In summary, the optimum use of these two studies is probably to use the cross-section of Wilson (Figure 2-6) for the shallow (e.g. < 5 km) structure and that of Dibblee (Figure 2-5) for a tentative model of the deeper (e.g. 5 to 10 km) features.

2.2.2 *FRANCISCAN EUGEOSYNCLINAL CORE COMPLEX*

The Franciscan formation is a heterogeneous unit of eugeosynclinal marine sedimentary and mafic marine volcanic rocks which consist predominantly of massively bedded graywacke with interbedded dark shale, minor amounts of chert and limestone, altered volcanic rock (greenstone) and various metamorphic rocks of the zeolite, blueschist, greenschist, and eclogite facies. In addition, they have been intruded by sill-like masses of peridotite, most of which have been serpentinized (Oakeshott, 1966).

Although generally characterized as a formation the Franciscan should not be visualized as a sequence with ordinary physical, spatial, and temporal coherence; rather, it should be thought of as a disorderly assemblage (*melange*) of certain characteristic rocks that have undergone unsystematic disturbance (Page, 1966). There are some coherent units within the Franciscan, although this is the exception rather than the rule: There are Cretaceous bedded sandstones, somewhat coherent chert graywacke sequences, and upper Jurassic chert-greenstone units included as blocks within the melanges, in addition to serpentinite, blueschist, conglomerate, and other materials all enveloped in an argillaceous matrix (Page, 1981).

Most of the Franciscan consists of sandstone (graywacke), although altered mafic volcanic rocks (greenstones) are widespread and comprise about 10% of the assemblage. The latter are chiefly derived from submarine eruptions and consist of pillows, tuffs, or breccias, although some of the massive units may be intrusive. The greenstones are generally depleted in olivine; plagioclase (bytownite or labradorite to albite) and augite predominate. Altered mafic glass is

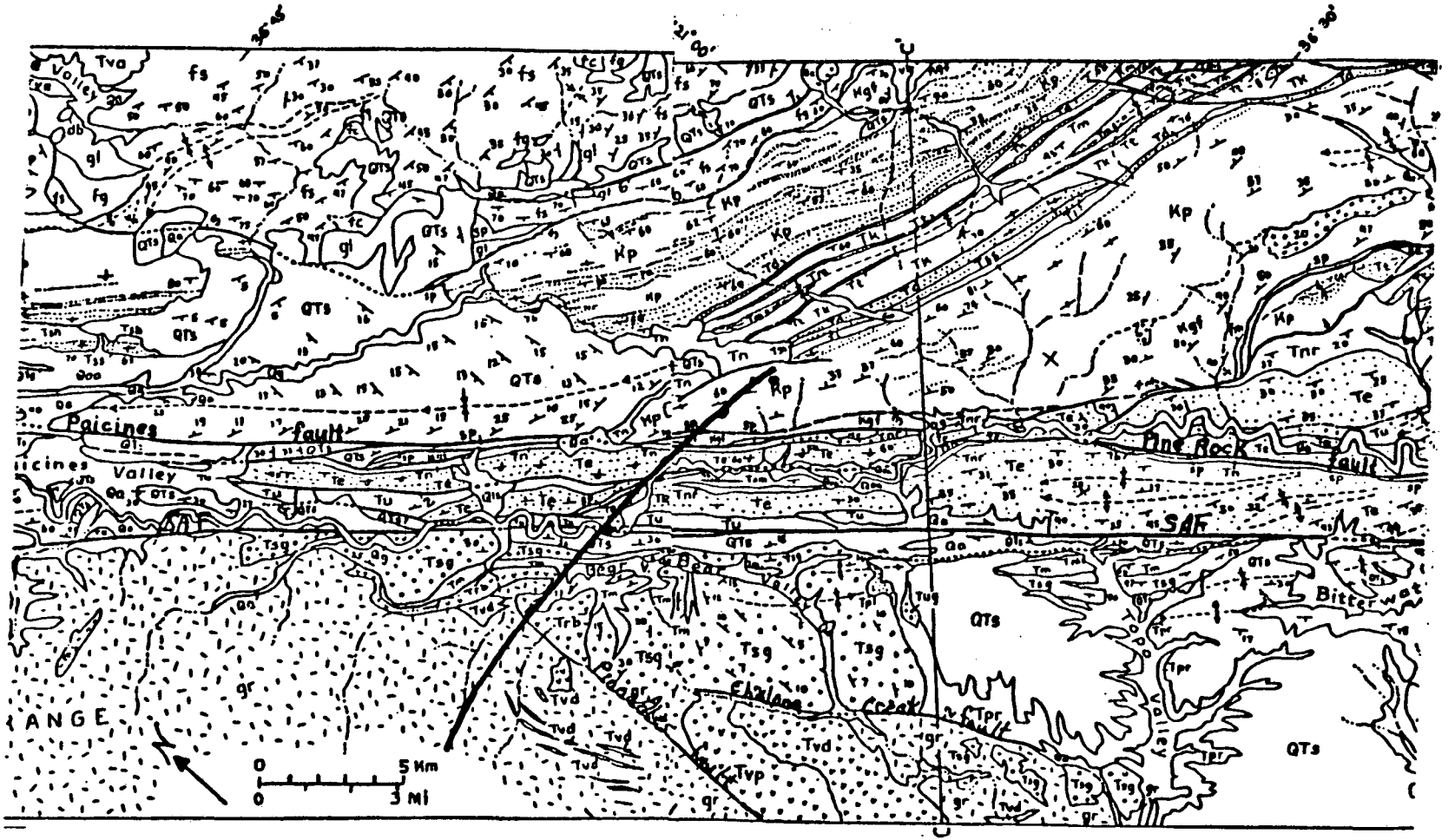

Figure (2-3) Geologic map of the same region as in Figure (2-2); adapted from Dibblee (1980). The prominent diagonal bar across the San Andreas fault represents the 1978 reflection profile.

pervasive. Most of these volcanics are abnormally hydrous and thus hydrochemically altered through reaction with sea water. Commonly associated with the greenstones are the Franciscan cherts which may in fact be formed by chemical precipitation of lava with sea water. They are distinctively thin-bedded closely jointed rocks composed of chalcedonic quartz and minor amounts of radiolaria, but generally lacking in clastic grains. Groups of these chert beds form discontinuous lenses up to 2 km in long.

Limestone is not common but does occur in some Franciscan terranes as rather small discontinuous bodies. It has been postulated that much of the Franciscan limestone originated by chemical precipitation in the presence of hot subaqueous lava; the lava may have supplied the lime to the water and the heat induced precipitation would have driven off the CO_2 (Page, 1966).

The most prevalent metamorphic rocks present in the Franciscan are actually the more uncommon kinds (e.g. glaucophane-bearing rocks, jadeitized graywacke, and eclogite are sporadically distributed in the form of lenses and masses). The glaucophane-bearing rocks were probably formed isochemically from basalts and in some instances from graywackes. Jadeite is commonly formed from alteration of graywacke and is therefore quite widespread as its replacement; this latter replacement often occurs without noticeable changes in outward appearance and thus may be responsible for suspiciously high densities in widely distributed graywackes (Page, 1966). The physical environment in which this type of metamorphism occurs is characterized by high pressures (5.5 to 7.5 kilobars) and low temperatures (150° to 300° C). This would correspond to lithostatic pressures at depths of 22 to 30 km, but at these depths the temperatures would be too high for this type of metamorphism; this paradox, as to the nature of the metamorphic environment, has intrigued many tectonophysicists . One common explanation is that burial (subduction) was rapid to depths of 20 to 30 km, followed by prompt uplift and erosion before the normal temperature gradient could be established. Alternatively, tectonic stresses may account for the high pressures without excessive temperatures. The eclogite that is found occurs as clumps that are tectonically enveloped in other rocks thus confusing any interpretations as to

its source (crust vs. mantle).

Essentially all of the coherent units within the Diablo Range are turbidite and related sandstones with thin mudstone intercalations. All sandstones within the coherent units and within the melanges are basically graywacke; about 35% of this is plagioclase feldspar. There is more than 10 volume percent of a fine matrix of chlorite and mica. The rest is quartz and lithic particles of greenstone, chert, shale and schist, with the shale constituting about 10%. There is essentially no orthoclase feldspar (Dibblee, 1980). These graywacke units are very immature, derived from turbidity currents and rapid erosion possibly of a granitic source material. Conglomerates appear locally in some of these units in the form of channel fillings and subordinate lenses. Many of the coherent sandstones are predominantly arkosic arenites containing, in general, more feldspar and a smaller proportion of lithic particles and matrix than many of the sandstone blocks of the nearby melanges. Actually, these units are metasandstones since nearly all of them have undergone incipient to pronounced blueschist facies metamorphism; however, because they retain most of their original megascopic textures and structures they are often classified as sandstones.

Some rather large coherent units of metagraywacke are included on the east side of the Franciscan core of the Diablo Range. For example, the "Orestimba metagraywacke", a somewhat tabular unit more than 7 km long, structurally underlies the extensive Garzas melange. It consists of massive to thin-bedded quartzofeldspathic graywacke with some minor amounts of intercalated siltstone. Turbidite features are found in some beds. Signs of metamorphism are found although metamorphic foliation is generally absent; various parts of the unit contain lawsonite, glaucophane or jadeitic pyroxene. This metamorphism is radiometrically dated at approximately 88 to 93 my (middle Cretaceous or older) (Page, 1981).

2.2.3 *SALINIAN PLUTONIC BLOCK*

The Gabilan Range and Mesa west of the San Andreas fault in central California is part of the large granitic "Salinian" plutonic block extending hundreds of kilometers to the north and south. The Gabilan terrane is the most elevated part of the Salinian Block adjacent to the fault, rising to an altitude of nearly 1000 m (Dibblee, 1980). It consists largely of granitic plutons and metasedimentary host rocks which are of amphibolite or higher metamorphic facies. The parent rocks of the metamorphics in the Salinian Block were predominantly, if not wholly, sedimentary—thinly bedded sequences of interbedded quartz-rich siltsone and impure sandstone plus lesser amounts of shaly and calcareous rocks (Ross, 1977).

The plutons of the Salinian Block are predominantly granodiorite and quartz monzonite with some examples of quartz diorite. These rocks are generally less variegated and apparently less deeply eroded than the plutons of the nearby Santa Lucia Range; in addition there are fewer remnants of metamorphic host rocks in the Gabilans. The exact ages of the Salinian plutons are a matter of some controversy: many estimates fall within the Cretaceous period, however a somewhat diffuse range of ages within this period exists based on K-Ar (92 to 70 m.y.) and U-Pb (117 to 106 m.y.) determinations. Page (1981) concludes that most of the Salinian is Early Cretaceous, though some may be Late Cretaceous. The age relationships between the plutonic block and sub-blocks, the pre-intrusive metamorphic host rocks, and the Franciscan assemblages bear critically on the tectonic history and development of the entire continental margin. For example, the initial determination that the granitic masses of the Coast Ranges were younger than some Franciscan rocks and the incongruent lack of plutonic activity and appropriate metamorphism in these Franciscan rocks lent great credence to the notion of large scale horizontal displacement on the San Andreas fault. Subsequently, many other pieces of evidence were compiled and such displacement is now widely accepted. (See section 2.3 below.)

The largest outcrop of Salinian pre-intrusive metamorphic rocks is in the Santa Lucia Range to the west of the Gabilans. These include biotite-feldspar quartzite, quartzofeldspathic granofels, and quartzofeldspathic gneiss plus lesser amounts of calc-silicate granofels,

amphibolite, aluminous schist, calcite marble, and metadolomite. In general the metamorphic grade within the Salinian Block is higher near the Pacific coast than elsewhere, reaching the granulite facies. The origin and geotectonic history of these pre-intrusive rocks is not well understood, however several investigators have attempted to correlate these rocks with those of other terranes (Wiebe, 1970; Ross, 1977). In general the evidence is insufficient to draw any definitive conclusions.

2.3 TECTONICS

2.3.1 *OVERVIEW*

The interpretation of the Bickmore Canyon/Bear Valley seismic reflection profile across the San Andreas fault depends, to some extent, on an accurate reading of the tectonic history of the fault and its bounding crusts. Specifically, the depth of the fault, the nature of the crust-mantle contact, the shallow structure at mid-crustal depths in the western granitic part of the section, the nature of the seismogenic zone, and the general question of the constitution of the upper and lower crusts and the fault zone itself are all critical problems bearing on the fault motion and observed seismicity patterns. An understanding of the tectonic history and development will greatly aid in the accurate determination of these structural features.

Several inactive faults exist on both sides of the main trace of the San Andreas; the Pinnacles fault to the west intersects the reflection line about midway into the Gabilan section, as indicated above and in Figure (2-3). Although inactive, this normal fault with its Miocene volcanics and sediments juxtaposed on the west with granite could extend to depth sufficiently to affect the seismic data. The low velocity wedge of Feng and McEvilly (1983) may be due in part to certain aspects of this contact, although this seems unlikely. Similarly, the San Benito and Pine Rock faults of the Diablo Range may contribute to the lack of spatially coherent reflectivity in the Franciscan half of the section; the presence of these faults to indeterminate depth may be viewed in the context of the general heterogeneity of the Franciscan medium.

The tectonic development of this region may be cast in terms of the history and development of the subduction zone Franciscan complex, the origin and emplacement of the Salinian Block, and a subsequent transformation to strike-slip or transform fault tectonics. The temporal and spatial correlation of these mammoth "events" can be most effectively understood by studying the relationship of continental geology to plate interactions at this active margin. The plate tectonic evolution of western North America has been extensively analyzed by Atwater (1970) in

terms of marine geophysical data; one of the more significant results of her thesis is the indication that a trench existed offshore from western North America in the mid-Tertiary period and that the onset of major strike-slip motion along a transform fault system did not begin until after the cessation of subduction. Hence, this model suggests that the San Andreas fault system and the attendant transverse motion of the Pacific and North American plates originated less than 30 m.y. ago. This subduction process is inferred from the pattern of magnetic anomalies west of the East Pacific spreading ridge and the "missing" eastern counterparts of these anomalies. From an analysis of the ages of the rocks in the vicinity of the Mendocino fracture zone off the coast of northern California it has been postulated that the consumption of the *Farallon* plate occurred from some undetermined time in the late Mesozoic or early Tertiary and was completed about 30 m.y. ago. Implied in this model is the assertion that the plate consumption or subduction rate (7 to 10 cm/yr) was greater than the rate of plate creation at the ridge (5 cm/yr), so that eventually the ridge itself was overrun by the trench. A prior Mesozoic subduction event is often associated with the formation of the Franciscan complex and the emplacement of the Sierran batholith and was unrelated to the later Farallon subduction event and the attendant transformation to a strike-slip plate boundary (Atwater, 1970). In this Mesozoic orogeny the Franciscan represents the eugeosynclinal complex, the Great Valley Sequence was accumulated in an elongate forearc basin within the arc-trench gap, and the Sierra Nevada batholith represents the intrusive roots of the magmatic arc. This earlier subduction process appears to have been active until about 80 m.y. ago (Atwater, 1970). The transformation to a strike-slip plate boundary marks the beginning of motion along the San Andreas fault and is correlated with the northwestward migration of the ridge-trench-transform fault triple junction; in this model the transform fault originated toward the southwest continental margin and migrated progressively northwestward with the locus of subduction activity due to oblique plate convergence. There is also evidence that ocean floor (e.g. Juan de Fuca plate) is presently being underthrust beneath the continental margin in the vicinity of Oregon and Washington; indeed, the andesitic volcanism of the Cascade mountains independently suggests such present-day

subduction.

2.3.2 *MESOZOIC SUBDUCTION AND FORMATION OF THE FRANCISCAN COMPLEX*

As discussed previously, the prevailing interpretation of the formation of the Franciscan Complex is that it was assembled by subduction of oceanic crust under western North America during the Mesozoic era as voluminous episodic offscrapings from a downgoing lithospheric slab. In such a scenario this tectonically stacked pile once formed the outer arc ridge alongside a paleo-subduction trench. However recent analysis of reflection data in central California indicates that a more complex tectonic wedging may have occurred (Wentworth et al., 1984; Zoback and Wentworth, 1986). In this model, the Coast Range Thrust fault, which forms the Franciscan-Great Valley boundary in much of central California, does not extend to depth in the crust and may be a roof thrust to a wedge of Franciscan which was presumably obducted over the Sierran basement. Hence the interjection of the Franciscan assemblage between the Sierran basement and the Great Valley Sequence would not in and of itself indicate a subduction origin, as previously accepted. However such a subduction zone origin is not precluded; the role of subduction in the generation of tectonic wedges is not clear. Evidence for the subduction zone origin of the Franciscan consists of the following:

i) its spatial position with respect to the (apparent) forearc basin deposits (e.g. Great Valley Sequence, "GVS") and the plutonic or magmatic arc (e.g. Sierra Nevada)

ii) paleomagnetic evidence for plate convergence in the late Mesozoic, contemporaneous with the period of Franciscan evolution

iii) the quasi-contemporary radiometric ages of Franciscan, GVS, and Sierran plutons

iv) the presence of highly sheared melanges within the Franciscan Complex

v) high P/T metamorphism within Franciscan, in part contemporaneous with the high P/T metamorphism and plutonism of the Sierra Nevada

vi) the mixture within the Franciscan of fragments of oceanic rocks, terrigenous sediments, and mantle material suggesting the convergence of oceanic and continental plates.

In addition to these indications the interbedding of radiolarian chert with graywacke, a terrigenous clastic sediment, can best be understood in the context of a subduction zone environment: Biogenic chert accumulations would favor a sheltered pelagic deep marine depositional environment and would not be expected to include clastic sediments. Conversely, turbidites such as graywacke represent a clastic influx within a somewhat unstable chaotic depositional environment. Alternating sequences of chert and graywacke are well represented in various Franciscan outcrops (Page, 1981). A deep sea floor on the oceanward side of a trench that receives clastic sediment from a continental shelf might fill during a period of slow subduction; subsequent turbidite flows could spread oceanward. During periods of more rapid subduction the troughlike character of the trench would be restored and chert deposition could prevail on the outlying sea floor. Furthermore, many of the observed chert-graywacke sequences have undergone blueschist facies metamorphism suggesting eventual subduction.

As mentioned previously (see section 2.2.2, above), the metamorphic environment in which the Franciscan Complex was incorporated was characterized by high pressures and low temperatures. In addition to the aforementioned scenario involving rapid subduction and prompt uplift, these high P/T conditions could have existed during a period of underthrusting; evidence for the underthrusting of the Franciscan beneath the GVS is noted by Page (1981) who suggests that the consequent tectonic stresses that would prevail would be sufficient to produce the observed metamorphic facies. Although no definite or coherent pattern exists in the distribution of the blueschist facies rocks in the Diablo (Raymond, 1973), within the Franciscan Complex as a whole there is a general but definite increase in the grade of blueschist metamorphism eastward (Ernst, 1981). This large scale trend reflects successively greater depths of subduction and is consistent with either of the aforementioned scenarios.

2.3.3 *ORIGIN AND EMPLACEMENT OF THE SALINIAN BLOCK*

Although the out-of-place Salinian Block basement of metasediments has not been definitively correlated with sequences elsewhere, it is believed that during the late Mesozoic it was situated between the Sierra Nevada and Penninsular-Baja California ranges, although there are difficulties in this scenario (Crowell, 1973). Specifically, K-Ar ages do not match exactly: those for the Salinian Block range from 92 to 62 m.y. whereas those for the Penninsular Range vary from 112 to 75 m.y. Of course it is important to realize that part of the Salinian Block was subducted during the Eocene and that much of the northern extent of the block is submerged off the coast of northern California. Hence, although this scenario would require the correlation of the southernmost Sierran rocks with the northernmost Salinian rocks, the inaccessibility of the latter precludes such a definitive examination. Crowell (1973) does point out, however, that no through-going fault or definitive tectonic scheme has as yet been recognized to tie the San Andreas fault with certain southern faults, notably the Newport-Inglewood fault zone, through the Transverse Ranges. In any case, even if the pre-intrusive metamorphic rocks did not originate in the region between the Sierra Nevada and Penninsular Ranges they were probably there in time to be invaded by the plutons of the Sierran-Penninsular magmatic arc (Page, 1981); that is, we know that the plutons were not transported with these host rocks from some locality beyond the Sierran-Penninsular axis. The question of whether these pre-intrusive metasediments were allochthonous prior to plutonism remains an intriguing mystery.

The main intrusive epoch of the entire core complex occurred in the early to middle Cretaceous (117-106 m.y. ago) and was contemporaneous with subduction to the west. At about the boundary between the Cretaceous and Tertiary (80-50 m.y. ago) while the Laramide orogeny was taking place far to the east, a general low angle subduction process was underway. Arc magmatism was extinguished in the Sierra Nevada by this time and the locus of inland deformation shifted eastward; by analogy with the modern Andes, such a magmatic lull may be associated with a transition from steep to shallow subduction: As the descending slab scrapes under the overriding plate during shallow subduction arc magmatism is suppressed and internal

deformation predominates. Evidence for such shallow subduction suggests the underthrusting of Franciscan beneath the Salinian Block at depths greater than 10 km (Dickinson, 1981). Uplifting of Franciscan terranes through the granitic crust of the Mojave Block is indicated along the San Andreas and Garlock faults as manifested by the Pelona, Orocopia and Rand schist terranes. Indeed, it has been proposed that the Salinian Block is a pre-San Andreas westward continuation of the Mojave Block (Dickinson, 1981). Further evidence of such a low angle subduction process is indicated by the presence of Franciscan-type eclogites in the Colorado Plateau suggesting a large eastward carry without significant depth of subduction. Simultaneous with this period of low angle subduction there was deep erosion of the plutons and uneven submergence of the Salinian Block. Additionally, local outcrops of deep-sea fan sedimentation can be found on the block.

The Paleocene (65-55 m.y. ago) was characterized by oblique plate convergence, rapid subduction of a gently dipping slab and the inception of strike-slip faulting. It is postulated that the initial 200 km of northwest movement of the Salinian Block occurred on a proto-San Andreas fault during the Paleocene (Page, 1981). [This is discussed in greater detail below.] The subduction or "destruction" of the western part of the Salinian Block occurred during the Eocene (53-38 m.y. ago) at which time the block was submerged. Page (1981) suggests that there may have been a lull in the northwest translation of the Salinian Block during this time.

The northwest migration of the triple junction began during the period from the Oligocene to early Miocene (38-21 m.y. ago) time. During this time the initial uplift and emergence of the Franciscan and the Salinian Block was occurring as well as limited basaltic and silicic magmatism within the block. Following this uplift and emergence, marine strata were deposited in and near the San Andreas fault zone in the Miocene and Pliocene. Such (channel) marine deposition is manifested in the San Benito or Hollister trough which may have extended northwest from the San Joaquin basin all the way across the San Andreas fault into the La Honda basin of the Santa Cruz Mountains. This is suggested by a Pliocene sequence through the fault (denoted by "QTs" in Figure (2-3)); this Pliocene sequence as well as the overlying Plio-Pleistocene valley

sediments are tightly folded, especially in the region between the San Andreas and Paicines faults.

The migration of the triple junction continued during the Miocene (23-5 m.y. ago) as subduction ceased and prolonged strike-slip faulting predominated. This strike-slip movement was accomodated along other areas in addition to the San Andreas such as the San Gregorio-Hosgri fault. Folding within the Salinian Block was occurring as well as continued magmatism during this period. Finally, the opening of the modern Gulf of California and the attendant northwest movement of Baja California began in the Pliocene-Quaternary (5-0 m.y. ago). It is believed that this northwest relative motion including, of course that of the Salinian Block, accelerated during this recent period (Page, 1981).

Current motion along the boundary between the Pacific and North American plates is estimated at 5.6 ± 0.3 cm/yr in the direction $N35°W \pm 2°$ from rigid plate models (Minster and Jordan, 1978); of this, 3.5 to 3.7 cm/yr is attributed to motion along the San Andreas fault system which accomodates slip along neighboring faults such as the Hayward, Calaveras, San Jacinto, et cetera (Savage and Burford, 1973); this latter figure is derived from geodetic measurements and detailed geologic evidence. The remainder is distributed over a broad zone of deformation and slip along faults located between the foot of the continental slope to the west and central Nevada. Extrapolation of these rates of motion back through geologic history poses several intriguing problems in part because of an apparent variability in the rate of right-lateral motion. The emplacement of the Salinian Block appears to have been a two stage process; the first pre-Eocene stage is difficult to document whereas the later stage is more generally acknowledged. Estimates of displacement along the San Andreas fault within the last 23 million years (post early Miocene) are based on several widely accepted geologic analyses and there is consensus that about 300 km of right-lateral displacement has occurred. Huffman (1972) analyzed facies distributions and clast content of upper Miocene rocks across the San Andreas fault in central California. Granitic and volcanic sources of clastic deposits west of the fault are located hundreds of kilometers to the southeast on the other side of the fault. Similarly,

voluminous coarse conglomerate beds east of the fault in the Temblor Range were correlated with the elevated granitic-metamorphic Gabilan Range and Mesa about 240 km to the northwest. Huffman concludes that 22 million year old rocks in central California have been displaced about 300 km in a right-lateral sense by strike-slip motion along the San Andreas fault in central California. Furthermore he suggests that the rate of slip was not constant and may have been episodic. Based on field, chemical, petrographic and radiometric considerations, Mathews (1973) has correlated the Pinnacles volcanic formation with the Neenach formation implying about 314 km of post early Miocene right-lateral displacement along the San Andreas fault. Mathews asserts that the lower part of the stratigraphic sequence of the northern Pinnacles formation is correlative with the Neenach volcanics and that this part of the Pinnacles is truncated by the Chalone Creek fault, an early Miocene trace of the San Andreas fault system (see section 2.2.1, above). Dickinson et al., (1972) analyzed early Miocene shoreline assemblages from the north end of the Gabilan Range (near San Juan Bautista) and matched them with assemblages in the San Emigdio Range suggesting 280 to 305 km of offset within the last 21.5 million years. These and several other convincing studies have lead to the widely held conclusion that about 300 km of right-lateral displacement of the Salinian block occurred over the last 21 to 23 million years.

After restoring the Salinian Block 305 km to the southeast to its early Miocene position one finds that Eocene rocks can be correlated across the San Andreas fault in addition to the Miocene rocks. Apparently there was a lull in the translatory plate motion during the Oligocene. Furthermore, at this position the Salinian Block is out of place with respect to the Sierran-Penninsular Ranges; based on the notion that the Salinian Block is part of the Sierran-Penninsular Range system one concludes that the entire block must have moved prior to the Eocene epoch. The actual amount of this pre-Eocene dextral displacement can be estimated by a comparison of several geological units across the fault. The most prominent formation that has been correlated is the Butano Eocene deep sea fan accumulation in the Santa Cruz Mountains with its counterpart, the Point of Rocks sandstone in the Temblor Range (see Figure 2-7,

adapted from Page, 1981). Detailed consideration of their respective basement rocks leads to the conclusion that significant pre-Eocene displacement occurred: The Butano sandstone is in direct contact with the underlying Salinian basement and there is strong geologic evidence that the Point of Rocks formation overlies Franciscan east of the San Andreas fault (Page, 1981). The length of mismatch of these basement rocks depends on assumptions as to the present location of the northernmost Salinian rocks and of the southernmost Franciscan rocks on opposite sides of the fault. Measuring from Point Arena to Eagle Rest Peak at the big bend of the San Andreas (Figure 2-7), the residual, displacement amounts to 290 km. Accounting for slip along the San Gregorio-Hosgri fault which may have contributed to the total length of mismatch, Page (1981) estimates that 175 to 210 km of pre-Eocene dextral displacement occurred along the proto-San Andreas fault and thus contributed partially to the emplacement of the Salinian Block. He estimates that this early partway emplacement occurred during the Paleocene (65-55 m.y ago). The evidence for this is largely conjectural and is based on contrasts in Paleocene thrust faulting on the two sides of the fault as well as certain paleogeographic arguments (Dickinson et al., 1972). In any case, the hypothesis is that due possibly to oblique plate convergence with attendant low angle subduction a strike-slip component was transmitted by the slab to the underside of the continental plate edge causing the observed displacement of the block. One of the more perplexing aspects of this scenario is that no pre-Miocene offset is required south of the Transverse Ranges; the general disparity of measurements to the north and south suggests that the proto-San Andreas fault may have bypassed the present San Andreas fault in the south and involved early movement of only part of the Salinian Block. The total offset during the Cenozoic era is estimated as 570 km (Dickinson, et al., 1981) although Howell (1975) estimates that as much as 700 km of displacement may have occurred along the entire system of northwest trending faults.

2.3.4 *RECENT HISTORY*

Subduction beneath the Diablo Range persisted until 6 to 17 m.y. ago (Page, 1981). Following erosion of the overlying GVS cover, the Diablo antiform was first exposed in the middle Miocene. The principal uplift of the Diablo antiform was in the late Pliocene, although it may still be going on. The Gabilan Range and Mesa was uplifted at the same time; this simultaneity may be an important clue to the tectonic history of the region. Many investigators propose that the Franciscan core bulged upward as a huge incipient diapir and cite several possible explanations ranging from gravitational buoyancy and related thermal inducements to tectonic or mechanical stresses. As it seems necessary in any scenario to include the simultaneous Gabilan uplift some have proposed that Franciscan is present at depth beneath this granitic metasedimentary complex. On the other hand, this regional perspective does not explain the apparent linear discretization of such bouyancy; specifically, the Salinas Valley and other structural valleys in the region appear to have been unaffected by any such bouyant behavior. One possible explanation would invoke the probable inhomogeneous composition and imbricate structure of the underlying subduction complex. However it is important to realize that the late uplift of these belts coincides with the onset of Neogene transform tectonics which post-dates the Mesozoic and early Tertiary subduction tectonics by some 2 to 20 million years (depending on location as suggested by the Atwater model). Furthermore these uplifted and depressed structural features parallel the range margins and the general fabric of the strike-slip motion. Of course these orientational relations may have just as plausibly been inherited from earlier subduction processes as these latter processes surely produced elongate slices and uneven crustal topography parallel to the plate boundary. However the chronological coincidence of these uplifts with the rifting in the Gulf of California, considerably after the cessation of subduction, strongly suggests that some aspect of Neogene transform tectonics had at least a prominent enhancing effect on these vertical adjustments.

2.4 DISCUSSION

The genesis of transform faulting along the continental margin in California may be traced to the Paleocene epoch at which time a change from a steep, more normal subduction environment to one characterized by oblique convergence and shallow underthrusting occurred. The consequences of this oblique convergence are manifested in the San Andreas fault system, although it is not clear how this transition actually occurred nor how the buried spreading center ('East Pacific Rise') has affected the tectonic development in the southwestern part of the continent. Indeed, the anomalous Transverse Ranges do not seem to fit any tectonic model; the geotectonic development of northern California appears to be difficult to explain in conjunction with the lithospheric structure of parts of southern California.

Plausible models of the formation of the Franciscan subduction complex have been offered that help to explain most of the geologic evidence, although not unambiguously; that is, the history of the oceanic crust prior to subduction during the Mesozoic era is not well understood and the notion of allochthonous terranes may be applicable to the subduction of what has become known as the Franciscan melange. The existence of Franciscan beneath portions of the upper granitic crust along the Coast Ranges west of the San Andreas fault is certainly not definitively shown, but a tectonic model has been offered which could explain how it might have been emplaced there prior to translation along the fault. The geologic evidence does not seem to provide an answer one way or the other, and thus the answer may lie in careful geophysical analyses. More detailed investigations of the seismic velocity within the crust are needed in addition to a more refined knowledge of the attenuation and heterogeneity properties of the medium. There are problems, however, in the application of seismic techniques to address this latter problem of lower crustal composition. Attenuation measurements may not provide unambiguous answers unless some method of delineating the relevant attenuation mechanisms is developed. On the other hand, although the results of attenuation measurements may not be sufficient to solve definitively the problem of the lower crustal composition(s), this type of

analysis provides the essential complement to the geologic data for an understanding of the general contrast in spatially coherent reflectivity across the fault (see Chapter 3). Velocity measurements may provide accurate, and in some respects, unambiguous results, but it is not clear how different Franciscan and granitic rocks may be at the temperatures and pressures appropriate for these depths. Indeed, although Walter and Mooney (1982) concluded that the average P-wave velocity of the lower Gabilan crust was almost 6% lower than that of the Diablo lower crust, it was largely on the basis of the field geology that they inferred a gneissic composition for the lower Gabilan crust. It is apparent that careful and detailed laboratory studies may help to solve the problems associated with velocity and attenuation measurements, particularly in such complex media.

The question of the apparent dip of the Moho may be explained by velocity modeling (see Chapter 3). That of the laminated appearance of the crust-mantle contact may require more geologic inference; this feature is not unique to the region of this study, but instead has been observed in numerous other areas, most of which are quite different in terms of geology and certainly in terms of tectonic history (see Hale and Thompson (1982) for a review). The actual depth to which the San Andreas fault zone extends remains a most intriguing mystery in the context of the fact that it represents the boundary between two lithospheric plates.

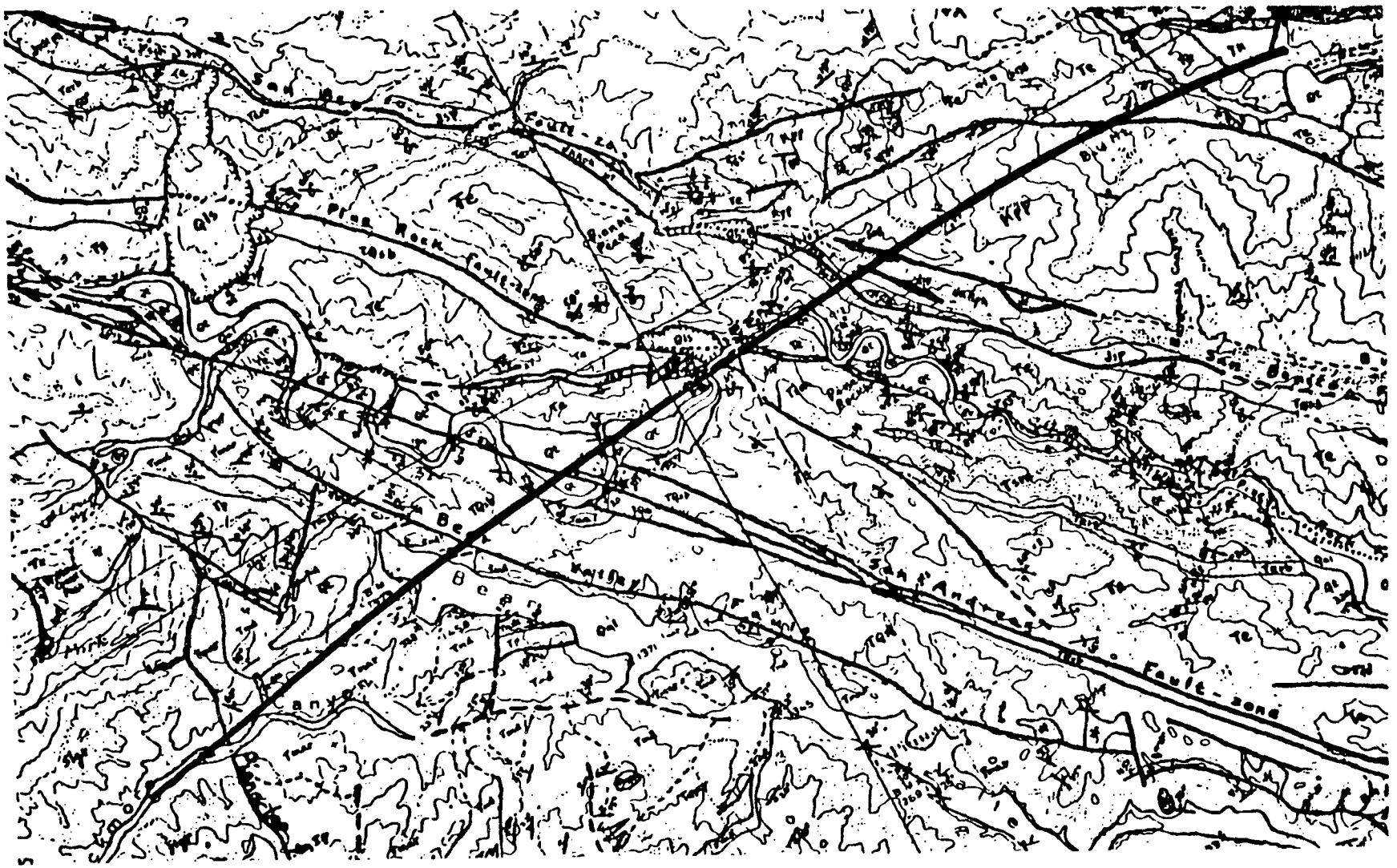

Figure (2-4) Detailed version of Figure (2-2) above; adapted from Wilson (1942). [Contour interval = 50 feet; Scale: one inch = 1 mile (1.609 kilometers)]

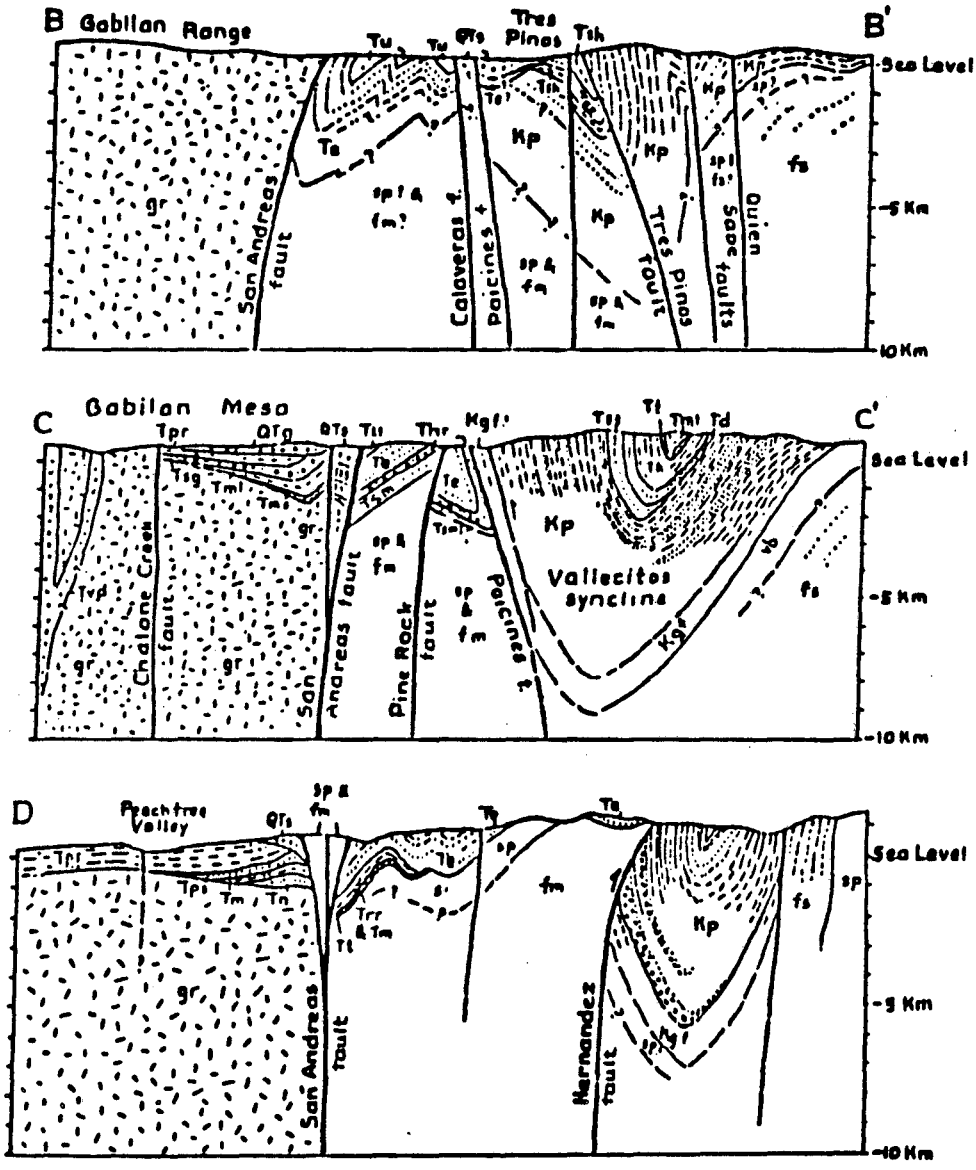

Figure (2-5) Geologic cross-section of Bickmore Canyon region of the San Andreas fault zone; after Dibblee (1980); (no vertical exaggeration).

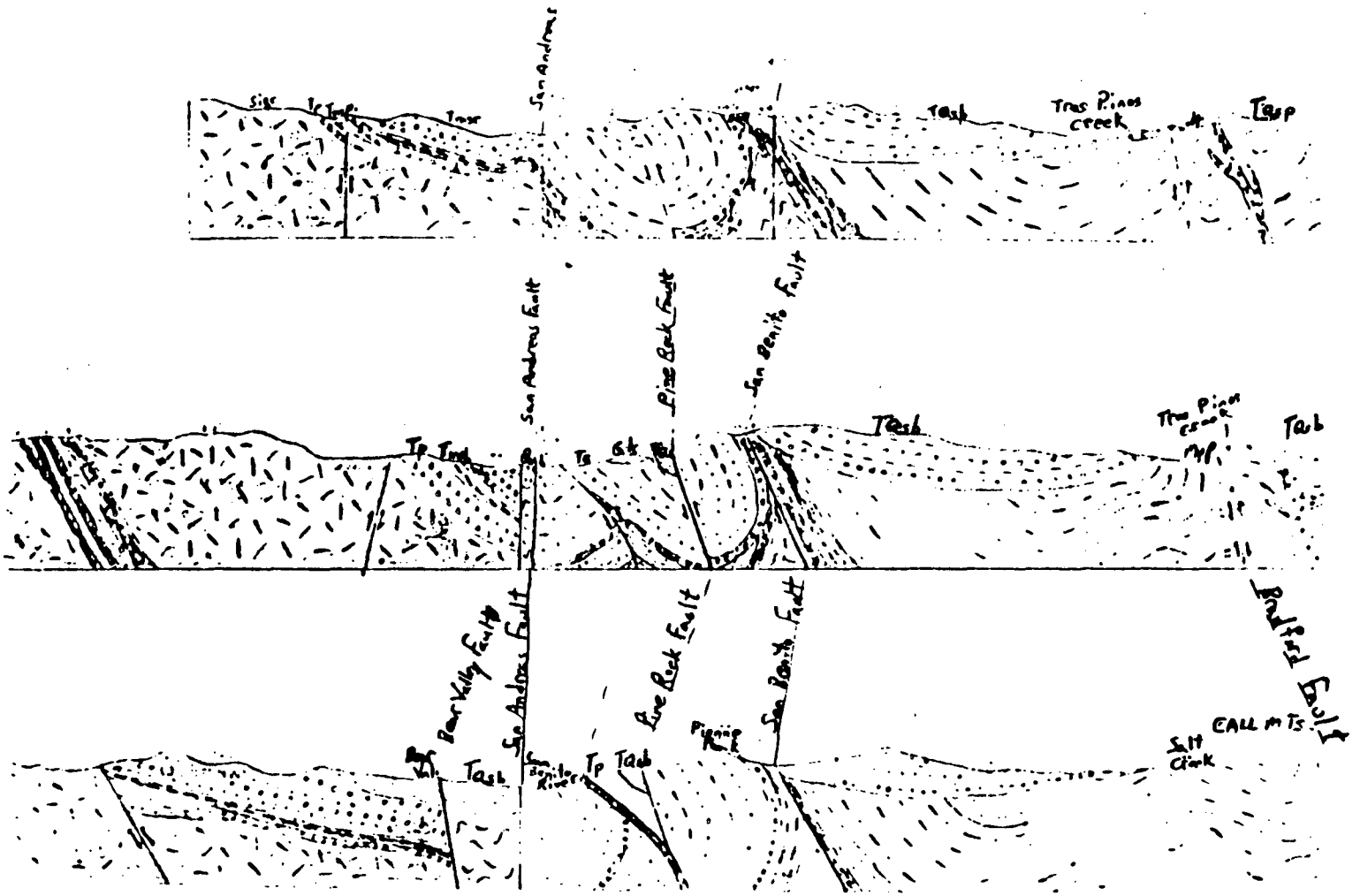

Figure (2-6) Geologic cross-section of Bickmore Canyon region of the San Andreas fault zone; after Wilson (1942); note that this cross-section spans a considerably shallower portion of the crust than the previous figure adapted from Dibblee (1980). [Scale: one inch = 1 mile (1.609 kilometers)]

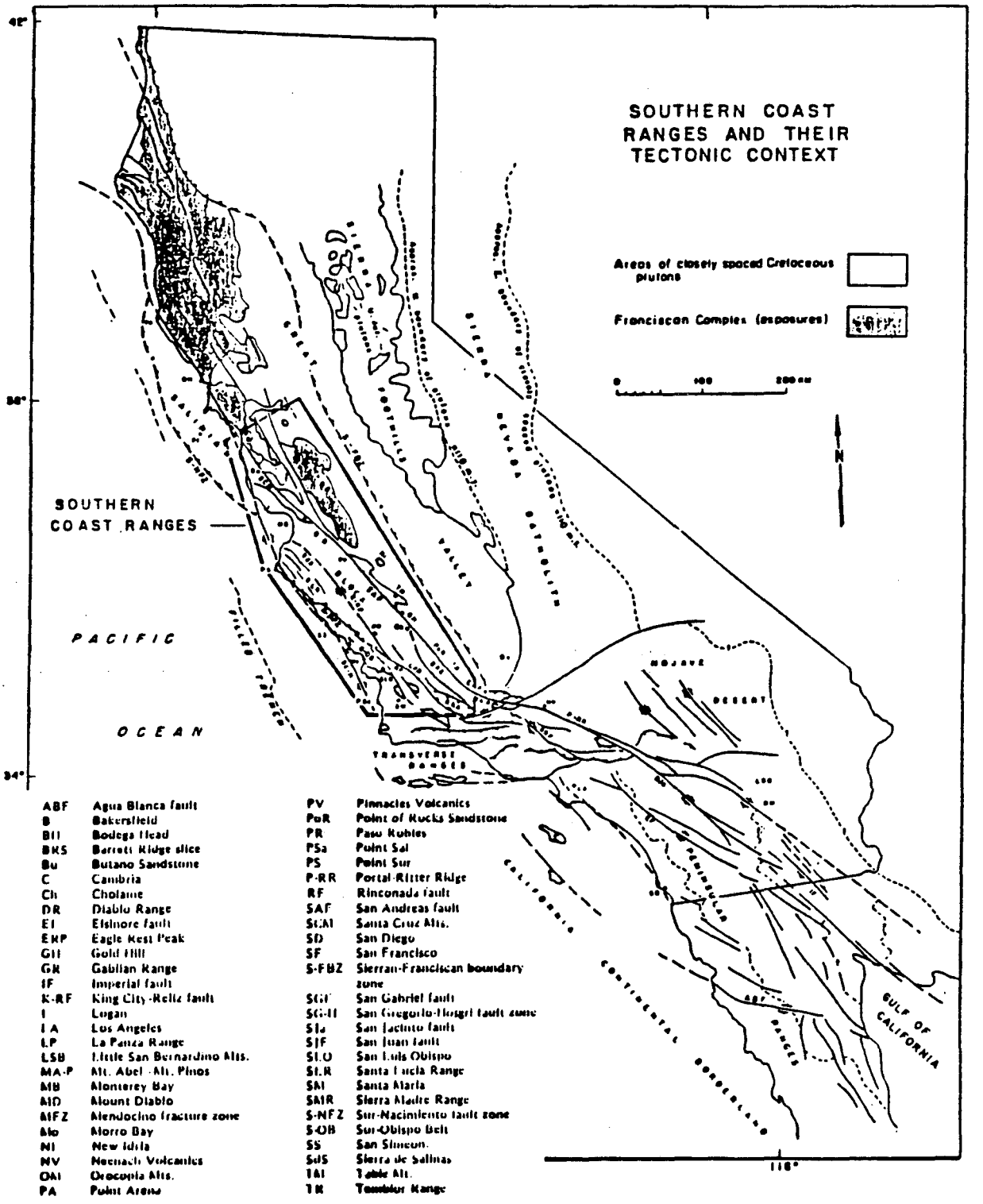

Figure (2-7) Tectonic map of the Southern Coast Ranges; adapted from Figure "13-2" of Page (1981).

References: Chapter 2

Atwater, Tanya, 1970. Implications of plate tectonics for the Cenozoic tectonic evolution of western North America *Geol. Soc. Am. Bull.*, **81**, 3513-3536.

Atwater, Tanya and Peter Molnar, 1973. Relative motion of the Pacific and North American plates deduced from sea-floor spreading in the Atlantic, Indian, and South Pacific oceans, in Kovach, R. L. and A. Nur, eds., Proc. Conf. on Tectonic Problems of the San Andreas Fault System: *Stanford Univ. Pubs. Geol. Sci.* **13**, 136-148.

Bakun, William H. and Marcia McLaren, 1984. Microearthquakes and the nature of the creeping-to-locked transition of the San Andreas fault zone near San Juan Bautista, California, *Bull. Seism. Soc. Am.*, **74**, 235-254.

Blumling, P. and C. Prodehl, 1983. Crustal structure beneath the eastern part of the Coast Ranges (Diablo Range) of central California from explosion-seismic and near-earthquake data, *Phys. Earth Planet. Interiors*, **31**, 313-326.

Blumling, Peter, Walter D. Mooney and W. H. K. Lee, 1985. Crustal structure of the Southern Calaveras fault zone, Central California from seismic refraction investigations, *Bull. Seism. Soc. Am.*, **75**, 193-210.

Crowell, John, 1973. Problems concerning the San Andreas fault system in southern California, *Stanford Univ. Pub. Geol. Sci.* **13**, 1245-135.

Dibblee, Thomas W., Jr., 1980. Geology along the San Andreas fault from Gilroy to Parkfield, *California Division of Mines and Geology, Special Report* **140**, 1-17.

Dickinson, W. R., et al., 1972. Test of new global tectonics - Discussion, *Am. Assoc. Petr. Geol. Bull.*, **56**, 375-384.

Dickinson, W. R., 1981. Plate tectonics and the continental margin of California, in *The Geotectonic Development of California*, W. G. Ernst, Editor, Prentice-Hall, New York, 1-28.

Ernst, W. G., 1981. Summary of the geotectonic development of California, in *The Geotectonic Development of California*, W. G. Ernst, Editor, Prentice-Hall, New York, 601-613.

Feng, R. and T. V. McEvilly, 1983. Interpretation of seismic reflection data for the structure of the San Andreas fault zone, *Bull. Seism. Soc. Am.*, **73**, 1701-1720.

Hale, L. D. and G. A. Thompson, 1982. The seismic reflection character of the continental Mohorovicic discontinuity, *J. Geophys. Res.* **87**, 4625-4635.

Howell, D. G., 1975. Hypothesis suggesting 700 km of right slip in California along northwest-oriented faults, *Geology*, **3**, 81-83.

Huffman, O. F., 1972. Lateral displacement of Upper Miocene rocks and the Neogene history of offset along the San Andreas fault in central California, *Geol. Soc. Am. Bull.*, **83**, 2913-2946.

Lynn, Heloise B., Laura D. Hale and George A. Thompson, 1981. Seismic reflections from the basal contacts of batholiths, *J. Geophys. Res.*, **86**, 10633-10638.

Mathews, Vincent III, 1972. Test of new global tectonics: Discussion *Am. Assoc. Petr. Geol. Bull.*, **56**, 371-374.

Mathews, Vincent III, 1973. Pinnacles-Neenach correlation: A restriction for models of the origin of the Transverse Ranges and the Big Bend in the San Andreas fault, *Geol. Soc. Am. Bull.*, **84**, 683-688.

McEvilly, T. V. and R. Clymer, 1975. Reflection seismic survey near the San Andreas fault, *U.S. Geol. Surv. Final Rept., contract no. 14-08-0001-14845.*

Minster, J. Bernard and Thomas H. Jordan, 1978. Present-day plate motions, *J. Geophys. Res.*, **83**, 5331-5354.

Mooney, Walter D. and Robert H. Colburn, 1985. A seismic-refraction profile across the San Andreas, Sargent, and Calaveras faults, west-central California, *Bull. Seism. Soc. Am.*, **75**, 175-192.

Oakeshott, Gordon B., 1966. San Andreas fault, in Geology of Northern California, *Cal. Div. Mines Geol.*, **190** 355-389.

Page, B. M., 1966. Coast Ranges Province, in Geology of Northern California, *Cal. Div. Mines Geol.*, **190** 253-322.

Page, B. M., 1981. The southern Coast Ranges, in *Geotectonic Development of California*, W. G. Ernst, Editor, Prentice-Hall, New York, 329-417.

Raymond, L. A., 1973. Tesla-Ortigalita fault, Coast Range thrust fault, and Franciscan metamorphism, northeastern Diablo Range, California, *Geol. Soc. Am. Bull.*, **84**, 3547-3562.

Ross, D. C., 1977. Pre-intrusive metasedimentary rocks of the Salinian block, California - a paleotectonic dilemna, in *Paleozoic Paleogeography of the Western United States: Pacific Section, Soc. Econ. Paleontologists and Mineralogists, Pacific Coast Paleogeography Symposium 1*, 371-380.

Savage, J. C. and R. O. Burford, 1973. Geodetic determination of the relative plate motion in California, *J. Geophys. Res.*, **78**, 832-845.

Scheiner, J. E., 1983. Attenuation near the San Andreas fault zone from reflection data, *Earthquake Notes*, **54**, 51.

Scheiner, J. E. and T. V. McEvilly, 1984. Seismic attenuation and crustal structure near the San Andreas fault from reflection profiling, *Earthquake Notes*, **55**, 10.

Stewart, Samuel W., 1968. Preliminary comparison of seismic traveltimes and inferred crustal structure adjacent to the San Andreas fault in the Diablo and Gabilan Ranges of central California, *Proc. Conf. Geol. Problems of San Andreas Fault System, Stanford Univ. Publ. Geol. Sci.*, **11**, 218-230.

Walter, A. W. and W. D. Mooney, 1982. Crustal structure of the Diablo and Gabilan Ranges, central California: A reinterpretation, *Bull. Seism. Soc. Am.*, **72**, 1567-1590.

Wang, Chi-Yuen, Feng Rui, Yao Zhengsheng and Shi Xingjue, 1986. Gravity anomaly and deep density structures in the San Andreas fault zone, in press, *Pageoph*, **124**, 127-140.

Wentworth, C. M., M. C. Blake, Jr., D. L. Jones, A. W. Walter and M. D. Zoback, 1984. Tectonic wedging associated with emplacement of the Franciscan assemblage, California Coast Ranges, *Franciscan Geology of Northern California: Pacific Section S. E. P. M.*, **43**, 163-173.

Wiebe, R. A., 1970. Pre-Cenozoic tectonic history of the Salinian block, western California, *Geol. Soc. Am. Bull.*, **81**, 1837-1842.

Wilson, Ivan, 1942. *Geology of the San Benito Quadrangle*, PhD thesis, University of California, Berkeley,

Zoback, Mark D. and Carl M. Wentworth, 1986. Crustal studies in central California using an 800-channel seismic reflection recording system, *Reflection Seismology: A Global Perspective, Geodynamic Series*, **13**, 183-196.

Chapter 3

Velocity and Attenuation Studies

3.1 INTRODUCTION

Seismic reflection profiling techniques provide a powerful and perhaps the only reliable approach to the study of the structural and compositional detail of the earth's crust, particularly in areas of complex structure. The small aperture and high frequencies of these studies generally allow for increased resolution while the attendant focussing capabilities offer the ability to target the structural features of interest. However, the resulting image, given this high resolution is very "fragile"; that is, it can be destroyed or distorted by errors in either data acquisition or in processing. Hence it is critical that the reflection survey be carefully planned and executed. Many of the early applications of the method to studies other than petroleum exploration were not so carefully planned; preliminary experiments to determine optimum sources, receivers, field configurations, recording parameters, spectral range of interest, listening times, etc. were not extensively carried out vis a vis the structural target of interest. This was due, in part, to cost considerations which can exceed 10k dollars per day. We have learned over the last decade that the reflection method can be very powerful given great care in the planning and execution stages.

In many different types of geological studies, the application of the reflection method is proving invaluable as improvements in the technique enable the interpretation of such data to be realized with greater confidence. One of the exciting areas of interest in which the method has been applied is in the study of the crustal structure across the San Andreas fault in central California. An expanding-spread (37-fold) survey in 1974 (McEvilly and Clymer, 1975) demonstrated the detectability of clear reflections from the base of the crust, which have subsequently been used in a monitoring program of travel-times in the vicinity of the seismogenic fault zone in a search for stress-related earthquake precursors (Clymer and McEvilly, 1981). A second,

extended reflection survey in 1978 involved common-depth-point, (CDP) profiling across the fault, including some long lateral and longitudinal offsets to about 20 km distance from the spread (McEvilly, 1981). The primary purpose of these studies was to determine the reflectivity of the crustal section in the vicinity of the fault zone in order to select appropriate segments of reflected and refracted arrivals which could be monitored in a long-term study of precursory travel-time and amplitude variations in the region where a M_L 5.0+ earthquake was expected within a few years or so. Furthermore, a refined understanding of the structure of this region was required to explain several important observations relating to earthquake data: The observed distortions in radiation patterns from local earthquakes recorded at the many stations of the U.S. Geological Survey (USGS) and U.C. Berkeley (UCB) networks, travel time anomalies within the same local arrays, and hypocenter location problems using a laterally homogeneous velocity model all emphasized the need for a more refined model of the velocity structure.

A summary of the travel time monitoring results is to be found in Clymer and McEvilly (1981). Recent analyses of this 1978 reflection line have shed light on several important aspects of the fault zone structure and of the bounding crusts. Feng and McEvilly (1983) have attempted an initial interpretation of the velocity structure from this 1978 CDP profile using the inverse ray method of May and Covey (1981). In addition to this approach, conventional reflection processing techniques have been applied. Using the DISCO software package of Digicon Corp., Inc., velocity and attenuation analyses have been carried out on this unique data set as part of this study. A model of the velocity structure, apparently more accurate, has been obtained for this seismically active region by detailed studies of the edited reflection data. In addition, a model of the attenuation characteristics as parameterized by the apparent Q operator has been formulated along the profile at mid-crustal depths under a weak scattering hypothesis. The application of this weak scattering approach to stacked reflection data requires the assumption that the stacked CDP seismogram represents the impulse response to the medium directly beneath the (coincident) source/receiver point at the surface; the difference

between this actual seismogram and a simple reflection series is assumed to be due to scattering of the *primary* wave energy by scatterers or heterogeneities in the propagation path. Hence the simple reflection series appears smeared in time as the energy of the *primary* wave is spread over the subsequent part of the seismogram in the form of later arrivals of secondary wave energy (e.g. coda). A critical assumption in this application is that these secondary arrivals do not include very late arrivals from previous (i.e. earlier in reflection time) impedance contrasts in the medium above the reflector associated with this coda. The definition of a *primary* wave in this scenario requires a relatively significant degree of spatial coherence in the stacked section.

Finally, this same attenuation analysis has been applied to microearthquake data obtained from a small array study undertaken in the same area in 1981. The velocity model is consistent with the trend of previous studies, (Eaton et al., 1970; Wesson, 1971; Boore and Hill, 1973; Healy and Peake, 1975; McEvilly and Clymer, 1975; Aki and Lee, 1976; Engdahl and Lee, 1976; McNally and McEvilly, 1977; Wang, et al., 1978; and Feng and McEvilly, 1983), toward a laterally heterogeneous structure representing the fault zone as a low velocity feature. The CDP attenuation analyses give relatively low Q values with no strong lateral variations; because of low signal strength in the fault zone it is difficult to obtain a very reliable Q structure there. In general, the Q values determined range from a low of 40 in the fault zone to about 155 in the granitic section in the far west portion of the line. There is a consistent tendency for the Q values to increase with frequency at all locations along the profile; this result is consistent with those of numerous other coda Q investigations, (Aki and Chouet, 1975; Rautian and Khalturin, 1978; Roecker, et al., 1982; Biswas and Aki, 1984; and numerous others).

The microearthquake study provided an interesting complement to the attenuation results from the reflection data; the apparent Q values for the microearthquake data are consistent with those obtained for the stacked CDP seismograms– generally about 100. Furthermore the tendency for Q to increase with frequency over a band from 3 to 24 Hz is also seen in the microearthquake results. As will be detailed below, the microearthquake coda analysis was

carried out primarily using the S-wave coda, yet the overall results were generally similar to those of the reflection data. Specifically, the dependence of the apparent Q, Q_c, on frequency was essentially the same for both data sets, although the Q_o, the apparent Q extrapolated to 1 Hz, were higher for the microearthquake data. Perhaps of the most significance, the contrast in the frequency dependence of the apparent Q values was consistent for both data sets: Q_c was consistently more frequency dependent in the Franciscan crust than in the Gabilan crust.

3.2 DATA

3.2.1 *1978 CGG REFLECTION PROFILE*

As a follow up of a previous project in 1974 consisting of two 37-fold expanding-spread reflection lines, one on each side of the San Andreas fault, (McEvilly and Clymer, 1975), an extensive seismic reflection survey using Vibroseis sources was conducted in 1978 by the Compagnie General de Geophysique, (CGG), in San Benito County in central California. Some 18 km of CDP coverage was obtained by this line which was roughly bisected by the San Andreas fault; the line is actually an extension of the 1974 line "XT2" along part of La Gloria Road in Bickmore Canyon (southwest quarter of the USGS 15 minute topographic sheet, San Benito quadrangle). The geographical limits of the CGG line are depicted in Figure (3-1) taken from Feng and McEvilly (1983); (also see McEvilly (1979) for more details on this line). The profile begins on La Gloria Road in Bickmore Canyon and continues eastward across open country in Bear Valley then descends to cross the San Benito River valley; from there it proceeds generally eastward past Bald Mountain to the headwaters of Salt Creek. Near the Lower Butts Ranch (Section 5, T16s-R8E) there is a 500 foot cliff to negotiate, necessitating a cable pullout (near VP 312) and the loss of some coverage. In addition some longitudinal and lateral offset data complement the main profile line, but were not used directly in this particular study.

The initial survey period was characterized by an in-line pattern with the recording spread advancing ahead of the vibrators, leaving a five station gap between vibrators and the first geophone group. The recording period was delayed for an extended period due to a combination of factors including permit problems, rugged topography, fire hazards, and inclement weather. Since the line could not be picked up at the point of departure a change of shot-receiver pattern was initiated using a split spread until the eastern end of the line was encountered at which time the vibrators moved through the line. This somewhat complicated variable shooting pattern enabled the profile to maintain nominal 24 fold coverage; however, as we shall see the

variable shot-receiver configuration precluded the ability to perform a pre-stack migration of the data. Other aspects of the equipment and field practice are indicated in Table (1).

The range of frequencies in the pilot sweep was limited on the high frequency end by the deep targeting intention of the experiment and by experience with the signal character in the 1974 survey; furthermore, scattering losses of seismic waves tend to be higher at the higher frequencies, (although Dainty (1981) suggests that for a weakly scattering environment scattering losses will dominate over intrinsic losses at the lower frequencies). For a frequency-independent or weakly dependent intrinsic Q operator, there will also be a greater degree of energy losses at the higher frequencies. On the low frequency end of the spectrum there is a constraint imposed by the limited stroke and mass of the vibrator reaction mass, and harmonic distortion in the signal produced. The Mertz (Model 9: 21900 lbs force) vibrators used in this survey had a lower limit of about 6 Hz. Therefore, the sweep frequency band chosen was the two octaves 24 - 6 Hz. To improve vibrator low-frequency stability a 32 second linear down sweep was chosen. At least three vibrators were operative at any one time although usually four were vibrating simultaneously. The recording array was set at 880 ft total group length, 440 ft group interval and consisted of 36 buried geophones. Recording was done at an 8 millisecond sampling rate. An ineffective radio relay provided by the contractor precluded acquisition of the long offset data.

3.2.2 *MICROEARTHQUAKE ARRAY*

As a complement to the reflection data study, results of a nearby microearthquake survey were analyzed in the hope of understanding the general characteristics of seismic wave propagation in severely heterogeneous media as well as the specific crustal attenuation properties near this active segment of the San Andreas fault zone. A small two-dimensional nested triangular array of ten portable seismographs was deployed by Don Vasco in 1982 approximately 3.9 kilometers from the main trace of the San Andreas fault. Although the original purpose of this array was to study the degree of coherence and the possibility of split or multi-path arrivals

within the S-wave from polarization and f $-k$ analyses, the data were later used in this investigation of attenuation contrast across the fault. Initially deployed on the Gabilan granite west of the fault on the Schmidt Ranch, the array recorded several small earthquakes of M_L up to approximately 3.0. The array geometry is depicted in Figure (3-2). Inter-station spacing ranged from about 50 meters to 200 meters allowing a 400 meter aperture. Subsequently, the entire array was redeployed about 4.5 km east of the fault in the Franciscan terrain of the Melendy Ranch. This latter redeployment included thirteen instruments and a somewhat larger aperture: inter-station spacing on this "Melendy array" ranged from 75 meters to about 300 meters and thus permitted an aperture of 600 meters, as indicated in Figure (3-2). Each station consisted of a three component seismometer and a DR100 Sprengnether recorder; the Schmidt array recorded data for 14 days, whereas the Melendy array was in operation for only six days due to indigenous bovine mayhem. Although abbreviated, the deployment of this array in such a seismically active area provided some useful data. The geographical setting of the two temporary arrays adjacent to the San Andreas fault is shown in Figure (3-3). These 3-component velocity transducers were 4.5 Hz Mark Products seismometers with system response characteristics as shown in Figure (3-4); The top figure shows the response for displacement and the bottom of Figure (3-4) shows the response for velocity. Both include the 50 Hz anti-alias filter for a sampling rate of 200 Hz. Each station triggered individually on the vertical component of the P-wave, however variations in detection sensitivity and other equipment related problems precluded complete recording of each earthquake. Those events that were well-recorded by the temporary arrays were correlated with those located by the USGS central California network; these hypocentral parameters are incorporated into the present study where necessary. A typical three component record from the Schmidt array is shown in the bottom part of Figure (3-5).

Based on the location given by the USGS this event was approximately 6.6 km from the station with a depth of 1.5 km and a local magnitude of 2.0. A typical recording from the Melendy array is also shown in Figure (3-5). This earthquake, located some 15.4 km from the station was given a depth of 5.8 km and a local magnitude of 1.9 by the USGS. Note the marked difference

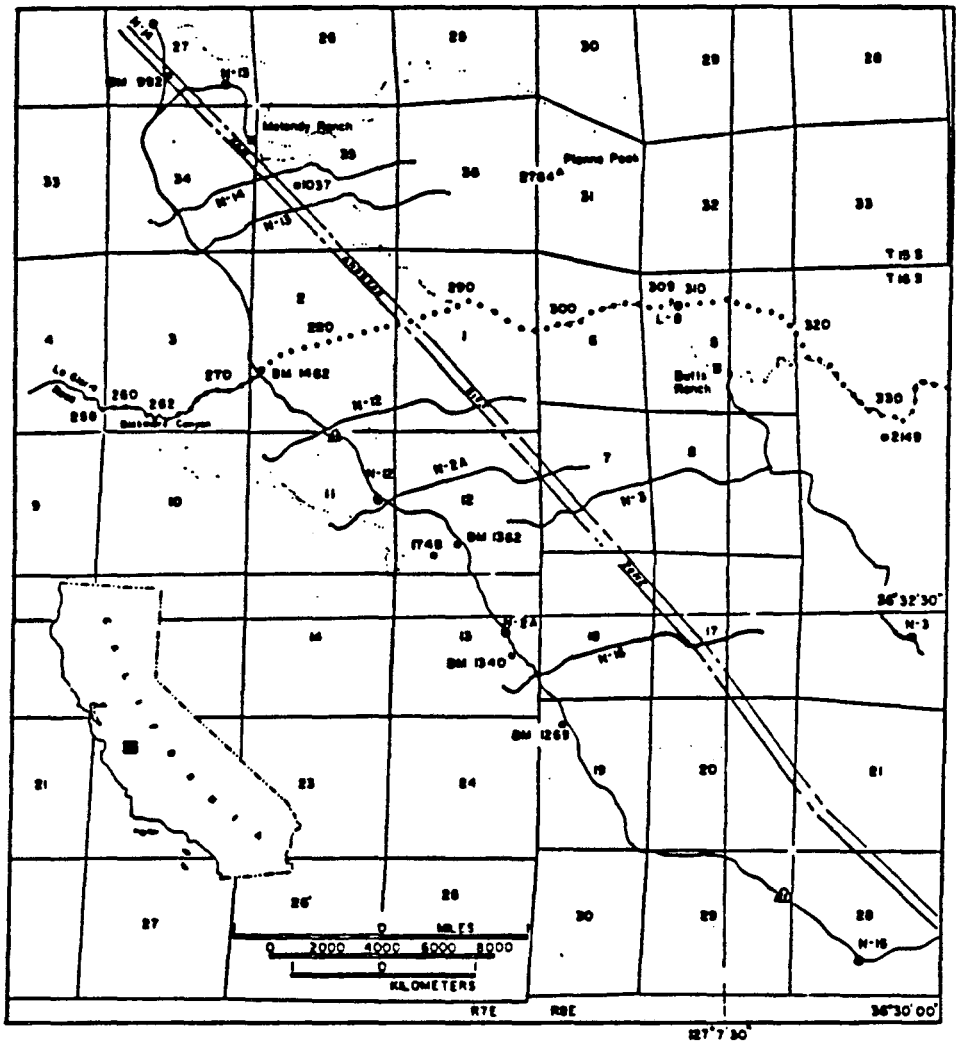

Figure (8-1) Map showing location of the 1978 CGG reflection survey (denoted by dotted line meandering east-west), crossing the San Andreas fault in San Benito, California (from Feng and McEvilly, 1983). Numbers along the profile are VP numbers (i.e. vibrator points).

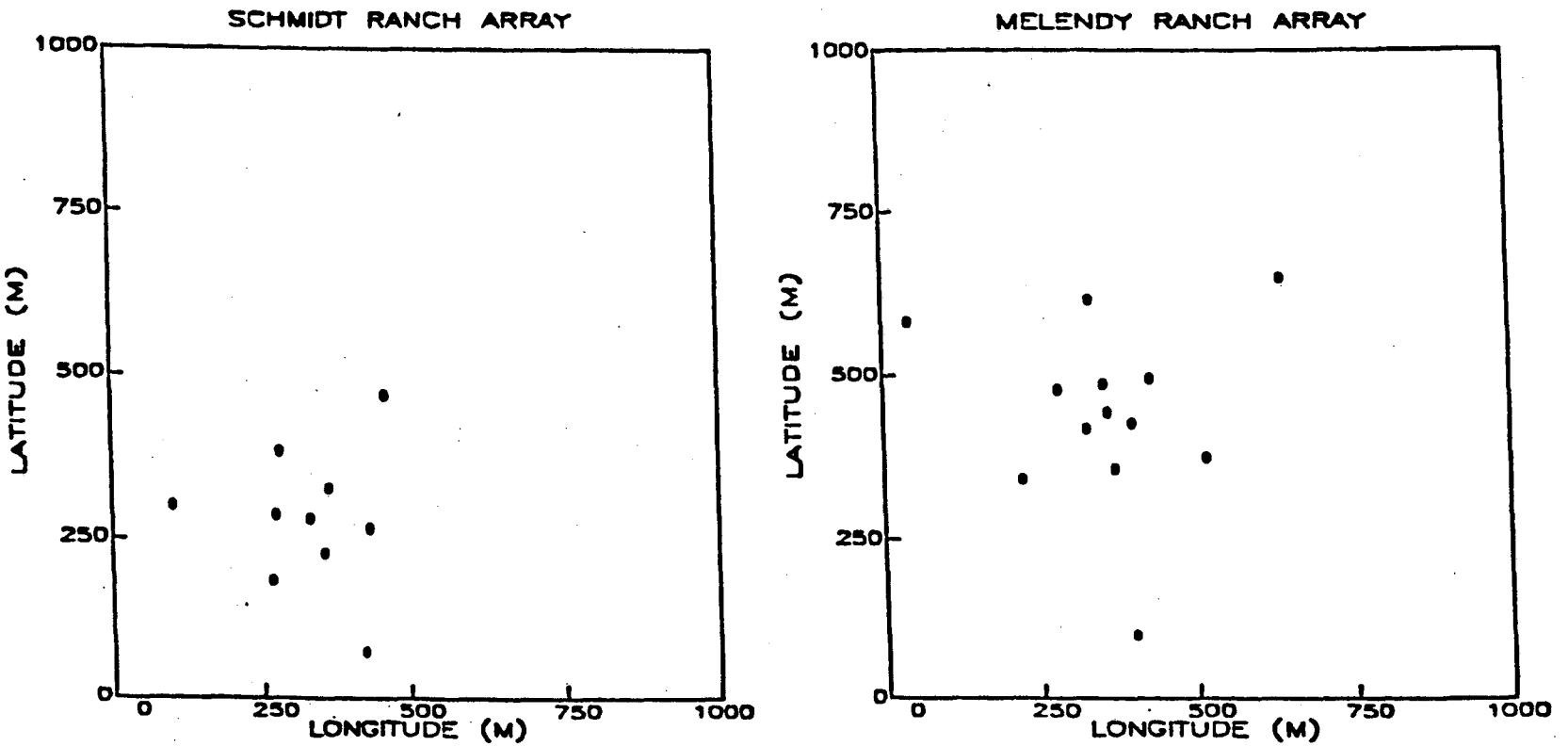

Figure (3-2) Array geometries for the 'Schmidt' microearthquake array on the western or Gabilan side of the San Andreas fault (left) and the 'Melendy' array on the eastern or Franciscan side of the fault (right). The actual locations of the arrays are shown in map view in Figure (3-3).

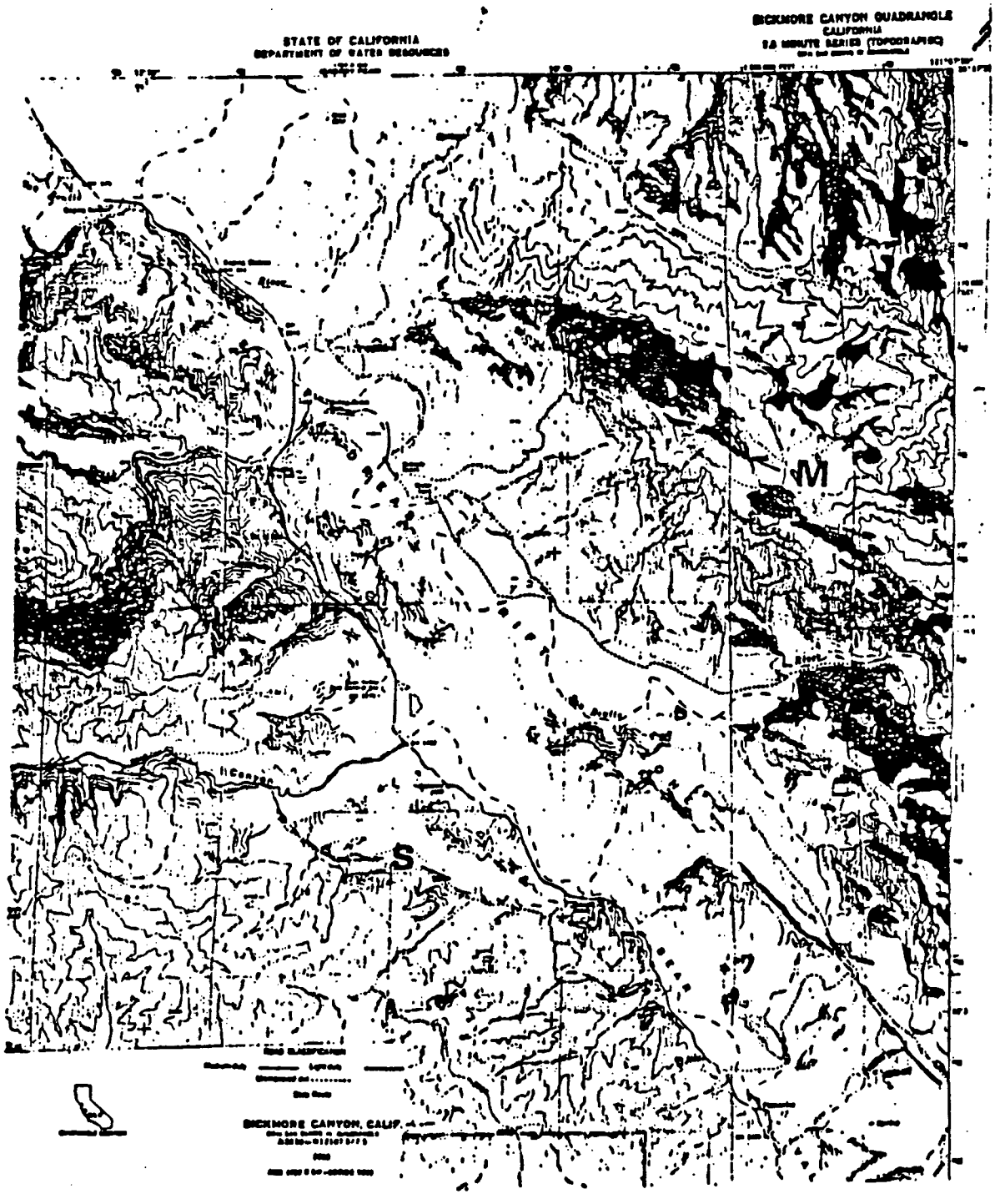

Figure (3-3) 7.5 minute topographic map of the Bear Valley/Bickmore Canyon region of the San Andreas fault in San Benito County showing locations of the temporary arrays of Figure (3-2) deployed for microearthquake study. The Schmidt array in the granitic western side of the fault is denoted by 'S' and is situated directly within the western portion of the reflection profile; the Melendy array to the east is denoted by 'M' and is somewhat to the north of the eastern extension of the reflection line. (Compare with Figure 3-1).

in frequency content between the two records; this is probably due to differences in the attenuation characteristics of the different bounding crusts and is similar to the robust spectral contrast noted across the CDP stacked section of the aforementioned reflection data, (see Figure (3-6)).

The microearthquake data were analyzed primarily to enhance our understanding of the attenuation characteristics in the region. In general the data provided a reasonable check on those attenuation results obtained from the reflection data, especially in the use of shear wave coda to complement the P-coda investigation of the CDP data. Unfortunately the quality of the microearthquake data was not amenable to such a detailed study for a variety of reasons (e.g. short records precluded coda decay analyses, clipping of records made accurate determination of amplitude changes difficult in the early part of the coda, persistent noise problems plagued several stations, and in some cases spurious glitches appeared that proved difficult to remove). In addition certain wave-propagation characteristics serve to contaminate the coda decay in terms of the utilization of this technique for the determination of attenuation parameters; these characteristics generally involve the presence of coherent energy within the assumed random incoherent scattered arrivals comprising the coda. This will be discussed later in detail as it constitutes a serious limitation in the application of this method of attenuation analysis to earthquake data.

Given the data available within the level of contamination described above, only four recordings were chosen for the coda decay analysis. The four seismograms consisted of two from each array (i.e. from each side of the San Andreas fault). For the Franciscan or Melendy array, two events produced two separate seismograms from neighboring stations which were analyzed for the decay factors; however for the Gabilan or Schmidt array two recordings of one event were used. Figures (3-7) and (3-8) show the three-component seismograms of the Melendy array from which one horizontal recording (e.g. middle seismogram) was chosen for analysis.

The USGS hypocentral parameters for these events, on 16 and 17 September, 1982 respectively, are listed in each figure caption in addition to the approximate source-receiver distances. Similarly, Figures (3-9) and (3-10) show the two sets of seismograms from the Schmidt array along

with their hypocentral parameters. Although preliminary analyses of the P-coda were carried out, the coda appear to be too short in duration to provide useful information; furthermore there are indications that these P-coda may be excessively contaminated with (converted) shear energy in the form of sharp coherent arrivals preceding the primary S-wave arrival.

Whereas the reflection data were analyzed in terms of both velocity and attenuation, the microearthquake seismograms were used only in the attenuation study; the attenuation results using the exclusively P-wave CDP seismograms were complemented by corresponding analyses of the S-wave coda decay on the microearthquake seismograms.

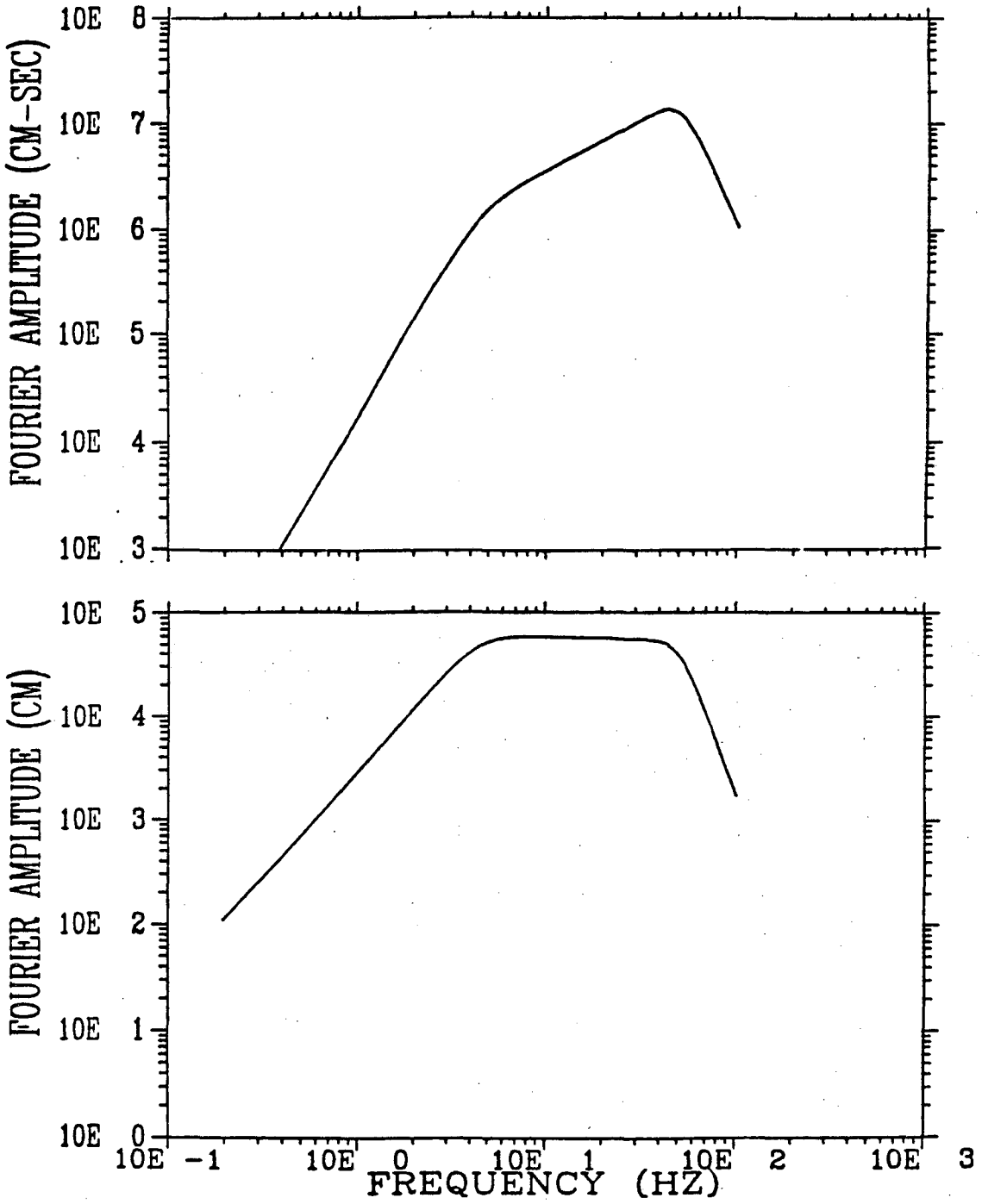

Figure (3-4) Instrument response curves for three-component seismometers used in microearthquake study; included is the 50 Hz anti-alias filter for a sampling rate of 200 samples per second. The top figure shows the response for displacement whereas that for velocity is shown at bottom.

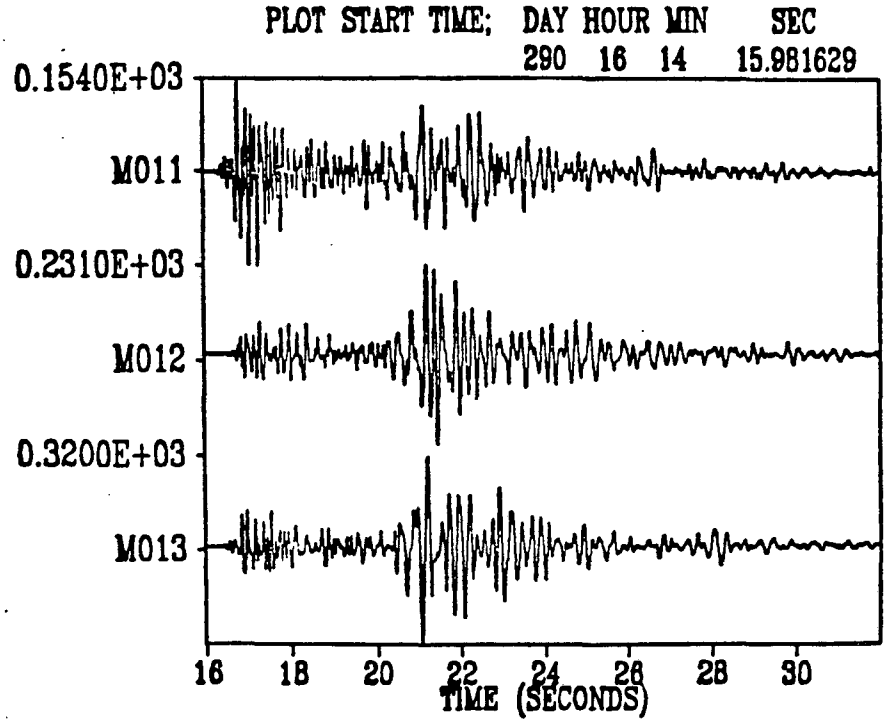

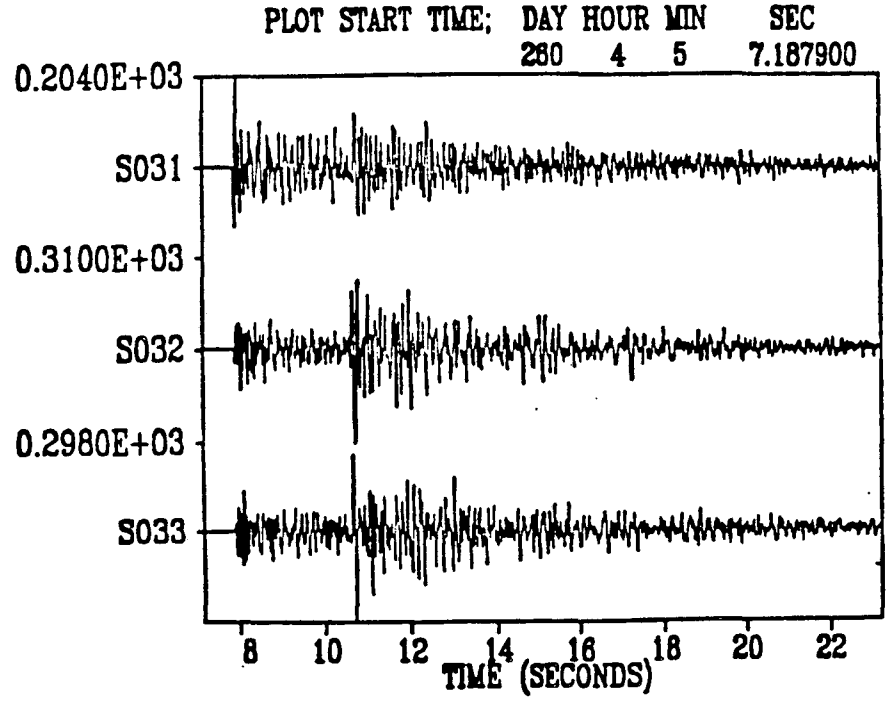

Figure (3-5 (Top) A typical three-component record for an earthquake recorded at the Melendy array on 10/17/82, at a source-receiver distance of 15.4 km; USGS hypocentral parameters: OT=161412.44, at 36°38.37′ N, 121°18.24′ W; depth = 5.8 km; M_L = 1.9. (Bottom) A typical three-component record for an earthquake recorded at the Schmidt array on 09/17/82, at a source-receiver distance of 6.6 km; USGS hypocentral parameters: OT=040503.84; at 36°39.88′ N, 121°20.49′ W; depth = 1.5 km; M_L = 2.0.

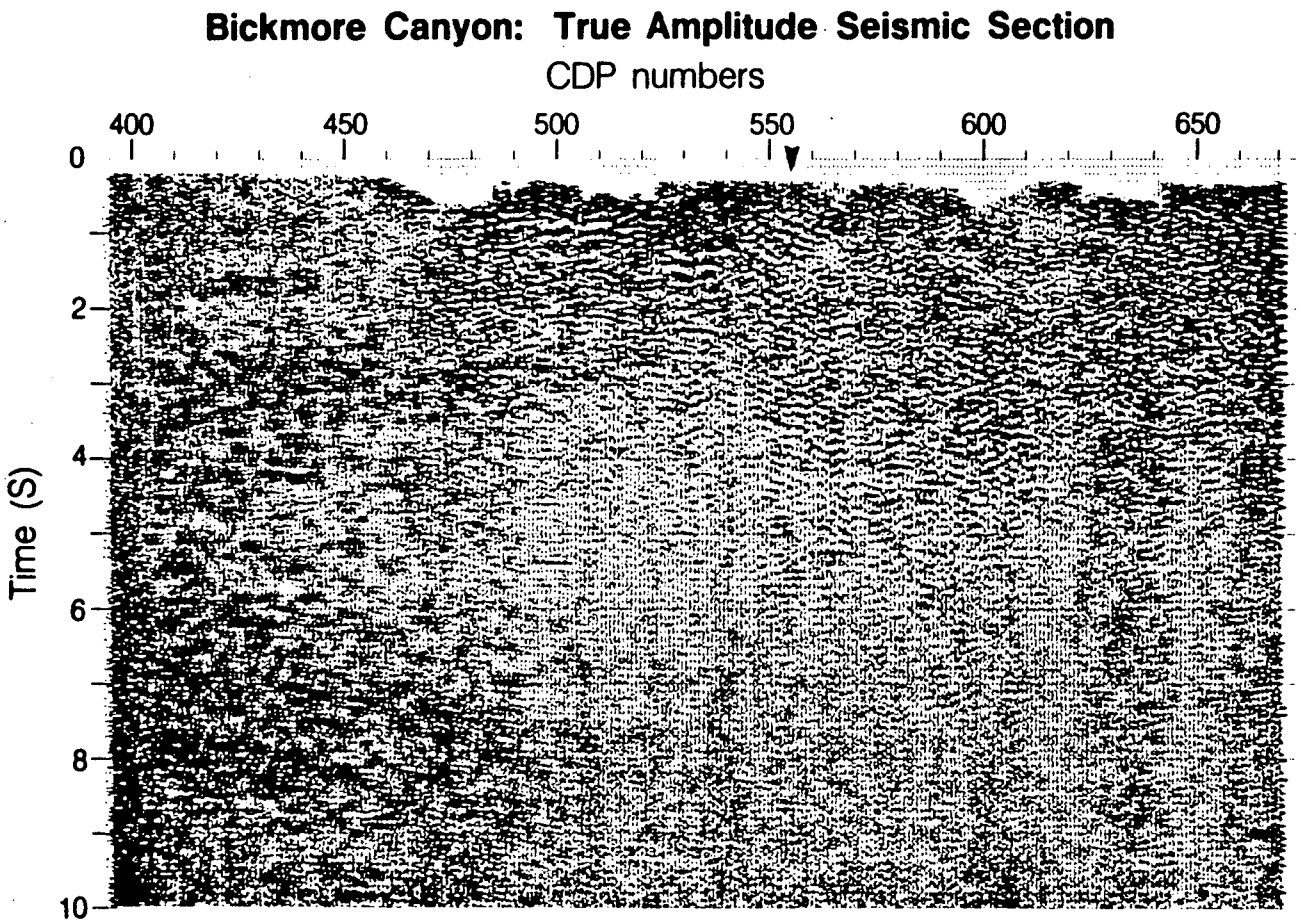

Figure (3-6) True amplitude stacked reflection section of the 1978 CGG data, processed using DISCO seismic data analysis package. San Andreas fault is depicted by arrow at top near CDP 550. Two-way reflection time is in seconds. Note the contrast in spatially coherent reflectivity between the Gabilan granitic part of the section to the west (left) and that of the Franciscan melange to the east; of specific interest are the mid-crustal structural features at about 3 seconds and the laminated (Moho?) structure at about 6 - 8 seconds within the western crust.

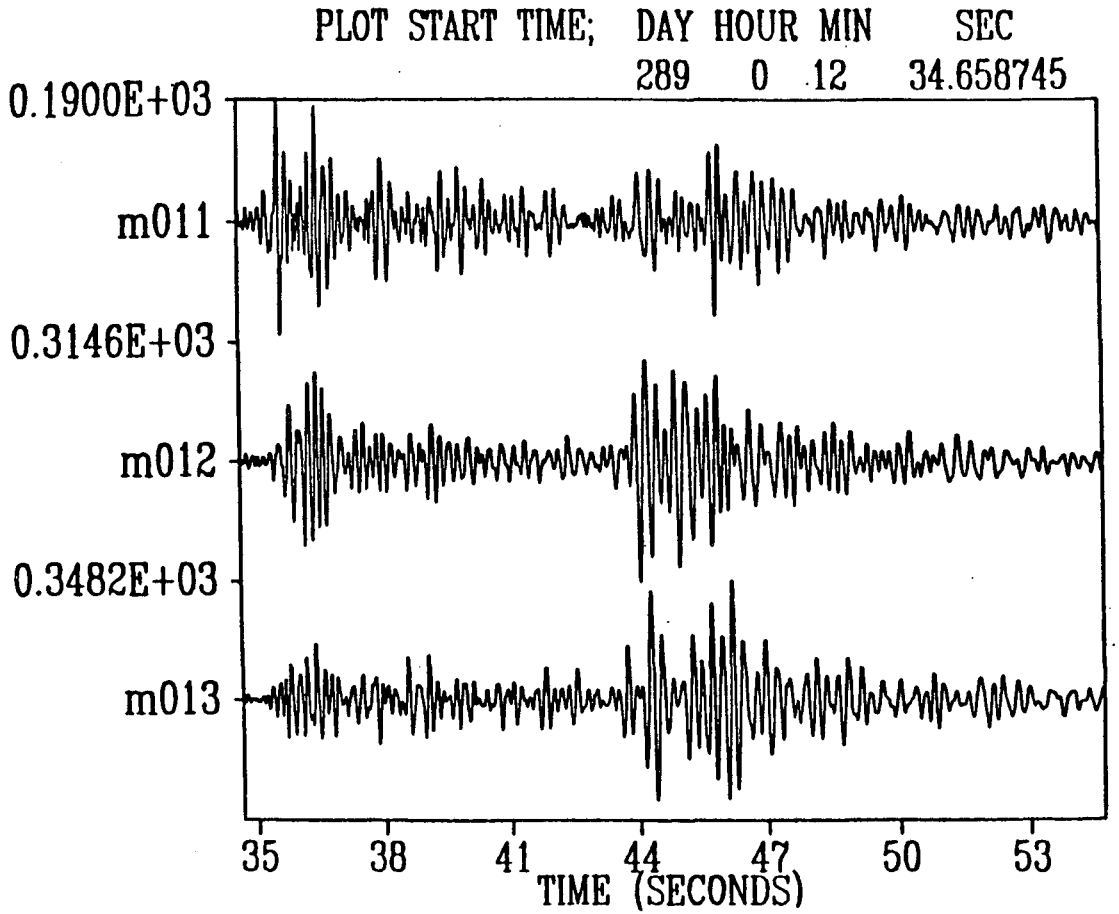

Figure (3-7) Three-component seismograms from the Melendy array for an earthquake recorded on 10/16/82 at an approximate source-receiver distance of 47.6 km and used in subsequent attenuation study. USGS hypocentral parameters for this event: OT=001225.17, at 36°49.54′ N, 121°35.35′ W; depth = 6.5 km; M_L = 2.6.

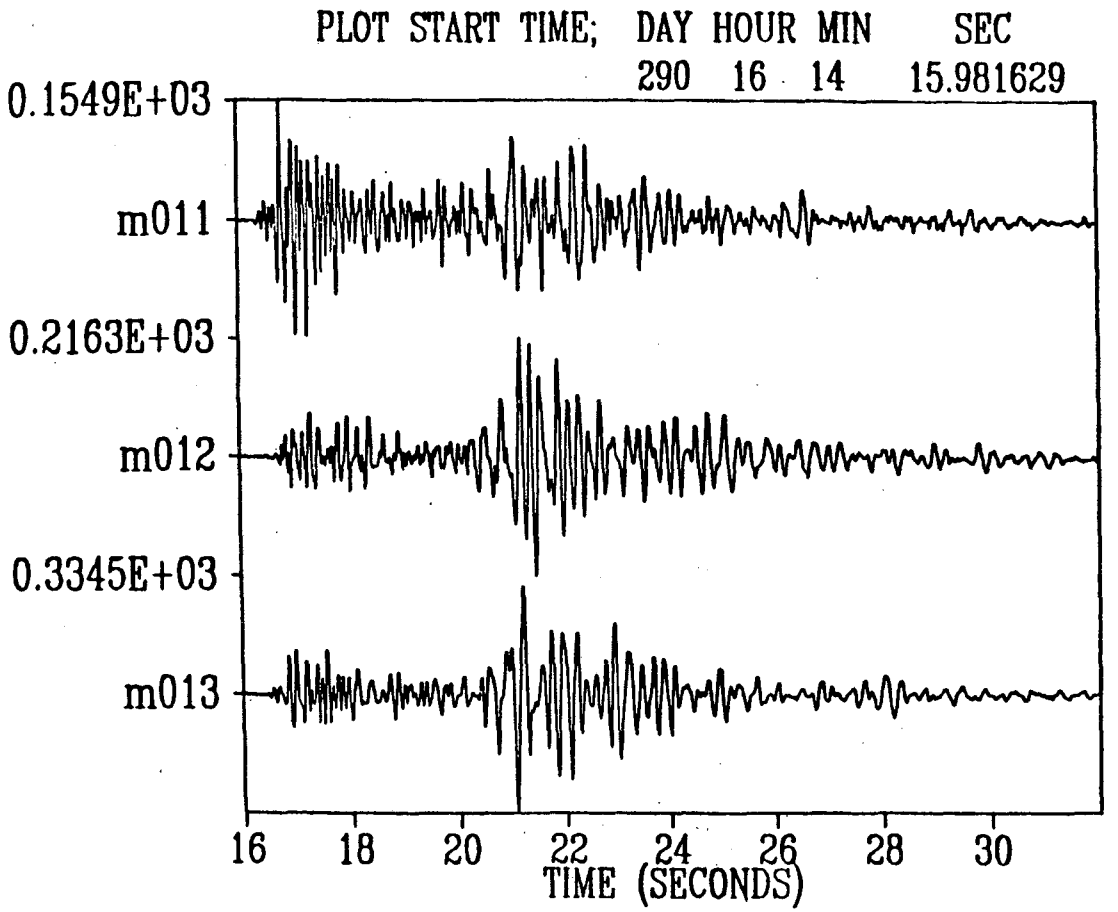

Figure (3-8) Three-component seismograms from the Melendy array for an earthquake recorded on 10/17/82 at an approximate source-receiver distance of 15.4 km and used in subsequent attenuation study. USGS hypocentral parameters for this event: OT=161412.44, at 36°38.37′ N, 121°18.24′ W; depth = 5.8 km; M_L = 1.9.

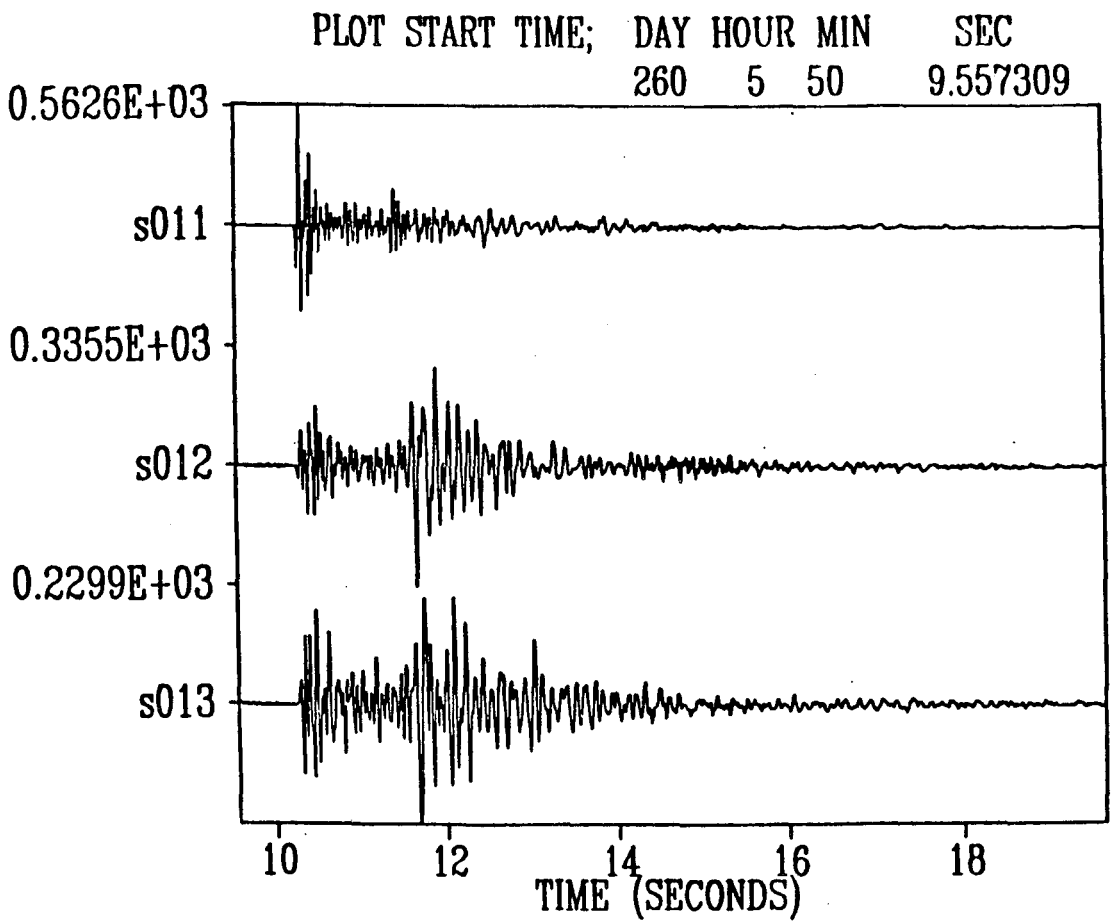

Figure (3-9) Three-component seismograms from the Schmidt array for an earthquake recorded on 09/17/82 and used in subsequent attenuation study. USGS hypocentral parameters for this event: OT=055008.46, at 36°35.53′ N, 121°13.85′ W; depth = 4.5 km; M_L = 1.2.

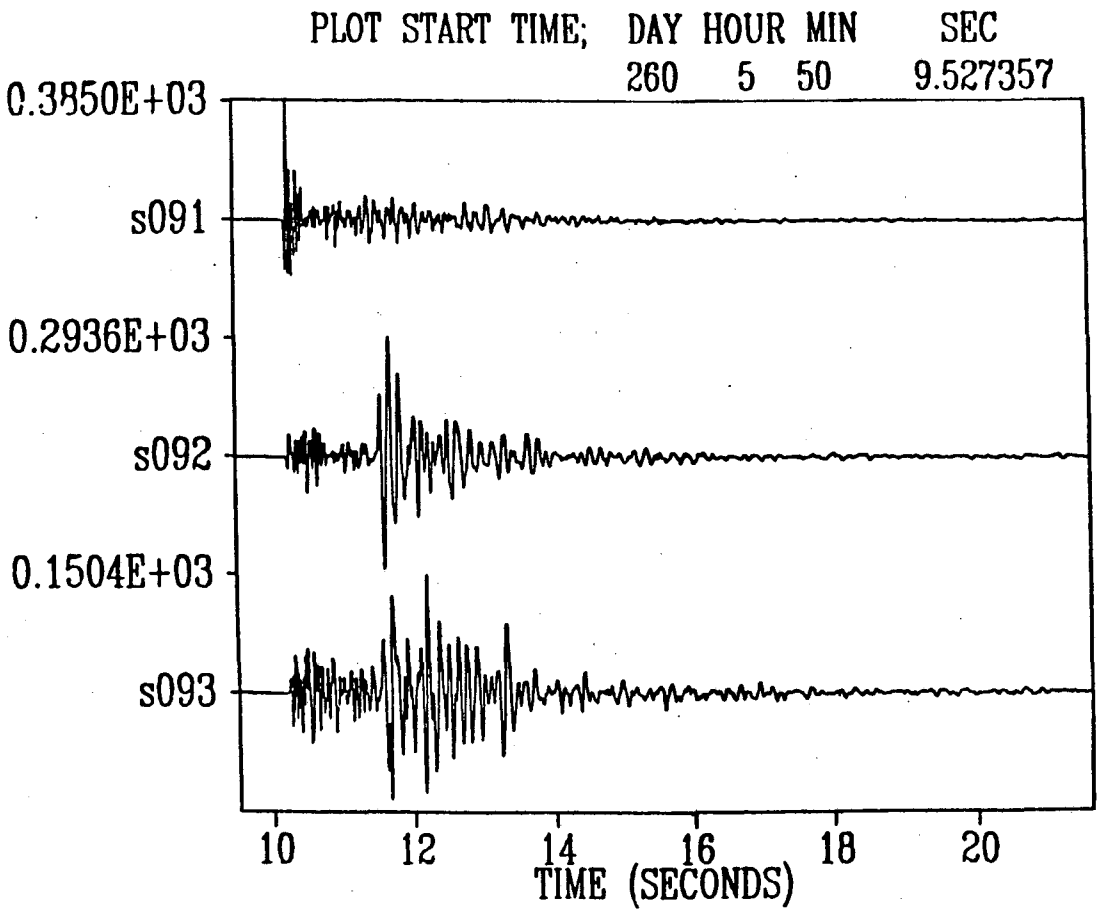

Figure (3-10) Three-component seismograms from the Schmidt array for an earthquake recorded on 09/17/82 and used in subsequent attenuation study. USGS hypocentral parameters for this event are the same as those for Figure (3-9); the station is about 265 meters from that of the previous figure.

3.3 VELOCITY ANALYSIS & STRUCTURAL INTERPRETATION

The marked contrast in reflectivity and frequency content of returned energy between the Franciscan (eastern) crustal melange and the granitic (western) crust, revealed in the true amplitude section of the 1978 data, (see Figure (3-6)), is a manifestation of fundamental differences in material properties. This data set has been studied extensively utilizing a wide range of conventional and unconventional methods. The modeling in this study has been aimed at refining our knowledge of the velocity and attenuation ("Q") characteristics of the fault zone and the structure of the crust on either side. As is clearly indicated in Figure (3-6) there are several intriguing structural trends that warrant attention in a detailed study of the San Andreas fault zone. Besides the contrast in reflectivity between the bounding crustal blocks, there are at least three major structural features of interest that are manifested in the true-amplitude stacked section, (Figures 3-6 or 3-16 to 3-19): One of the more striking features is seen in the shallow structure at about 3 seconds time on the western side of the section(s). Lynn et al. (1981) have studied this section independently and in comparison with other deep seismic sections and suggest that this represents the basal contact of the granitic batholith. The subhorizontal aspect of these reflections indicates a tabular shaped batholith. Walter and Mooney (1982) suggest that the Gabilan crust can be characterized by a granitic upper crust to a depth of 9 ± 1 km overlying gneissic material below. The transition to such a gneissic material may be complex, as these banded and tapered reflections suggest. Alternatively, the model of Wentworth et al. (1984) and Zoback and Wentworth (1986) regarding crustal structure along the boundary of the Franciscan and Great Valley Sequence east of the San Andreas fault may offer a different interpretation. In their model, a tectonic wedging process is hypothesized in which an allochthonous Franciscan terrane underthrust the Great Valley Sequence over virtually the entire western margin of California during the Mesozoic era. Because this tectonic wedging process is expected to have been contemporaneous with the formation of the Salinian Block at the southern part of the Sierran-

Penninsular axis, the existence of Franciscan material within or beneath the granitic upper crust may be especially plausible. The model depends on the interpretation of a series of seismic reflection profiles as well as that of an aeromagnetic survey (Griscom, 1982; 1983). The presence of Franciscan beneath the Gabilans has been suggested in a previous study of two seismic refraction profiles in this region by Stewart (1968), who proposed that the granitic Gabilan block may be structurally underlain by lower velocity Franciscan formation; his suggestion was based on an observed amplitude attenuation of a refracted P-wave phase as a function of distance in the range 40 to 75 km wholly within the Gabilan Range. The depth of this proposed transition was given as roughly 10 km, consistent with the aforementioned feature at about 3 seconds on the stacked reflection data. Lynn et al. (1981) considered several models to explain these features; the general process of accumulation of granitic magma above higher density basaltic magma was not favored due to the appreciable thickness of the reflection zone. Instead, a model describing a reaction melting process with the resultant formation of sub-batholithic cumulates was proposed. Although Franciscan rocks are not present in surface exposures of the Gabilan crust, it is still an open question as to its composition at depth, which has critical bearing on the presumed large-scale lateral motion of the Salinian block (see Chapter 2, above). Walter and Mooney (1982) have suggested that if this gneissic material in the lower Gabilan crust is the same rocks found at the surface west of the fault then the proposed block motion has taken place at or below the crust-mantle boundary as opposed to motion along a mid-crustal slip plane. The model of Lynn et al. (1981) does not preclude this hypothesis although it is important to note that it does not rule out the possibility that these shallow reflectors represent regularly bedded sediments and metasediments. However the presence of highly deformed and/or poorly stratified (Franciscan melange) pre-batholithic rocks in the region tends to weaken the hypothesis that the lower Gabilan crust must be of a granitic origin while lending credence to Stewart's suggestion. The model of Wentworth et al. (1984) and Zoback and Wentworth (1986) would seem to provide a mechanism to support the suggestion of Stewart (1968). The existence of a low velocity wedge extending westward from the fault zone at these mid-crustal depths as

proposed by Feng and McEvilly (1983) and later by the gravity modeling of Wang et al. (1986) may provide an additional constraint on the constitution of the lower Gabilan crust. However it may well be that velocity information derived from both refraction and reflection studies is not adequate to resolve the dilemma. The adopted velocity model of Walter and Mooney (1982) shows a somewhat higher average velocity (e.g. 6.9 km/sec) for the lower Diablo crust ($16 < z < 30$ km) than for that of the Gabilan crust (6.5 km/sec; $10 < z < 24$ km) west of the fault. Compositional arguments that have been offerred to explain the seismic data generally reguire a mafic crystalline material, notably of a gneissic or gabbroic composition. At the pressures and temperatures expected in the lower crust the velocities of gneissic and gabbroic materials may be quite similar (Stewart and Peselnick, 1977, 1978; Lin and Wang, 1980). Lin and Wang (1980) have shown that for certain compositions containing gneissic material there may be a tendency for a negative velocity-pressure gradient. Hence since no such negative velocity-depth gradient has been noted in the seismological literature for these shallow crustal depths Walter and Mooney (1982) have concluded that a probable composition for the lower Diablo crust would consist of a gabbro and amphibolite mixture without any gneiss or norite.

Another structural feature manifested in the processed sections of the Bickmore data is the apparent dip of the Moho on the granitic side (near 7-8 seconds). This apparent dip has far reaching consequences regarding the coupling of the crusts and the depth extent of the San Andreas fault. Feng and McEvilly (1983) have suggested that this feature is indicative of a general crustal thickening in the east-southeastward direction, although they acknowledge that a primary cause for this feature is probably a sort of push-down effect due to the presence of a low-velocity wedge extending westward from the San Andreas fault near 3 seconds. Such a wedge was inferred from an analysis of the 1974 reflection data; it was subsequently incorporated into the starting model for the velocity inversion of the 1978 Bickmore Canyon data and tended to remove some of the apparent dip. However this dip may be indicative of a more complex process related to shearing of the shallow formations (McEvilly, 1979). The shearing is expected to be more intense near the fault zone. Thus, due to the lower velocities associated

with this zone, there may be an appearance, in the time domain, of a deepening of the "Moho event" toward the fault. In such a model one would expect that the Moho reflection within the Diablo crust, if observed, would show a similar thickening (westward) toward the fault if a similar process were occurring there. Absence of such an effect to the east, if corroborated, would argue for different mid-crustal conditions across the fault.

The third major structural feature that appears in these sections is the laminated nature of the reflection from the crust-mantle boundary. This laminated appearance of the Moho horizon has been noted in several other continental areas (Hale and Thompson, 1982) and has critical bearing on the crust-mantle transiton. Instead of a sharp compositional discontinuity, this contact may be more accurately modeled as a diffuse boundary; however, this interpretation of the Moho as a "transition zone" given a smooth change of pressure and/or temperature with depth would not favor rapid changes in the acoustic impedance. The lamination is observed over some 7 km thickness and is apparently independent of the rms velocity model used to stack the data; given this wide band of reflections, "peg-leg" multiples including reverberations at the source and receiver near surface layers are probably insufficient to explain fully the persistent laminated appearance. Changes of velocity and/or density over "layers" from 125 m to 0.5 km thick appear to be necessary to explain the observations at least partially. Furthermore this observation of a laminated Moho is not unique, as noted above. Such a stratified seismic structure has been observed in the Laramie Mountains of southeastern Wyoming from a COCORP reflection profile, in the Hardeman Basin in southeastern Oklahoma, (also COCORP data), in the southern Appalachians, (COCORP again), several CALCRUST lines in the Mojave-Sonoran region of southeastern California, and in a USGS reflection line offshore Charleston, South Carolina. Louie and Clayton (1985) have modeled the laminations in the CALCRUST lines as velocity steps, gradients, and as thin layers, concluding that the thin-layer model best fit the data. Hale and Thompson (1982) have suggested a number of geologic models to explain these observations including tectonic banding due to ductile flow and segregation, relatively undeformed metasediments, cumulate layering, and lenses of partial melt. Clearly any geologic model must

explain the seismic character of the Moho; in addition, a single model must be general enough to apply to the crust-mantle transition in widely divergent tectonic environments. In light of the observed structure of the Moho transition as manifest by its dip, lamination, and in some cases (e.g. Bickmore Canyon) by its apparently abrupt terminus at the fault zone, it may be necessary to model the boundary as a dynamic transition zone rather than as a static boundary.

Thus far, most investigations of the crust in this region of the San Andreas fault zone have concentrated on the refinement of velocity structure; this study attempts to extend the refining process using conventional and unconventional techniques as well as to incorporate a parameterization in terms of the attenuation and scattering characteristics of the medium. Velocity modeling has proceeded using conventional reflection processing methods. The DISCO software package includes the constant velocity analysis technique as well as more sophisticated and somewhat less subjective coherency techniques. These conventional reflection processing methods were useful in converging on a plausible velocity model for the study area; due to the inherent non-uniqueness of the process, the choice of final models was influenced by prior knowledge obtained from several previous studies. These include refraction surveys, Walter and Mooney (1982), reflection surveys, (McEvilly and Clymer, 1975), earthquake studies, (Eaton, et al., 1970; Boore and Hill, 1973; Aki and Lee, 1976; Engdahl and Lee, 1976; McNally and McEvilly, 1977;), and laboratory studies, (Wang, et al., 1978).

A sense of the difficulty can be realized by noting in the true-amplitude stack that, particularly in the eastern, Franciscan crust, coherent reflectivity is not prominent and certainly not as spatially coherent as in the western, granitic crust. All of the conventional seismic reflection velocity analysis techniques involve a search for maxima in spatial coherency upon application of some dynamic correction for moveout. Hence, in areas of high (intrinsic) attenuation, (low Q), or in regions where significant heterogeneity may lead to considerable wave scattering at the wavelengths of interest, rms velocity analyses may be quite difficult to apply in a meaningful fashion.

As can be seen in Figure (3-11) the 1978 CDP profile was a somewhat crooked line. This is due in part to the rugged topography and to land access problems (McEvilly, 1979). In order to account for this without any appreciable loss of accuracy or coverage, great care was required to redefine the CDP line through the "cloud" of scattered points. In Figure (3-11) we see the surface projections of the many subsurface midpoints. By specifying a rectangular collection space about each surface station within which subsurface midpoints can be collected, it was possible to obtain a reasonably straight CDP line with only a 25% loss in data redundancy. At a particular station the rectangle was defined as 220 feet in line by 660 feet perpendicular to the line; note that the receiver station spacing was 440 feet (see section 3.2.1, above). Of the 6672 traces recorded from 139 shots in the field, 4988 shot-receiver combinations (i.e. traces) were gathered by this method into common depth point gathers. Essentially the entire range of offsets was retained (e.g. up to 20,680 feet in some cases) although in a considerably less continuous manner. The resulting mean fold for the unedited data was therefore about eighteen.

Analysis of the data also required careful and extensive editing of noisy traces. In addition to all 48 traces of shot #7 which could not be demultiplexed, 1009 traces were zeroed due to persistent noise problems. Among other sources of noise, the most persistent problem was apparently introduced systematically at low signal levels by the field summing system (ADIT), (McEvilly, 1980). As most of these aspects of noise were within the frequency range of interest, simple bandpass filtering was an inadequate solution. Furthermore, the ambient ground noise and the source-generated signal, particularly west of the fault, was so low as to put the information into the lower significant bits, precisely where system noise was dominant. Hence, to improve the signal-to-noise ratio and to correct properly for the crookedness of the line some 41% of the raw data were omitted and thus not considered in many aspects of subsequent analysis.

Velocity studies generally were performed using both edited and relatively unedited data, however, the 1684 traces omitted in redefining the CDP line were not considered at all. For the attenuation studies, only the fully edited data were analyzed. While a considerable reduction in

coverage resulted from these corrections, the improvement in data quality was enough to provide substantial confidence in the results and conclusions. Furthermore, comparison of the velocity modeling results using both edited and unedited data revealed no significant differences.

Careful study of refractions led to a somewhat detailed subweathering velocity model, (Figure (3-12)), which was applied to the datum statics adjustment. The datum was chosen as 1000 feet above sea level. Note the consistency of this model with the surface geologic cross-sections of Wilson (1942) and Dibblee (1980) in Figures (2-6) and (2-5), respectively (both in Chapter 2). the low velocity trough is due essentially to fault bounded sediments and gouge. The statics obtained using this model were compared with the statics obtained using a homogeneous weathering velocity model. Statics in either case were of the order of tens of milliseconds and no significant differences in the character or continuity of spatially coherent reflectivity were noted between the two methods of near-surface correction. In addition, a mute schedule was computed based on this study of refractions and applied to the shot gathers to facilitate subsequent velocity analysis. Specifically, coherency analyses of the CDP gathers for velocity estimation are contaminated by refraction energy and thus it was necessary to mute these high amplitude first arrivals prior to velocity analysis.

As noted above, the lateral variations of material properties in this complex region complicated the velocity analysis. CDP gathers were corrected for moveout at various constant time-invariant velocities. Visual inspection of these panels for spatial coherency led to the best first guess of a velocity model. This constant velocity analysis (CVA) technique involves a certain degree of subjectivity. With some geophysical savvy and some knowledge of the geology of the study region, this subjectivity can be minimized as considerable confidence in the interpretation is achieved; despite its simplicity this CVA method has proven to be the most reliable technique for estimating optimum stacking velocities. As a check of the results several coherence estimating techniques were used to estimate velocities; in one such method, coherence over user-specified gates was computed for a range of times and rms velocities, (see Figure (3-13)).

One must discriminate those 'desired' coherency peaks due to the moveout correction from those due to near surface effects and noise. This can be a somewhat subjective determination and requires experience not only with the reflection data processing procedure but also with the other geological and geophysical data available for the region. In this case, the velocity analyses were guided by a wealth of information on the lateral heterogeneity of the region from earthquake studies and geologic mapping as well as several tectonic models of the fault's bounding crustal blocks. As can be seen in the stacked sections, the signal-to-noise level is considerably better in the granitic or western side of the profile than in the eastern Franciscan side; this is in turn reflected in the coherence plots. Two representative plots of the coherence for a reasonably wide range of velocities at mid-crustal depths are shown in Figure (3-13). This figure shows contours of coherence vs. rms velocity for the granitic and Franciscan crusts. Note how much more ambiguity is present in the Franciscan (lower) plot; it is not possible to draw any definitive pattern of stacking velocities from this plot for CDP 651 alone. It is difficult enough to discern a velocity function for the CDP gather for the granitic crust (upper plot). The high velocity contours are probably due to noise contamination, although the large amplitudes in the plot for CDP 651 are puzzling.

Once some idea of the velocity structure is obtained, one may use more advanced techniques offered by DISCO to refine the model. One of those attempted, a layer stripping method, involves a slanted plane wave stack of the data over a range of ray parameters based on a range of appropriate interval velocities. After such a slant stack, each trace of a CDP ensemble will contain arrivals of a single ray parameter. A contoured coherence display of interval velocity versus time is produced based on an analysis of three types of arrivals possible for the ray parameter range input: subcritical reflections, supercritical reflections and critical refractions. By using all three available arrivals, (Schultz, 1982) has shown that the velocities determined are more accurate than interval velocities obtained by reducing rms velocities with the Dix formula. Based on such a coherence display, the interval velocities are picked and the respective layer is stripped off; subsequent layers are examined in a similar manner as the time and ray

parameter range is adjusted. An example of an intermediate step is shown in Figure (3-14) for a CDP gather in the Gabilan granite west of the fault. The contours at the left of the plot are not well understood and are neglected in the determination of velocity for this range of reflection times at this CDP location, (i.e. 423). A sample resultant model is shown in Figure (3-15) along with the appropriate time-depth function.

Multiple reflections proved not to be a problem for these data, perhaps because of the lateral heterogeneity and significant departure from planar subsurface topography. A predictive deconvolution procedure was undertaken and applied to the stacked data; Figure (3-16) shows the resulting section. It is quite similar to the section (Figure (3-6)) which had no such deconvolution. Note the histogram of multiplicity or fold at the bottom of the section; the irregularity of the coverage is due to the crookedness of the line as well as the extensive editing.

In areas of such complex laterally varying structure it is important to perform a pre-stack migration of the reflection data. This is generally a difficult computational task; current algorithms require constant geometries for all CDP gathers which is effectively precluded by varying patterns in source-receiver geometry along the line. The irregularity of shooting patterns in these data resulted from an attempt to compensate, with respect to subsurface midpoints, for the crooked nature of the profile line as well as for gaps in the data caused by land access problems, (see section 3.2.1, above). The crookedness of the line and attendant non-uniform shooting patterns combined to thwart an effective pre-stack migration since most migration algorithms require a uniformity of source-receiver patterns. In many cases it is possible to re-define the profile line according to both a relatively straight-line configuration and a more uniform pattern of sources and receivers; a pre-stack migration of this approximation to the real line can then be performed and will, in most cases, represent a reasonable approximation to that of the actual profile. Attempts to re-define the shooting patterns for the 'Bickmore' line resulted in a profile that was not a reasonable approximation to the actual line. Nevertheless a post-stack migration using a finite difference approximation to the wave equation was applied with some interesting results, (Figure (3-17)). Because of low coverage at the ends of the line and the

resulting higher noise, this section was truncated prior to migration. This was done to prevent the propagation of noise along the diffraction curve; this phenomenon was somewhat more pronounced in the unedited data since the signal to noise ratio was lower than with the edited data. In general the "smiles" are still quite evident, though less so with this truncated version; they are also confined to a shallow region. By sampling more coarsely in the summation along the hyperbola one can minimize the "smiling" nature of the migrated section seen in Figure (3-17)). Figure (3-18) represents such a coarser migration; (in fact, the sampling is four times coarser.) Note the apparent upper mantle structure in these migrated sections, (Figures (3-17), (3-18)); these are examples of why sections which are not true-amplitude ought to be viewed with caution especially in areas of high noise levels.

In addition to migration, there are some powerful signal enhancement applications possible with the current level of sophistication in seismic reflection processing. Figure (3-19) is an example of an enhanced post-stack migration section. This particular enhancement technique allows one to reject or minimize the contribution from trace samples that do not exceed a certain cross-correlation or coherence threshold. One can specify the horizontal extent of "reflectors" allowed in the calculation as well as the range of dips to pass in the enhancement stage. Finally, one mixes the enhanced data with the processed but unenhanced data according to a reasonable weighting scheme. As these parameters are arbitrary (and perhaps capricious), one must be careful in the interpretation of such enhanced versions. There are, however, some intriguing features in Figure (3-19) that are not apparent in the other sections. In particular, one notices the arrivals, (Moho?) on the eastern end of the section at about 8.5 seconds; although the Moho reflection does not appear in the Franciscan crust in this survey, a previous survey wholly on the east side of the San Andreas fault, ("XT1", in the aforementioned 1974 survey—see McEvilly and Clymer, 1975), with 37-fold coverage did show a Moho reflection. It may just be that the multiplicity in the 1978 data is insufficient to bring it out, in which case the signal enhancement process could be a trustworthy aid. Of course the 1978 data was not from exactly the same location as that of the 1974 data and this may be sufficient to explain the discrepancy,

although this poses the problem of understanding the lateral continuity of the crust-mantle contact, in addition to the observed laminated character. Another feature indicated in Figure (3-19) that is not apparent in the previous unenhanced sections is the apparent upper mantle structure suggested by coherent reflectivity at times greater than 10 seconds; this may represent nothing more than an artifact of the signal enhancement process. Finally, it is important to keep in mind while examining these enhanced versions that noise may contaminate the interpretation depending on its location in time and space vis a vis the specific signal enhancement parameters input.

The tentative rms velocity model chosen is primarily based on the results of the constant velocity analysis although in areas of clear and spatially coherent reflectivity (e.g. western crust), the model was refined using one or more of the various coherency techniques discussed above. Figure (3-20) shows this model which was used to stack the data in Figures (3-6), and (3-16 to 3-19); an alternative view of this model is indicated in the velocity functions of Figure (3-21), (recall that CDP numbers increase eastward; the fault zone is centered at about CDP 555). Notice how this model is consistent with the trend of such modeling efforts as indicated in Figure (3-22) taken from Feng and McEvilly (1983), though perhaps not as refined or detailed. For example, the low velocity wedge that extends westward at seismogenic depths in their model is not resolvable in either the constant velocity analyses or in the various coherency studies. Nevertheless, the overall trend is reflected in both.

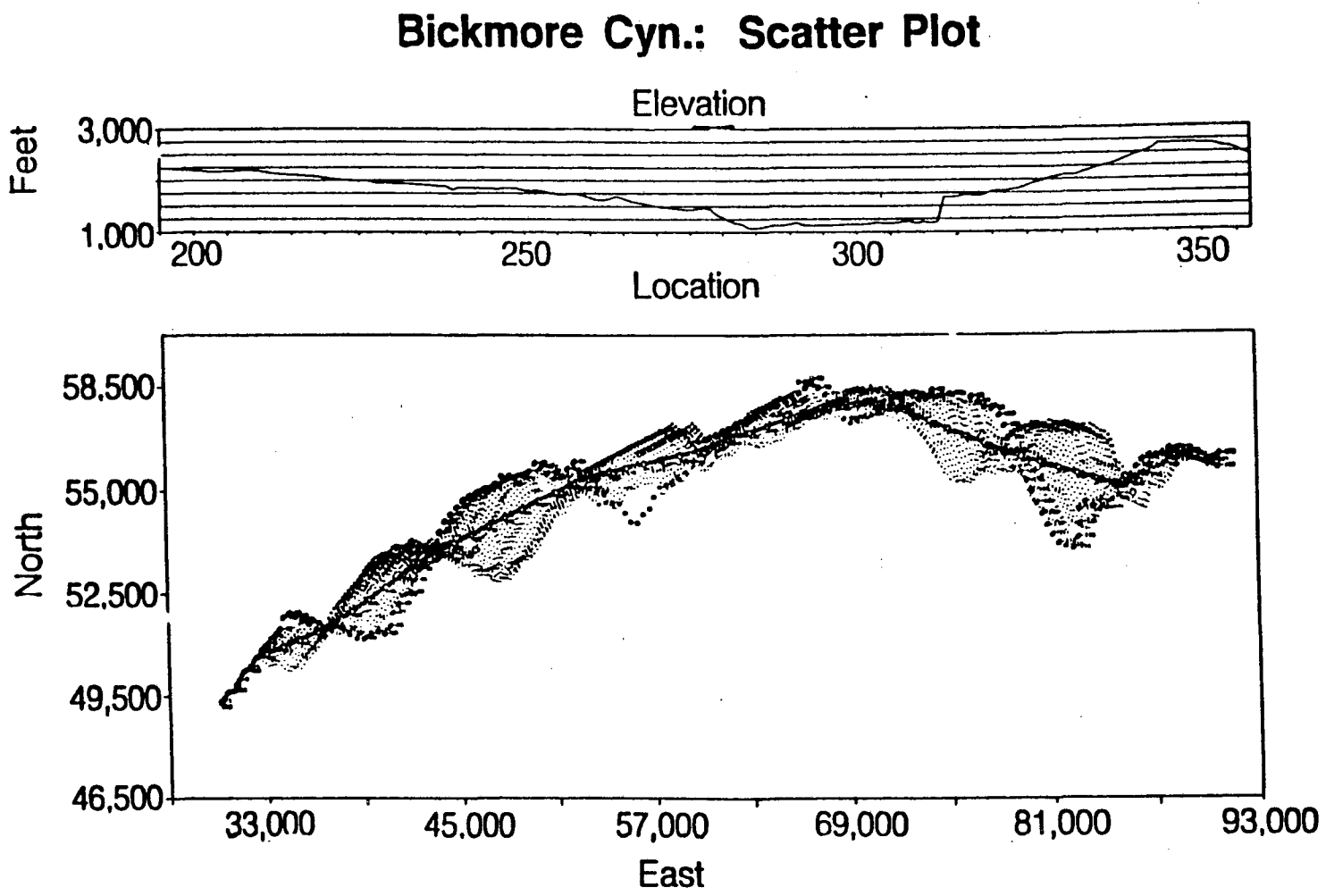

Figure (3-11) Scatter plot of 1978 reflection line in map view with elevations shown at top; units of distance in lower plot are feet in the east and north directions from an arbitrary origin. The cloud of points represent the projections of the subsurface midpoints for the surface source-receiver pairs. The line through this cloud is the approximated CDP line fit through the cloud and used as the representation of the profile line in further processing.

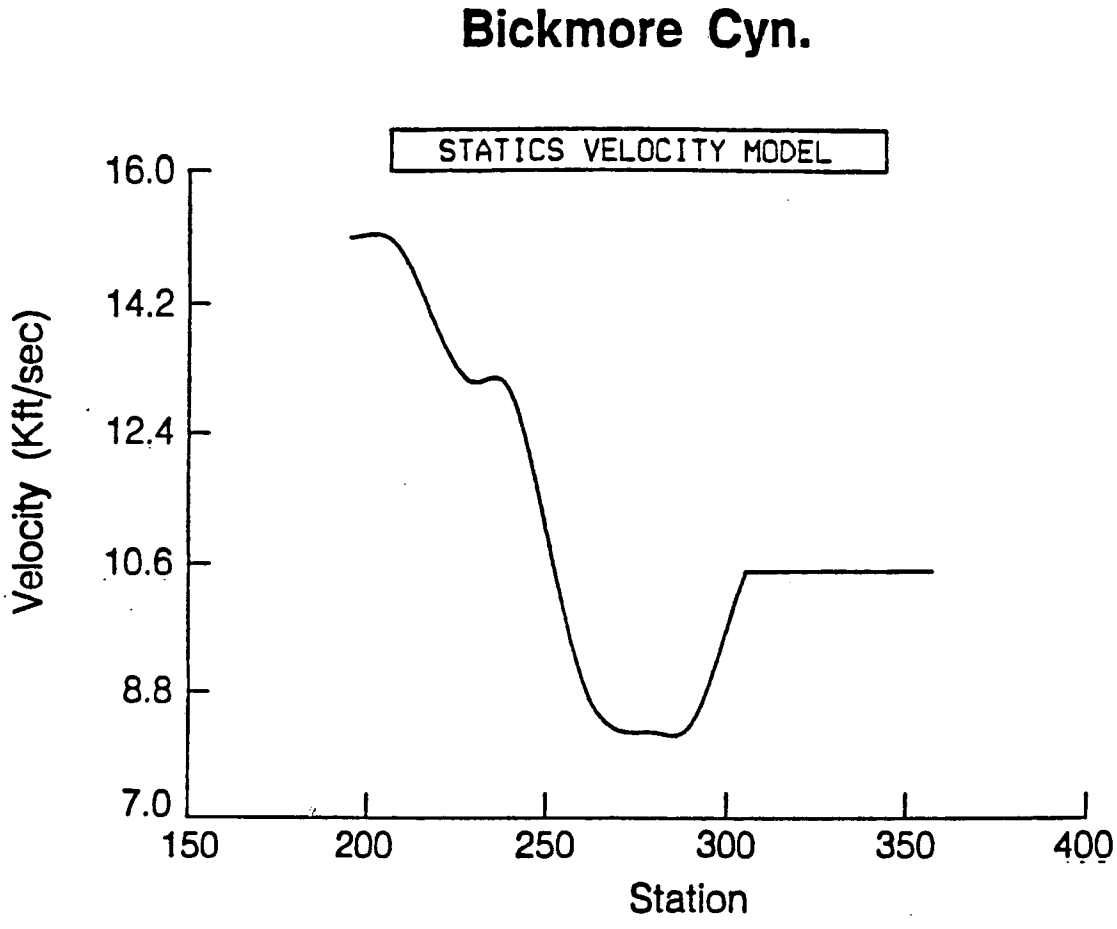

Figure (3-12) Velocity model used to perform statics correction to the data; station locations are in VP or vibrator point positions along the line (see Figure 3-1). The low velocity trough represents the sedimentary basin on the eastern margin of the Gabilan Range (i.e. against the San Andreas fault). The statics velocity model is taken from an analysis of the refractions in the reflection shot gathers.

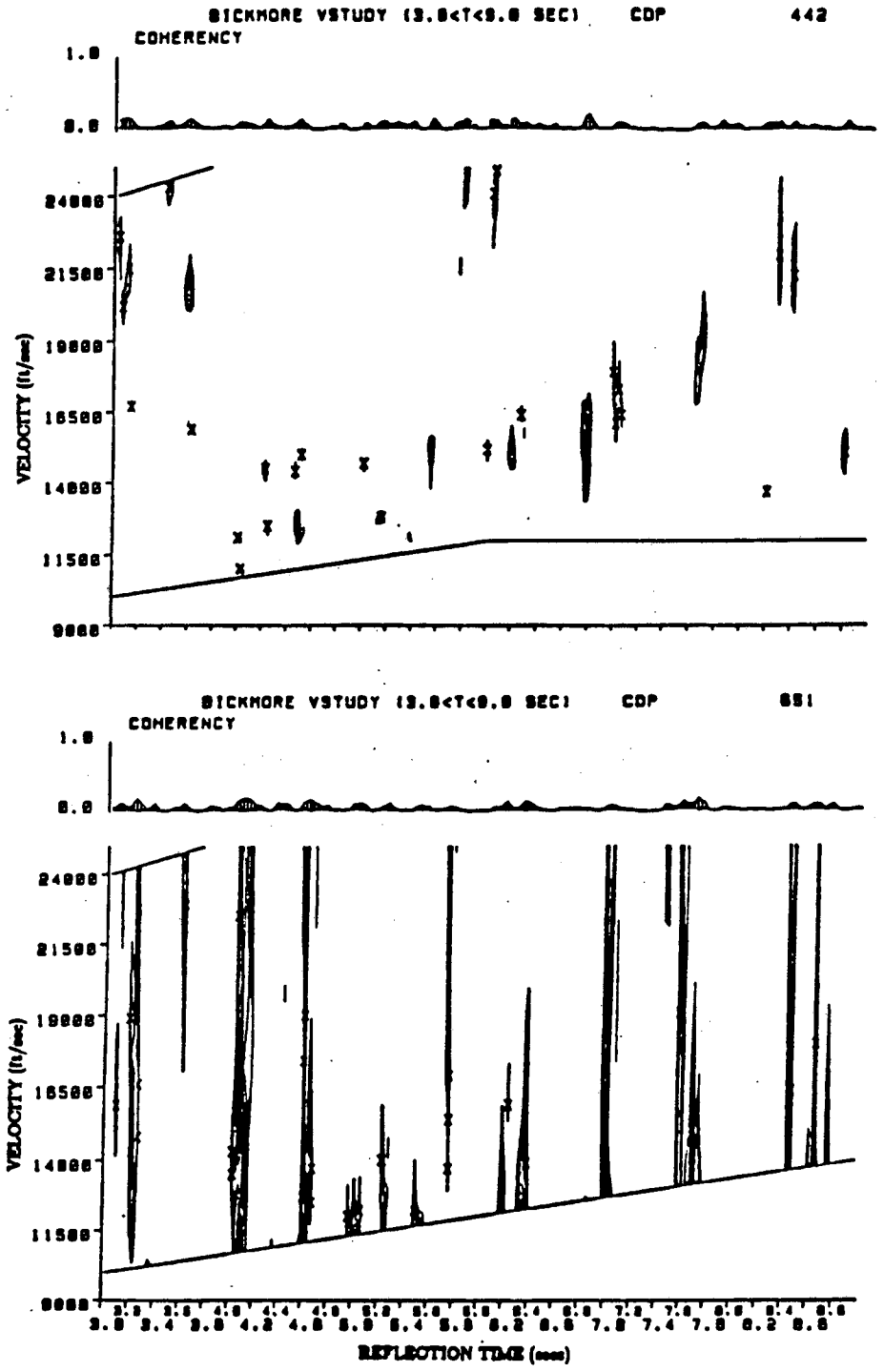

Figure (3-13) Coherency plots from CDP 442 in the Gabilan portion of the profile (top) and from CDP 651 in the Franciscan portion (bottom). Such contours represent the coherence across the traces of the CDP gather at each time over the range of velocities given and are used to find an optimum stacking velocity for a normal moveout correction (NMO) prior to stacking. The coherency contours are relatively straightforward for the Gabilan CDP, whereas for CDP 651 the contours of coherence are smeared across the range of velocities given; this is because there is significant lack of spatially coherent reflection energy return in this eastern part of the line.

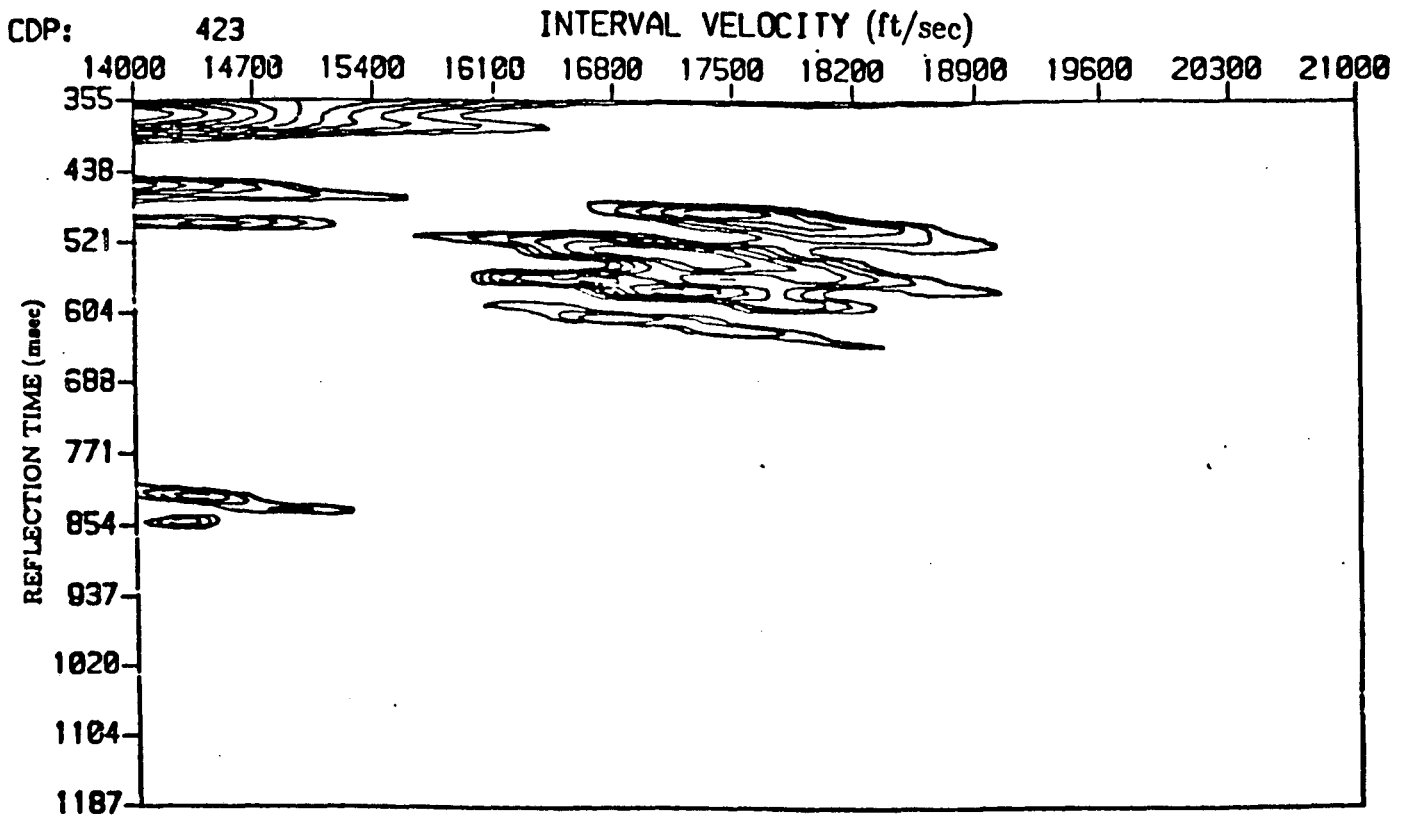

Figure (3-14) Coherency plot for interval velocities from CDP 423 in the Gabilan portion of the line. The method used to estimate coherence here is different from that used in the previous two figures; based on the analysis of Schultz (1982) and involving a slant stack of the traces in the gather, it includes the ray parameter inputs corresponding to subcritical reflections, supercritical reflections and critical refractions; this method is believed to be more accurate than the more common method of picking interval velocities using a transformation of the rms stacking velocities by the Dix equation.

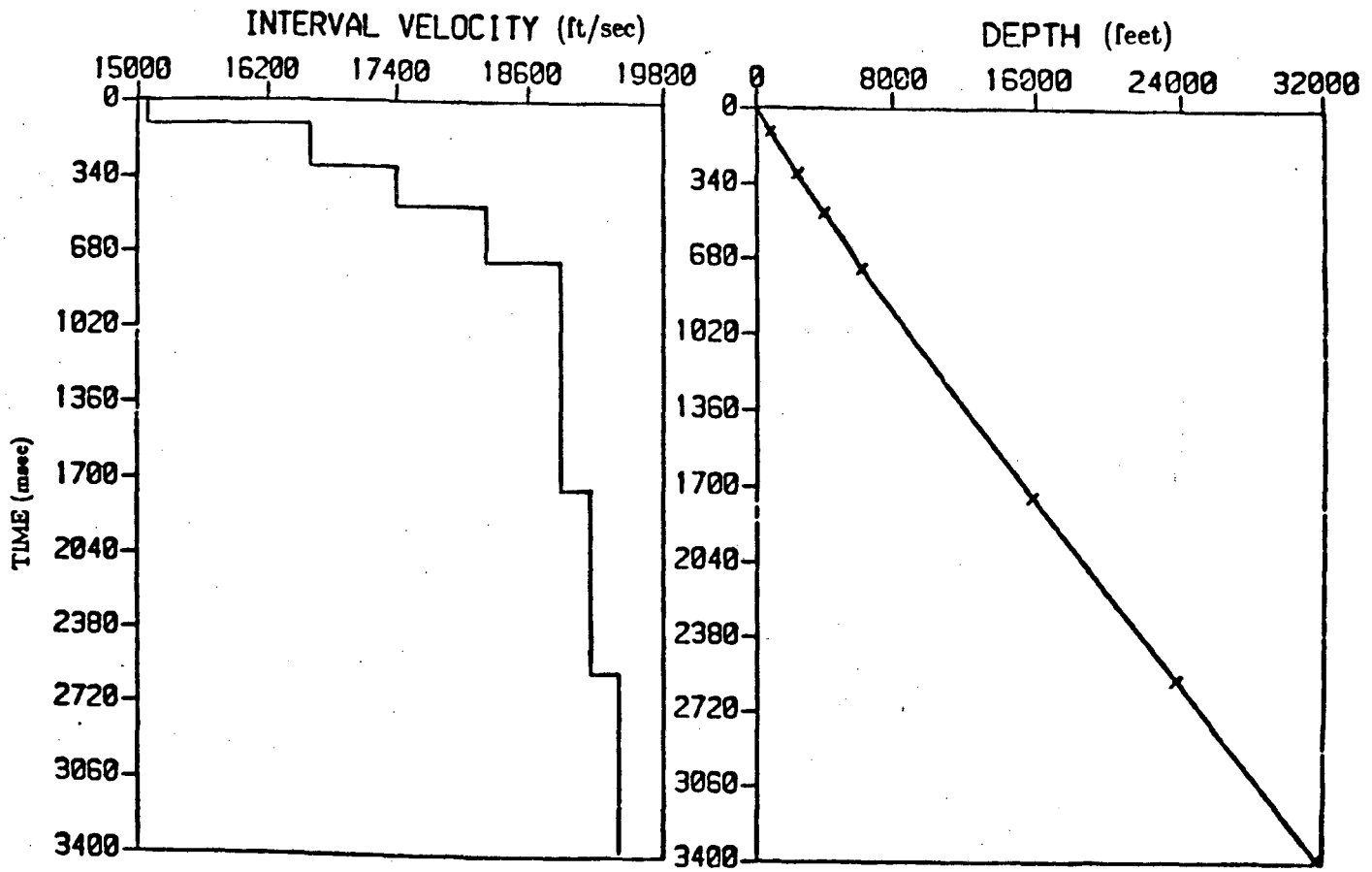

Figure (3-15) The resulting interval velocity model and corresponding time-depth function for the previous coherency plot.

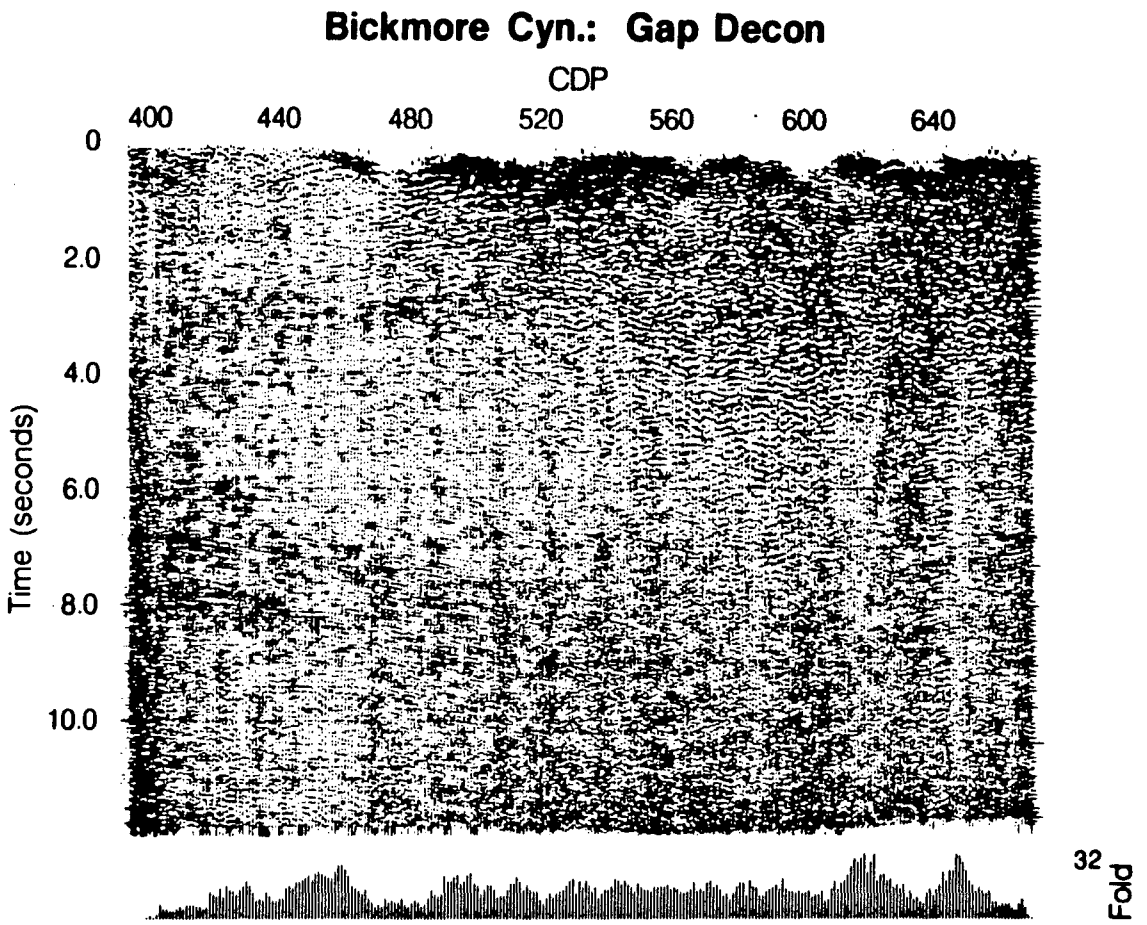

Figure (3-16) Same as Figure (3-6) but includes a predictive deconvolution step applied in an effort to mitigate the contributions from multiple reflections; As is noted by comparing the two figures, multiples were probably not a serious problem in the actual data, owing possibly to the rather severe departure from planar homogeneous structure that characterizes this crustal section. The histogram at the bottom represents the fold or multiplicity as a function of CDP position along the profile. The irregularity of the coverage is due both to the crookedness of the line (see Figure 3-11) and to the rather extensive editing of the data, as described in the text.

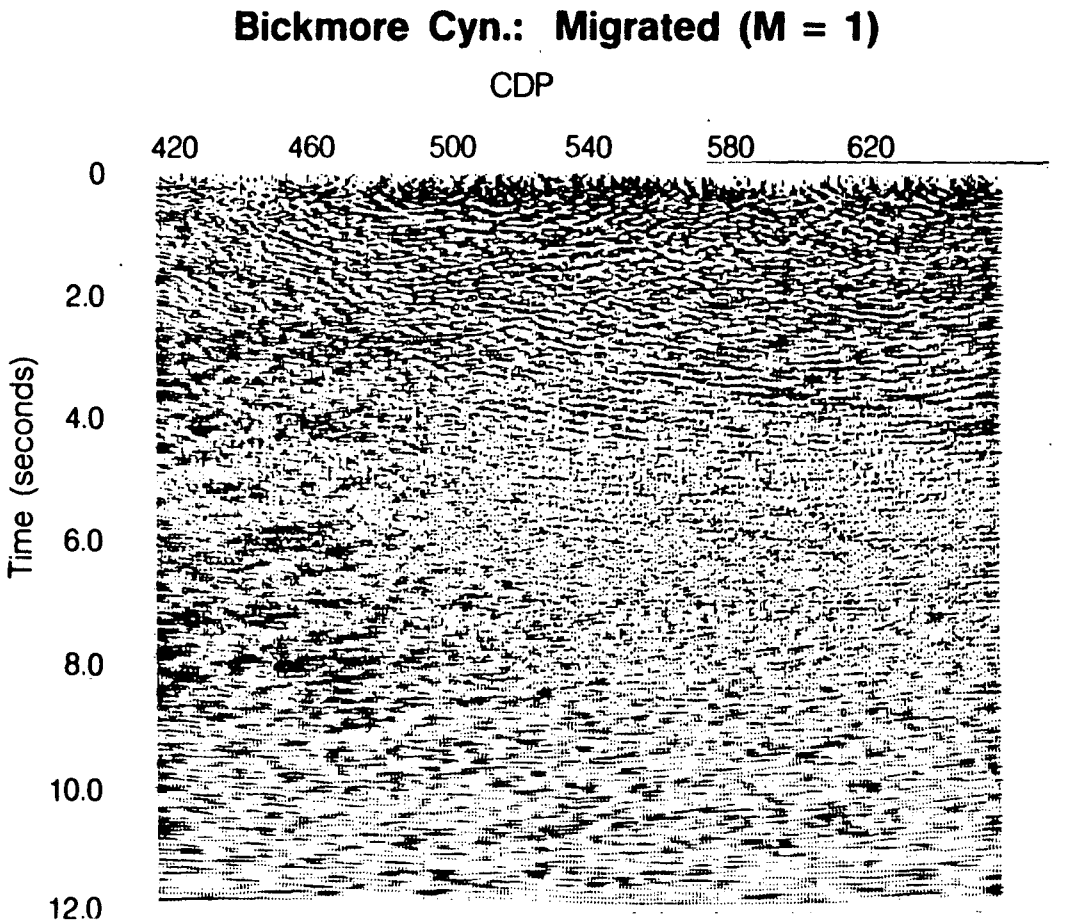

Figure (3-17) Migrated (post-stack) version of Figure (3-6). Certain features observed here are notable in their contrast to the unmigrated Figure (3-6): The 'smiles' evident throughout the shallow portion of the section are certainly not present in the unmigrated version and may be due, in part, to a somewhat slow velocity model for this shallow data. The apparent structure at about nine seconds in the eastern part of the section may be representative of the Moho contact that is not evident in the unmigrated section, however the presence of apparent (upper mantle?) structure at times greater than this throughout the lower portion of the stack may cast doubt as to the accuracy of this interpretation.

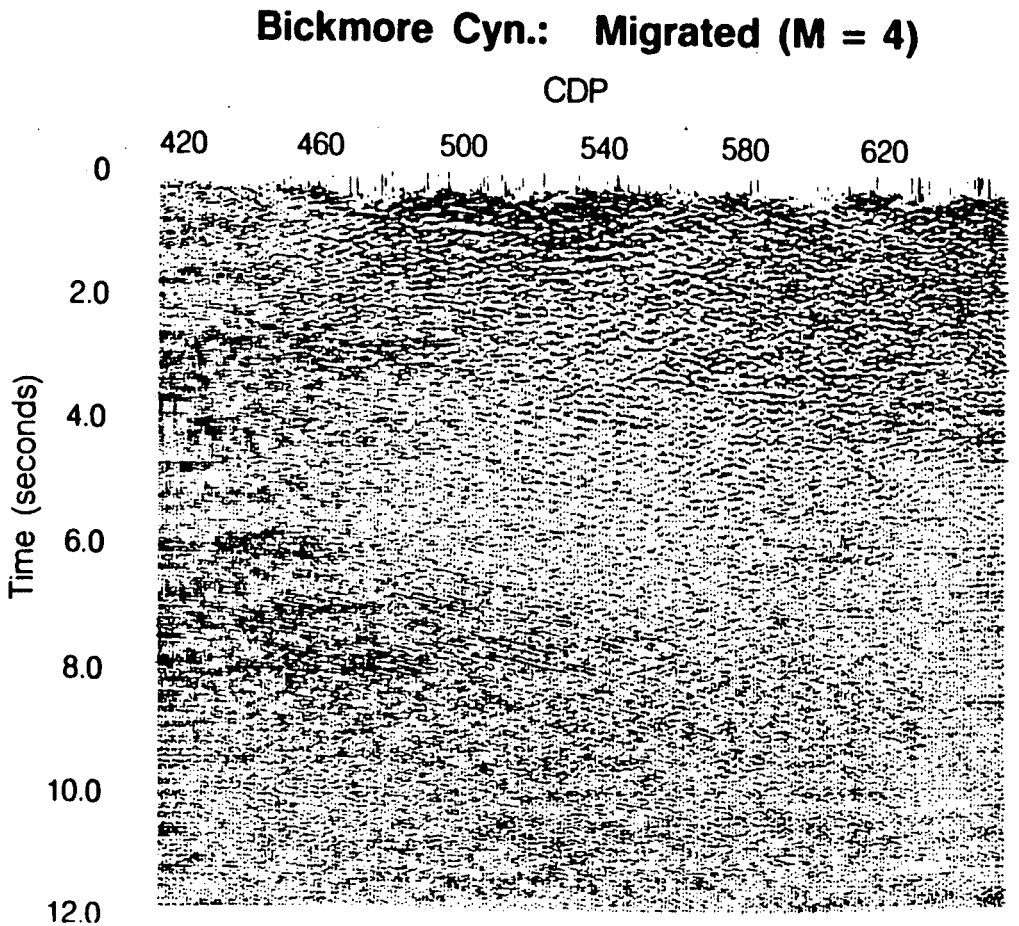

Figure (3-18) Same as Figure (3-17) however the migration is 'coarser' in that the summation along the hyperbola is four times coarser.

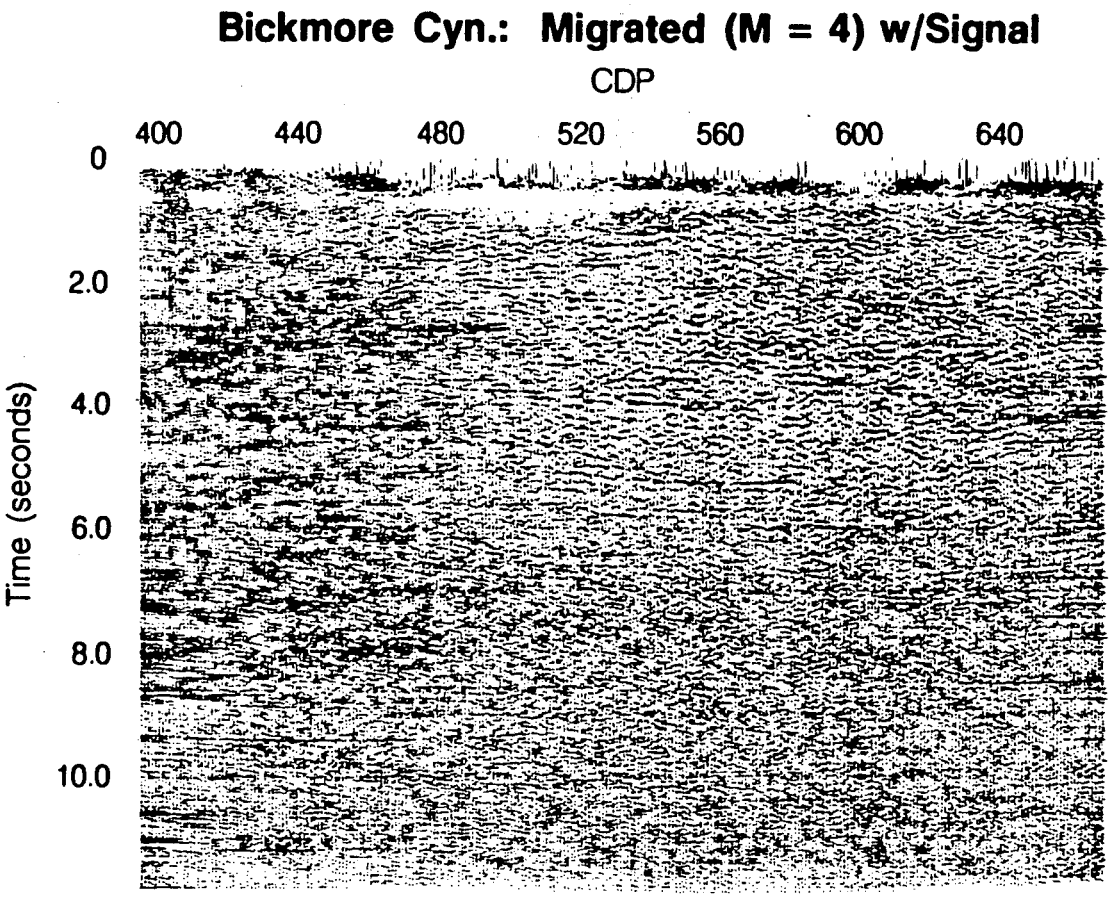

Figure (3-19) Same as Figure (3-18) however, in addition to the coarse migration the data is enhanced by a coherency process that allows the processor to extract from the stacked data certain desired features and then add them back to the data. In this case a range of dip of ±16 ms/trace) was specified, as well as a lateral range of CDP's (e.g., 11) over which to calculate coherence; in addition, a threshold coherence of 0.33 was specified, above which the data are separated and retained. Finally, these data are added to the unenhanced data such that, in this case, the result is enhanced 33%.

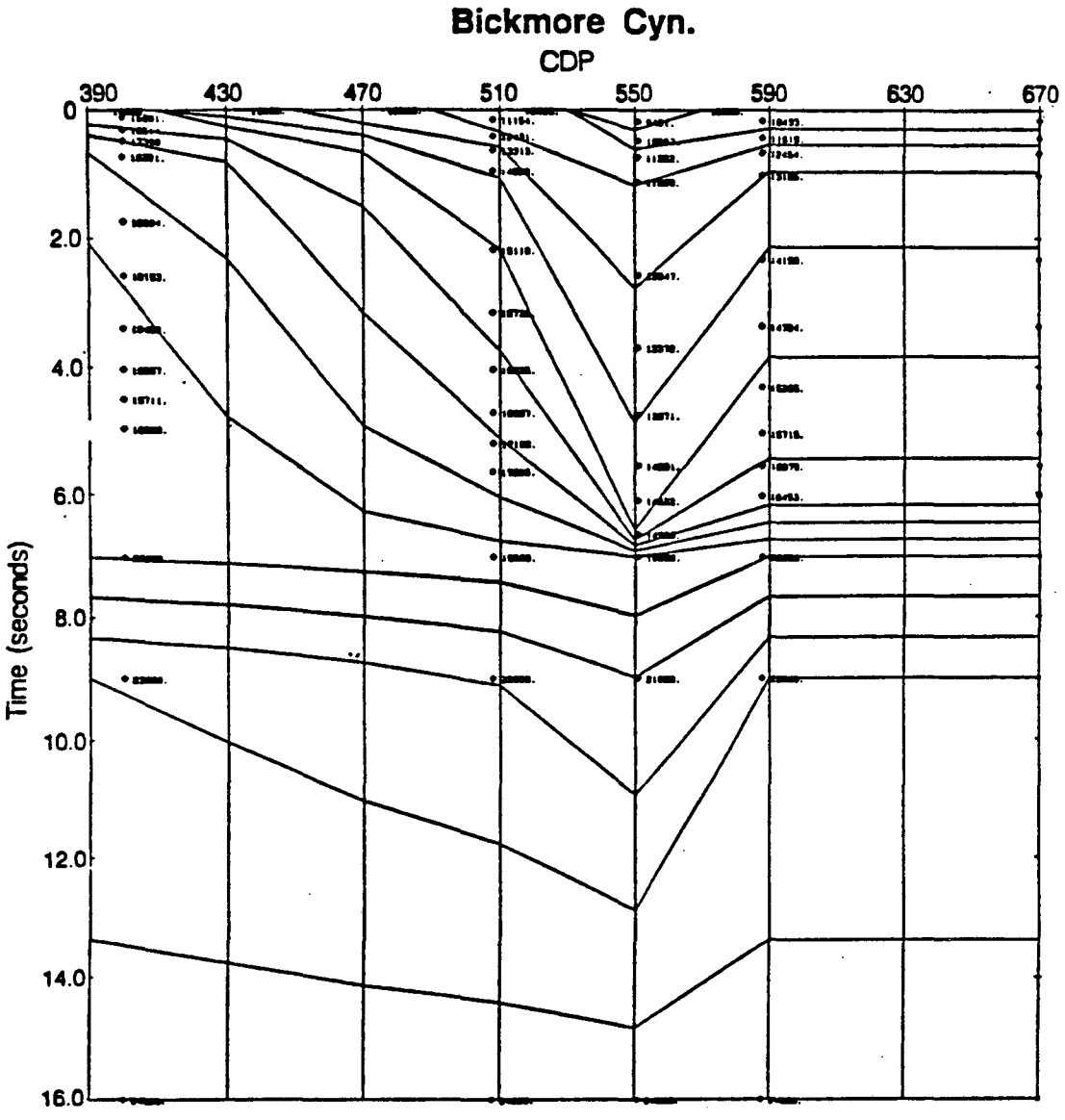

Figure (3-20) NMO velocity model used to stack the data; this model was determined from various constant velocity and coherency analyses. Two-way reflection time is indicated at the left of the figure in seconds. Note the low velocity trough in the center that represents the San Andreas fault zone.

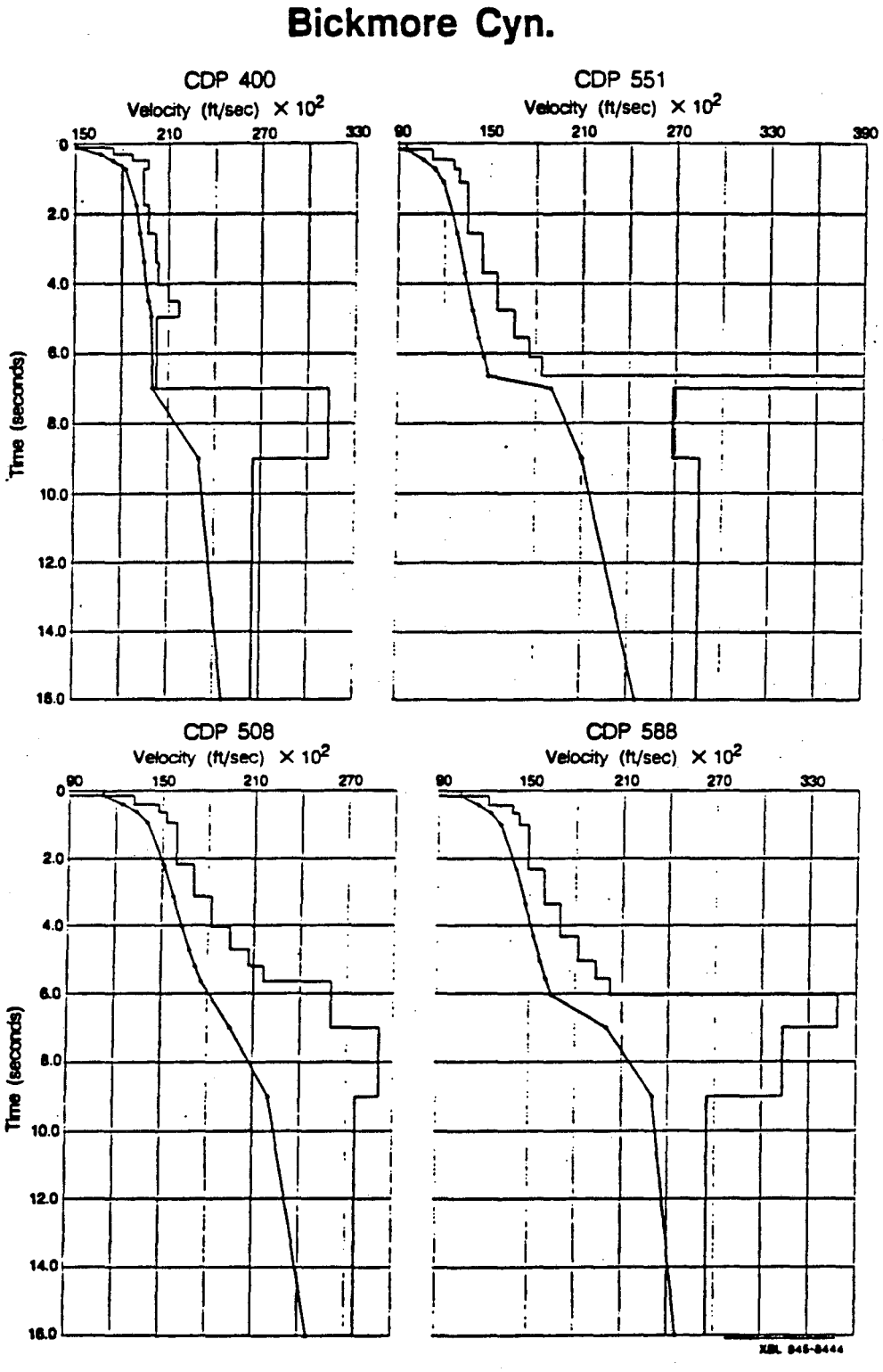

Figure (3-21) Alternate perspective of the stacking velocity model depicted in the previous figure showing the corresponding interval velocities also (calculated from the Dix formula). Recall that the CDP numbers increase eastward, with the fault zone centered at about CDP 555 (i.e., upper right part of this figure).

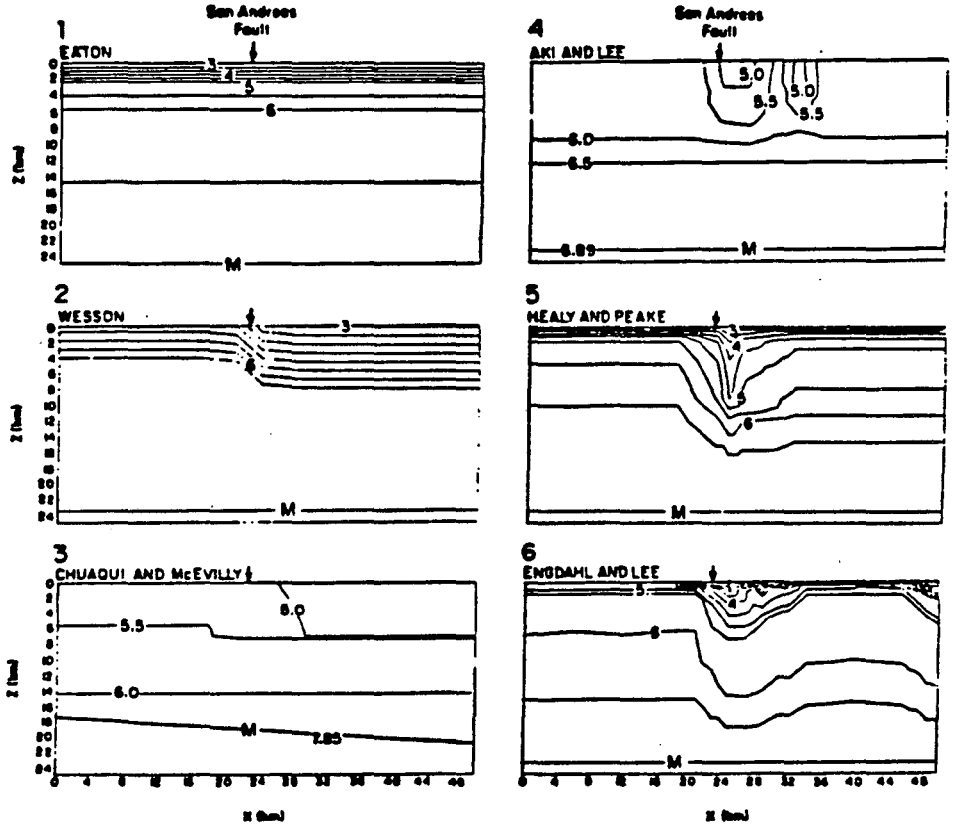

Figure (3-22) Historical view of the trend of velocity modeling in this region, taken from Feng and McEvilly (1983). The sequence of models is represented by the numbers at the upper left of each. Note the progression by which the fault zone is modeled as a low-velocity trough, bounded on either side (particularly to the west) by higher velocity media. [It is important to realize that, unlike these models, the model depicted in Figures (3-20) and (3-21) does not necessarily represent the actual wave velocity at those depths, although the interval velocities may approximate such velocities; rather, the velocity model obtained by the constant velocity and coherency analyses represents, merely, that velocity as a function of time that *best* stacks the data (i.e., that results in the most spatially coherent reflectivity representing, ideally, the pattern of subsurface impedance contrasts).]

3.4 ATTENUATION ANALYSES

3.4.1 *OVERVIEW*

In addition to a parameterization in terms of velocity, it is believed that an understanding of the attenuation ("Q") profile will greatly enhance our knowledge of the earth's crust, particularly in critically important areas such as this active segment of the San Andreas fault. Attenuation of seismic wave energy can be decomposed in terms of the intrinsic dissipative properties of the medium and its scattering characteristics. The partitioning of these processes, which may not be independent, is especially difficult and elusive; this problem is most important in the lithosphere because of considerable heterogeneity and the more intense scattering that is expected in such an environment. Most of the seismological approaches to the problem which focus on the scattering attenuation are statistical; whereas primary body waves (e.g., P and S-waves) are modeled accurately in terms of amplitude and phase by deterministic approaches, the complexity and apparent randomness of the coda of P and S-waves are virtually impossible to model deterministically. Energy loss due to scattering from a random inhomogeneous structure has been studied as a dominant factor in both primary amplitude attenuation and P and S-coda wave excitation (Aki and Chouet, 1975; Sato, 1977, 1978; Rautian and Khalturin, 1978; Dainty, 1981; Roecker et al., 1982; Pulli, 1984; Biswas and Aki, 1984; Rhea, 1984; Wu, 1985; and many others). Most investigators concentrate on models of heterogeneity parameterized by velocity perturbations because impedance contrasts are generally dominated by such contrasts in velocity, although Wu and Aki (1985) have recently indicated a theoretical decompostion into velocity-type scattering and impedance-type scattering. In the weak scattering environment of the perturbation model the Born approximation is generally adopted; under this approximation the depletion of energy in the primary wave due to scattering is neglected, although the transfer of energy from the primary to the secondary wave field constitutes the heart of the model.

Thus the law of energy conservation is violated. Alternatively one may assume a strongly heterogeneous medium in which multiple scattering is important. The multiple scattering approach tends to be somewhat cumbersome mathematically, making it somewhat difficult to apply to actual inversion of data; thus it has often led to a diffusion model (Wesley, 1965; Dainty and Toksoz, 1977; Nakamura, 1977; Dainty, 1981; Scheiner and McEvilly, 1981; and others), although this may not be applicable to terrestrial applications (Kopnichev 1977). "Lunargrams" show long relatively unattenuated coda; the assumed explanation is that the absence of water leads to a very low level of intrinsic attenuation in the propagation medium and hence even a small amount of heterogeneity would be sufficient to generate intense coda. The unknown amount of intrinsic attenuation in the lithosphere of the earth makes the problem of determining the relative contributions of the intrinsic and elastic scattering mechanisms difficult in the case of seismic wave propagation. In any case, the high level of scattering on the moon is amenable to a diffusion model as applied by Nakamura (1977), Dainty and Toksoz (1977), and others.

The weak or single scattering model is by far the most widely used in earthquake and microearthquake studies, in sharp contrast to the lunar studies noted above. In fact, the model has been extended recently in an attempt to detect changes in the coda Q premonitory to seismicity (Novelo-Casanova et al, 1985; Sato, 1986; Jin and Aki, 1986; Aki and Jin, 1986). In these latter investigations the temporal variation of the coda Q value is compared with the seismicity. In this model the increasing stress levels and consequent increases in crack density are presumed to result in lowered Q values. Furthermore there have been observations of an attendant decrease in the b-values for several regions (Novelo-Casanova, et al., 1985; Jin and Aki, 1986) in the period preceding major earthquakes. This latter correlation of Q with b-values is most interesting; it is based quite simply on the assumption that in the shallow crust increasing tectonic stress levels tend to preferentially increase the crack density for large-sized and large aspect ratio cracks. Since this will, in general, involve both an increase in the scattering intensity or heterogeneity (i.e. lower Q_s) as well as a decrease in the b-value, the observed

(apparent) Q and b-value should decrease in tandem prior to a significant earthquake (Aki, 1985; Novelo-Casanova, et al., 1985; Jin and Aki, 1986).

The model of Sato (1977), Aki and Chouet (1975) and others pertains primarily to S-wave coda; however, there is no reason why it cannot be applied to P-wave data. In general, given the weak scattering model, the scattered (isotropic) energy will be a maximum when $ka \approx 2\pi$ or when $\lambda \approx a$, where k is the wavenumber and a is the correlation or scale length (the scale length is defined according to a particular correlation function assumed for the medium). The requirement for the formation of P-coda is the existence of impedance perturbations (generally modeled as perturbations to the mean velocity) over a geometrical range comparable to the wavelengths of the incident wavefield (i.e., $\lambda \approx a$). When this condition is satisfied for P-waves it may be manifested in the P-coda. Of course the P-coda for earthquake data will in general include shear energy, however in the application to reflection data we can minimize the shear wave contribution by application of the stacking process. In fact, the stacking process inherent in CDP profiling leads ideally to an exclusively P-wave data set; hence the often neglected problems of wave conversions and those of surface wave contamination in the coda are generally not relevant in the application to reflection data. To a first approximation, the stacked reflection seismogram, or vertically propagating coda, represents the impulse response of the medium to a point source at the observation point on the earth's surface. Thus both the single scattering and diffusion models are applicable to this type of data if the environment is assumed to be either weakly or strongly heterogeneous, respectively.

3.4.2 *EARLY STUDIES: CDP REFLECTION DATA & ABSORPTION MECHANISMS*

Prior to the application of the single scattering model the diffusion approach was applied to the 1978 CDP data with some interesting results. Preliminary observations of unstacked near-source, (x=670m) recordings suggested that the seismic energy decay could be fit to the solution to the diffusion equation (McEvilly, 1981):

$$\frac{\partial E}{\partial t} - D\nabla^2 E + \frac{\omega}{Q}E = 0 \tag{1}$$

where $E = E(x, y, z, t, \omega)$ is the seismic energy density in a unit frequency band about ω, D is the diffusivity constant for the medium, and Q is the apparent quality factor; this Q represents the combined intrinsic and elastic scattering attenuation effects. The diffusivity was assumed to be related to the wave scattering process by analogy with the scattering of particles moving with a certain mean free path, L, as $D \approx V\ L$, given a characteristic velocity, V, for the medium. The point source solution to equation (1) is:

$$E(0, t, \omega) = S(\omega)\ t^{-\frac{3}{2}}\ e^{-\frac{\omega t}{Q}} \tag{2}$$

where r, the source-receiver distance, is assumed small with respect to the effective path lengths of the multiply scattered arrivals in the coda. $S(\omega)$ the "source term" is

$$S(\omega) = \frac{W_o(\omega)}{(4\pi D)^{\frac{3}{2}}}$$

where $W_o(\omega)$ is the source energy spectrum. In this case the *primary* energy was the first arrival and the coda decay over the entire seismogram was analyzed. Though crude, this preliminary study of near offset unstacked data encouraged more detailed analyses of both unstacked and stacked data.

Because the stacking process theoretically results in purely compressional wave energy and tends to enhance the signal-to-noise, or *primary*-to-secondary wave energy, the analysis of the coda decay was carried out predominately on the stacked seismograms. The stacked data were divided into two full octave bandwidths and point-source solutions to the diffusion equation for amplitudes:

$$Log_{10} A(t, \omega) = C(f) - \frac{3}{4} Log_{10}\ t - bt \tag{3}$$

where $C = Log_{10} S$ and $b = \frac{(Log_{10}\ e)\pi f}{Q}$, were fit in the least squares sense to the coda of the primary arrival. Examples of such fits are shown in Figure (3-24).

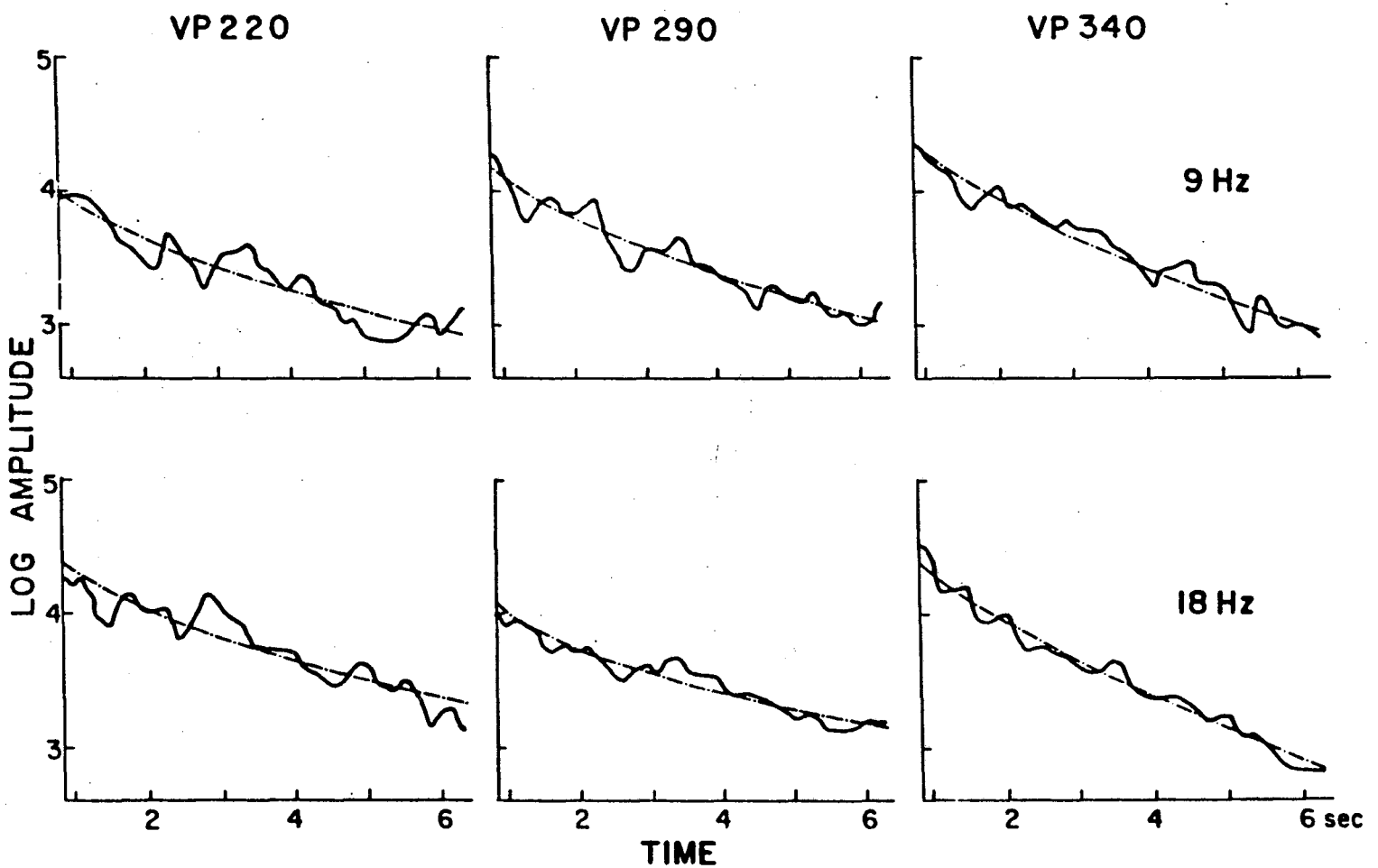

Figure (3-24) Least square fits of equation (3) (Section 3.4.2) through three representative stacked CDP data traces along the profile for arbitrary center frequencies of 9 Hz (upper three plots) and 18 Hz (lower three plots) of the filtered data; the data were filtered into two octave bands spanning the sweep range of the data. As before, the western Gabilan data is at left (i.e., lower VP numbers), and the eastern Franciscan data is at right. Two-way reflection time is shown at two-second increments at the bottom of each plot.

DIFFUSION MODEL

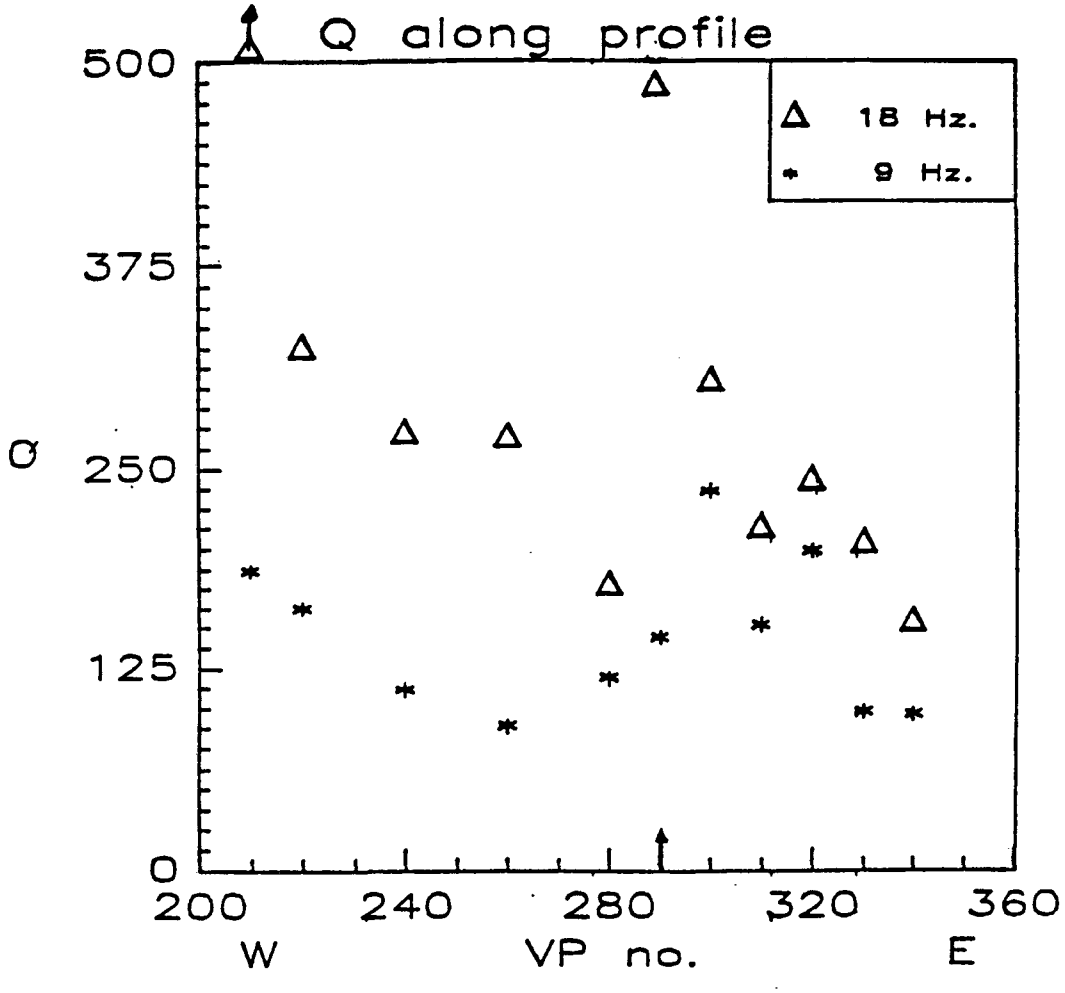

Figure (3-25) Composite of results for the diffusion analysis for all the CDP data according to VP number; data is divided according to the appropriate filtered band by center frequency with the higher octave denoted by the triangles. The fault is shown by the arrow at bottom near VP 290. Note that the higher frequency data have consistently higher apparent Q values than the lower octave data.

The center frequency of each octave was used in the calculation. The results are summarized in Figure (3-25). Though somewhat difficult to interpret, there is a tendency for the apparent Q values to decrease eastward (i.e. toward higher VP numbers). It is not a particularly unambiguous effect but it is interesting to note that this general trend is consistent with the results obtained from the single scattering model described in the next section.

The motivation to model the energy propagation as a diffusion process was based on the observation of the stacked reflection section, particularly the apparent lack of reflectivity in the eastern Franciscan crust. The diffusion model is not unknown to geophysical problems; in conjunction with the lunar studies alluded to earlier, numerous ultrasonic model experiments have been carried out in the laboratory (see Dainty and Toksoz, 1977 for a summary). In such experiments the medium is represented by a thin aluminum plate through which ultrasonic pulses were propagated; scatterers were represented by circular holes (with diameters smaller than the dominant wavelength) or by grooves of random orientation. The densities and sizes of both scatterers and scattering regions were varied in these experiments. The intensity of coda generation was clearly proportional to the density of scatterers and the size of the scattering region. Furthermore, the application of the diffusion theory to the resulting coda decay showed that the diffusion model was an appropriate theoretical model for this problem. There was, on the other hand, one discrepancy in the fit of the amplitude decay to the solution to the diffusion equation including an exponential loss term: The resulting Q values were as low as 70 yet the Q for aluminum is greater than 1000; it was suggested that this extreme lowering of the Q value may have been due to absorption in the clay sealant at the edges of the plates. Although this tends to compromise the reliability of this method in the determination of apparent attenuation values, the close fit of the data using the diffusion model encouraged its continued application.

The diffusion approach is also widely used in studies of electromagnetic wave propagation in the earth. This is essentially due to the fact that earth materials have relatively high conductivity and thus constitute a rather dissipative medium with respect to electromagnetic wave propagation. Hence the wave field may be thought of as a very damped wave and energy is

generally diffused through the medium. The popularity of this approach in electromagnetic problems due to these attenuative properties therefore provides an attractive example for the seismic case where attenuation is believed significant. However certain aspects of the diffusion model pose troubling interpretational problems in this latter case. In the first place, the model assumes extremely intense scattering and thus a purely random medium. The obvious presence of coherent reflection energy in the Gabilan crust would thus seem to preclude the application of this diffusion model there. In addition, the physical interpretation of the diffusivity parameter is not clearly understood in terms of the structure of the medium. Nevertheless, the results of both the preliminary application of the diffusion model to unstacked data and the more careful least-squares analysis (Figures 3-24, 3-25) of stacked data were quite interesting, and warranted further scrutiny.

Finally, it is perhaps important to note that, in general, the higher frequency data have higher Q values, and as indicated above, this pattern has been reported in numerous other seismic studies (Aki and Chouet, 1975; Console and Rovelli, 1981; Roecker et al., 1982; Del Pezzo et al., 1983; Rodriguez et al., 1983; Rhea, 1984; Del Pezzo and Zollo, 1984; Scherbaum and Kisslinger, 1985; Campillo et al., 1985; Jin et al., 1985; Carpenter and Sanford, 1985; Rebollar et al., 1985; Agnew et al., 1986; and others), in marked contrast with the laboratory data: The results of many different laboratory studies indicate that Q is constant over a wide spectral range, from 1 to 10^6 Hz (for summaries of the data, see Knopoff, 1964 and Jackson and Anderson, 1970). Indeed, a reasonably consistent pattern has been emerging from the results of numerous seismological analyses (see Figure 3-26) which indicates an apparent Q^{-1} that increases with frequency from less than 10^{-3} Hz to about 1 Hz and decreases with frequency from about 1 Hz to 25 Hz (Aki, 1980; Sato, 1984; Aki, 1985; and others). The theoretical curve fit through the various data in this figure (e.g. dotted curve) is based on the weak scattering theory of Chernov (1960) and involves certain *a priori* assumptions regarding the fractional velocity perturbation of the inhomogeneous media (Sato, 1984). As is clearly seen in Figure (3-26) the low frequency data is lacking relative to the data above 1 Hz. An enhanced view of the

box for surface wave data in the left part of the figure may be provided by Figure (3-27) adapted from Jackson and Anderson (1970). The data in this figure are taken from their compilation of the available surface wave and free oscillation observations; (most of the upper data points are from Love waves and torsional mode oscillations). The general consistency of this frequency dependence of the free oscillation data has been shown in subsequent studies as well (see Anderson and Hart (1978) for a summary). Although Jackson and Anderson (1970) were able to fit this latter data with a relaxation model of intrinsic dissipation neglecting all scattering losses, it is interesting that the data fall neatly within Aki's (1985) model of the apparent Q based exclusively on a scattering theory. Actually the fit of Jackson and Anderson deteriorated at the short period end of the data because most relaxation models predict a peaked and somewhat symmetric (in log-log domain) frequency dependence for Q^{-1}, and their data were sparse and inconclusive at short periods (Figure 3-27). The data for both these Figures (3-26 and 3-27) refer to conditions relevant within the entire lithosphere (and deeper) as well as those exclusively within the earth's crust. The dominant mechanisms of intrinsic attenuation for the earth's crust are expected to be different from those in the mantle where temperatures and pressures (as well as composition) are quite different. Laboratory measurements as well as theory indicate that Coulomb frictional sliding across crack surfaces and grain boundaries is an attenuation mechanism that would give a Q constant with frequency, (Born, 1941; Knopoff, 1964; Walsh, 1966); this is an appealing mechanism of attenuation in the shallow crust where cracks would be open under the low ambient pressures, but may not be important in the lower crust and are certainly not expected to be relevant in the mantle. (The depth extent to which cracks are likely to be open may be extended to the lower crust by the presence of fluids which could provide a resistance force to counteract the ambient lithostatic load within the pore spaces.) Walsh (1966) has suggested that because the frictional sliding mechanism is non-linear it may not be important at relatively small strain amplitudes (e.g., $< 10^{-5}$ or 10^{-6}). On the other hand, the presence of even a minute amount of fluid will tend to lubricate the crack surface, thereby facilitating sliding and increased dissipation. (Actually, the presence of fluids on

the crack surfaces or within pore spaces is expected to have a perhaps more important effect on the intrinsic dissipation in the form of a viscous relaxation process.)

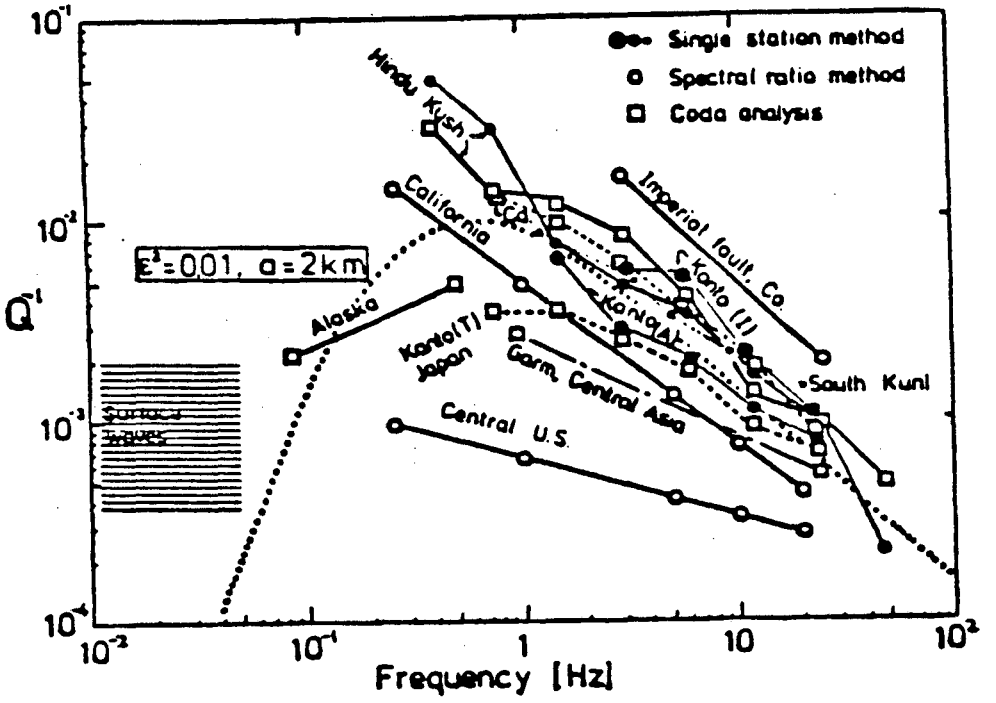

Figure (3-26) Composite of available seismological data of apparent Q^{-1} as a function of frequency; superimposed on this data is the theoretical curve (dotted) expected from Chernov's (1960) weak scattering model given a mean square fractional velocity perturbation of 0.001 (ϵ^2), and a correlation scale length ('a') of 2 km. All of the body wave data indicated are of shear waves and/or their coda. (Adapted from Aki, 1985.) Note that all curves for data above 1 Hz show Q proportional to frequency; data below 1 Hz are lacking and thus the peaked nature of the dependence of apparent Q on frequency as predicted by theory is not manifested here.

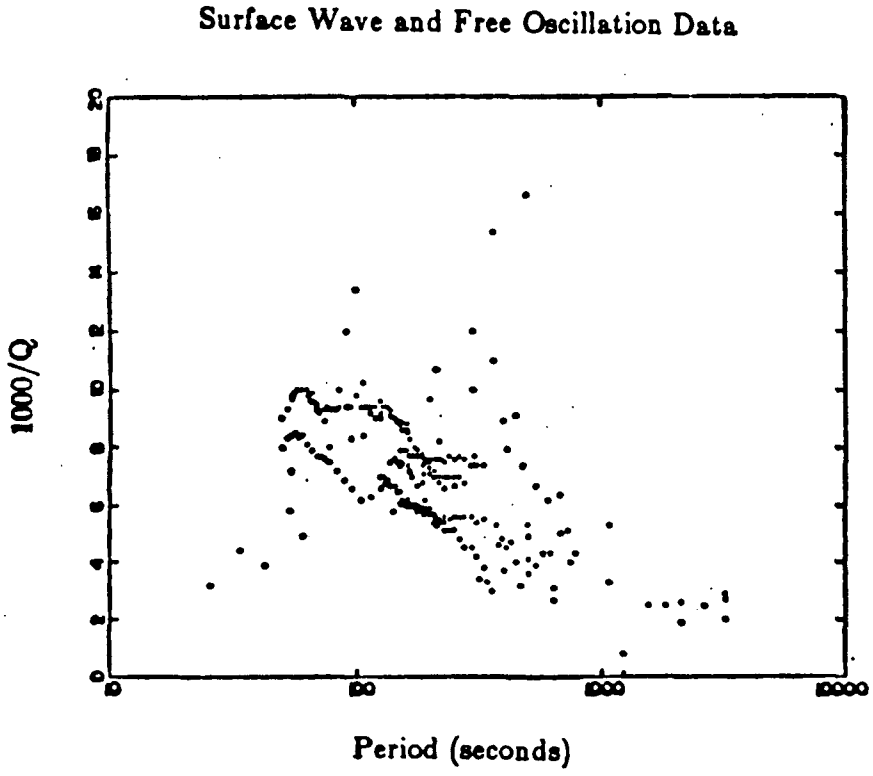

Figure (3-27) Pattern of frequency dependence of Q^{-1} derived from the available surface wave and free oscillation data. The upper data points are primarily from Love waves and torsional mode oscillations. (Adapted from Jackson and Anderson, 1970.) Note the general trend of increasing Q^{-1} with frequency (i.e., with decreasing period) over a wide spectral range.

Although any relaxation model of intrinsic dissipation will be rather strongly frequency dependent, a superposition of such linear models is thought to have a 'smearing' effect on the peak, leading to a quasi-constant "absorption-band" attenuation model (Liu, et al., 1976). O'Connell and Budiansky (1977) have shown that a spectrum of crack geometries would be sufficient to cause such a smearing of the frequency dependence for an absorption model involving viscous relaxation of shear stresses within pore spaces; however at seismic frequencies, they suggest that crystalline rocks are most probably in a state of uniform pore pressure and thus any dissipation would be due to fluid flow between cracks as opposed to relaxation of shearing stresses within the pore fluid. In either case, a variation of crack geometries would be mapped into a variation of the peak absorption frequencies and thus a weakening of the dependence of Q_i on frequency. A similar conclusion was found by Mavko and Nur (1979) who added that the flatter pores (e.g., aspect ratios $< 10^{-5}$) would be more sensitive to the details of the fluid and its ability to support compressional and shear loads; hence, even a small concentration of very flat pores would greatly accentuate the dissipation of seismic waves given a slight amount of fluid.

One of the most interesting aspects of the study by Mavko and Nur (1979) is the conclusion that in a partially saturated medium, the ratio Q_P/Q_S is expected to be *less* than unity, implying that losses in compression exceed those in shear; in fact, much of the laboratory data involving partially saturated media seem to corroborate this inference (Birch and Bancroft, 1938; Peselnick and Zietz, 1959; Savage, 1966). This result is, however, not supported by the majority of seismological data, particularly that of surface waves (Jackson and Anderson, 1970). It may be that the answer depends on the depth extent of the data of interest; that is, for crustal rock under relatively low lithostatic load, bulk attenuation may be more important than at much higher pressures where different intrinsic attenuation mechanisms may dominate. Certain mechanisms of attenuation are more likely than others to be relevant over a larger pressure-temperature regime. Examples of such mechanisms include the motions of lattice defects under transient stresses (Mason, 1969), grain boundary relaxation (Gordon and Nelson, 1966), and

various thermally activated relaxation mechanisms (Zener, 1948; Anderson and Archambeau, 1964).

Aki (1980) has reviewed the literature in terms of the scattering attenuation as well as the various models of intrinsic absorption, primarily for shear waves. In discussing these results he points out that the pattern indicated in Figure (3-26) is rather suggestive of a relaxation mechanism with a relaxation time for the lithosphere of $1/(2\pi \cdot 0.5) \approx 0.3s$. Based on the assumption that the observed pattern of frequency dependence is due to a particular intrinsic relaxation mechanism, Aki shows that, with the possible exception of the thermoelastic attenuation effect in dry rocks containing cracks (Zener, 1948; Savage, 1966), the relaxation time of 0.3 seconds implies either unreasonable fluid viscosities or excessive temperatures. As the thermoelastic effect predicts a decreasing Q with frequency (Savage, 1966), one is led to suggest that, at least for the crust, it may be the scattering process that is responsible for the observed frequency dependence of the apparent Q.

Finally, the role of water and other fluids in the actual intrinsic absorption process in the crust is expected to be quite significant, although the precise nature of its effects, particularly as relates to the frequency dependence of the apparent Q, is uncertain. Several investigators have shown that anomalous fluid pressures exist in this general region of the San Andreas fault, particularly in the Franciscan media (Berry, 1973; Irwin and Barnes, 1975). Although they stress the important role that these fluids play on the pattern of seismicity, facilitating creep in certain regions, these analyses also indicate that the concentration of metamorphic fluid is generally high; it is thus suggested that the depth of closing of cracks and pore spaces due to lithostatic pressures may be extended to the lower extent of the seismogenic zone (e.g., about 10 km).

The question of what mechanism of intrinsic dissipation predominates is certainly complicated by the role of scattering on the seismic data; in addition, it is important to bear in mind that most laboratory studies involve very high frequencies and the extrapolation of these results to seismic frequencies may not be straightforward.

Besides these theoretical obstacles to understanding the mechanism of attenuation of seismic waves in the crust, there are technical problems associated with the reduction of actual data. The most difficult such problem exists when signal strength decreases in the presence of noise. High Q values near VP 290 in the fault zone may be due to low signal-to-noise ratio; as signal strength drops near or below the noise level an artificial enhancement of apparent Q occurs. Of course, in the limit of all noise, Q will appear to go to infinity! In fact this latter point was tested in the context of the diffusion study of the stacked traces; data in the range 13 to 16 seconds (two-way transit time) were fit to equation (3) above. Signal-to-noise in this part of the record is expected to be significantly less than unity. The resulting Q values were consistently "infinite" (i.e. negative) over a wide range of position along the profile, as anticipated. Given the important role of attenuation in seismic wave propagation it is essential that an understanding of such crustal properties be addressed despite these serious obstacles. The analysis of high quality data from many different tectonic settings may provide a database from which accurate conclusions may be drawn regarding the heterogeneity and dissipative properties of the particular region.

In addition to the marked contrast in reflectivity between the two crusts as seen in the stacked sections (Figures (3-6), (3-16 to 3-19)) there is a clear difference in frequency content across the section. Dominant frequencies in the granitic western part of the profile are noticeably higher (12-18 Hz) than those in the Franciscan crust of the Diablo range (8-15 Hz) to the east. This notable spectral contrast can be seen in Figure (3-28) in which the smoothed spectra for a representative CDP stacked trace from the granitic crust, CDP 445, is juxtaposed with the spectra of CDP 645 from the eastern Franciscan end of the profile. These spectra are taken over the coda of a "reflector" at mid-crustal depths. A "reflector" has been identified from the stacked data based on the identification of large amplitude spatial coherency. The onset times of the reflectors range from 2.624 seconds, (two way travel time), to 4.328 seconds and the windows over which the spectra are computed are generally 1-2 seconds. The corresponding depth range is about 6 to 17 km. The response of the instrument, an 8 Hz GSC 20D geophone

(McEvilly, 1979) has not been removed from the spectra in these figures. As the sweep range was 24-6 Hz, the low frequency decay ($f < 6$ Hz) is expected. This general observation of spectral contrast in reflectivity between the two crusts may be explained by a simple intrinsic absorption model with a constant or weakly frequency dependent Q_i; alternatively, the spectral contrast may be explained by a frequency dependent scattering process. The ambiguity in the determination of the partitioning of these two attenuation mechanisms is once again apparent.

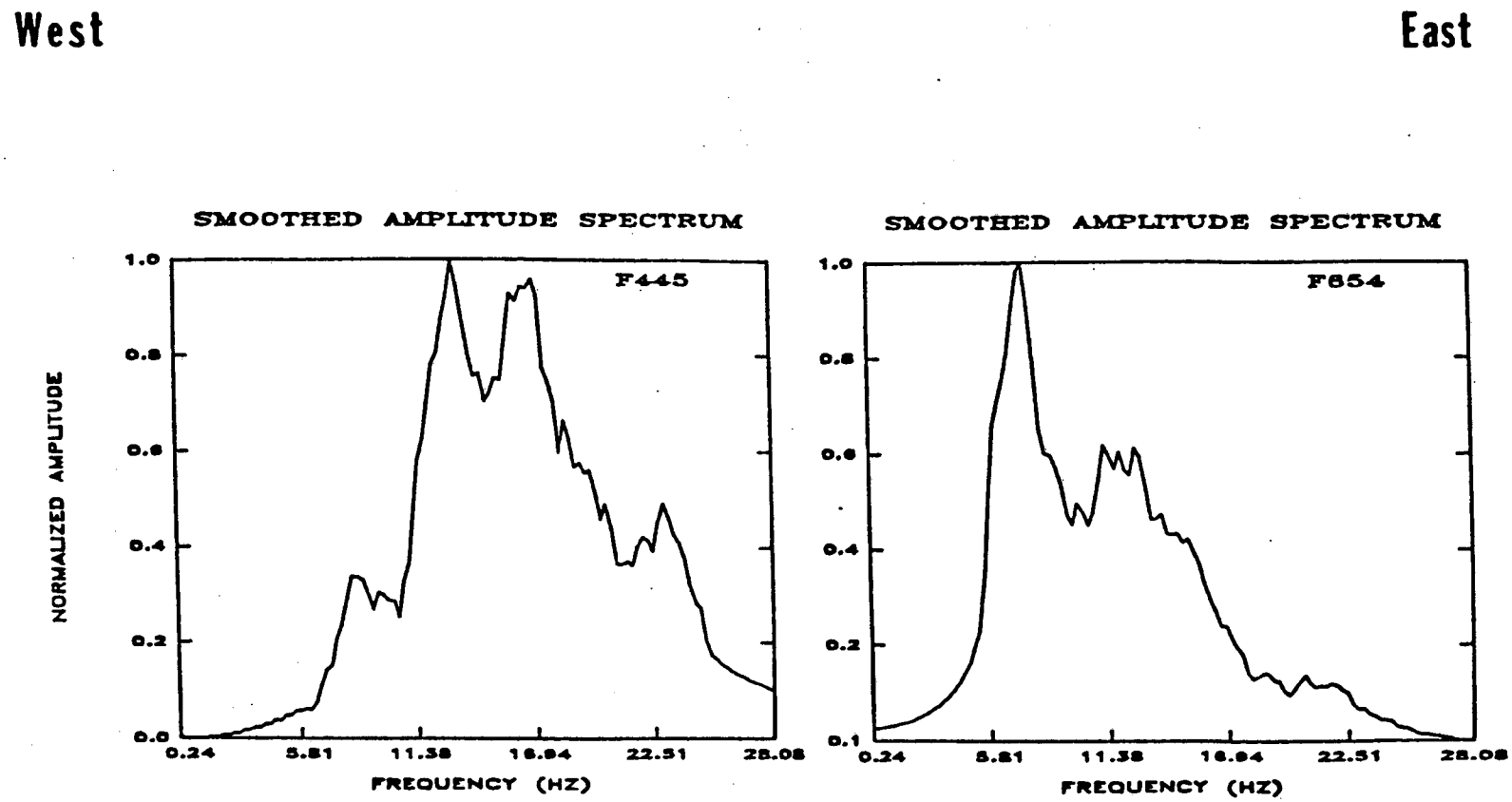

Figure (3-28) Smoothed Fourier amplitude spectra for two representative CDP coda windows; F445 is the spectra for CDP 445 in the western Gabilan portion of the section; F654 is that for CDP 654 in the Franciscan portion. Neither spectra is corrected for instrument response. Note that the sweep range was 6-24 Hz, which is adequately represented by the Gabilan spectra, in contrast to the relative depletion of the high frequencies for the Franciscan spectra.

3.4.3 *WEAK SCATTERING APPROACH: THEORETICAL DEVELOPMENT*

Based on the work of Sato (1977, 1978, 1982), Aki and Chouet (1975), Roecker et al. (1982), and others a technique has been developed for analyzing the coda of a coherent seismic signal in terms of the scattering attenuation properties of the sampled medium. As in the diffusion model a primary arrival must be identified and windowed judiciously so as to study its coda but the window must not include subsequent primary arrivals. In this application of the aforementioned techniques to reflection data, it is important to realize that the 'primary' arrival has actually been (coherently) scattered once between the source and the co-located receiver. This differs from the cases studied by Sato (1977, 1978), Aki and Chouet (1975), Roecker et al. (1982) and others in which the earthquake source and the receiver are at different positions and the primary arrival has not been scattered. The scattered 'primary' wave of the stacked CDP seismogram studied here differs from those scattered 'secondary' arrivals that follow it in the coda in two important ways: the secondary arrivals have undergone at least one more scattering subsequent to the initial reflection; in addition, the initial scattering or reflection is said to be spatially coherent because the process of stacking tends to enhance its amplitude relative to that of the subsequent secondary arrivals within the coda. In general these secondary arrivals within the coda are not spatially coherent and thus tend to cancel upon stacking.

In contrast to the application of the diffusion model to reflection data, some coherent energy is expected within the weak scattering model; in fact, such energy should predominate but should be accompanied by scattered arrivals in the form of signal-generated noise. Results from analysis of the CDP reflection data indicate that in *well-behaved* layered media a clear and spatially coherent arrival can be discerned and its coda analyzed, whereas in extensively fractured or strongly heterogeneous media such coherent 'primary' arrivals are more difficult to locate. The application of this weak scattering model to the reflection data is rather appealing in the sense that the stacked form of the data is not plagued with shear wave contamination resulting from wave conversions; this is in marked contrast to the more common application of

the method to earthquake data. A generalized form of this method has been applied to numerous earthquake and microearthquake data sets from many different tectonic settings, and as discussed below a pattern seems to be emerging. Although by no means unambiguous the general pattern suggests that, in *active* tectonic regions such as those involving convergent plate margins or intense seismicity, apparent Q values tend to be somewhat low and the degree of frequency dependence is significant (Console and Rovelli, 1981; Rodriguez, et al., 1983; Scherbaum and Kisslinger, 1985). This is contrasted by seismically quiescent regions, in which the Q values may be higher and, more clearly, the degree of dependence of these Q values on frequency appears to be less (Rhea, 1984; Jin, et al., 1985). In fact these preliminary results (Console and Rovelli, 1981; Rodriguez, et al., 1983; Del Pezzo, et al., 1983; Rhea, 1984; Del Pezzo and Zollo, 1984; Scherbaum and Kisslinger, 1985; Jin, et al., 1985; Agnew, et al., 1986; Huang and Wyss, 1986) have inspired several recent attempts to determine if temporal and/or spatial variations of these scattering attenuation parameters may be indicative of processes premonitory to seismic activity (Novelo-Casanova, 1985; Jin and Aki, 1986; Aki and Jin, 1986).

The weak scattering theory that forms the basis of the inversion for apparent Q and mean free path in this work is outlined in the Appendix; similar to the theory of Chernov (1960), the scatterer is represented by a small perturbation to the mean velocity field and acts as a secondary source. The Green's function for this weak scattering environment is derived as well as an expression for the far-field scattered energy. The analysis follows the model of Sato (1977, 1978); the scattered wave field is expressed in terms of amplitude (equation (A28) of the Appendix) and is applied both to the P-wave coda of the CDP reflection data and to the S-wave coda of the microearthquake data. This equation, rewritten here as equation (4) includes the correction for geometrical spreading and incorporates the Green's function for the secondary scattering source. An exponential loss effect has been assumed to represent the attenuation of primary wave energy:

$$a_{corr}^{s^2}(t) = S(\omega, L, t_o)\, t \ln\left(\frac{t + t_o}{t - t_o}\right) e^{-\frac{\omega t}{Q_c}} \tag{4}$$

The left side represents the squared envelope of the scattered arrivals in the coda, corrected for geometrical spreading; t is the arrival time of scattered energy in the coda; $S(\omega, L, t_o)$ is the "coda source factor" and includes the source energy spectrum, the density of the medium, the arrival time or "onset time" of the primary arrival, t_o, and the mean free path for the medium. This last parameter, L, is also defined as the reciprocal of the *turbidity*, which is in turn defined as the product of the number density of scatterers and the *scattering cross-section* * for the medium. Hence, this quantity describes the general heterogeneity structure of the scattering domain and is, in general, frequency dependent. As the single scattering model is the lowest order approximation in scattering theory, the importance of this parameter in inferring structural characteristics for the medium must not be exaggerated. Several geologic bodies have been mapped within the Franciscan of the Diablo Range that indicate the scale of heterogeneity that may be anticipated. For example, numerous discontinuous lenses have been noted up to 2 km in length (Wilson, 1942). Dikes up to 3 km in length have been mapped and large tabular units such as the Orestimba metagraywacke are expected to have length scales of more than 7 km beneath the extensive Garzas melange (Page, 1981).

For the weak scattering assumption the mean free path is taken to be large with respect to source-receiver distance to ensure few, indeed only one, scattering event per wave. This is a critical assumption and in turn poses a rather troubling obstacle in any effort to separate the effects of intrinsic and scattering attenuation. We can assume that such a partitioning can be theoretically accomplished if we accept equation (A23) (Dainty, 1981; Richards and Menke, 1983)

$$Q_c^{-1} = Q_i^{-1} + Q_s^{-1} \tag{5}$$

where Q_i^{-1} expresses the intrinsic dissipation and Q_s^{-1} denotes the seismic energy loss due to elastic scattering; and if we further accept the definition (Dainty, 1981; Roecker, et al., 1982).

*The scattering cross-section, or σ, is defined as the ratio of the time average of the scattered wave energy per unit time to the mean energy flux density of the incident wave, and evidently has units of cm^2, (Morse and Feshbach, 1953; Ishimaru, 1977 for example).

$$Q_s = \frac{\omega L}{V}. \tag{6}$$

Given these relationships, the constraint that the mean free path must be large relative to the source-receiver distance implies of course that Q_s^{-1} is much smaller than Q_i^{-1} and thus that intrinsic attenuation greatly predominates over scattering losses. Such an *a priori* assumption compromises the degree of partitioning that can be determined by any inversion procedure. But the problem is even worse than that. For example: Sato (1978) applied a linearized (e.g. logarithm was taken) form of the above equation to an investigation of earthquakes near the Kanto district of Japan. In studying the decay of S-wave coda amplitudes from 69 regional earthquakes recorded in 1976 Sato assumed that the observed attenuation, denoted by Q_c^{-1} here, was due entirely to intrinsic dissipation. In addition, using an empirical magnitude-energy relation he was able to decompose the coda source factor and thus determine the values of the mean free path for S-waves as well as the Q values for the region. Two significant flaws are associated with his approach: As indicated above, some attenuation must surely be attributed to elastic scattering losses and therefore his resulting Q values (Q_i) are underestimated. Furthermore despite the *a priori* assumption of large values for the mean free path, Sato's resulting values were of the same order as the source-receiver distances (100 km) and in some cases actually less than that.

The proper way to approach the problem, within the constraint on the magnitude of L and given the above assertions relating the different attenuation parameters (i.e. equations (5) and (6)) involves a non-linear least squares inversion with constraints. In addition, since the parameters L and Q_i are coupled a complex search procedure is necessary which depends strongly on a reasonable first guess at the values for these parameters. As there is such considerable uncertainty in our understanding of both the heterogeneity structure of the medium and of the intrinsic attenuation values, such an approach is not favored at this time.

Finally, in addition to these difficulties, another important obstacle in the determination of the mean free path involves the significant ambiguity in our understanding of the actual source energy spectrum. For the microearthquake data, although it may be possible to determine the

spectral amplitude of the filtered seismogram it is not clear what the source spectrum was prior to application of the earth filter; indeed this is part of the problem to be addressed. In addition, because the measured amplitudes for the microearthquake data were so small, the problem had to be scaled prior to taking the logarithm (i.e. in going from equation (A28) to (A29)) so as to maintain positive amplitude values. Hence, the computed values of the coda source factor are only relative. Finally, the difficulty associated with the determination of the coda source factor is excacerbated in the case of the CDP data because, although we know the input frequency band of the source, coupling variations of the baseplate-soil interaction with frequency and along the profile are difficult to ascertain. In other words the actual source spectrum input to the earth below the very shallow near surface veneer is strongly dependent on the coupling of the baseplate to the soil at its drive frequencies. This difficulty has been addressed by several investigators and remains an area of great interest, particularly within the seismic exploration community. Lerwill (1981) studied the problem from a theoretical perspective and compared these results with field observations. Analysis of baseplate velocity over the sweep band on a variety of different surfaces showed considerable variation. The observed variation over a wide band of frequencies (e.g. 10 - 90 Hz) was measured at the baseplate and as such is a very conservative indication of the total distortion; it is probably not inaccurate to expect considerably more complex variations in signal characteristics actually propagated into the ground. One solution to this problem may be realized by measuring the spectrum of the signal of an identical source sweep at various down-hole receivers along the profile. Such measurements were attempted in the spring of 1984 using only one Failing compressional vibrator having roughly the same peak force of 15000 pounds used in the 1978 survey. Down-hole geophones existed at depths of 140 feet at four sites along the old profile, however several sites in the Diablo Range were inaccessible due to a recent washout of the road. Consequently this test was abandoned; nevertheless, in future studies this may provide an adequate and reliable method of determining the source spectrum which would not be plagued by (very) near surface effects such as compaction, soil type, and degree of saturation. Such knowledge would allow correction of the source

sweep and thus aid in efforts to understand the filtering characteristics of the crust.

The approach adopted here is to invert for C (see equation (A29) of the Appendix) and the slope, b, (e.g. apparent attenuation factor) and, making assumptions for the value of L (see equations (A24 & A28), determine the appropriate value of Q_i^{-1} from the slope. This approach makes no assumption about the relative contributions to the total attenuation from scattering versus intrinsic mechanisms. A minimum value of the mean free path may be calculated in which Q_i is taken as infinite. In this case L_{min} is calculated by application of equation (6) where Q_c or the apparent coda Q is substituted for Q_e.

3.4.4 *WEAK SCATTERING APPROACH: METHOD*

The inversion procedure is a rather simple two-dimensional linear least squares process. No constraints are imposed and the attenuation parameter is accepted as the "apparent coda Q"; after taking the logarithm of equation (4) (or equivalently (A28)), the resulting equation (A29) is linear in Q_c and the coda source factor.

The criteria employed in choosing the data for this study were different for the reflection data as compared to those for the microearthquake data; those for the microearthquake data were, in some respects, more straightforward. Only those events that were located by the USGS central California network were analyzed. As explained above (see section 3.2.1), due to equipment-related problems many recordings were not amenable to detailed analysis. In addition, S-wave coda were chosen based on uniformity of decay, or equivalently, the relative absence of coherent arrivals. Such coherent arrivals generally consisted of clear converted phases, although the possibility exists that multipathing may have been the origin for some of these apparently coherent arrivals within the coda (McLaughlin, 1982). Such coherent energy was, in some cases, present on seismograms at certain stations within an array yet absent on seismograms from neighboring stations for the same event. In fact, the general variation of coda generation efficiency between stations in close proximity was surprisingly evident. Figure (3-29)

shows two recordings of the same event at stations only 270 m apart in the Schmidt (Gabilan) array. The earthquake, an M_L 1.2 on 17 September 1982, was a shallow focus event, with a depth of 4.5 km according to the USGS. Even at a distance of only 6.6 km, significant variations in propagation path among the various scattered arrivals may be invoked to explain the observed differences in coda generation. Similar phenomena were noted by McLaughlin (1982) and Chouet (1979) in their investigations of microearthquake data in the same area. McLaughlin (1982) studied the spatial coherency of these waveforms across equally small arrays in addition to an analysis of polarizations. His detailed investigation of an aftershock to an M_L 4 event on the San Andreas fault 3 km away revealed considerable differences in character of both P-wave and S-wave coda. These differences were reflected both in $f-k$ analysis and in the polarization study. Chouet (1979) interpreted the observed variation in coda envelopes as due to temporal changes in either the source or the propagation region since in his study the earthquakes analyzed occurred over several months. Observations such as these are in some respects in contradiction with the accepted theory of coda generation as proposed by Aki and Chouet (1975). Although coda excitation is expected to be strongly dependent on the local geologic conditions at the receiver site (Aki, 1969), the observation of distinct differences in character at receiver sites characterized by essentially identical geologic conditions may not be anticipated (Aki, 1969; Aki and Chouet, 1975; Aki, 1982). On the other hand, even a modest level of experience with seismic reflection data would suggest that given the oft-observed trace-to-trace variations on most shot gathers one may certainly expect such variations in coda excitation over relatively small distances. Aki and Chouet (1975) also indicate that for $\Delta < 100$ km, the total duration of the combined coda (P and S) is independent of Δ or azimuth; this however is not consistent with the aforementioned variations. In spite of these inconsistencies it is believed that some useful information on the overall average spatial attenuation structure of the medium can be gleaned from the application of this method; however it is important to exercise some restraint in the interpretation of the results. In particular, the presence of coherent energy in the coda as well as potential contamination by surface wave energy (direct and scattered) must be

considered when interpreting the overall decay rates.

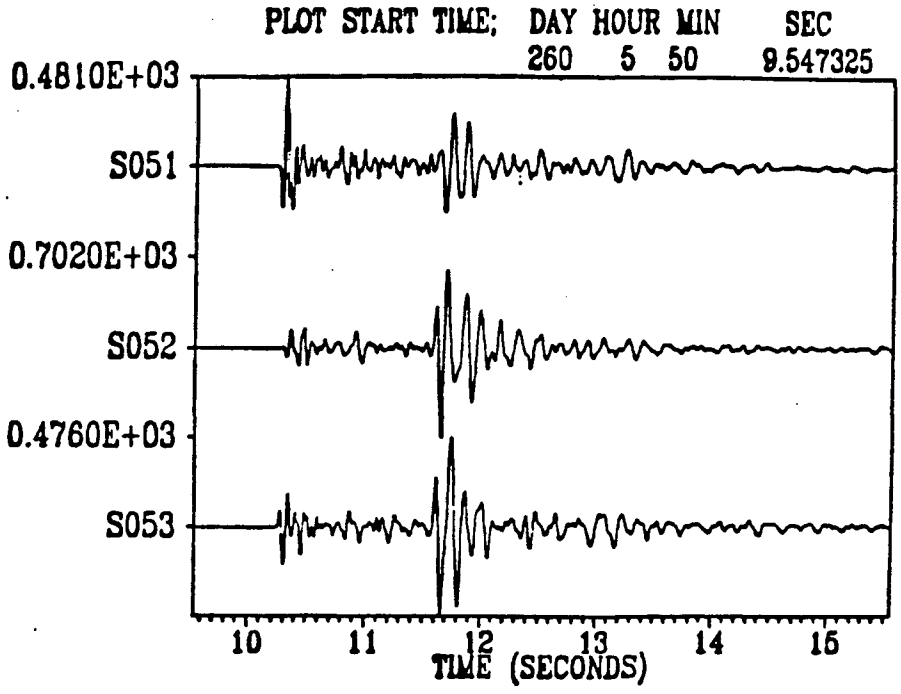

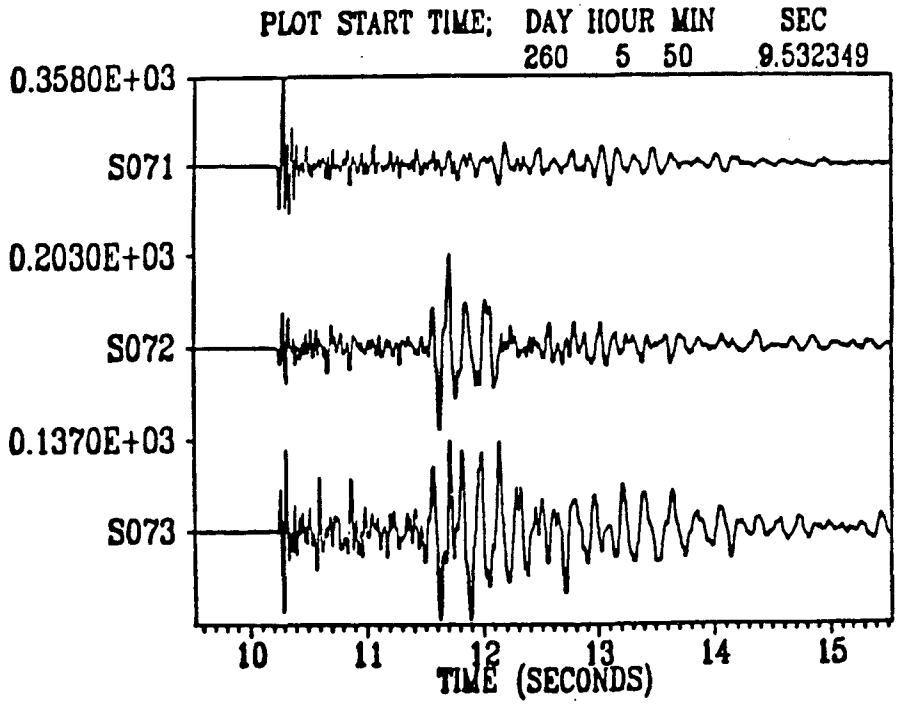

Figure (3-29) Two recordings of the same earthquake at stations separated by about 270 meters in the Schmidt array. USGS hypocentral parameters are given in the caption for Figure (3-9). Note the relative difference in coda intensity between the two stations on the horizontal components.

Whereas the presence of shear wave energy and surface wave contamination is minimized in the case of the stacked CDP seismogram, several other factors may hamper the investigation of coda decay. These factors fall into two distinct categories: the interpretational problems that bear upon the model of coda generation and various technical problems associated with the nature of the particular data set. The interpretational problems arise from the realization that even in plane-layered laterally homogeneous media one does not expect the normal moveout and stacking process to result in a simple reflection series; the presence of intrabed multiple reflections alone will 'smear' the primary reflections in an identical fashion as that of scattering from random inhomogeneities: pulse broadening, primary amplitude attenuation, and spectral shifts of energy will result (O'Doherty and Anstey, 1971; Schoenberger and Levin, 1974; Menke, et al., 1985). The presence of intrinsic loss mechanisms will compound these effects. These ambiguities are all related to the interpretation of the results, not to the actual application of the method to the reflection data. There are basically two very different technical limitations involved in the application of the coda method to the stacked reflection data. In media characterized by plane layers with a moderate degree of lateral inhomogeneity or containing a random but weak distribution of scattering sources the primary reflectors will, of course, appear smeared indicating the presence of coda. Application of the single scattering analysis to such media would seem to be appropriate; the only problem would be the potential limitation on coda duration by primary arrivals from a subsequent reflector and the attendant contamination of the coda of one primary with that of a previous one. On the other hand, for intensely fractured media or media with no discernible layering the identification of primary reflected energy in the stacked section would be the most limiting problem. Both of these two extremes are actually present in the Bickmore Canyon section. Identification of primary arrivals is relatively straightforward in the Gabilan portion to the west; windowing of the coda required some care to avoid the incorporation of primary coherent energy. The Franciscan portion to the east was plagued by a general absence of spatially coherent energy. These problems served only to limit the amount of data to which the attenuation analysis could be applied.

Following the identification of spatially coherent reflection energy, the seismograms constituting such a primary arrival were summed into one and a window up to 2 seconds in length was chosen; the peak of the primary is chosen as the onset time, t_o. (All windows in the CDP study were approximately two seconds in length.) Although not completely successful, it was hoped that by summing the various stacked seismograms, each composed of a number of traces itself, spurious coherence would be suppressed. These windows were all located in the same mid-crustal depth range, approximately 6 to 17 km. The average number of CDP seismograms summed into one was about eight, but varied from three to sixteen. The envelope of the coda energy, (a^2) in this window is then computed by adding the square of the amplitude values to the square of the Hilbert transforms of these values. Finally, the logarithms of these amplitudes are computed resulting essentially in the left side of equation (A29), and these are then fit in the least squares sense to obtain the apparent attenuation, Q_c and the relative value of the coda source term.

As mentioned previously, both the CDP reflection data and the microearthquake data were corrected for spherical divergence prior to inversion. (In fact the spreading correction precedes the envelope calculation.) This was accomplished in both cases within the DISCO program package (as was the Hilbert transformation). In the case of the summed reflection seismogram the correction consisted of multiplication by the product of a smoothly varying velocity model and the travel time at that sample value. Although the theoretical development outlined in the appendix assumed a constant density and velocity to characterize the medium, it was seen as an improvement to apply a correction using a smoothed version of the velocity model used to stack the data. If over the depth (i.e. temporal) range of these windows the velocity does not vary appreciably, the departure from the theory will not be significant. Moreover the use of a time-varying velocity model is considered to be a more accurate correction. In the case of the microearthquake data, the correction was time-varying in the sense that amplitudes prior to the S-wave arrival were multiplied by the product of the P-wave velocity appropriate for that region (e.g. Franciscan vs. Gabilan) and the transit time, whereas those arriving after the primary S-

wave were corrected according to the appropriate shear velocity.

Although various advanced analysis techniques were applied to the reflection data in several stages of the processing, as described above (see section 3.3), only the true-amplitude data were analyzed in the attenuation study; no deconvolution, migration, or gain control operations were applied to the data used in this analysis of amplitude decay. Of course a considerable degree of spatial averaging was involved due to the long (880 feet) geophone groups; however, as with the actual stacking process, the principal effect of this spatial averaging was to enhance the coherent vertically-propagating signal relative to the relatively incoherent or randomly scattered "noise". On the other hand, the operations listed above involve severe nonlinear manipulation of the data and were thus avoided for this 'true' amplitude analysis.

3.4.5 *SCATTERING ANALYSIS RESULTS: UNFILTERED DATA*

The procedure for identification and isolation of a window of coda energy is illustrated in Figure (3-30). Eight CDP seismograms, from 518 to 525, were summed into one after the identification of a "primary" reflector at about 2.5 seconds. This unfiltered composite seismogram is recorded in the western part of the San Andreas fault zone and is essentially the only useable data in this high noise, low reflectivity zone. In Figure (3-31) the corresponding energy envelope is plotted; note that the center CDP no. (522) is assigned to the summed coda as is the convention for all of the coda analyzed. Figure (3-32) shows the logarithm of the previous figure and the corresponding fit through the data according to equation (7), where the center frequency of the sweep ($f \approx 15\ Hz$) was arbitrarily assumed in the computation. (Note that the theoretical model assumes a delta function source and a monochromatic component of the source as a *primary* wave which interacts with the various scatterers. When analyzing filtered data, the center frequency of the filtered band is used in the calculation according to equation (7), however when analyzing unfiltered data an arbitrary determination of "center" frequency must be made. In the case of the Vibroseis data, the center frequency of the sweep is used; in the case of

the microearthquake data, the dominant frequency of the seismogram is used: 6 Hz for the Melendy data and 9 Hz for the Schmidt data.) The apparent or coda Q (Q_c) for these data is 40. The sharp and relatively large dips in the data in Figure (3-32) due to the logarithm are easily removed by a moving window smoothing function; although tests indicate that such an operation has little effect on the inversion results and thus no smoothing was applied in these computations. The coda Q values for eight unfiltered CDP seismogram windows are plotted in Figure (3-33) as a function of position along the 16 km profile. While there is a hint of a pattern of decreasing Q eastward it is not prominent. The Q values range from 40 for CDP 522 to 151 at the westernmost CDP 423 in the Gabilan granite. There is a paucity of useable data in the fault zone (near CDP 555) due to the general lack of spatially coherent reflectivity. (In fact this method may be more aptly suited to a more *regular* plane layered structure where primary reflectors and their coda are more clearly discernible.) The tendency for Q to decrease slightly eastward may be due to increased scattering losses attributable to the more heterogeneous structure of the Franciscan melange relative to the Gabilan granite of the western crust. Alternatively, the intrinsic "lossiness" of the media may be manifested in this trend. The incorporation of independently derived information regarding the scale lengths of inhomogeneity in these media, in addition to modeling of the scattering properties of such anomalies, would greatly aid in the delineation of these disparate attenuation mechanisms. On the other hand, it is important to realize that some ambiguity may always remain: Although Q_s will always be affected by the distribution of scale lengths of heterogeneity, a high intrinsic attenuation (i.e. low Q_i) will dominate over any degree of scattering attenuation, and thus it may be difficult to determine the partitioning of these two effects in certain degenerate cases. Furthermore there are many assumptions invoked in the weak scattering model that may not be strictly appropriate. An important test of the method should include an application to more planely layered sections. This is especially important in the application to CDP data from inhomogeneous media because the entire rationale for using the stacked data rests on the assumption that the stacking process will yield a one dimensional seismogram representing the impulse response of the medium to a

point source at the surface midpoint. The ability to recognize spatially coherent primary reflections is but one, albeit important, precondition for applying this method. One must be wary of any peaks in the coda wave train that may represent quasi-coherent scattered energy from dipping or otherwise irregular interfaces. A versatile and effective pre-stack migration algorithm would greatly aid in the application of this model to such data. It is interesting that the presence of spurious coherent energy plagues the application of the single scattering theory to both reflection data and microearthquake data, although such coherence is attributed to different causes in the two forms of data. On the other hand, one may generally classify such spurious coherence as some form or other of multi-pathing phenomena, thus providing a reasonable and common explanation for both cases.

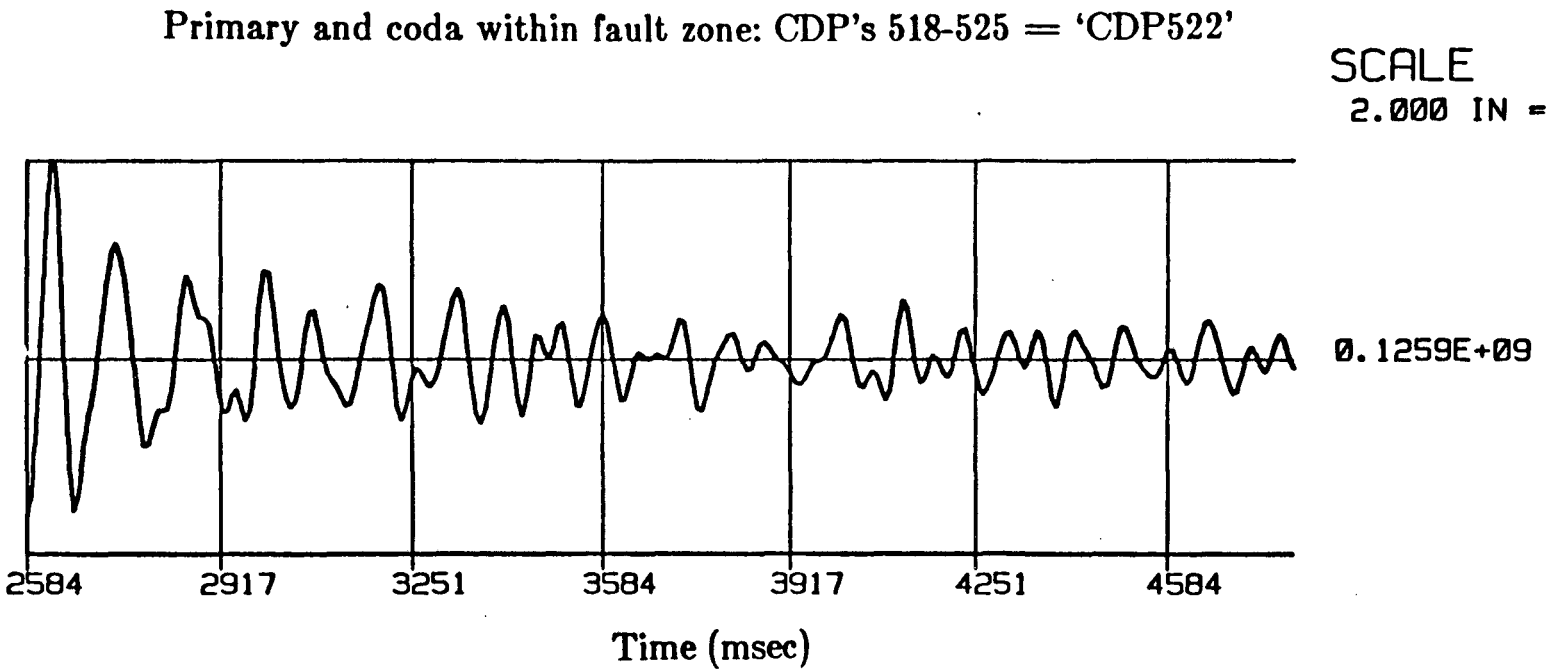

Figure (3-30) Coda window for CDP 522 within the western part of the San Andreas fault zone. This coda is actually a composite of the coda for eight CDP's centered on #522.

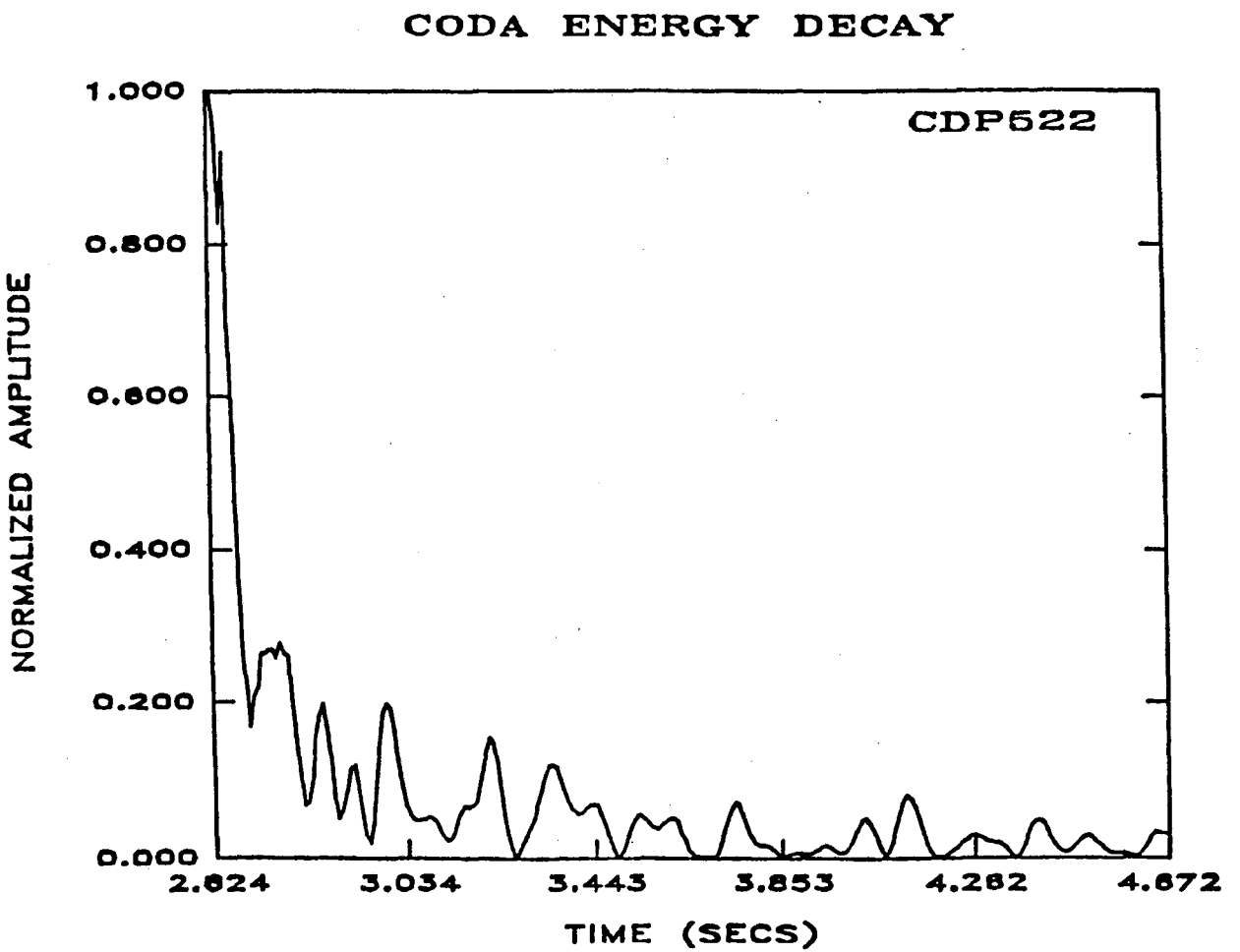

Figure (3-31) The corresponding energy envelope for the previous composite coda; it is calculated by addition of the squared seismogram to its squared Hilbert transform. For further discussion, see the Appendix for this chapter.

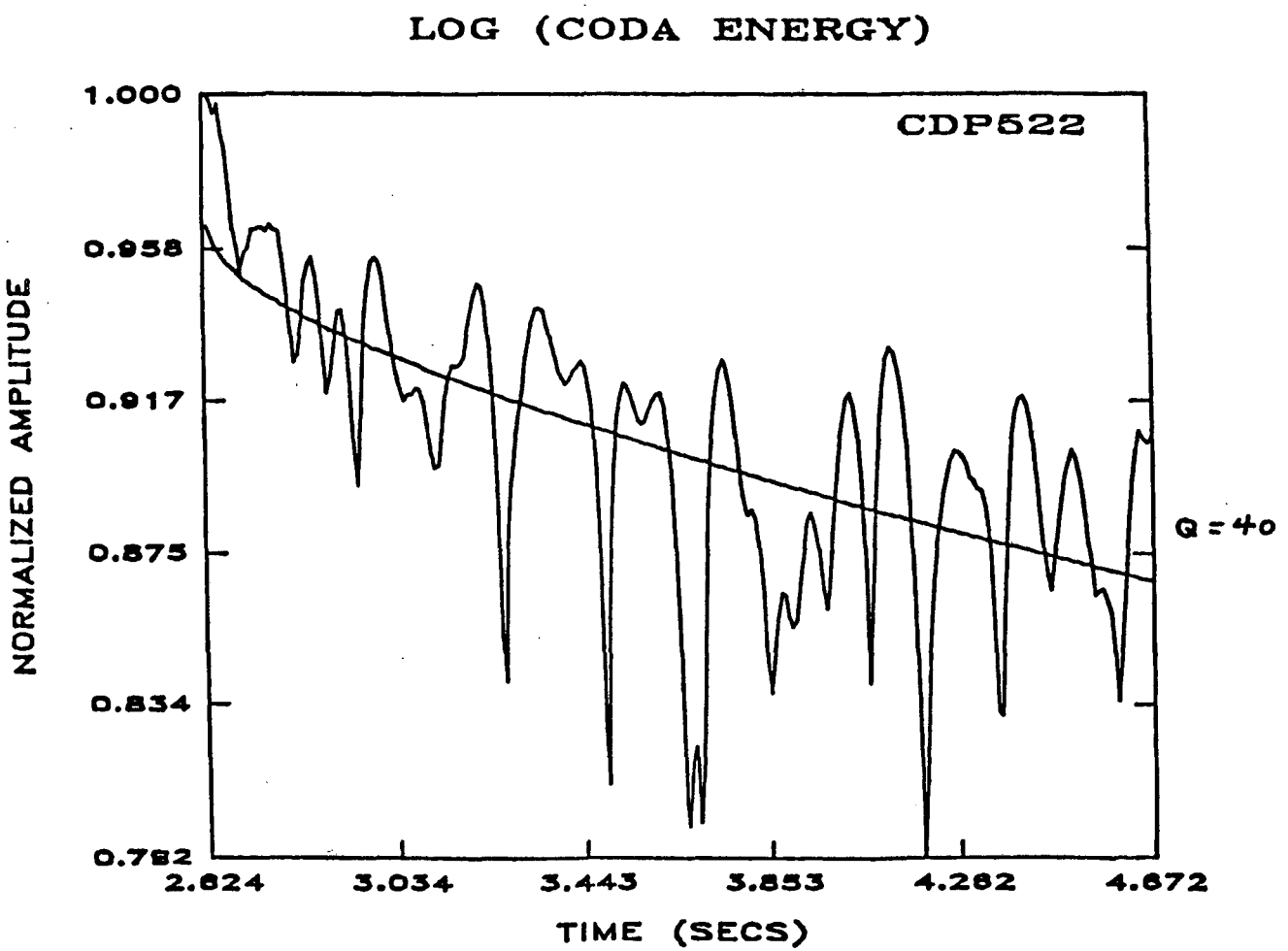

Figure (3-32) Logarithm of the previous figure and the least squares fit through it according to equation (A29) of the Appendix. An apparent Q of 40 as indicated at right is obtained by the fit.

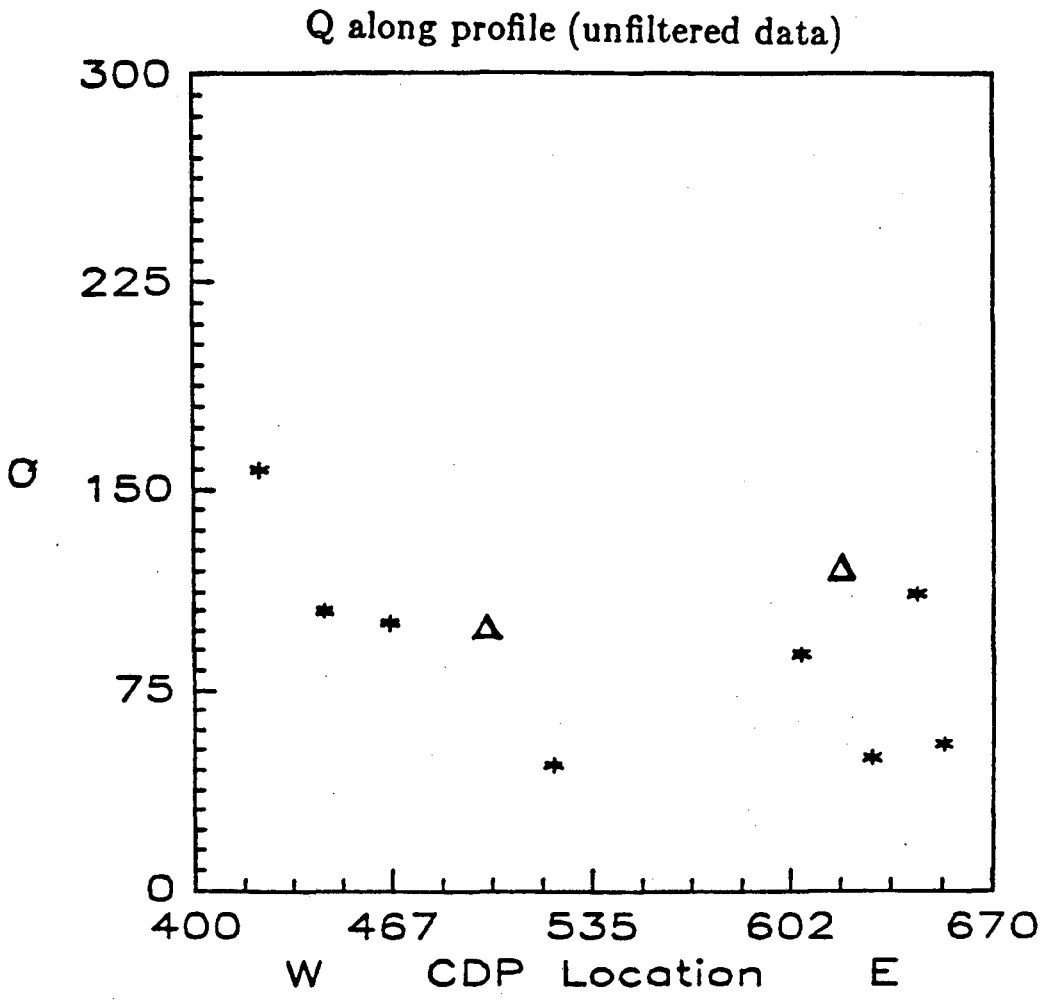

Figure (3-33) Pattern of apparent Q values across the profile of the 1978 reflection survey for the unfiltered data from the analysis of coda decay according to the weak scattering model. Asterisks correspond to the CDP data; the two triangles represent the average of the results for the unfiltered microearthquake coda.

Although in some respects the application of the single scattering method to microearthquake data is more straightforward (e.g. no difficulty exists in discerning primary arrivals and their coda), some care is required in choosing data that are not contaminated by surface wave energy or clear coherent arrivals due either to structural factors or to conversions. Furthermore, relatively few of the events recorded met all the requirements of data length and quality, as discussed above. Figures (3-7) through (3-10) show the full three component seismograms from which the four S-coda were chosen. The two Franciscan seismograms were the middle components of Figures (3-7) and (3-8); the two Gabilan seismograms were the middle components of Figures (3-9) and (3-10).

The most striking difference between the S-coda which propagated through the Franciscan and that which propagated through the Gabilan is manifested in the relative frequency content. As with the (P-wave) reflection data, the Franciscan microearthquake coda is markedly depleted in the higher frequencies relative to the Gabilan coda. This can be readily observed in these figures but is even more apparent in their spectra. Figures (3-34) and (3-35) show the spectra for the four S-coda used in the decay analysis. These coda were initially corrected for the instrument response and then high-pass filtered above about 1 Hz. (The choice of the low frequency cutoff in the filter was chosen based on observation of the instrument-corrected spectra; due to the low seismometer response below about 2 Hz the and recorder's limited dynamic range, the spectra when corrected produced an exaggerated high amplitude trend at these low frequencies (see Figure (3-4). The corner frequencies for the Melendy data average about 2.8 Hz whereas those for the Schmidt data average about 7.5 Hz. Although it is entirely possible that the differences in corner frequencies may be completely explained by differing source characteristics, it is interesting that this robust spectral contrast is very common, persisting throughout the data from these arrays. Actually, the decay rate of the high frequencies may be a more accurate indicator of crustal scattering properties than the corner frequencies. One possible application of this idea would be to examine the time rate of change of the spectral decay slope for increasing lengths of the coda window. For a given seismogram (i.e. for a given source-receiver

path), this rate of change of specral decay is expected to indicate the nature of the low-pass filtering inherent in the scattering attenuation characteristics of the medium. On the other hand, the depletion of high frequencies in waves propagating through the Franciscan is not expected to be manifested in the time domain inversion for apparent Q, although the dependence of Q on frequency should reflect this effect.

The resulting Q_c values for the microearthquake study are indicated in the composite figure for the CDP analysis as triangles (see Figure 3-33). Although generally of similar magnitude, the Q values of the western Schmidt data are somewhat lower than those of the eastern Melendy data, in contrast to the CDP results; however it should be noted that in both the acoustic and shear wave cases, the tendency for Q to decrease or increase eastward, respectively, is rather weak. As will be examined below there is a more unambiguous trend between the eastern and western crusts in terms of the dependence of the quality factor on frequency, in contrast to the actual Q_c results.

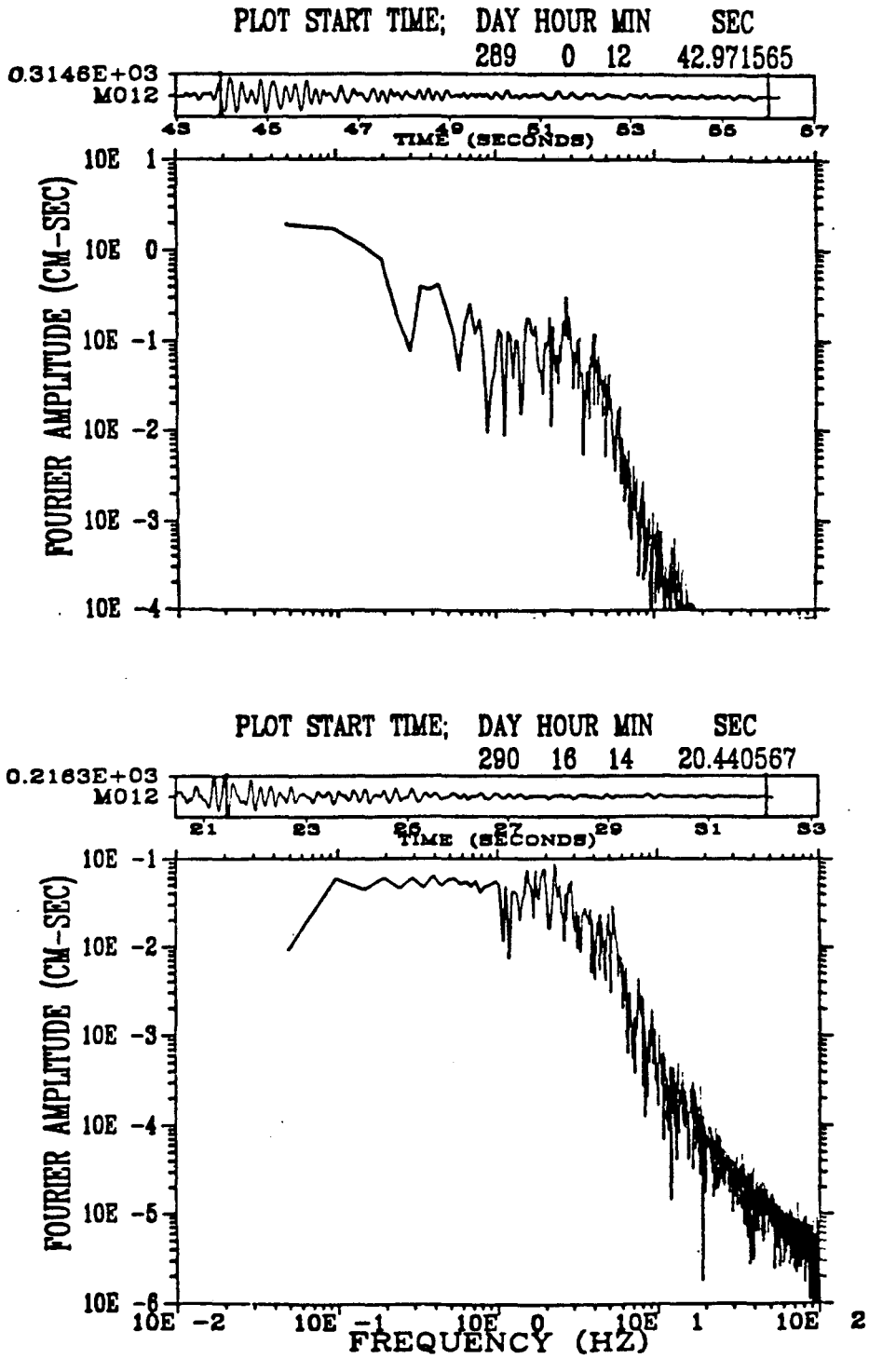

Figure (3-34) Fourier amplitude spectra for coda windows used in the Q study for the microearthquake data recorded at the Melendy array, east of the San Andreas fault. The time windows over which these spectra are computed are shown at the top of each spectra.

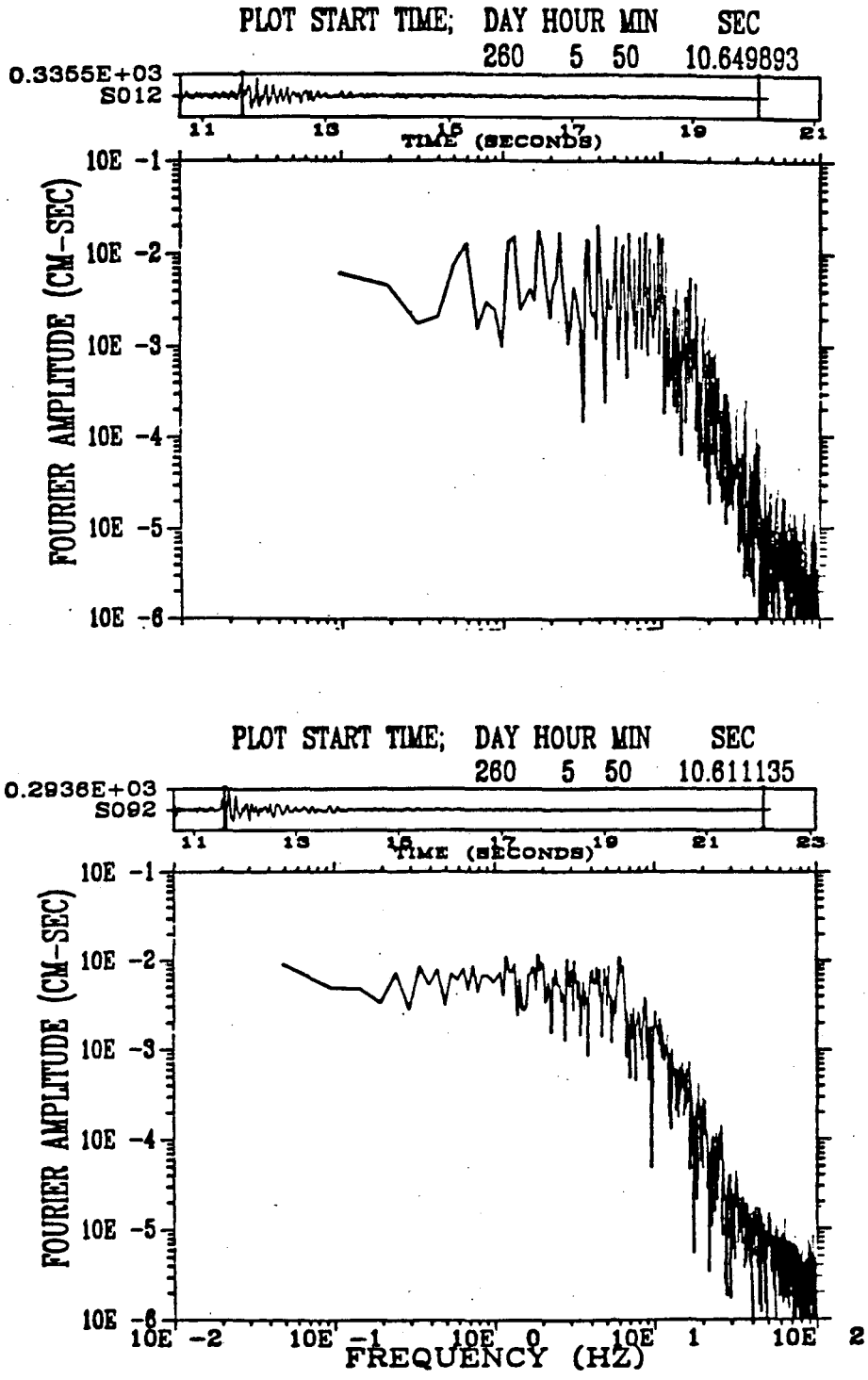

Figure 3-35) Fourier amplitude spectra for coda windows used in the Q study for the microearthquake data recorded at the Schmidt array, west of the San Andreas fault. The time windows over which these spectra are computed are shown at the top of each spectra.

3.4.6 *SCATTERING ANALYSIS RESULTS: FILTERED DATA*

This single scattering inversion scheme was applied to the CDP data over four narrow bandwidths after application of appropriate Butterworth filters. The filters were carefully designed to avoid the introduction of numerical artifacts associated with such narrow band filtering and in general the large taper zones of the filters overlapped. The center frequency of each band was used in the calculation of the attenuation coefficient: The center frequencies 9, 12, 18, and 21 Hz encompassed the entire sweep range 6 - 24 Hz. In all cases the apparent Q values increased smoothly with increasing frequency. What is especially interesting is that the degree of frequency dependence of the apparent Q values differs consistently between those computed from data on the eastern half of the profile and those from the granitic side.

The microearthquake seismograms were filtered over five narrow bands with center frequencies ranging from 3 to 24 Hz. The filters were designed in much the same manner as with the reflection data; that is, the decay rates were chosen to be rather broad to prevent the incorporation of any artificial ringing contamination.

As noted above, it has become common to fit the results of these scattering attenuation analyses to a function of the form:

$$Q = Q_o f^n \tag{7}$$

The degree of frequency dependence is embodied in the power of the frequency: typical values are generally between 0.1 and about 1.5 for seismic data in the range 0.5 to about 25 Hz. There are indications that this power, n , may be a useful parameter in attenuation studies as it may serve as an indicator of the scattering attenuation regime for many different tectonic settings. Numerous studies utilizing the "coda Q" method described above have been carried out recently using earthquake and microearthquake data and a consistent pattern has been emerging for the body wave data above about 0.5 Hz. In addition to the variations of the Q_o parameter in which there are the rather expected lower values for tectonically active regions relative to the more

quiescent regions such as continental shields and cratons (see Singh and Herrmann, (1983) for a summary of results within the continental U.S.), there appears to be a pattern of higher values of the parameter n (i.e. Q_c is more strongly dependent on frequency) for tectonic regimes characterized by active subduction, volcanism, and plate convergence. Stable tectonic zones such as shields and continental interiors tend to have lower values indicating that in these regions the dependence of the apparent quality factor on frequency is noticeably less over this range of frequencies (approximately 0.5 to 25 Hz). Although not exactly using the same method as the coda Q method Singh and Herrmann (1983) have tabulated values of Q_o and n within the entire continental U.S. and report the highest values of n in the western or Pacific coast region ($n \approx 0.4 - 0.6$) and the lowest values in the central and south-central U.S. ($n \approx 0.1 - 0.3$); eastern and northeastern U.S. are characterized by intermediate values. However more detailed studies in specific regions using the coda Q method suggest that there may be areas within the continental U.S. in which both the attenuation (Q_o^{-1}) and the n parameter are even higher: Pulli (1984) found values of n as high as 0.95 in New England for lapse times less than 100 seconds within the coda, although for lapse times greater than this the values for n were as low as 0.4 over the spectral range $0.75 < f_{Hz} < 10$. Following up on the analysis by Pulli (1984), Agnew, et al. (1986) found values of n as high as 1.11 for short lapse times and 0.50 for longer lapse times in the same northeastern region. Similarly, Rhea (1984) reports values of n as high as 0.94 across the South Carolina coastal plain over the range $2. < f_{Hz} < 10.$ by the same method. A relatively high value of 0.87 for n is reported in an investigation of microearthquakes in northern Baja California by Rebollar, et al. (1985). This pattern for Q_o and n is also apparent in results of investigations outside the coterminous U.S. Consistently high values of n are apparent for subduction zones. Analysis of 32 aftershocks of the Petatlan (14 March 1979, $M_s = 7.6$) earthquake in the Middle American trench of southern Mexico revealed a value of n of 0.87 (Rodriguez, 1983). In the Adak Islands region of the active Aleutian subduction zone Scherbaum and Kisslinger (1985) report values of n of 1.05. In Kanto, Japan and Stone Canyon, central California Aki and Chouet (1975) and Aki (1980)

report values of n of between 0.6 and 0.8. These results are of particular interest to this paper since both the reflection data and the microearthquake data used here are essentially in the same region of the San Andreas fault zone as Stone Canyon.

Several studies in Italy indicate a regional trend in the parameter values: the highest values ($n = 1.1$ are reported in the northeastern Friuli region by Console and Rovelli (1981); the lowest values ($n = 0.45$) are found in the Aeolian Islands of southern Italy by Del Pezzo, et al. (1983) and intermediate values ($n = 0.6$) are reported in central Italy in the Umbria region by Del Pezzo and Zollo (1984). Studies in Asia and India manifest similar trends: Roecker, et al. (1982) interpreted their results for different lapse times in the coda to represent variations of the parameter values with depth in the Hindu Kush region of Afghanistan. Based on this assumption they reported values of n of 1.0 for shallow depths and 0.5 for deeper paths. In the Indian subcontinent a general trend is reported in which the more geologically complex and seismically active northeastern zones are characterized by values of 0.4 - 0.6 whereas the more stable southern parts of India show values of 0.2 - 0.3 (John and Nuttli, 1983). In China, Chen, et al. (1984) report higher values of n (up to 0.4) for the more seismically active Yunnan province in southern China than for the more stable Beijing region to the north ($n \approx 0.0$). Only one study of the frequency dependence of the apparent quality factor is reported for the oceanic lithosphere: Jin, et al. (1985) studied S-coda from 22 WWSSN records of island arc events at regional distances by the coda Q method and found that for the younger oceanic lithosphere (e.g. near Iceland), $n \approx 0.61$ whereas for the older oceanic lithosphere (e.g. near Guam), $n \approx 0.46$. They found that in general the Q values were proportional to, and the n values inversely proportional to the age of the lithosphere; in addition they noted some convergence of the Qs at the higher (i.e. 4 Hz) frequencies.

In the vast majority of coda Q investigations the value of n has been determined for a given region; it is only in a few cases that a detailed study has been done to delineate the actual variation of n within a given region. In the present study, variations of coda Q and n are investigated over a rather small geographic area although across a major plate boundary. Such

detailed analysis is allowed, in part, by the extension of the coda Q method to CDP reflection data. The results appear to be generally consistent with the aforementioned pattern emerging from other such studies: n is consistently larger in the more heterogeneous Franciscan than in the (presumably) more homogeneous Gabilan batholithic crust for both acoustic and shear wave energy. Furthermore the results reported here for n and, in general, for Q_c, for this region of central California are consistent with those reported by Aki and Chouet (1975).

If the degree of frequency dependence of the quality factor is an indication of the degree to which scattering interactions dominate the attenuation process, then these results suggest that for the wavelengths involved here scattering by heterogeneities in the Franciscan crust is more prominent than in the Gabilan granitic crust and, by extension, the attenuation is dominated by the scattering more so in the Franciscan. However the role of intrinsic dissipation must be considered; it is not at all clear how the combined effects of intrinsic and scattering attenuation can be decomposed from such results. The consistency of these results with the aforementioned pattern suggests that for the range of seismic frequencies (from approximately 0.5 Hz to 25 Hz) scattering effects may be more important in more heterogeneous and geologically active regions than in more homogeneous and/or quiescent regions.

Table (2) shows the results of fits of the P-coda decay rates to equation (7) for the CDP reflection data and those of the S-coda decay rates for the microearthquake study; included are the standard deviations of the least squares fit for each of the two parameters. (The data from CDP 645 were omitted because of very large variances.) The inversion procedure was similar to that described above for the coda decay rates: The equation was linearized by taking the logarithm and a simple two dimensional linear least squares process obtained the parameters Q_o and n. While the values of n are within the range given by other investigators the values of Q_o, are unacceptably low. If we interpret this parameter as denoting the Q at 1 Hz, it is especially disturbing; however, this physical meaning may not be accurate simply on the basis of a dimensional analysis (i.e., the units of Q_o are actually Hz^{-1}). Nevertheless, assuming that Q_o does indeed represent the apparent Q value extrapolated to 1 Hz, we may make the following

comments: Although the depth range of these time windows is mid-crustal (i.e. 6 to 17 km) and the Q values are expected to be low in this tectonic regime, these values are much too low to be consistent with numerous observations of local, regional and teleseismic P-waves. Indeed, such low values at 1 Hz would virtually preclude the observation of P-waves from all but the largest earthquakes at regional distances. Hence, one may suppose that this functional form for the frequency dependence of Q is either not applicable or is only accurate for higher frequencies and thus extrapolation to 1 Hz may not be warranted. On the other hand, note that if the values of n are small the frequency dependence weakens and the value of Q at 1 Hz is essentially the same as that at higher frequencies (i.e. up to approximately 25 Hz). There is certainly no useful or reliable seismic information at frequencies below the spectral bands of the respective sources and their corresponding receivers; that is, below about 6 Hz for the reflection data (recall that the sweep range was 6 - 24 Hz) and about 3.0 Hz for the microearthquake data (the response of the 4.5 Hz geophone is down about 10 db at 3.0 Hz) there are essentially no useful data. Hence the value of any parameter derived from such data corresponding to these low frequencies would constitute an extapolation from results within the respective spectral bands. The results for Q_o suggest that such an extrapolation may not be appropriate. Indeed, extrapolation of this functional form for the frequency dependence of the observed Q to surface wave frequencies would be especially unreasonable; the resulting low values of Q would contradict a wealth of data at periods of about 20 seconds, a period at which surface wave propagation appears to be quite efficient. Although at this point it remains unclear to what extent this functional form may be applicable to either data set, and although the extrapolated values of Q at 1 Hz are indeed too low, the consistency of the dependence of Q on frequency as manifested in the values of the n parameter is accepted as an indication of the usefulness of these results.

Roecker, et al. (1982), Pulli (1984), and Agnew (1986) have all reported a general increase in the value of n as a function of lapse time within the coda and have asserted that this corresponds to a tendency of Q_c to be less frequency-dependent as the depth of the sampled medium increases. Similarly, larger values of Q_o for the coda decay at larger lapse times have

been explained along the same line of reasoning (Rautian and Khalturin, 1978). Gao, et al. (1983) have offered an alternative hypothesis: they suggest that in examining coda to large lapse times after the primary S-wave arrival one must include the effects of multiple scattering unless either the intrinsic attenuation predominates or the medium under investigation is indeed a very weakly scattering medium. In other cases the neglect of this multiple scattering will lead to an over-estimation of the apparent Q by a factor of 1.4. Hence the apparent change in coda decay as a function of lapse time as noted by these aforementioned studies may not be due to depth-dependent variations in the parameter values but may reflect the contribution to the wave train of multiply scattered arrivals. Of course, it is important to realize that in these studies of coda decay based on the weak scattering theory, it is self consistent to assume that variations of decay profile with lapse time are due to depth-dependent properties rather than multiple scattering.

In order to draw any definitive conclusions about the frequency dependence of Q over this band and in this region, much more data would have to be analyzed. This is especially important given the many possible sources of contamination to individual coda from coherent (converted) energy and surface waves as well as from generally low signal-to-noise levels. Nonetheless, the results given in Table (2) indicate that for both the P-wave reflection data and the S-wave microearthquake data, Q_o is uniformly greater and n uniformly lower in the western Gabilan region than in the Franciscan region. This may be intuitively gratifying in the sense that the Franciscan is known to be a more heterogeneous medium and may scatter elastic waves more efficiently. Alternatively, the result may simply indicate that the Franciscan is a more intrinsically *lossy* medium than the Gabilan, and that the combination of the active intrinsic dissipation mechanism(s) and the scattering interactions is reflected in the greater dependence on frequency.

3.4.7 *MEAN FREE PATH*

The weak scattering formalism assumes that the mean free path is large with respect to the source-receiver distance. A value for the minimum mean free path may be calculated by assuming the extreme case of no intrinsic attenuation, even though this would seem to violate the weak scattering assumption. Such a minimum mean free path, L_{min} represents the upper bound to the scattering attenuation or Q_s^{-1} as given in equation (6). Similar analyses have been carried out by other investigators and, as in the case of the n parameter discussed above, may be useful in characterization of the general heterogeneity or scattering environment of various tectonic regimes. Sato (1978) found values of L (not necessarily minima) of about 100 km in the Kanto district of Japan. In his analysis of coda decay profiles as characterized by the lapse time, Pulli (1984) found values of L_{min} of about 80 km for the early part of the coda and values of about 400 km for the study of larger lapse times in the coda. As discussed above he attributed these differences to depth-dependent variations. In addition Pulli noted a $1/f$ variation of L_{min} for the "deeper" coda and a frequency independent L_{min} for the "shallow" coda. For northern Baja California, Rebollar, et al. (1985) reported values of L_{min} similar to those found in this investigation: Using the same method they determined values of 15.7 ± 2 km. As is shown in Tables (3b, 3c) these results for Baja California are analogous to the microearthquake results found here for central California, although the latter values are somewhat lower. Tables (3a, 3b) show the values of the minimum mean free paths for the filtered CDP and microearthquake data, respectively. The composite results are given in Table (3c). As indicated in these tables, the minimum mean free paths are calculated from equation (6) according to the assumption of an elastic heterogeneous environment. In the calculation of L_{min} for the CDP data mid-crustal velocities of 6.0, 4.7, and 4.9 km/sec are assumed for the Gabilan, San Andreas fault zone, and Franciscan media, respectively. For acoustic wave energy, the average L_{min} for the western granitic crust is approximately 7.4 km whereas for the Franciscan crust the average is 3.4 km. In the calculation of L_{min} for the microearthquake data, mid-crustal velocities of 3.55 and 3.30 km/sec were assumed for the Gabilan and Diablo crusts, respectively; the shear

velocity chosen for the Gabilan crust was based on the model of Healy and Peake (1975), whereas V_s for the Franciscan medium was taken from the work of Levander and Kovach (1981). For shear wave energy, the average L_{min} for the granitic medium is 6.4 km, less than that for the Franciscan medium (9.7 km). This general difference between the shear and acoustic values of L_{min} across these major crustal blocks may indicate fundamental differences between the scattering environments for shear versus acoustic energy. However, such a conclusion may be premature; the contrast in these results may not be due to the actual material properties of the propagation media. Certainly the contrast in L_{min} between the Melendy and Schmidt microearthquake data can be traced to that of the Q_s (i.e. Q_c) values. That is, the lower Q_c of the Schmidt data results in lower L_{min} values. It is probably too simplistic to conclude that the scattering and attenuation of shear wave energy is greater in the Gabilan than in the Franciscan. Unlike the CDP data, the source functions of the microearthquakes may be very different from event to event and there are far fewer microearthquakes than (controlled) vibrator sources in the reflection survey. Although some caution is advised in assuming that the source spectrum of the vibrator is invariant along the entire 18 km profile, the variation is not expected to be significant here (Quaternary sediments blanket the entire region--see Chapter 2). Many more microearthquake events would have to be analyzed to enable any statistically definitive conclusions to be drawn. It is, at present, rather difficult to explain why the results for Q_s (i.e. Q_c) should be so different for the shear wave data relative to the acoustic data, especially in light of the wealth of results from this seismic band in the literature which appear to suggest otherwise.

While not directly related these values for the L_{min} are of the same order as the anticipated scale lengths of heterogeneity, at least for the Franciscan medium. As noted above and in Chapter 2, inferences from geologic mapping suggest that discontinuous lenses and dikes up to 3 km in length are expected to be somewhat common throughout the Diablo Range. In addition, large (tabular) metagraywacke units have been *observed* to be greater than 7 km in length within the Franciscan. The similarity of the magnitudes of the length scale of heterogeneity

and the calculated L_{min} may be completely fortuitous. In order to characterize adequately a scattering medium, one must determine both the mean free path and the correlation scale length of inhomogeneity, in addition to the actual impedance contrasts involved in the scattering process. Several methods exist for determining the scale lengths of heterogeneity on a statistical basis. These methods are generally based on the work of Chernov (1960) and involve certain correlation techniques. Recent modeling using finite difference calculations have been carried out by Frankel and Clayton (1986) and suggest that a self-similar medium (i.e. one characterized by a Von Karman correlation function) may be appropriate for this seismic frequency band. To date, there have been few successful applications of the technique to actual seismic data, however it appears that the approach of Frankel and Clayton (1986) is amenable to some sort of waveform analysis.

3.5 SUMMARY AND DISCUSSION

Interpretation of an 18 km long seismic reflection profile crossing the San Andreas fault in central California reveals important information about the velocity and attenuation characteristics of the fault zone and particularly of the bounding crustal blocks. The western granitic crust is characterized by a significant degree of spatially coherent reflectivity indicative of several interesting structural features. This is in marked contrast to the eastern Franciscan crustal block which is generally devoid of any clear structure (see Figure 3-6, for example). The most prominent feature apparent in the granitic portion of the sections is the Moho reflection at a two-way reflection time of about 7 - 8 seconds; the laminated appearance of this contact is consistent with numerous other seismic reflection studies from varying tectonic regimes. It has been modeled as a cyclic series of thin layers by Clowes and Kanasewich (1970) with layers approximately 200 m thick; speculation as to the geologic cause of such a structure is not definitive at this point and more careful modeling is needed to refine our understanding of its seismic (see Chapter 4) and geologic character. A hint of a Moho reflection in the Franciscan crust appears in the migrated sections (see Figures 3-18 and 3-19) at about the same reflection time, but its meaning is inconclusive. The apparent eastward dip of the Moho reflection in the granitic crust is probably due to a 'velocity push-down' effect due primarily to the low-velocity trough of the fault zone (see Figure 3-20) and possibly to a low-velocity wedge extending westward at mid-crustal depth from the fault (Feng and McEvilly, 1983). A third structural feature prominent in these sections is evident at about 3 seconds in the western crust and is believed to represent the basal contact of the granitic batholith. This contact may indicate the boundary between the granitic upper crust and a Franciscan lower crust, Stewart, 1968) although this hypothesis is disputed by Walter and Mooney (1982), who favor a gneissic composition for the lower crust. In any case, some contrast in impedance is evident at this depth of about ten kilometers.

Finally, the velocity model obtained by analysis of the reflection data is consistent with the trend of previous investigations of earthquake data (Figures 3-20, 3-22). This model shows

the prominent low-velocity trough associated with the San Andreas fault zone bounded by the higher velocity Gabilan and Diablo crusts. The data analysis techniques used in the processing of this data were not sufficient to resolve the low-velocity wedge proposed by Feng and McEvilly (1983) and extending westward at mid-crustal depths.

In an attempt to explain the observed contrast in reflectivity across the fault as well as to understand the attenuation characteristics and heterogeneity of the medium, two extreme scattering models of P-wave propagation have been applied to these data, leading to essentially similar results: Both a diffusion approach and a weak scattering model show that although the apparent attenuation (Q^{-1}) is greater in the Franciscan portion of the section it is only slightly greater than that of the granitic crust. The apparent Qs average about 115 in the western crust and about 70 in the eastern crust with a Q of 40 for the fault zone itself. These values of Q for the unfiltered data are consistent with those of a similar analysis of S-wave coda from a microearthquake data set in the region; however, unlike the CDP data, the S-wave coda show a somewhat higher Q for the Franciscan medium (e.g., $Q = 114$) than for the S-coda recorded in the Gabilan granite to the west (e.g., $Q = 92$). This may be due to a different attenuation mechanism for the shear wave data than for the P-wave data, but this explanation requires further analysis; a more likely explanation may be that the coda method is not precise enough for such a conclusion, particularly for such a small data set. It has been shown in the investigation of the microearthquake data that significant variations in coda intensity may exist at neighboring receiver sites for a common source. Such variations would further complicate the interpretation of the attenuation results. The tentative conclusion is that in order to employ this method of Q determination a significantly large data set is required; the attendant averaging afforded by such a large data set may help to smooth these local variations and thus to aid in the determination of an unambiguous profile of the average crustal attenuation. In any case, it is noted that these Q values, for both the P and S-wave data, are consistent with those obtained by Aki and Chouet (1975) in the same general region, although this consistency of absolute Q values is greater at the lower frequencies (the range of frequencies used in the study

by Aki and Chouet ranged from about 1 Hz to 25 Hz); while their values for the apparent Q range from a low of 70 at 1 Hz to almost 1000 at 20 Hz, those computed in this study range from a low of 45 at 3 Hz to a high of 593 at 24 Hz for the microearthquake data).

In contrast to the ambiguity regarding the absolute values of the apparent Q parameter, analysis of the filtered data for each data set reveals a consistent difference in the degree of frequency dependence of the apparent Q between the bounding crusts of the fault. (Results within the fault zone itself are relatively lacking owing primarily to the lack of discernible structure in this portion of the stacked reflection section.) Consistent with numerous other studies of body waves at frequencies above about 0.5 Hz (see text–section 3.4.6 for a summary of published results) the apparent Q values were found in all cases to increase with frequency; of perhaps greater significance is the trend toward greater frequency dependence in the "Franciscan" data relative to the "granitic" data (P and S-waves). This may be part of an emerging pattern for body wave data; whereas several studies have detailed the relation between the degree of frequency dependence of Q and the degree of heterogeneity or tectonic activity, very few studies have sought to determine the fine structure associated with the comparison of this frequency dependence over a small regional area (Chen, et al., 1984; Rhea, 1984). The results of these studies are, in general, consistent with the emerging pattern suggesting that there is a greater degree of frequency dependence for heterogeneous and/or tectonically active regions than for more homogeneous and/or quiescent regions.

The observed frequency dependence of the apparent Q for this study as well as for the numerous other studies cited here for frequencies spanning all seismic data is consistent with the theoretical predictions for a Q derived from a model of weak scattering (see Figures 3-26, 3-27). In light of the fact that laboratory measurements of (intrinsic) attenuation overwhelmingly suggest that Q is independent of frequency over a very large spectral range, it may be that the observed functional form of the frequency dependence of the apparent Q is dominated by scattering. Although the presence of water and other fluids in cracks and pores would lead to an intrinsic absorption process that is frequency dependent (by a functional form similar to that

observed over the entire range of seismic data), in contrast to that predicted for a frictional sliding mechanism, any reasonable range of crack geometries would tend to smear the frequency dependence of Q_i. Whereas both frictional sliding and viscous relaxation due to the presence of fluid-filled cracks are believed to be relevant mechanisms for the crust, and whereas a range of crack geometries is a reasonably plausible condition for the crust, it is suggested that the observed frequency dependence for the attenuation parameter is due to the (weak) scattering process. Further investigation of the observed attenuation is surely needed; it is recommended that such investigations be carried out by a variety of techniques, in addition to the "coda-Q" method used here so as to yield a relatively unambiguous (i.e., not 'method-dependent') picture of the attenuation of seismic data.

One perplexing result of this difference in frequency dependence between the two bounding crusts in this region of the San Andreas fault relates to the observed contrast in spectral content between data from the two media. For both P and S-wave data, and for either Vibroseis or microearthquake sources, it has been consistently observed that the high frequencies are depleted in the Franciscan relative to that of waves propagating in the western granitic medium. This is not consistent with the result that Q is nearly proportional to frequency within the Franciscan crust because, given an exponential attenuation mechanism, a functional form for Q such as that given by equation (7) (see section 3.4.6) implies a frequency *independent* attenuation if n is nearly unity. This discrepancy may be due to the difference in the actual source functions associated with the Vibroseis source on the different shallow crustal material across the fault. Given the different soil properties along the profile it is probably unreasonable to assume that the same frequency content of the Vibroseis source sweep is actually input into the earth below the upper soil-baseplate coupling layer. As indicated at the end of section 3.4.3 an attempt to determine the actual source input spectrum using down-hole geophones along the profile was attempted without success; nevertheless it would be interesting to re-examine selected traces of the shot-gathers from certain points along the profile in such a way as to more accurately determine the exact spectral characteristics of the input source energy.

One interesting hypothesis which may be proposed to explain the observed variation in frequency dependence of Q is that this observed frequency dependence, as parameterized by the exponent n in equation (7) is dominated by surface wave dispersion in scattered surface wave energy converted by and scattered from topography at the receiver site; in such a scheme the higher frequency components of the surface waves would be characterized by slower velocities and would thus 'linger' in the coda, giving a higher Q. This effect would be more pronounced for the tectonically active or heterogeneous regions than for the stable, more homogeneous regions thus giving a lower n value. This hypothesis requires considerably more investigation in both a theoretical and observational sense.

The results of this investigation of both velocity and attenuation structure are consistent with the trends of other crustal studies in the same region (in the case of velocity) and in numerous other regions (in terms of attenuation).

TABLE 1: Field Parameters

PARAMETER NAME	VALUE or DESCRIPTION
Sweep range (Hz)	24 - 6
Sweep time (seconds)	32
Listening time (seconds)	48
Geophone	GSC 20D (8 Hz, digital)
Amplifier	Sercel 338 B
Correlator	Mandrel DC 2400
No. channels	48
Array length (feet)	880
Group interval (feet)	440
Geophones/group	36
Sample rate (msecs)	8
Range of offsets (feet)	[2200, 22880]
Geometry pattern	split-spread & offend

TABLE 2: Q(f) Results

$$Q = Q_o f^n$$

P-coda decay (CDP Data)

CDP	Q_o	σ_{Q_o}	n	σ_n	$Q_{sn/}$
423	9.905	3.960	1.0314	0.1491	151
445	2.146	1.558	1.3880	0.2707	99
467	3.543	1.343	1.2157	0.1414	94
522	0.080	0.156	2.4827	0.7233	40
606	5.245	2.474	0.9624	0.1759	82
630	0.076	0.078	2.4579	0.3843	43
654	1.614	0.890	1.3260	0.2057	48

S-coda decay (Microearthquake Data)

Location	Q_o	σ_{Q_o}	n	σ_n	$Q_{sn/}$
Melendy a	18.051	6.247	1.0306	0.1435	120
Melendy b	15.016	5.557	1.0469	0.1535	108
Schmidt a	29.361	12.968	0.5793	0.1833	91
Schmidt b	16.494	3.756	0.7879	0.0945	93

COMPOSITE RESULTS:

P-coda (CDP Data)

Crustal Block	Q_o	σ_{Q_o}	n	σ_n	$Q_{sn/}$
West	4.223	3.000	1.2117	0.2649	115
East	0.863	0.560	1.5821	0.2420	58

S-coda (Microearthquake Data)

West	22.006	5.269	0.6836	0.0994	92
East	16.464	3.863	1.0387	0.0973	114

TABLE 3a CDP Data

$$L_{min} = \frac{V}{\omega_c} Q(\omega_c); \qquad \omega_c \equiv 2\pi f_c$$

CDP	V(km/sec)	f_c(Hz)	$Q(f_c)$	L_{min}(km)
423	6.0	9	105	11.1
	6.0	12	115	9.2
	6.0	18	202	10.7
	6.0	21	241	11.0
	6.0	[15]	151	[9.6]
445	6.0	9	52	5.5
	6.0	12	54	4.3
	6.0	18	107	5.7
	6.0	21	165	7.5
	6.0	[15]	99	[6.3]
467	6.0	9	56	5.9
	6.0	12	64	5.1
	6.0	18	119	6.3
	6.0	21	151	6.9
	6.0	[15]	94	[6.0]
522	4.7	9	21	1.8
	4.7	12	37	2.3
	4.7	18	196	8.1
	4.7	21	127	4.5
	4.7	[15]	40	[2.0]
606	4.9	9	45	3.9
	4.9	12	50	3.3
	4.9	18	84	3.6
	4.9	21	95	3.5
	4.9	[15]	82	[4.3]
630	4.9	9	20	1.7
	4.9	12	32	2.1
	4.9	18	88	3.8
	4.9	21	173	6.4
	4.9	[15]	43	[2.2]
654	4.9	9	30	2.6
	4.9	12	47	3.1
	4.9	18	83	3.6
	4.9	21	92	3.4
	4.9	[15]	48	[2.5]

TABLE 3b Microearthquake Data

$$L_{min} = \frac{V}{\omega_c} Q(\omega_c); \qquad \omega_c \equiv 2\pi f_c$$

Location	V(km/sec)	f_c(Hz)	$Q(f_c)$	L_{min}(km)
Melendy a	3.30	3	69	12.1
	3.30	6	93	8.1
	3.30	12	190	8.3
	3.30	18	351	10.2
	3.30	24	593	13.0
	3.30	[6]	120	[10.5]
Melendy b	3.30	3	57	10.0
	3.30	6	86	7.5
	3.30	12	156	6.8
	3.30	18	288	8.4
	3.30	24	553	12.1
	3.30	[6]	108	[9.5]
Schmidt a	3.55	3	74	13.9
	3.55	6	59	5.6
	3.55	12	103	4.9
	3.55	18	157	4.9
	3.55	24	234	5.5
	3.55	[9]	91	[5.7]
Schmidt b	3.55	3	45	8.5
	3.55	6	59	5.6
	3.55	12	101	4.8
	3.55	18	163	5.1
	3.55	24	230	5.4
	3.55	[9]	93	[5.8]

TABLE 3c COMPOSITE RESULTS:

$$L_{min} = \frac{V}{\omega_c} Q(\omega_c); \qquad \omega_c \equiv 2\pi f_c$$

Crustal Block	V (km/sec)	f_c (Hz)	$Q(f_c)$	L_{min}(km)
CDP Data				
West	6.0	9	71	7.5
	6.0	12	78	6.2
	6.0	15	115	7.3
	6.0	18	143	7.6
	6.0	21	186	8.4
East	4.9	9	32	2.7
	4.9	12	43	2.8
	4.9	15	58	3.0
	4.9	18	85	3.7
	4.9	21	120	4.5
Microearthquake Data				
West	3.55	3	60	11.2
	3.55	6	59	5.6
	3.55	12	102	4.8
	3.55	18	160	5.0
	3.55	24	232	5.5
East	3.30	3	63	11.0
	3.30	6	90	7.8
	3.30	12	173	7.6
	3.30	18	320	9.3
	3.30	24	573	12.5

Appendix

Initially, we consider a three dimensional infinite elastic medium in which a random homogeneous distribution of scatterers exist. The scatterers are essentially small-scale perturbations in the mean velocity field. The medium is thus characterized by a mean velocity, V, and a mean density, ρ; the heterogeneity, or distribution of scatterers, is characterized by a scale or correlation length, a, and a mean free path, L.

A source, of size considerably smaller than the wavelength of seismic waves emitted, radiates a band limited signal or wavelet over a very short time interval, u. That is, the mean seismic energy generation is expressed as:

$$\Lambda_s(t,\omega) = \frac{W_o(\omega)}{u} S_s(t) \tag{A1}$$

where

$$S_s(t) = \begin{cases} 1 & 0 \leq t \leq u \\ 0 & \text{otherwise} \end{cases}$$

and $W_o(\omega)$ is the total radiated seismic energy within a unit frequency band around ω. Hence, $\Lambda_s(t;\omega)$ is the mean energy generation rate of the wave within a unit frequency band around (ω) at the source.

For the source at the origin, the mean seismic energy flux density is:

$$\mathbf{J}^o(r,t,\omega) = \frac{1}{4\pi r^2} \Lambda_s(t - \frac{r}{V}, \omega)\, \hat{\mathbf{r}} \tag{A2}$$

where the $1/4\pi r^2$ expresses the geometrical spreading, and V is velocity.

We consider an "intermediate" field case:

$r >> \lambda$, the wavelength (actually, $\lambda = \lambda(\omega)$) such that a spherical wave may be accurately approximated as a plane wave. For frequencies as low as 6 Hz this condition will be easily satisfied in the upper crust (V $\approx$ 3.5 km/sec for S-waves, 6.0 km/sec for P-waves) at distances greater than about 10 km; we may accurately assume plane wave conditions at somewhat less

than this distance, (i.e. $r \geq 10\lambda$).

Since we are considering a weakly scattering situation, the source-receiver distance is limited by the mean free path: $r << L$. Hence, our region of applicability for the weak scattering model can be expressed as:

$$\lambda << r << L$$

[The lower limitation on source-receiver distance is not problematical; however, due to the unknown value of L and its probable and also unknown frequency dependence, estimation of the upper limit may prove difficult.]

Given this plane wave approach, the mean *primary* wave energy density, $E^{o}(r, t, \omega)$ and the mean flux density may be related as:

$$\mathbf{J}^{o}(r, t, \omega) = E^{o}(r, t, \omega)\ V\ \hat{\mathbf{r}} \tag{A3}$$

The energy depletion of the primary wave field over a propagation distance, x, may be characterized as a decaying exponential: $exp\,(-x/L)$ where L is the mean free path and is the reciprocal of the turbidity [see Chernov (1960) for details]. Accounting, then, for the loss of energy in the primary wave field, we amend the incident flux density, (A2), as:

$$\mathbf{J}^{o}(r, t, \omega) = \frac{e^{-\frac{r}{L}}}{4\pi r^2}\,\Lambda_s\,(t - \frac{r}{V}, \omega)\,\hat{\mathbf{r}} \tag{A4}$$

For a weak or single scattering environment ($r << L$) we may approximate this exponential as: $e^{-r/L} \approx (1 - r/L)$. Note that although this is not as strong an assumption as the Born approximation, in which the loss of primary wave energy to scattering is neglected entirely, the assumption that $r << L$ poses a somewhat severe *a priori* restriction on the range of values of L. E^0 is then:

$$E^{o}(r, t, \omega) = \frac{(1 - \frac{r}{L})}{4\pi r^2 V}\,\Lambda_s\,(t - \frac{r}{V}, \omega) \tag{A5}$$

The total seismic energy is the sum of this (depleted) primary wave energy and the scattered

energy "pool": $E = E^{\circ} + E^{s}$. At the ith scatterer,

$$\mathbf{J}^{\circ}(\mathbf{r}_i, t, \omega) = \frac{(1-\frac{\mathbf{r}_i}{L})}{4\pi r_i^{\,2}} \Lambda_s \left(t - \frac{r_i}{V}, \omega\right) \hat{\mathbf{r}}_i \tag{A6}$$

Each scattering event can be considered as a secondary source and hence can be characterized by an equivalent (spherically symmetric)* energy generation rate:

$$\Lambda^{s}_{equiv} = \sigma \mid \mathbf{J}^{\circ} \mid \tag{A7}$$

where σ is the effective cross-section of the scatterer and is defined as the ratio of the time average of the scattered wave energy per unit time to the mean energy flux density of the primary or incident wave (Morse and Feshbach, 1953; Ishimaru, 1977, for example).

Hence, the mean energy flux density of the *scattered* wave from the ith scatterer is (see Figure AF1, below):

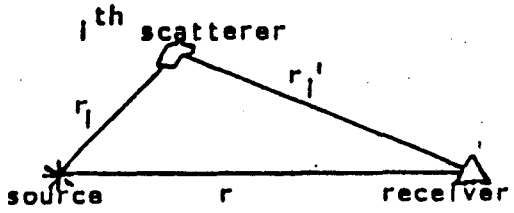

(AF1)

$$\mathbf{J}_i^{s}(\mathbf{r}, t, \omega) = \frac{(1-\frac{\mathbf{r}_i'}{L})}{4\pi r_i'^{\,2}} \Lambda^{s}_{equiv} \hat{\mathbf{r}}_i' \tag{A8}$$

$$= \frac{(1-\frac{r_i'}{L})}{4\pi r_i'^{\,2}} \sigma \mid \mathbf{J}^{\circ}(r_i, t - \frac{r_i'}{V}, \omega) \mid \hat{\mathbf{r}}_i' \ .$$

*The product ka (k = wavenumber, a = correlation length) is a critical parameter in scattering analyses as it relates to the distribution of scattered energy as a function of angle between source and scatterer [see Aki and Richards (1980) or Chernov (1960) for details]. Large ka ($ka >> 1$) comprises the forward scattering domain; small ka ($ka << 1$) is generally viewed as the backscattering or Rayleigh scattering domain (Chernov, 1960), although the actual radiation pattern is complicated and depends on the choice of correlation function (Lerche, 1986; Dainty, 1984). In this study an intermediate value is assumed *a priori*. In such a "Mie scattering" domain (i.e. $ka \approx 2\pi$), we may assume isotropic scattering, although it is necessary to determine the value of the correlation length, a, independently in order to test this.

In order to relate this expression for the scattered flux density to the mean energy density, it is useful to define the turbidity, g :

$$g \equiv n\,\sigma = L^{-1} \tag{A9}$$

where n is the number density of scatterers and σ is the effective cross-section. The aforementioned assumption of a large mean free path in the weak scattering theory can thus be restated in terms of turbidity which essentially implies a small σ. From equation (A3), (A8) and (A9), we may then express the mean energy density for this (single) scattered wave as:

$$E_i^s(\mathbf{r},t,\omega) = \frac{|\,\mathbf{J}_i^s\,|}{V} = \frac{(1-\frac{\mathbf{r}_i{}'}{L})}{4\pi r_i{}'^{\,2}V}\,\Lambda^s_{equiv} \tag{A10}$$

$$= \frac{(1-n\,\sigma r_i{}')}{4\pi r_i{}'^{\,2}V}\,\sigma\,|\,\mathbf{J}^o\,|$$

Substituting equation (A6) for the (scalar) $|\,\mathbf{J}^o\,|$,

$$E_i^s(\mathbf{r},t,\omega) \approx \frac{\sigma}{(4\pi)^2 V\; r_i{}^2 r_i{}'^{\,2}}\Lambda_s\,(t-\frac{r}{V},\,\omega) \tag{A11}$$

where $r \equiv |\,\mathbf{r}_i + \mathbf{r}_i{}'\,|$, and where terms of order σ^2 and higher have been neglected.

The sum of all single scattered waves gives $E^s = \sum_{i=1}^{n} E_i^s$; since we have assumed a homogeneous distribution of scatterers, the summation can be changed to an integral:

$$E^s\,(\mathbf{r},t,\omega) = \frac{n\,\sigma}{(4\pi)^2\,V}\int\int_{-\infty}^{\infty}\int\frac{1}{r_1^{\,2}\;r_2^{\,2}}\Lambda_s\,(t-\frac{(r_1+r_2)}{V},\,\omega)d^3x \tag{A12}$$

where

$r_1 \equiv |\,\mathbf{x}'\,|$ .....r_i

$r_2 \equiv |\,\mathbf{x}-\mathbf{r}\,|$ .....r'_i

and $\mathbf{x} \equiv$ coordinate vector of scatterer.

Let

$$G^s(r,t) = \frac{1}{(4\pi)^2 V} \int\int_{-\infty}^{\infty}\int \frac{1}{r_1^2 r_2^2}\, \delta(t-t',\omega)\, d^3x \tag{A13}$$

(where $t' = t - \frac{r_1+r_2}{V}$) be the Green's function for the single scattering environment. Then equation (A12) can be written as a convolution:

$$E^s = n\sigma G^s * \Lambda_s \tag{A14}$$

$$= n\sigma \int_{-\infty}^{\infty} G^s(r,t-t')\Lambda_s(t',\omega)\,dt'$$

To integrate equation (A13), we transform to prolate spheroidal coordinates with source and receiver at the foci (see Figure AF2):

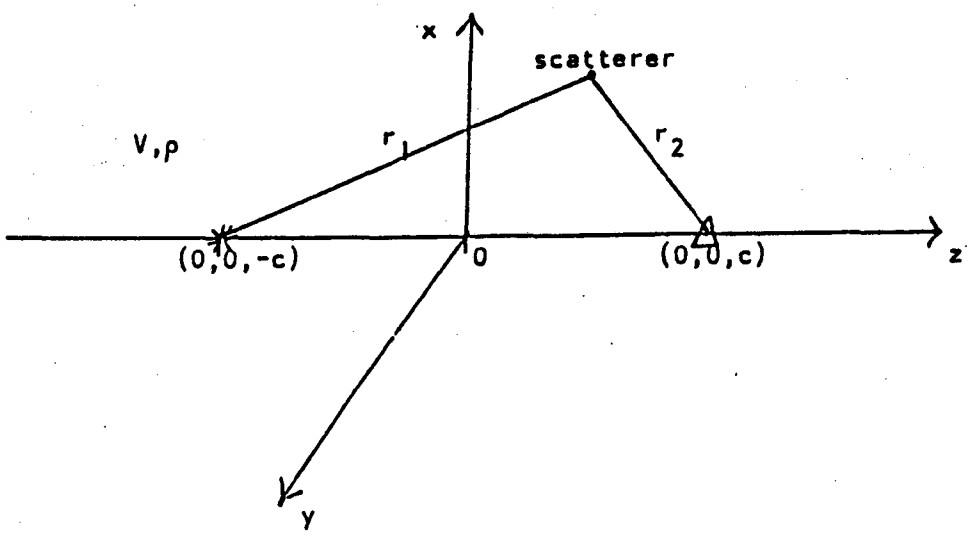

(AF2)

$$x = c\sqrt{\alpha^2-1}\,\sin(\eta)\cos(\varsigma)$$

$$y = c\sqrt{\alpha^2-1}\,\sin(\eta)\sin(\varsigma)$$

$$z = c\,\alpha\cos(\eta)$$

Domains of variables: $\begin{cases} 1 \le \alpha < \infty \\ 0 \le \eta \le \pi \\ 0 \le \varsigma \le 2\pi \end{cases}$

This defines the transformation from [x,y,z] to $[\alpha, \eta, \varsigma]$, in which $\alpha = \frac{Vt}{r}$. Following the transformation, equation (A13) becomes:

$$G^{e}(2c,t) = \frac{1}{16\pi c^2}\int_1^{\infty}\frac{d\alpha}{2\pi}\delta(\alpha - \frac{Vt}{2c})\int_0^{2\pi} d\varsigma \int_0^{\pi}\frac{\sin\eta}{\alpha^2-\cos^2\eta}d\eta \tag{A15}$$

$$= \frac{1}{4\pi(2c)^2}\int_1^{\infty} d\alpha\, \delta(\alpha - \frac{Vt}{2c})\, K(\alpha)$$

The transformation back to r, t reveals that for $\alpha>1$, (i.e. causality),

$$G^{e}(r,t) = \frac{1}{4\pi r^2}K(\frac{V\ t}{r}) \tag{A16}$$

where $K(\alpha) = \frac{1}{\alpha}\ln\left(\frac{\alpha+1}{\alpha-1}\right)$.

Rewriting (A5) and (A14) using our relation for the source time function, (i.e. equation (A1)) we get

$$E^{o}(r,t,\omega) = \frac{(1-\frac{r}{L})}{4\pi r^2 V}\frac{W_o(\omega)}{u}S_u(t-\frac{r}{V}) \tag{A17}$$

$$E^{e}(r,t,\omega) = \frac{n\sigma W_o(\omega)}{u}\int_{-\infty}^{\infty} G^{e}(r,t-t')S_u(t')dt'$$

As we let u -> 0 [i.e. $\frac{S_u(t)}{u} \rightarrow \delta(t-t')$],

$$E^{e}(r,t,\omega) = \frac{n\sigma W_o(\omega)}{4\pi r^2}K(\frac{Vt}{r}) \qquad \text{for } Vt > r \tag{A18}$$

$$= \frac{W_o(\omega)}{4\pi r^2 L}K(\frac{V\ t}{r})$$

A graph of this function is shown below in addition to an approximate form valid for large lapse times in the coda. For such later arrivals one may accurately use this approximation. The method of Aki and Chouet (1975) for single scattering essentially uses this approximate form, with some minor adjustments in the definition of the coda source term. Numerous investigators have applied this method in studies of crustal structure in diverse tectonic environments. (See

section 3.4.6 of Chapter 3 for a discussion of these analyses.)

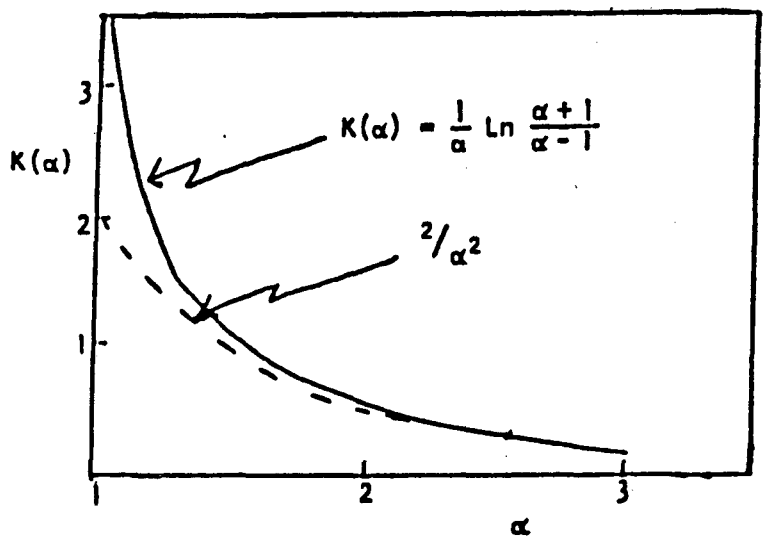

(AF3)

In the application to seismic wave propagation in general and coda decay in particular, the analysis is performed relative to a fixed point in space: $r = r_o$; thus, if we let t_o be the arrival time of the primary wave at this fixed source-receiver distance, $\alpha \rightarrow \frac{t}{t_o}$, equation (A18) may then be expressed as:

$$E^e(r_o, t, \omega) = \frac{W_o(\omega)}{4\pi r_o^2 L} K\left(\frac{t}{t_0}\right) \tag{A19}$$

We note, in passing, that for arrivals at times greater than twice that of the primary wave one may accurately use the approximate form of $K(\alpha)$, $K(\alpha) \approx 2/\alpha^2$; furthermore, when examining coda decay at a fixed receiver location, $r_o = V\ t_o$, and large lapse times (i.e. at times much greater than the arrival time of the primary wave), as is generally done, the resulting expression for the elastic case is very simple:

$$E^e(r_o, t, \omega) = \frac{W_o(\omega)}{4\pi V^2 t_o^2} \frac{2t_o^2}{L\ t^2} = \frac{W_o(\omega)}{2\pi L V^2 t^2} \tag{A20}$$

$$\text{for} \begin{cases} t & \geq 1.5\ t_o \\ r_o & = Vt_o, \text{ fixed} \\ K(\alpha) & \rightarrow 2/\alpha^2 \end{cases}$$

Since for propagating plane waves, the seismic energy density is twice the mean kinetic energy density (Bullen, 1963), we can express equation (A19) in terms of amplitudes as recorded on a vertical wide-band velocity transducer; assuming sinusoidal wave motion,

$$E(t) = \frac{1}{2}\rho A^2(t) \tag{A21}$$

where ρ is density and $A^2(t)$ is the time-averaged squared amplitude of the (velocity) seismogram. Hence, equation (A19) can now be expressed in terms of amplitude:

$$A^{*2}(r_o,t,\omega) = (\frac{2}{\rho})\frac{W_o(\omega)}{4\pi r_o^2 L} K(\frac{t}{t_o}) \tag{A22}$$

$$= \frac{W_o(\omega)}{2\pi\rho r_o^2 L} K(\frac{t}{t_o})$$

Thus far we have assumed an infinite elastic inhomogeneous medium. Since we have assumed that the distribution of secondary sources (scatterers) is uniform, a factor of $\frac{1}{2}$ will account for observations on the surface of a half-space, as is the case here. The effects of intrinsic and scattering attenuation on the energy of a propagating plane wave may be expressed in terms of a decaying exponential, $e^{-\beta t}$, where $\beta = \omega/Q_c$, and Q_c is an apparent coda quality factor. It has been suggested, and tentatively shown (Richards and Menke, 1983), that the apparent coda quality factor may be simply and accurately related to the intrinsic quality factor, Q_i, and a scattering quality factor, Q_s, as:

$$Q_c^{-1} = Q_i^{-1} + Q_s^{-1} \tag{A23}$$

The intrinsic quality factor denotes the frictional or viscous dissipation; (the intrinsic attenuation mechanism may be more clearly demonstrated by studying the frequency dependence of Q; see text). Q_s^{-1} denotes the seismic energy loss due to elastic scattering. It can be expressed as:

$$Q_s = \frac{\omega L}{V} \tag{A24}$$

following Roecker et al. (1982), and Dainty (1981). Equation (A22) for amplitudes may be amended accordingly:

$$A^{*2}(r_o,t,\omega) = (\frac{1}{2})\frac{W_o(\omega)}{2\pi\rho r_o^2 L} K(\frac{t}{t_o})e^{-\frac{\omega t}{Q_c}} \tag{A25}$$

$$= s(\omega,L)\, K(\frac{t}{t_o})e^{-\frac{\omega t}{Q_c}}$$

$$= s(\omega,L)\left\{(\frac{t}{t_o})^{-1} \ln\left(\frac{t+t_o}{t-t_o}\right)\right\}e^{-\frac{\omega t}{Q_c}}$$

where $s(\omega,L) = \dfrac{W_o(\omega)}{4\pi r_o^2 \rho L}$.

The left side of this equation is simply the squared peak amplitudes on a velocity seismogram recorded at a certain hypocentral distance, r_o, and filtered in a narrow band about ω. In the application of standard time series analysis techniques it is useful to note that the energy content of a time series, $f(t)$, is the same as that of its Hilbert transform. The above theoretical development is in terms of energy, and since an investigation of coda decay is essentially one involving the change in the overall shape of the wave train as opposed to phase fluctuations of its individual components, it is appropriate to focus on the envelope of the seismogram. The envelope of a signal, $Env\left\{f(t)\right\}$ is:

$$Env\left\{f(t)\right\} = [f^2(t) + f_H{}^2(t)]^{\frac{1}{2}} \tag{A26}$$

where $f_H(t)$ is the Hilbert transform of $f(t)$. Finally in correlating the energy content of the squared envelope of the seismogram to the above analysis we define:

$$a^{*2}(t) \equiv \frac{1}{2}Env^2\left\{A^*(t)\right\} \tag{A27}$$

$$= s(\omega,L)(\frac{t}{t_o})^{-1} \ln\left(\frac{t+t_o}{t-t_o}\right)e^{-\frac{\omega t}{Q_c}}$$

Equation (A27) may be applied to the problem of the decay of seismic coda energy whether the source is an earthquake, an explosion, or a sinusoidal source at the surface (i.e.

Vibroseis). Noting that in either case, $r_o = Vt_o$, $s(\omega,L)$ becomes:

$$s'(\omega,L,t_o) = \frac{W_o(\omega)}{4\pi V^2 \rho L t_o}$$

In an investigation of the decay of scattered seismic energy as manifested in the envelope of the coda, it may be useful initially to correct the data for spherical spreading using a suitable velocity, V; For the two-dimensional application this geomerical spreading correction may be approximated as a multiplicative factor $(Vt)^2$ where t is the travel time of the primary and/or scattered wave. In this case, equation (A27) is modified to:

$$a_{corr}^{s^2}(t) = S(\omega,L,t_o)\, t \, \ln\left(\frac{t+t_o}{t-t_o}\right) e^{-\frac{\omega t}{Q_c}} \tag{A28}$$

where $S(\omega,L,t_o) = \dfrac{W_o(\omega)}{4\pi\rho L t_o}$ is the modified form of $s'(\omega,L,t_o)$ to reflect this correction, and where the left side of equation (A28) represents the squared envelope of the scattered arrivals in the coda, corrected for geometrical spreading.

Finally, the logarithm of this expression is taken to linearize the problem in terms of the coda source term, $S(\omega,L,t_o)$ and the apparent coda Q, Q_c :

$$\log_{10}(a_{corr}^2) = C + \log_{10}(t) + \log_{10}\left[\ln\left(\frac{t+t_o}{t-t_o}\right)\right] - bt \tag{A29}$$

where $C \equiv \log_{10} S$; $b = \dfrac{2(\log_{10} e)\,\pi f}{Q_c}$ f = frequency . (We have dropped the superscript s and the functional arguments for clarity.)

The foregoing derivation provides an expression for the time domain analysis of the coda of a filtered seismic signal. The results of such inversions for the apparent quality and coda source factors may be compared with similar results at different frequencies. As discussed above, there are certain limiting assumptions:

i) weak or single scattering environment (i.e. small turbidity or $r << L$)

ii) isotropic scattering (i.e. $ka \approx 2\pi$)

iv) slowly varying density and velocity fields in the background medium

iii) point source (i.e. source size $<<$ wavelength, λ)

v) source time duration is short

vi) plane wave propagation (i.e. $r \geq 10\lambda$).

The first two assumptions are probably the most difficult to satisfy because they involve parameters that describe the heterogeneity structure of the medium *a priori*. Although the density and velocity fields and the source size and time function may be more or less unknown, they are considered better constrained than those characterizing the randomness of the medium. Despite these limiting assumptions it is believed that this approach can be successfully applied to a wide range of data. In fact, a general form of this method has been applied to numerous earthquake and microearthquake data sets from a wide variety of tectonic regimes, as is discussed in the text (see section 3.4.6 of Chapter 3). In the present study this method is applied to both microearthquake and zero offset (stacked) seismic reflection data.

References: Chapter 3

Agnew, J. D., R. C. Quittmeyer and C. T. Statton, 1986. Attenuation of coda waves in the northeastern United States, *Earthquake Notes*, **57**, 8.

Aki, K., 1969. Analysis of the seismic coda of local earthquakes as scattered waves, *J. Geophys. Res.*, **74**, 615-631.

Aki, K., 1980. Attenuation of shear-waves in the lithosphere for frequencies from 0.05 to 25 Hz, *Phys. Earth Planet. Interiors*, **21**, 50-60.

Aki, K., 1981. Source and scattering effects on the spectra of small local earthquakes, *Bull. Seism. Soc. Am.*, *71*, 1687-1700.

Aki, K., 1982. Scattering and attenuation, *Bull. Seism. Soc. Am.*, **72B**, 5319-5330.

Aki, Keiiti, 1985. Theory of earthquake prediction with special reference to monitoring of the quality factor of lithosphere by the coda method, *Earthq. Predict. Res.*, **3**, 219-230.

Aki, K. and B. Chouet, 1975. Origin of coda waves: source, attenuation, and scattering effects, *J. of Geophys. Res.*, **80**, 3322-3342.

Aki, K. and W.H.K. Lee, 1976. Determination of three-dimensional velocity anomalies under a seismic array using P-arrival times from local earthquakes: 1. A homogeneous initial model, *J. of Geophys. Res.*, **81**, 4381-4399.

Aki, K. and Anshu Jin, 1986. Relation between long-term seismicity and coda Q, *Earthquake Notes*, **57**, 25.

Anderson, Don L. and C. B. Archambeau, 1964. The anelasticity of the earth, *J. Geophys. Res.*, **69**, 2071.

Berry, Frederick A. F., 1973. High fluid potentials in California Coast Ranges and their tectonic significance, *Amer. Assoc. Petrol. Geol. Bull.*, **57**, 1219-1249.

Birch, Francis and Dennison Bancroft, 1938. The effect of pressure on the rigidity of rocks, 1 *J. Geol.* **46**, 59.

Biswas, N. N. and K. Aki, 1984. Characteristics of coda waves: central and southcentral Alaska, *Bull. Seism. Soc. Am.*, **74**, 493-506.

Boore, D. M. and D. P. Hill, 1973. Wave propagation characteristics in the vicinity of the San Andreas fault, *Proc. of the Conference on Tectonic Problems of the San Andreas fault system, Stanford Univ. Publ.*, **13**, 215-224.

Born, W. T., 1941. The attenuation constant of earth materials, *Geophysics*, **2**, 625-660.

Chen, Peishan, Otto W. Nuttli, Wenhua Ye and Jiazheng Qin, 1984. Estimates of short-period Q values and seismic moments from coda waves for earthquakes of the Beijing and Yunnan regions of China, *Bull. Seism. Soc. Am.*, **74**, 1189-1207.

Chernov, L. A., 1960. *Wave Propagation in a Random Medium*, McGraw-Hill, New York.

Chouet, Bernard, 1979. Temporal variation in the attenuation of earthquake coda near Stone Canyon, California, *Geophys. Res. Let.*, **6**, 143-146.

Clymer, R. W. and T. V. McEvilly, 1981. Travel time monitoring with Vibroseis, *Bull. Seism. Soc. Am.*, **71**, 1902-1927.

Console, R. and A. Rovelli, 1981. Attenuation parameters for Friuli region from strong-motion accelerogram spectra, *Bull. Seism. Soc. Am.*, **71**, 1981-1991.

Dainty, A. M., 1981. A scattering model to explain seismic Q observations in the lithosphere between 1 and 30 Hz, *Geophys. Res. Let.*, **8**, 1126-1128.

Dainty, A. M. and M. N. Toksoz, 1977. Elastic wave propagation in a highly scattering medium – A diffusion approach, *J. Geophys.*, **43**, 375-388.

Del Pezzo, E., F. Ferulano, A. Giarrusso and M. Martini, 1983. Seismic coda Q and scaling law of the source spectra at the Aeolian Islands, southern Italy, *Bull. Seism. Soc. Am.*, **73**, 97-108.

Del Pezzo, Edoardo and Aldo Zollo, 1984. Attenuation of the coda waves and turbidity cefficient in central Italy *Bull. Seism. Soc. Am.*, **74**, 2655-2659.

Dibblee, Thomas W., Jr., 1980. Geology along the San Andreas fault from Gilroy to Parkfield, *California Division of Mines and Geology, Special Report* **140**, 1-17.

Eaton, J. P., W. H. K. Lee and L. C. Pakiser, 1970. Microearthquakes in the study of the mechanics of earthquake generation along the San Andreas fault in central California, *Tectonophysics*, **9**, 259-282.

Engdahl, E. R. and W. H. K. Lee, 1976. Relocation of local earthquakes by seismic ray tracing, *J. Geophys. Res.*, **81**, 4400-4406.

Feng, R. and T. V. McEvilly, 1983. Interpretation of seismic reflection data for the structure of the San Andreas fault zone, *Bull. Seism. Soc. Am.*, **73**, 1701-1720.

Frankel, Arthur and Robert W. Clayton, 1986. Finite difference simulations of seismic scattering: Implications for the propagation of short-period seismic waves in the crust and models of crustal heterogeneity, *J. Geophys. Res.*, **91**, 6465-6489.

Gao, L. S., L. C. Lee, N. N. Biswas and K. Aki, 1983. Comparison of the effects between single and multiple scattering on coda waves for local earthquakes, *Bull. Seism. Soc. Am.*, **73**, 377-390.

Gordon, R. B. and Carl Nelson, 1966. Anelastic properties of the earth, *Rev. Geophys.*, **4**, 457.

Griscom, Andrew, 1982. Magnetic interpretation of ophiolites and batholiths in California, *Geol. Soc. Amer. Abs. with Programs*, **14**, 503.

Griscom, Andrew, 1983. The contact between the Great Valley sequence and the Franciscan assemblage, California, from magnetic data, *(abs.): Amer. Geophys. Union, Transactions, EOS*, **64**, 867-868.

Hale, L. D. and G. A. Thompson, 1982. The seismic reflection character of the continental Mohorovicic discontinuity, *J. Geophys. Res.* **87**, 4625-4635.

Healy, J. and L. Peake, 1975. Seismic velocity structure along a section of the San Andreas fault near Bear Valley, California, *Bull. Seism. Soc. Am.*, **67**, 1177-1197.

Irwin, William P. and Ivan Barnes, 1975. Effect of geologic structure and metamorphic fluids on seismic behavior of the San Andreas fault system in central and northern California, *Geology*, **12**, 713-716.

Ishimaru, A., 1976. *Wave propagation and scattering in random media*, **vols. 1, 2**, Academic Press, New York.

Jackson, David D. and Don L. Anderson, 1970. Physical mechanisms of seismic-wave attenuation, *Reviews of Geophys. and Space Phys.*, **8**, 1-63.

Jin, Anshu and Keiiti Aki, 1986. Temporal change in coda Q before the Tangshan earthquake of 1976 and Haicheng earthquake of 1975, *J. Geophys. Res.*, **91**, 665-673.

Jin, Anshu, Tianqung Cao and Keiiti Aki, 1985. Regional change of coda Q in the oceanic lithosphere, *J. Geophys. Res.*, **90**, 8651-8659.

Kikuchi, M., 1981. Disperion and attenuation of elastic waves due to multiple scattering from inclusions, *Phys. Earth Planet. Interiors*, **25**, 159-162.

Knopoff, L., 1960. Q, *Rev. Geophys.*, **2**, 625-660.

Kopnichev, J. F. 1977. The role of multiple scattering in the formation of a seismogram's tail, *Izv. Earth Physics*, **13**, 394-398.

Lerwill, W. E., 1981. The amplitude and phase response of a seismic vibrator, *Geophysical Prospecting*, **29**, 503-528.

Levander, Alan R. and Robert L. Kovach, 1981. S-Wave observations in the Franciscan terrane, central California, *Bull. Seism. Soc. Am.*, **71**, 1863-1874.

Lin, Wunan and Chi-Yuen Wang, 1980. P-wave velocities in rocks at high pressure and temperature and the constitution of the central California crust, *Geophys. J. R. Astr. Soc.*, **61**, 379-400.

Liu, H. P., D. L. Anderson and H. Kanamori, 1976. Velocity dispersion due to anelasticity: Implications for seismology and mantle composition, *Geophys. J. Royal Astro. Soc.*, **47**, 41-58.

Louie, J. N. and R. W. Clayton, 1985. A multi-offset study of deep crustal reflectoors in southeastern California, *(abs.): Amer. Geophys. Union, Transactions, EOS*, **66**, 978.

Lynn, Heloise B., Laura D. Hale and George A. Thompson, 1981. Seismic reflections from the basal contacts of batholiths, *J. Geophys. Res.*, **86**, 10633-10638.

Mason, W. P., 1969. Internal friction mechanism that produces an attenuation in the earth's crust proportional to frequency, *J. Geophys. Res.*, **74**, 4963-4969.

Mavko, G. M. and A. Nur, 1979. Wave attenuation in partially saturated rocks, *Geophysics*, **44**,

161-178.

May, B. T. and J. D. Covey, 1981. An inverse ray method for computing geologic structures from seismic reflections – zero offset case, *Geophysics*, **46**, 268-287.

McEvilly, T. V., 1979. Extended reflection survey of the San Andreas fault zone, *U. S. Geol. Surv., Technical Rept. 1, contract no. 14-08-0001-16804*, McEvilly, T. V., 1980. Extended reflection survey of the San Andreas fault zone, *U. S. Geol. Surv., Final Report, contract no. 14-08-0001-16804*,

McEvilly, T. V., 1981. Extended reflection survey of the San Andreas fault zone, *U.S. Geol. Surv. Open-File Rept., 81-388.*

McEvilly, T. V. and R. Clymer, 1975. Reflection seismic survey near the San Andreas fault, *U.S. Geol. Surv. Final Rept., contract no. 14-08-0001-14845.*

McLaughlin, K. L., 1982. *Spatial coherency of seismic waveforms*, PhD thesis, University of California, Berkeley.

McNally, K. C. and T. V. McEvilly, 1977. Velocity contrast across the San Andreas fault in central California: Small-scale variation from P-wave nodal plane distortion, *Bull. Seism. Soc. Am.*, **67**, 1565-1576.

Menke, W. and R. Chen, 1984. Numerical studies of the coda falloff rate of multiply-scattered waves in randomly layered media, *Bull. Seism. Soc. Am.*, **74**, 1605-1614.

Menke, William, Dean Witte and Rolin Chen, 1985. Laboratory test of apparent attenuation formulas, *Bull. Seism. Soc. Am.*, **75**, 1383-1393.

Morse, P. M. and H. Feshbach, 1953. *Methods of Theoretical Physics*, McGraw-Hill, New York.

Nakamura, Y., 1977. Seismic energy transmission in an intensively scattering environment, *J. Geophys.*, **43**, 389-399.

Novelo-Casanova, D. A., E. Berg, V. Hsu and C. E. Helsley, 1985. Time-space variation of seismic S-wave coda attenuation (Q_c^{-1}) and magnitude distribution (b-values) for the Petatlan earthquake, *Geophys. Res. Let.*, **12**, 789-792.

O'Connell, Richard J. and Bernard Budiansky, 1977. Viscoelastic properties of fluid-saturated cracked solids, *J. Geophys. Res.*, **82**, 5719-5735.

Page, B. M., 1981. The southern Coast Ranges, in *Geotectonic Development of California*, W. G. Ernst, Editor, Prentice-Hall, New York, 329-417.

Peselnick, L. and I. Zeitz, 1959. Internal friction of fine-grained limestones at ultrasonic frequencies, *Geophysics*, **24**, 285-296.

Pulli, J. J., 1984. Attenuation of coda waves in New England, *Bull. Seism. Soc. Am.*, **74**, 1149-1166.

Rautian, T. G. and V. I. Khalturin, 1978. The use of the coda for determination of the earthquake source spectrum, *Bull. Seism. Soc. Am.*, **68**, 923-948.

Rebollar, Cecilio J., Carlos Traslosheros and Rosa Alvarez, 1985. Estimates of seismic wave

attenuation in northern Baja California, *Bull. Seism. Soc. Am.*, **75**, 1371-1382.

Rhea, Susan, 1984. Q determined from local earthquakes in the South Carolina coastal plain, *Bull. Seism. Soc. Am.*, **74**, 2257-2268.

Richards, P. G. and W. Menke, 1983. The apparent attenuation of a scattering medium, *Bull. Seism. Soc. Am.*, **73**, 1005-1022.

Rodriguez, M., J. Havskov and S. K. Singh, 1983. Q from coda waves near Petatlan, Guerrero, Mexico, *Bull. Seism. Soc. Am.*, **73**, 321-326.

Roecker, S. W., B. Tucker, J. King and D. Hatzfeld, 1982. Estimates of Q in central Asia as a function of frequency and depth using the coda of locally recorded earthquakes, *Bull. Seism. Soc. Am.*, **72**, 129-150.

Sato, H., 1977. Energy propagation including scattering effects: single isotropic scattering approximation, *J. Phys. Earth*, **25**, 27-41.

Sato, H., 1978. Mean free path of S-waves under the Kanto district of Japan, *J. Phys. Earth*, **26**, 185-198.

Sato, H., 1982. Attenuation of S waves in the lithosphere due to scattering by its random velocity structure, *J. Geophys. Res.*, **87**, 7779-7785.

Sato, H., 1984. Attenuation and envelope formation of three-component seismograms of small local earthquakes in randomly inhomogeneous lithosphere, *J. Geophys. Res.*, **89**, 1221-1241.

Sato, H., 1986. Temporal change in attenuation intensity before and after the eastern Yamanashi earthquake of 1983 in central Japan, *J. Geophys. Res.*, **91**, 2049-2061.

Savage, J., 1966. Thermoelastic attenuation of elastic waves by cracks, *J. Geophys. Res.*, **71**, 3929-3938.

Scheiner, J. E. and T. V. McEvilly, 1981. Attenuation contrast across the San Andreas fault from reflection seismic profiling, *Earthquake Notes*, **52**, 34.

Scherbaum, F. and C. Kisslinger, 1985. Coda Q in the Adak seismic zone, *Bull. Seism. Soc. Am.*, **75**, 615-620.

Schoenberger, M. and F. K. Levin, 1974. Apparent attenuation due to intrabed multiples, *Geophysics*, **39**, 278-291.

Singh, Sudarshan and Robert B. Herrmann, 1983. Regionalization of crustal coda Q in the continental United States, *J. Geophys. Res.*, **88**, 527-538.

Stewart, R. and L. Peselnick, 1977. Velocity of compressional waves in dry Franciscan rocks to 8 kilobars and 300°C, *J. Geophys. Res.*, **82**, 2027-2039.

Stewart, R. and L. Peselnick, 1978. Systematic behavior of compressional velocity in Franciscan rocks at high pressure and temperature, *J. Geophys. Res.*, **83**, 831-839.

Stewart, Samuel W., 1968. Preliminary comparison of seismic traveltimes and inferred crustal structure adjacent to the San Andreas fault in the Diablo and Gabilan Ranges of central

California, *Proc. Conf. Geol. Problems of San Andreas Fault System, Stanford Univ. Publ. Geol. Sci.*, **11**, 218-230.

Schultz, P. S., 1982. A method for direct estimation of interval velocities, *Geophysics*, **47**, 1657-1671.

Walsh, J. B., 1966. Seismic wave attenuation in rock due to friction, *J. Geophys. Res.*, **71**, 2591-2599.

Walter, A. W. and W. D. Mooney, 1982. Crustal structure of the Diablo and Gabilan Ranges, central California: A reinterpretation, *Bull. Seism. Soc. Am.*, **72**, 1567-1590.

Wang, C. Y., W. Lin and F. T. Wu, 1978. Constitution of the San Andreas fault zone at depth, *Geophys. Res. Let.*, **5**, 741-744.

Wang, Chi-Yuen, Feng Rui, Yao Zhengsheng and Shi Xingjue, 1986. Gravity anomaly and deep density structures in the San Andreas fault zone, in press, *Pageoph*, **124**, 127-140.

Wentworth, C. M., M. C. Blake, Jr., D. L. Jones, A. W. Walter and M. D. Zoback, 1984. Tectonic wedging associated with emplacement of the Franciscan assemblage, California Coast Ranges, *Franciscan Geology of Northern California: Pacific Section S. E. P. M.*, **43**, 163-173.

Wesley, J. P., 1965. Diffusion of seismic energy in the near range, *J. Geophys. Res.*, **70**, 5099-5106.

Wesson, R. L., 1971. Travel-time inversion for laterally inhomogeneous crustal velocity models, *Bull. Seism. Soc. Am.*, **61**, 729-746.

Wilson, Ivan, 1942. *Geology of the San Benito Quadrangle*, PhD thesis, University of California, Berkeley,

Wu, R. S., 1985. Multiple scattering and energy transfer of seismic waves – separation of scattering effect from intrinsic attenuation - I. theoretical modeling, *Geophys. J. Royal Astr. Soc.*, **82**, 57-80.

Wu, R. S. and K. Aki, 1985. Scattering characteristics of elastic waves by an elastic heterogeneity, *Geophysics*, **50**, 582-595.

Zener, C. M., 1948. *Elasticity and anelasticity in metals*, Univ. of Chicago Press, Chicago Illinois.

Zoback, Mark D. and Carl M. Wentworth, 1986. Crustal studies in central California using an 800-channel seismic reflection recording system, *Reflection Seismology: A Global Perspective, Geodynamic Series*, **13**, 183-196.

Chapter 4

Forward Modeling

4.1 INTRODUCTION

In an effort to model the velocity and attenuation properties of the crust in this region of the San Andreas fault zone, one-dimensional synthetic seismograms were computed based on the results of the previous analyses, (see Chapter 3). The synthetic (two-way) reflection seismograms were calculated for normal incidence plane waves propagating through a stack of homogeneous layers in which the effects of absorption and dispersion were included. The attenuation was parameterized by an exponential Q operator derived from the coda-Q inversion of the true amplitude stacked CDP section described in Chapter 3; the dispersion effect was based on the absorption-dispersion relation given by Futterman (1962). The four parameters necessary for the calculation of a single synthetic seismogram were the layer thicknesses and the values of the velocity, density, and Q within each layer; in all cases these parameters were taken to be constant within each layer, the only exception being, of course, the dependence of the velocities on frequency. Although the coda-Q analyses indicated a significant frequency dependence of the Q factor, this parameter was held constant within each layer and thus the input values of the Q in each layer were taken from the results of the coda-Q study using the unfiltered reflection data.

In all calculations the source was represented by a band-limited minimum phase Butterworth wavelet having low and high frequency corners of 6 and 24 Hz, respectively; this of course was the range of the Vibroseis source sweep used in the 1978 CGG reflection data. Hence, the synthetic seismogram calculated for a given one-dimensional model corresponds to the CDP stacked trace having this variation of velocity, density, and Q with depth. The variation of the parameter values with depth was adjusted to correspond to the different CDP traces along the 18 kilometer profile. By juxtaposing the synthetic seismograms according to their representative CDP's along the (horizontal) profile, a stacked seismic section was simulated.

The appearance of spatially coherent reflectivity in these 'pseudo-sections' (see Figures 4-7a to 4-7d) is indicative of subsurface structural features; qualitative comparison of these pseudo-sections with the actual seismic sections (e.g. Figure 3-6), from which these synthetics are derived, suggests that such structural features ought to be more clearly discernible in the actual data. The fact that these *reflectors* are not more clearly illuminated in the actual stacked section suggests that out-of-the-plane scattering may have been an important factor or that the systematic problems involved in the field recording have served to severely limit the signal-to-noise ratio or the resolution of these features (McEvilly, 1980). Of course, the possibility that there are no plane horizontal reflectors in this crustal section must be considered since the region is generally characterized by intense lateral heterogeneity; this is especially important for this data set in light of the fact that a pre-stack migration was not applied. These synthetic pseudo-sections also suggest that the laminated appearance of the crust-mantle contact may be modeled by a cyclic variation of velocity (and density) over layers at least 600 meters in thickness and having a total depth extent of 3.2 kilometers or more; relatively large contrasts in impedance are required to model this laminated feature.

Finally the spectral contrast between a relatively low Q *Franciscan* crust and a higher Q *Gabilan* crust is confirmed by the synthetic results; (this is, of course, not surprising given the constant Q exponential operator used in the calculation of the synthetics). The fact that a constant Q operator was sufficient to illustrate this spectral contrast between the two bounding crusts suggests that if the apparent Q values derived from the coda-Q analysis are accurate, then the degree of frequency dependence of Q, as expressed by the n parameter (see equation (7), Chapter 3), must not be especially significant (i.e. n must be less than 1).

4.2 MODEL DESCRIPTIONS

Four basic models of the two-dimensional velocity variation were chosen. The first, model 'SS', was derived from the rms velocities used in the processing of the reflection data; that is, interval velocities for a given CDP were calculated from the Dix formula. The resulting velocity-depth function served as the input values of the velocities and layer thicknesses for the calculation of the one-dimensional synthetic associated with that particular CDP location. A typical series of input functions is shown in Figure (4-1) for CDP 460. In all models the density was calculated from a velocity-density function given by Fluh (personal communication).

$$\rho = 1.67 + 0.174\ V_P \tag{1}$$

where ρ is given in g/cm^3 when V_P is given in km/sec. Except for model 'FM', in which the upper mantle density was taken from equation (1), all models had a fixed upper mantle density of 3.27 g/cm^3 as suggested by Bott (1971). As noted in Chapter 3, velocity model 'SS' is quite similar to that of Feng and McEvilly (1983), although it is not as detailed as theirs. Hence the second model ('FM') is derived from their results (i.e. Figure 10 of Feng and McEvilly (1983)). Finally, in an effort primarily to model the laminated character of the Moho as noted on the aforementioned stacked reflection section (see Figure 3-6) as well as in several other areas (Hale and Thompson, 1982) two perturbations of model 'FM' were used. In these models, denoted as 'C1' and 'C2', layers of alternating velocities over thicknesses of 400 and 600 meters, respectively, were inserted at the crust-mantle contact. In model 'C1' there were four such layers of velocities 7.5 $\pm$ 0.35 km/sec whereas in model 'C2' there were six such layers, resulting in a cyclic series of laminae with reflection coefficients of about 0.067. These relatively high reflection coefficients were necessary to reproduce the strong Moho reflections noted in the stacked section(s). Similarly high reflection coefficients were used by Clowes and Kanasewich (1970) in modeling the same laminated appearance of deep crustal reflections. Unlike their study, in which layers of alternating velocity (with constant density) were of thicknesses less than 200 meters over a total depth extent for the transition zone of less than 1 km, this study

required a significantly thicker transition zone with correspondingly thicker layers. Analysis of the three reflection records depicted in their study shows a considerably less pronounced 'Moho' transition, albeit for a thicker crust (i.e., the approximate 'Moho' reflection time was almost twice that for the Bickmore data). Hence for their study relatively thin layers within the model transition zone were sufficient to fit the data qualitatively.

To model the random heterogeneity of the medium the aforementioned velocity models were "randomized" by addition of a random variation of the velocity within a given layer as generated by a random number generator function. In this case a ten percent perturbation to the layered velocity-depth function was chosen; this relatively large value for the velocity perturbation was chosen somewhat arbitrarily. In a study of amplitude and phase anomalies across the LASA array in Montana from teleseismic sources Aki (1973) found fractional rms velocity perturbations of about four percent. In light of the fact that LASA was originally chosen because of its presumed lateral homogeneity in a stable cratonic part of the continent, a value of ten percent for the velocity perturbation in an intensely inhomogeneous medium such as this crustal section bounding the San Andreas fault did not seem excessive. This perturbation of the deterministic velocity-depth function was superimposed or added to the initial nine to fourteen layer model, with the exception of the nth layer, which in all cases represented the upper mantle and had a fixed velocity of 7.85 km/sec. The result was a series of layers each several hundred meters thick with a random variation of velocity superimposed on the initial layers which were generally up to three kilometers thick. Because of the relatively large perturbations introduced by this procedure the depths at which large impedance contrasts are located may be shifted somewhat. Figure (4-2) shows a typical velocity-depth model for a given "CDP seismogram" (e.g. CDP 620) before and after such a randomization. Models 'SS' and 'C1' had random layer thicknesses of 400 meters; in model 'FM' the random layer thicknesses were 500 meters and in model 'C2' the random layer thickness was 600 meters. This range of thicknesses was chosen to be roughly midway within the range of wavelengths for the P-waves propagating through the model(s), in the expectation that the maximum scattering effect would thus be simulated.

MODEL ('SS') PARAMETERS: CDP 460

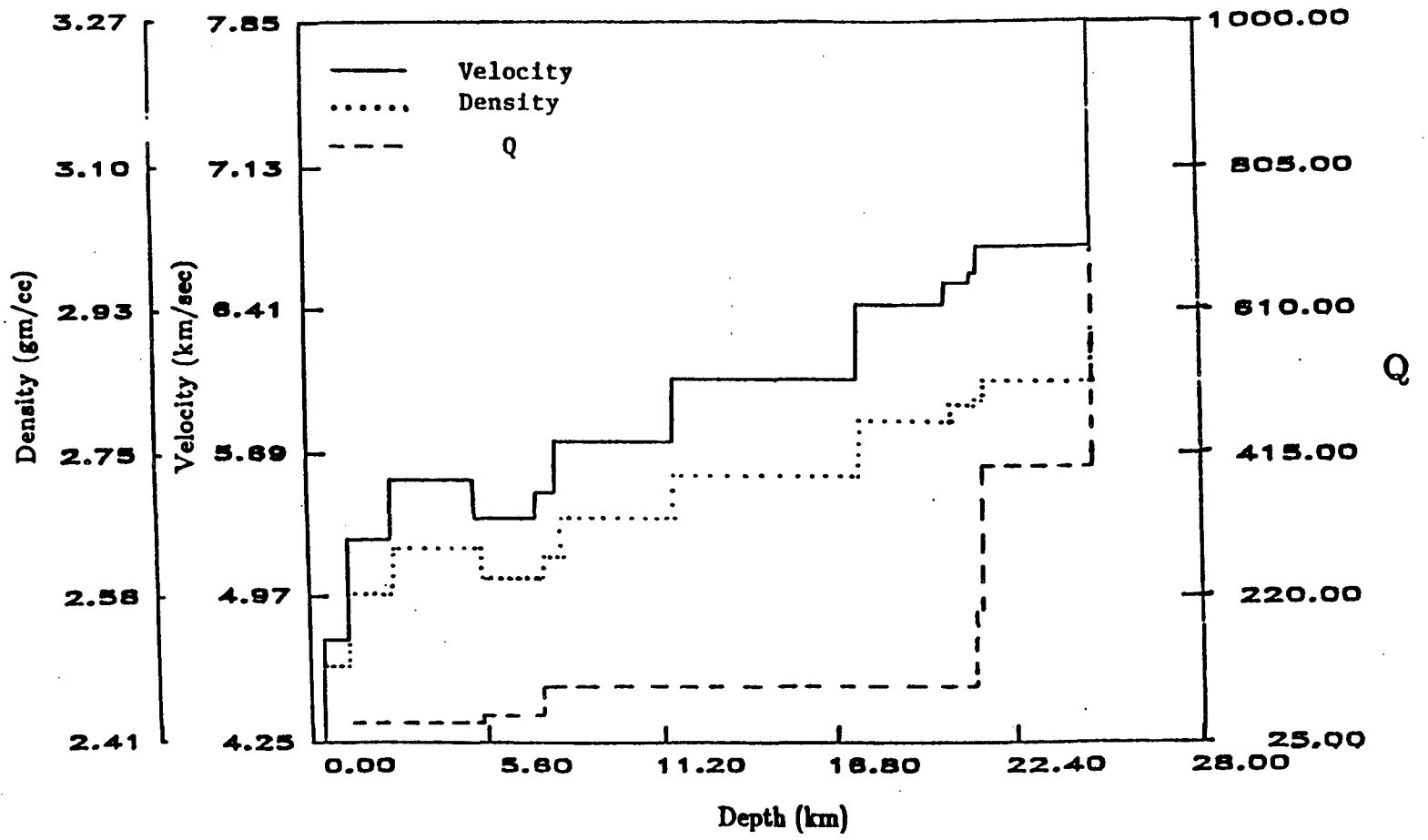

Figure (4-1) Layered model parameters of model 'SS' input for CDP 460. Note the crust-mantle discontinuity at a depth of about 24 km; an upper mantle velocity and density of 7.85 km/sec and 3.27 g/cc, respectively are assumed for all models. The Q(z) function, derived from the coda-decay analysis of the stacked CDP seismograms (see Section 3.4), is used for CDP 460 in all models.

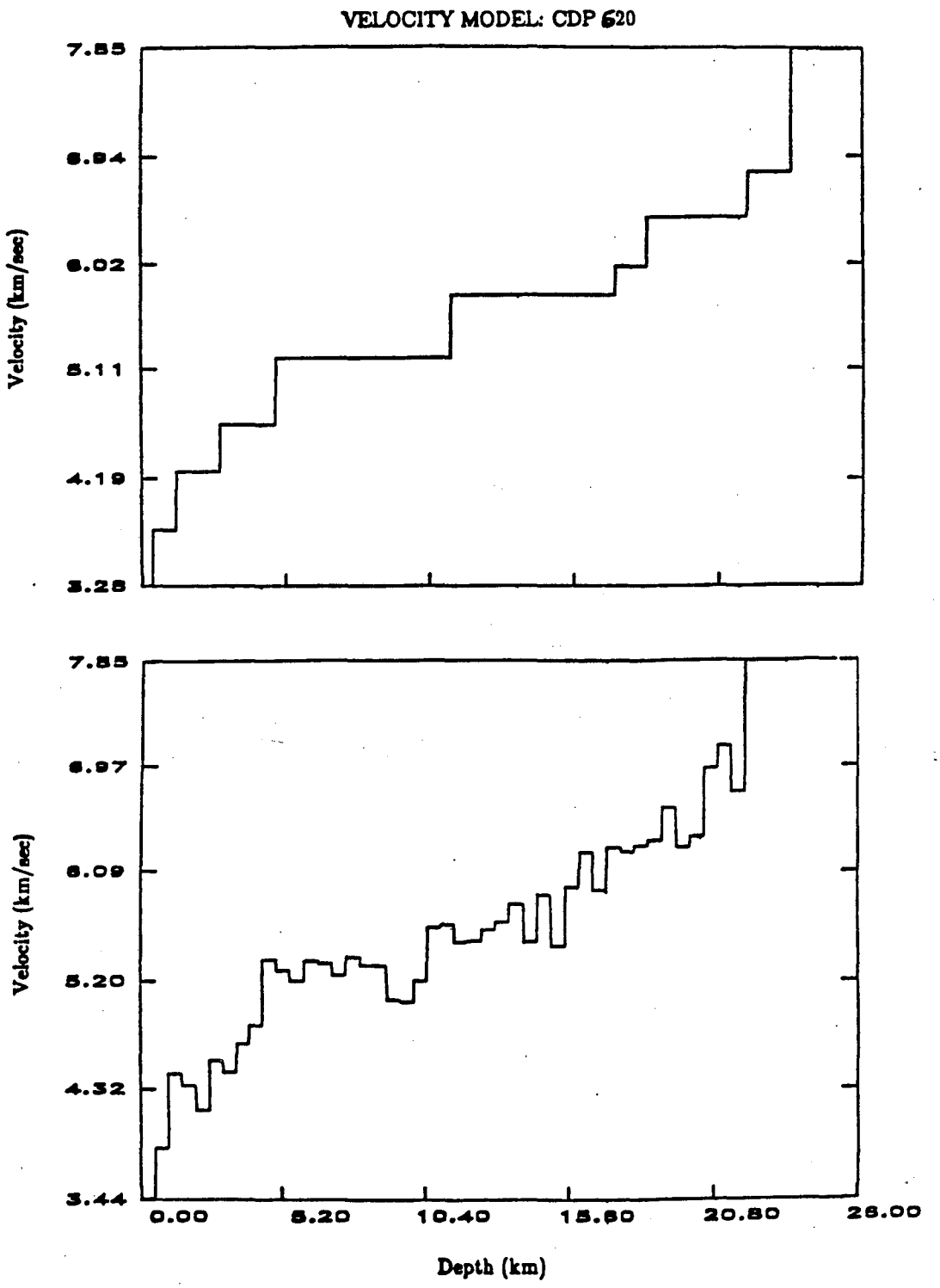

Figure (4-2) Layered velocity model for CDP 620 before (top) and after (bottom) randomization; this randomization procedure uses a layer mini-thickness of 400 meters and a percent randomization factor of 10% superimposed on the initial (top) velocity model.

The Q(z) variation was invariant among the various four basic models. Since the Q results from the coda analysis did not vary with depth but instead gave an average Q for a given CDP over a general mid-crustal depth range, the adoption of a depth varying Q model was somewhat ad hoc. The chosen model bhas a thin veneer several hundred meters thick in which the Q is assumed to be one-eighth of the mid-crustal value derived from the coda analysis. The subsequent values of Q increase by factors of two up to the core value given in Chapter 3 (see Q_{ssf} values in Table 3-2); this core value corresponds to that in the depth range 6 to 17 kilometers. For the layers at greater depth, the Q increases by a factor of two until the crust-mantle contact at which point it is assigned an arbitrary upper mantle value of 1000. Figure (4-1) shows a typical Q(z) model for a CDP (#460) within the Gabilan crust. Note that the Q value at mid-crustal depths is constant at a value of 99, the value given for the unfiltered coda of that CDP. Although admittedly arbitrary this Q model was believed to be quite plausible and since it was primarily based on the results of the coda-Q study over most of the roughly 25 km thick crust it represented the most credible model available.

Finally after computation of the synthetic seismogram a signal-to-white-noise ratio of five was ensured by addition of twenty percent white noise as generated by a random number generator function. Figure (4-3) shows that the spectrum of the noise is indeed white. As this noise is added after the computation of the seismogram it is to be distinguished from the effects of the random perturbation of the velocity model whose spectrum is certainly not white.

Figure (4-4) shows typical seismograms calculated for CDP 650 in the Franciscan and for CDP 460 in the Gabilan calculated using velocity model 'SS'. Note the contrast in reflectivity at depth (i.e. Moho reflection) between the two; this is primarily due to the generally lower Q values in the Franciscan relative to those within the Gabilan medium. Given the frequency independent Q model used here, this contrast in attenuation between the two media is expected to be manifested in the spectral content of the two seismograms. The contrast in frequency content between these two seismograms is evident in the general difference in sharpness of the reflections, particularly in those at depth. Figure (4-5) also shows the spectral contrast between

the coda of the two seismograms shown in the previous figure (prior to the addition of white noise, of course); the windows over which these spectra are computed are indicated above each spectral plot. Note that the corner frequency of the Gabilan coda ($f_c \approx 8$ Hz) is about twice that of the Franciscan coda ($f_c \approx 4$ Hz). Although these corner frequencies are lower than those of the actual field data the relative differences in spectral content between the bounding crusts in these synthetic seismograms are consistent with both the CDP reflection data (e.g. Figure 3-28) and the microearthquake data (e.g. Figures 3-34 and 3-35). Absolute differences in the corner frequencies between the actual reflection data and these synthetic data may be due to differences in the source spectra, however it is important to realize that the time windows for these latter spectra (e.g. top of Figure 4-5) are very late in the record and therefore correspond to greater travel paths and increased attenuation.

FOURIER SPECTRUM: WHITE NOISE

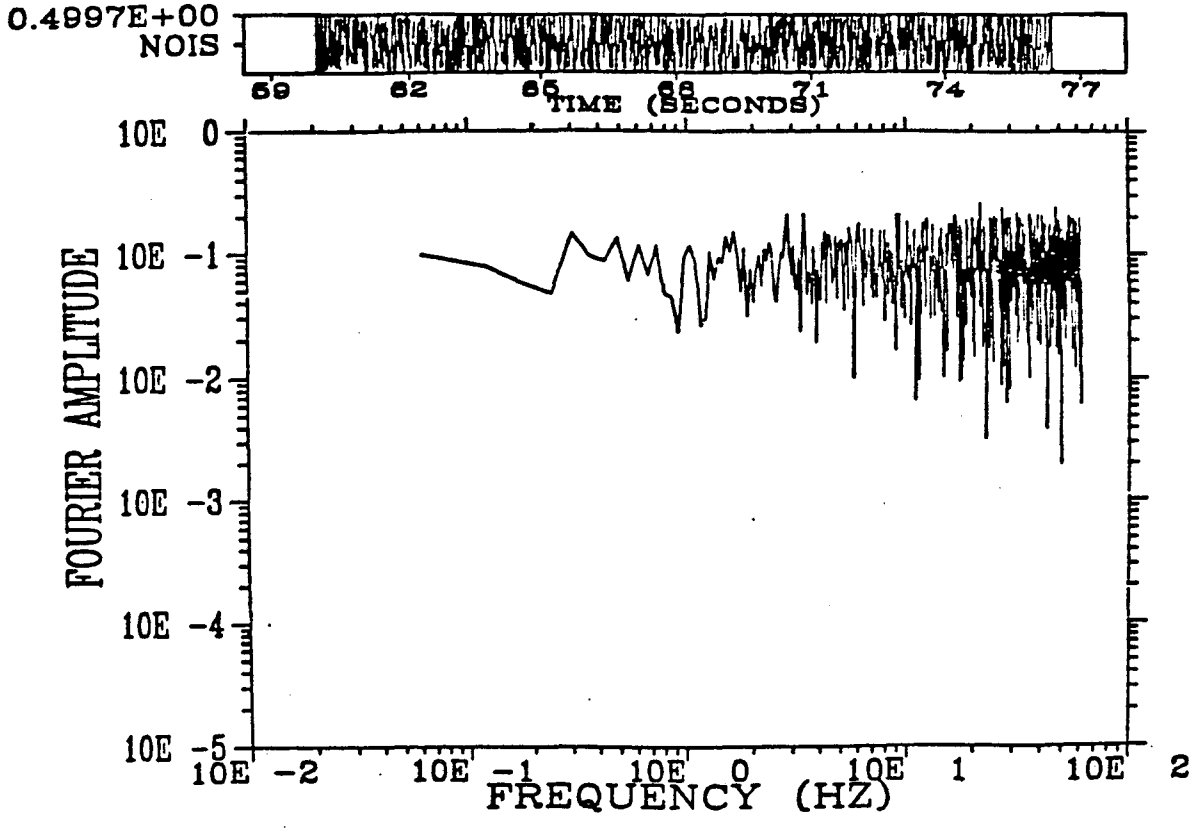

Figure (4-3) Fourier spectrum (bottom) of the noise function (top) added to the synthetic seismograms after computation. Note that the spectrum is indeed 'white' thus ensuring that no spectral contamination is associated with this step. A signal-to-noise ratio of five was achieved by the superpostion of this white noise such that the amplitude of the noise is no greater than 20 % of the signal strength. This type of random noise is to be distinguished from that arising from impedance contrasts arising from the randomization of the velocity field (see Figure 4-2); this white noise represents that due to field instruments and other equipment, cultural noise, microseismic noise, etc. and does not include any effects associated with the actual reflectivity of source-generated energy.

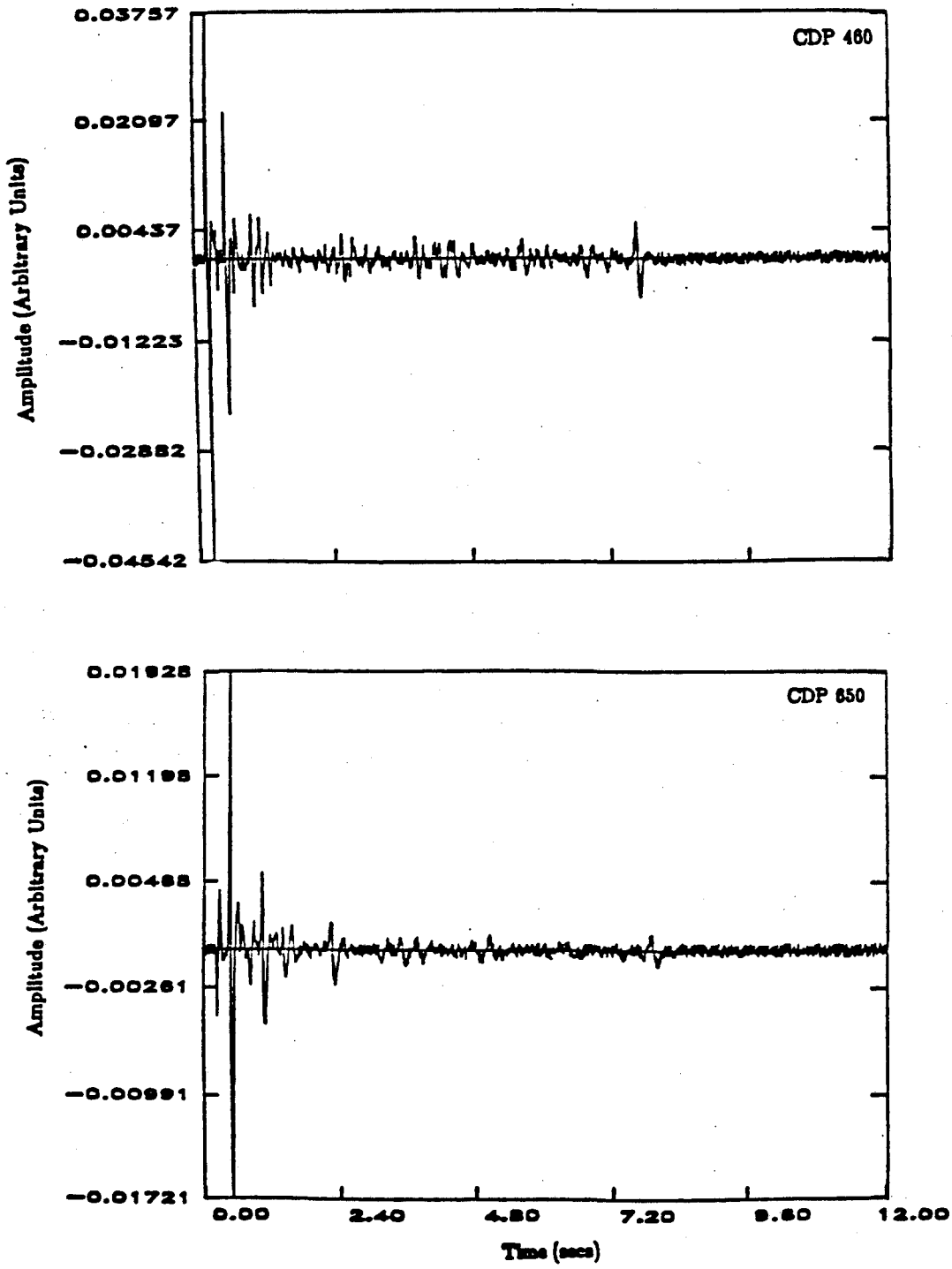

Figure (4-4) Synthetic seismograms for CDP 650 (East) and CDP 460 (West); amplitude is in arbitrary units. Note the relative lack of reflectivity at depth in the seismogram for CDP 650 with respect to that of CDP 460; this is surely due to the generally lower Q values for the 'Franciscan' CDP's east of the fault than those for the 'Gabilan' CDP's to the west; this is also manifested in the generally lower amplitudes for CDP 650 relative to those of CDP 460.

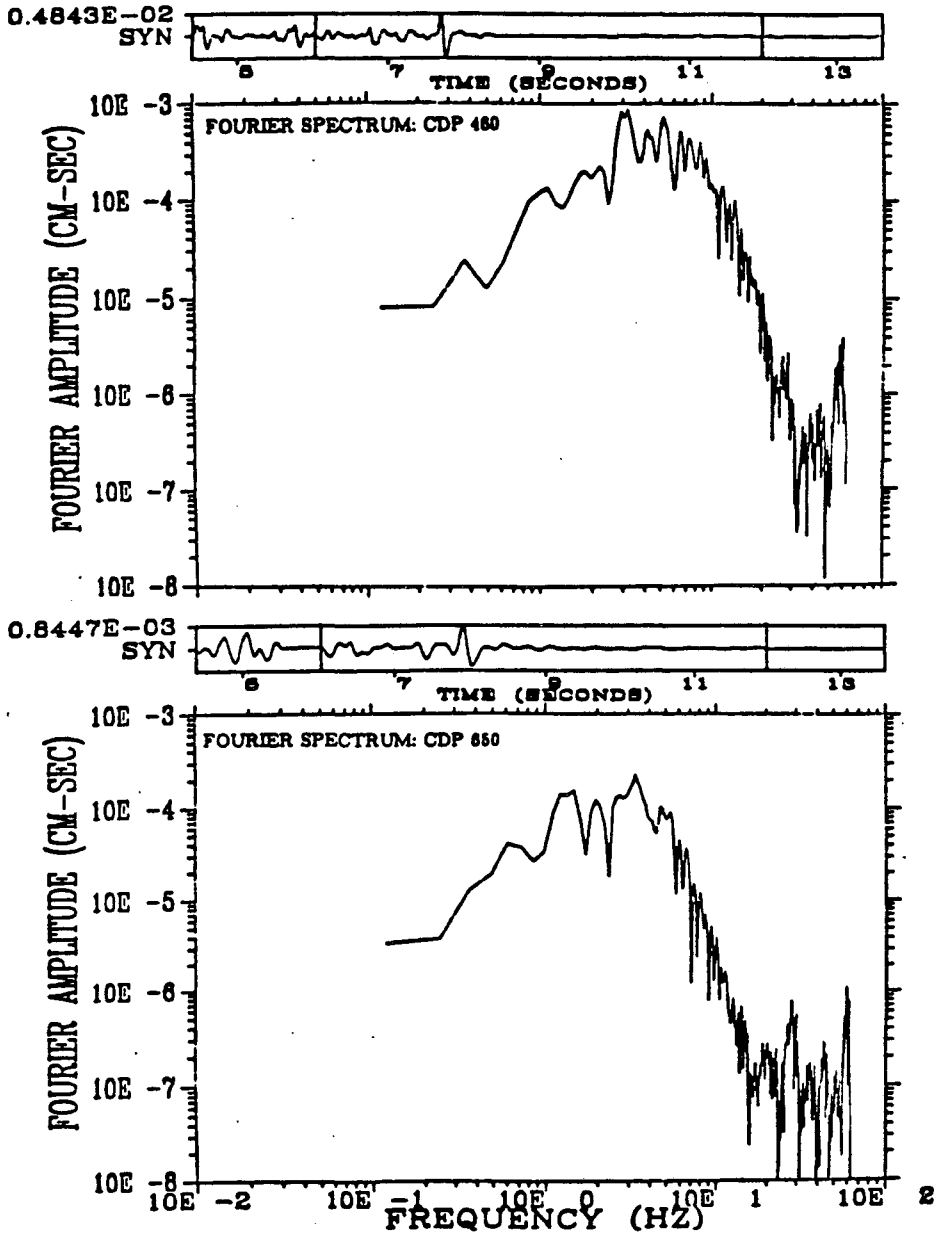

Figure (4-5) Fourier spectra for the coda of the seismograms in Figure (4-4). Note the higher amplitudes and corner frequency (e.g. 8 Hz) for the spectrum of CDP 460 relative to that of CDP 650 (e.g. 4 Hz); the higher spectral amplitudes for CDP 460 is due entirely to the higher Q values at this western CDP location, whereas the higher corner frequency is due, additionally, to the assumption of a frequency-independent Q model.

4.3 METHOD

Although two and three-dimensional synthetic seismogram algorithms exist, it was considered that a one-dimensional forward modeling scheme would be sufficient to test the results of the previous velocity and attenuation studies; in those studies the stacked CDP seismogram was interpreted as the impulse response of the medium to a point source at the observation point on the surface, and the resulting velocity and attenuation profiles were interpreted as representative of the medium directly beneath that observation point. (Although such an interpretation may be reasonable it is only strictly true if the data are migrated (before stack); hence, this interpretation is only approximately true.) In this way a two-dimensional image of the reflectivity was produced, essentially by a juxtaposition of one-dimensional traces or seismograms. In the forward modeling approach the set of one-dimensional velocity and attenuation functions from the results of the inversion of the reflection data served as successive inputs to a synthetic seismogram algorithm; in this way a similar juxtaposition procedure was formulated resulting, it is hoped, in a similar *stacked* seismic section.

The algorithm is a variation of one introduced by Gouppilaud (1960) and modified by Ganley (1981) to include attenuation and dispersion. Essentially a propagator technique, it is applicable to plane waves in a flat layered model in which the source wavelet is propagated through the attenuating stack of layers. As described by Ganley (1981) the downgoing wave at the bottom of the ith layer may be expressed in terms of the value of the wave function at the top of the layer, D_o modified by its propagation through that layer of thickness d :

$$D_i(\omega) = D_o(\omega)\, e^{-\alpha d_i}\, e^{-i\omega d_i/c_i} \tag{2}$$

Here the familiar exponential dissipation effect is embodied in α which is simply related to the quality factor:

$$\alpha \approx \frac{k}{2Q} \tag{3}$$

where k is the propagation constant and the phase delay is represented by the second exponential. Note that the phase velocity c_i in this layer is a function of frequency, although Futterman (1962) has shown that the dispersion effect is quite small at moderate values of Q; as an example, he shows that the phase velocity for 1 Hz waves is less than 10^{-3} greater than that at 0.05 Hz. Even for a Q as low as 30 the fractional dispersion effect over this wide spectral band is only about 4%. The dispersion is determined from Futterman's (1962) "third absorption-dispersion pair." The complex velocity is given in terms of Q:

$$V(\omega) \approx V_r \left[1 + \frac{i \ \mathrm{sgn}(\omega)}{2Q} \right] \tag{4}$$

where sgn (ω) is equal to +1 for positive values of ω and -1 for negative values of ω and V_r, the real part of the complex velocity, may be expressed in terms of the non-dispersive elastic phase velocity, c:

$$V_r = \frac{c}{2} \left[1 + \left(1 + \frac{1}{Q^2} \right)^{-1/2} \right] \tag{5}$$

The upgoing wave in the ith layer is similar to that expressed in equation (2); its wave function is determined from the (frequency-dependent) reflection and transmission coefficients for a plane wave in medium 1 normally incident at the boundary with medium 2:

$$R = \frac{\rho_1 V_1 - \rho_2 V_2}{\rho_1 V_1 + \rho_2 V_2} \tag{6a}$$

$$T = \frac{2\rho_1 V_1}{\rho_1 V_1 + \rho_2 V_2} \tag{6b}$$

Note that these are frequency-dependent through the complex velocities. These coefficients reduce to the usual constant coefficients when there is no contrast in Q across the boundary; in the general case of different Q values across adjacent strata, both reflection and transmission introduce a phase shift in the incident wave (Spencer et al., 1982).

The propagation within a given layer is governed by expressions similar to that in equation (2), modified to include contributions from other upgoing (or downgoing) waves according

to the appropriate reflection and transmission coefficients. The method is generalized to express in matrix form the displacement (in the spectral domain) at the surface due to transmission and reflection through an n-layer medium. Figure (4-6) shows in diagrammatical form the algorithm used here. The impulse response is computed step by step for increasing i, then j. Finally the response is multiplied by the band-limited wavelet to get the signal. This technique involving propagator matrices is fundamental to many forward modeling schemes in seismology; the difference here is primarily the inclusion of absorption and dispersion. All computations involved in the calculation of the synthetic are carried out in the frequency domain and thus the effects of attenuation and dispersion are easily incorporated.

In an effort to model the effects of elastic scattering the layered velocity functions used in each of the four models were vertically *randomized* in the sense that a 10% random variation of velocity was superimposed on the deterministic (9 to 14 strata) layered velocity function. However, what is actually modeled in this scheme is not the effects of random scatterers or "blobs" but the effects of multiple reflections in the bedding planes. Lerche (1986) has shown that while the stratigraphic filtering effects of bedding planes may be similar to both that of random scatterers and intrinsic dissipation, as shown by O'Doherty and Anstey (1971), the spectral range over which these mechanisms dominate are probably different. These effects generally involve phase delays and amplitude attenuation of the primary wave as well as pulse broadening. Lerche's analytical approach using mean field renormalization techniques show that for elastic media the stratigraphic or multiple reflection effects dominate at the lower frequencies (i.e. low ka, where k is the propagation constant and a is the correlation scale length of the scatterers or bedding planes) whereas the random scatterers or blobs dominate at the higher frequencies. At the higher frequencies the general effect of the blobs is to cast energy into directions transverse to the normal to the bedding planes. While this must surely be relevant in the actual field data, it was not possible to model this within the framework of homogeneous layers and a one-dimensional propagation scheme. The spectral domain used in the forward modeling approach here is essentially that in which $ka \leq 1$; thus the maximum stratigraphic or multiple

reflection effect is assured.

PROPAGATION ALGORITHM

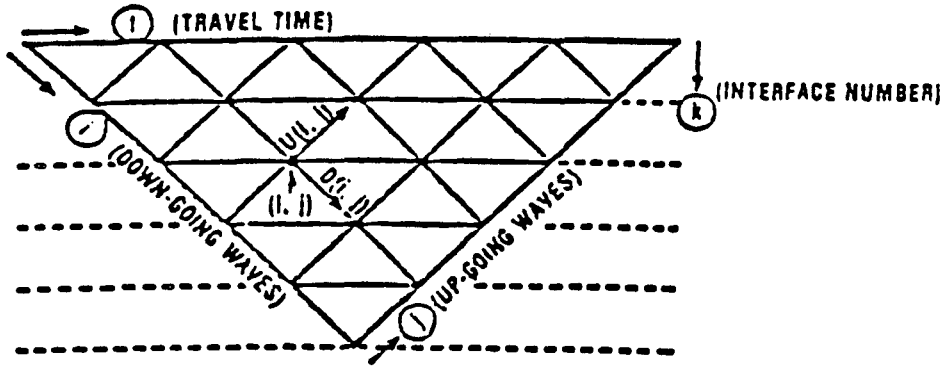

$$\begin{cases} U(I, J) = U(I, J-1) \times [1 + R(k)] + D(I-1, J) \times R(k) \\ D(I, J) = U(I, J-1) \times [-R(k)] + D(I-1, J) \times [1 - R(k)] \\ R(k) = \text{Reflection Coefficient at the } k\text{th Interface} \end{cases}$$

Figure (4-6) Schematic view of 1-D propagation algorithm (adapted from Morlet et al., 1982).

4.4 RESULTS

Probably the most striking manifestation of the effects of attenuation can be observed in the synthetic seismic 'pseudo-sections' resulting from the juxtaposition of the seismograms according to their respective CDP location along the profile. Figures (4-7a to 4-7d) show the sections for each of the four basic models used in this analysis. The most persistent aspect of these sections is the general contrast in spatially coherent reflectivity across the profile, similar to that of the actual data shown in the processed sections of Chapter 3 (see Figures 3-6, 3-16 to 3-19). Although the effects of the differing velocity-depth functions for these sections are certainly evident, the general contrast in spatially coherent reflectivity across each of these sections is surely due to the laterally varying attenuation functions. The Q(z) functions are essentially velocity-model-independent; thus, the observed variations in reflectivity at depth between models are due entirely to differences in the velocity functions. By comparing structural features of interest between the different models in conjunction with the actual data (e.g. Figure 3-6) we can refine our understanding of the velocity structure, while our knowledge of the attenuation profile of this crustal section can be enhanced by an overall comparison between the data and the ensemble of synthetic sections.

In plotting the pseudo-sections it was necessary to mute the first half-second of data because the relatively large amplitude reflections at early times tended to dominate the subsequent signals even with the incorporation of automatic gain control (AGC); this process is analogous to the muting of refractions in the processing of reflection data, although there are other important reasons for this mute procedure in the case of actual field data that are not applicable here. Since we are primarily interested in the large scale structural features of the entire crustal block, the loss of information at very shallow depths is not critical. These synthetic sections would probably resemble the actual processed sections more closely if variable area display was applied, but the general structural features are rather clearly evident. In all such plots an AGC

window of 2.0 seconds was applied.

In addition to the general contrast in reflectivity laterally across each of the four sections in Figure (4-7), one observes, albeit subtly, that the San Andreas fault zone apppears as a light, empty patch centered about CDP 560. This can be attributed to the same attenuation effect as that noted above; input Q values for the fault zone were the lowest among all CDP's for each model.

For (two-way) times less than about 1.5 seconds (i.e. for $0.5 < t < 1.5$), model 'C1' shows the most pronounced structural features (e.g. Figure 4-7a). Below this region is the proposed basal contact of the Gabilan batholith at about 3 seconds within the western granitic block evident in the data section (Lynn et al., 1981). The nature of this latter contact has critical bearing on the geotectonic development of the region in light of the controversy regarding the possible existence of Franciscan material beneath the Gabilan granite (Stewart, 1968). The lateral extent of this relection is apparently greatest for model 'SS' and as such this model may best image this proposed basement contact; given the low velocity wedge proposed by Feng and McEvilly (1983) it is not clear what to infer about the lateral extent to which this contact should be imaged on the reflection section. The outlines of the batholith are somewhat evident in the data as a broad tabular mass that seems to thin eastward toward the fault zone. A reflector may be observed at about 2.2 seconds in all four models within the Franciscan crust. The relative absence of such a spatially coherent reflector within the corresponding part of the data section suggests that out-of-the-plane scattering may be responsible. This is suggested for much of the data section, but especially in the shallow to mid-crustal region of the Franciscan crust; because there is a clear, though relatively low amplitude, Moho reflection within the Franciscan portion of all four sections of Figure (4-7), one is led to assert that scattering may indeed be a factor in the wave propagation in this region and, in particular, for the Franciscan crust.

One of the most dominant structural features of both the actual data section and the synthetic sections is the laminated Moho within the Gabilan crust. Considerable effort was devoted to the modeling of this feature in the forward modeling approach. The eastward dipping nature

of this reflection is due to the low velocity trough associated with the fault zone resulting in a sort of 'push-down' effect. The laminated appearance, which has been widely noted in other data sets (e.g. Hale and Thompson (1982) have documented this observation for deep reflection data from the Laramie Mountains of southeastern Wyoming, the Hardeman Basin in southeastern Oklahoma, the southern Appalachians, and offshore Charleston, South Carolina.) has been imaged most reasonably well by model 'C2', in which a cyclic series of layers was inserted above the 7.85 km/sec mantle. There are five such layers, each 600 meters thick having velocities of 7.5 $\pm$ 0.35 km/sec and giving reflection coefficients of about 0.067. Model 'C1' has only three, somewhat thinner layers above the mantle and thus has a more limited total depth extent. The actual depth extent of the laminated transition zone in the data section is quite large, spanning over two seconds, (two-way reflection time) or almost seven kilometers. As noted above, modeling efforts such as these were carried out by Clowes and Kanasewich (1970) using one-dimensional plane wave synthetics. Their data, from dynamite sources in southern Alberta, showed a thicker crust; the proposed Moho transition was at a (two-way) reflection time of more than 14 seconds. The entire depth extent of the zone in their data was only about 0.5 seconds, thus requiring thinner layers spanning less overall depth extent. Even a 0.5 km thick crust-mantle transition zone is somewhat difficult to explain geologically; the much thicker transition zone observed in this forward modeling study is especially perplexing. Hale and Thompson (1982) have proposed several geologic models of formation including tectonic banding due to ductile flow and segregation, relatively undeformed metasediments, cumulate layering, and lenses of partial melt. Clowes and Kanasewich (1970) considered similar geologic models, favoring an explanation involving the effects of partial melting or incomplete mixing and gravitational separation of the more basic, high velocity material from the more acidic-intermediate, lower-velocity rocks. These geologic models that have been proposed are, of course, purely speculative; the important aspect of these studies in widely divergent tectonic settings is that there seems to be a persistent fine structure to the crust-mantle contact. One purpose of these synthetic modeling efforts is to provide some constraints on the seismic nature of this fine

structure in the hope that it will help to determine a plausible geologic model of the Moho. Although no geologic model seems more plausible than another at this point, the results of this synthetic modeling experiment seem to suggest some reasonable values of the layer thicknesses and the possible impedance contrasts that may be involved.

Finally, it is interesting to note that a somewhat faint but discernible reflection is apparent at these depths (i.e. about 25 kilometers) within the Franciscan crust in all four of these models. Its relatively distinct character may be due to the general lack of random arrivals so prevalent in the actual data section. As noted earlier, the neglect of random scatterers in this forward modeling approach may be a factor in the relative clarity of the reflections as well as the general 'emptiness' of these pseudo-sections. Specifically, it seems quite plausible that the inclusion of such three-dimensional effects as are expected to result from the scattering process in the actual wave field would serve to 'randomize' or otherwise camouflage the already faintly coherent signal from the crust-mantle boundary.

The contrast in spatially coherent reflectivity across these pseudo-sections is also manifested in the degree of signal strength at depth in the individual seismograms (Figure 4-4). This is particularly evident in the comparison of "Moho arrivals" for the two seismograms depicted here. While a hint of a reflection is observed at about 7.5 seconds in the eastern or Franciscan seismogram (bottom of Figure 4-4), it is markedly less pronounced relative to the background noise than that shown at the top of Figure (4-4) for the Gabilan seismogram. In addition the level of reflection signal strength is greater for the entire western trace, especially at times greater than about 2.0 seconds. Finally, there is significantly greater sharpness to each reflection in the Gabilan trace than for the eastern seismogram. All of these features can be related to the differing Q(z) models; the values of Q are simply lower for the Franciscan layers than for the Gabilan layers. Of course, due to the frequency independent Q model (i.e. exponential attenuation is proportional to frequency), this contrast in sharpness is also manifested in the spectra for these seismograms (Figure 4-5).

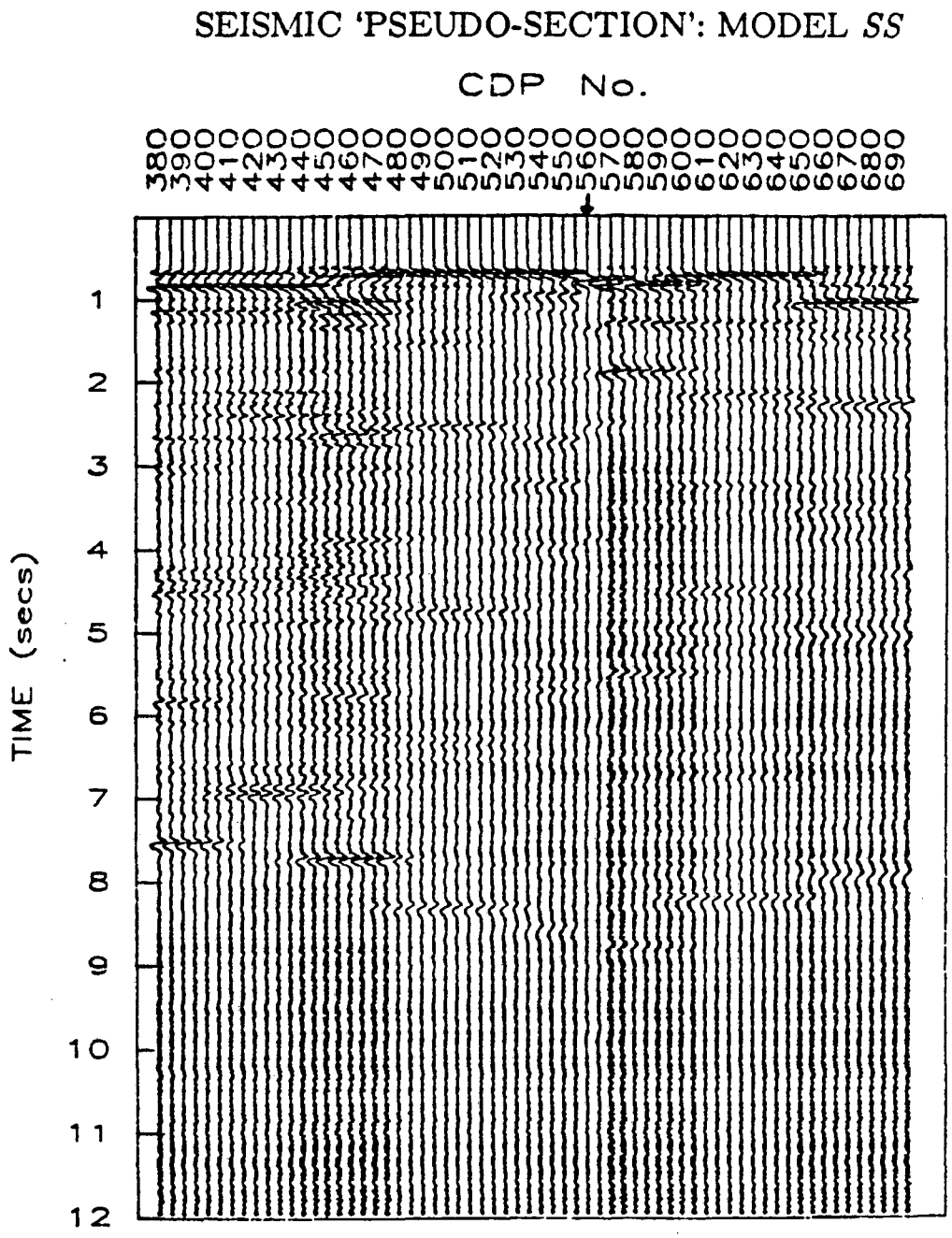

Figure (4-7a) Synthetic ('pseudo-section') seismic reflection section formed by juxtaposition of the individual 1-D synthetic seismograms calculated using the velocity model ('SS') derived from conventional analysis of the Bickmore Canyon seismic reflection data. In this figure as well as in the following three pseudo-sections, the first half-second of data has been muted and an automatic gain control (AGC) using a 2.0 second window has been applied to visually enhance the deeper features. In addition, each individual seismogram is actually plotted twice consecutively for improved lateral continuity. Note the general contrast (east vs. west) in laterally coherent reflectivity in all four pseudo-sections; this is due to the lower Q(z) values east of the San Andreas fault; the fault appears as a light empty patch beneath the arrow at top (e.g. near CDP 560). Note the pronounced lateral extent of the basal contact at about 2.5 seconds (two-way) time.

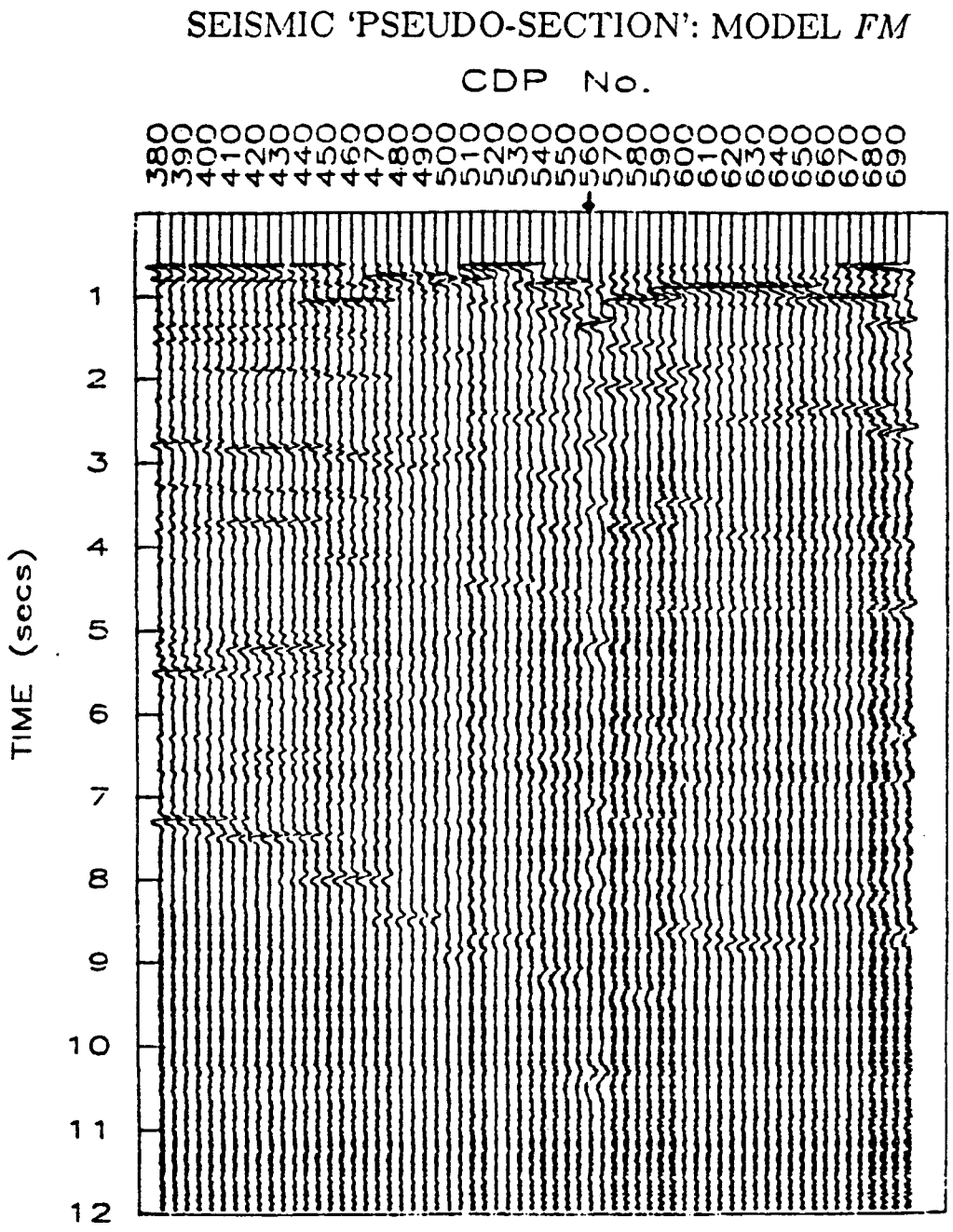

Figure (4-7b) Pseudo-section of the synthetic seismograms based on the velocity model of Feng and McEvilly (1983) ('FM'). Note the pronounced eastward increase in the depth of the Moho reflection due, probably, to a velocity 'push-down' effect associated with the low-velocity fault zone as well as the low-velocity wedge at mid-crustal depth in their model.

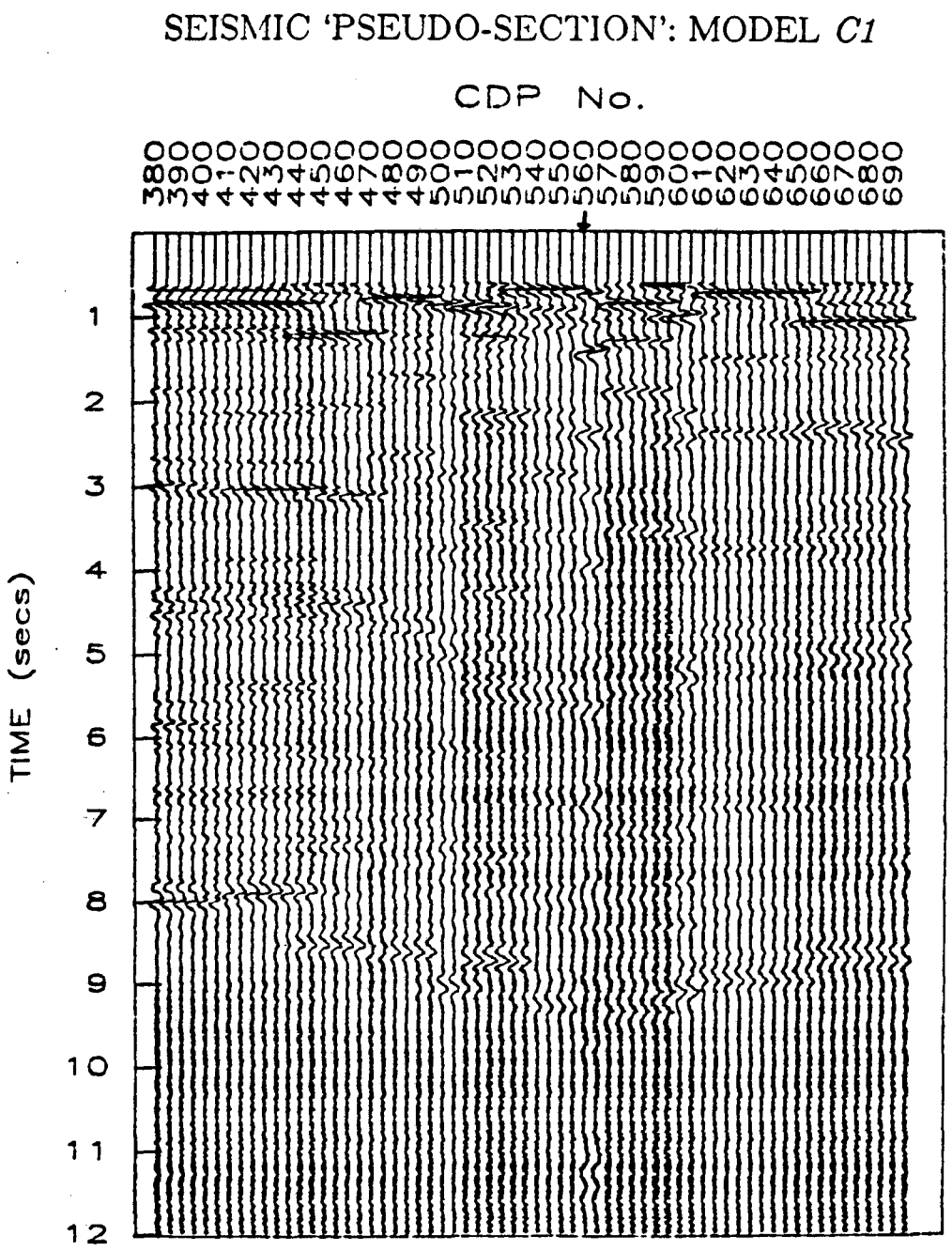

Figure (4-7c) Pseudo-section using a perturbation of the velocity model used in (4-7b) such that the Moho consists of four laminae of thickness 400 meters. Notice the increased complexity of the Moho reflection relative to that of (4-7b).

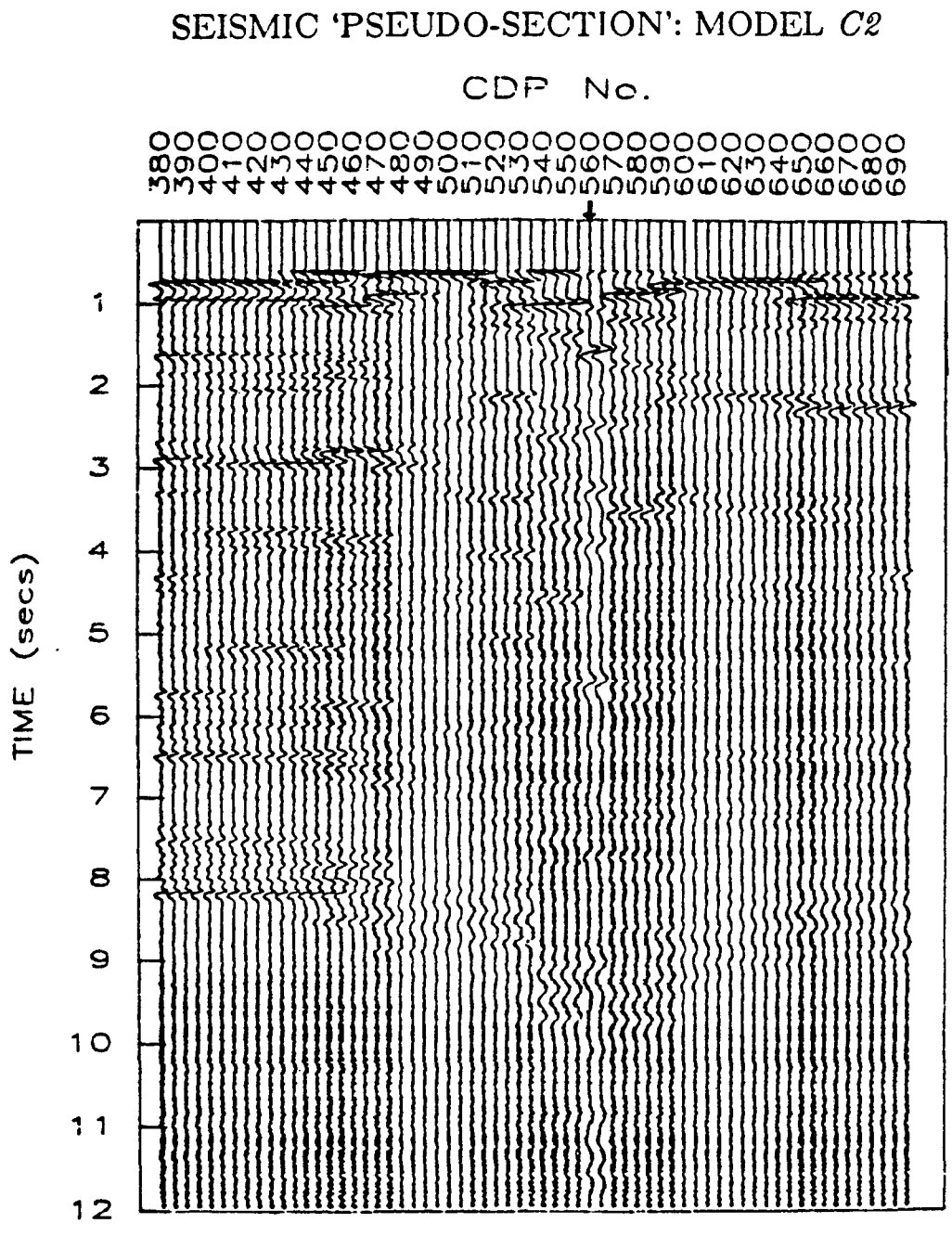

Figure (4-7d) Pseudo-section using a perturbation of the velocity model used in (4-7b) such that the Moho consists of six laminae of thickness 600 meters. Notice the increased depth extent of the Moho reflection relative to that of the other three pseudo-sections; this figure most closely resembles that of the data section (Figure 3-6).

4.5 SUMMARY AND DISCUSSION

The results of detailed investigations of the velocity and attenuation structure of the crust within and bounding the San Andreas fault zone in central California have been incorporated into a simple forward modeling scheme in an attempt to re-create the original seismic reflection section. Synthetic 'pseudo-sections' have been formed by the juxtaposition of one-dimensional synthetic reflection seismograms calculated based on the velocity and Q structure previously obtained by analysis of the actual stacked seismic sections (e.g. Figures 3-6, 3-16 to 3-19). Perturbations to the velocity model(s) allow for a refinement of our understanding of the structure by a visual qualitative comparison of the resulting pseudo-sections with the actual data section. This essentially one-dimensional method is crude – they are basically 'credibility tests' – and hence the ability to glean any useful information from these pseudo-sections is limited. Major structural features, such as the mid-crustal reflection at about 3 seconds time (two-way) in the Gabilan (western) portion of the section and the Moho reflection at about 7 seconds (also in the Gabilan part of the section) are modeled reasonably well; however these features are considerably more complex in the actual data. The general contrast in crustal reflectivity is reproduced in these synthetics, however this is accomplished exclusively by the incorporation of lower Q values within the Franciscan crust and within the fault zone. In general, the complexity associated with the actual data is due primarily to scattering, but also to instrument noise (McEvilly, 1980).

A major structural feature of interest that is prominent in the data and is also evident in each of these synthetic sections is the basal contact of the Gabilan batholith, represented by a series of reflectors at about 2 to 3 seconds time. Unlike the actual data which show a faint outline of the easternmost edge of the batholith, the pseudo-sections show only its lower boundary. Model 'SS', which was derived from conventional processing of the reflection data, shows the greatest lateral continuity of this contact and may be the most accurate model in this regard.

The question of whether a gneissic composition characterizes the lower Gabilan crust, as suggested by Walter and Mooney (1982), or a Franciscan-type composition as indicated by the refraction study of Stewart (1968) and the geotectonic arguments of Dickinson (1981) is not adequately addressed by qualitative comparison of these synthetic sections with the data. Furthermore, the existence of a low velocity wedge extending westward from the fault at the same approximate depth (i.e. 10 km) as the aforementioned basal contact (Feng and McEvilly, 1983) is not resolved by this study nor by the conventional processing of the actual reflection data.

Modeling of the laminated Moho by a cyclic series of layers over about three kilometers indicates that such a fine structure is likely for the crust-mantle boundary; in fact, comparison of model 'C2' (Figure 4-7d) with the data suggests that this type of cyclic layering may be present over an even greater depth extent than that given by this model (i.e. $\geq$7.5 km). Reflection coefficients of as much as 0.067 are required over these laminae in order to give rise to such a significant and persistent layered structure as is evident in all the stacked data sections (i.e. Figures 3-6, 3-16 to 3-19). No plausible geologic models are offered in this study to explain this fine structure.

The presence of a faint but discernible Moho-type reflection at depths of about 25 kilometers within the Franciscan crust in these pseudo-sections is intriguing. The general absence of such spatially coherent reflection energy in the data suggests that random scattering of the wave field has camouflaged any signature of crust-mantle contact within the Franciscan medium. The inclusion of such random scattering effects in a two or three-dimensional synthetic seismogram algorithm would probably tend to wipe out this already faint feature. In the present study an apparent Q operator that is significantly lower throughout the Franciscan crust than in the Gabilan crust has accomplished a similar result, however a crust-mantle reflection does appear. It is interesting to note that such a feature has also been observed in the migrated and coherency-filtered sections of the actual data (e.g. Figures 3-17 to 3-19). A careful reflection survey that is not plagued by the instrument problems characterizing the Bickmore Canyon data (McEvilly, 1980) might well show a more clearly defined Moho reflection within the Franciscan

crust in this region. Indeed, the 37-fold reflection survey by Western Geophysical Company for the University of California, Berkeley revealed just such a reflection at a reflection time of about 8.5 seconds (McEvilly and Clymer, 1975). This north-south profile was wholly within the Franciscan crust, about 25 km north of the Bickmore Canyon survey.

The contrast in spectral content between the data on either side of the San Andreas fault is evident in both the actual data and in these synthetics; this contrast is consistently manifested in both the individual seismograms and in the stacked sections. Such a contrast suggests that if the apparent Q is frequency independent, as assumed in these synthetic calculations, then the Q is simply lower in the eastern crust than in the western Gabilan medium. However the results of the analysis of the filtered data (e.g. Section 3.4.6) indicate that the apparent Q is proportional to frequency -- indeed, that this proportionality is greater in the eastern medium than in the western crust. Such a proportionality would tend to mitigate the observed spectral contrast as it would lead to an almost frequency-independent attenuation, assuming an exponential decay function. The consistently observed spectral contrast across the fault must be due to the difference in input spectra of the Vibroseis source along the profile, due to differences in soil-baseplate coupling. In other words, the assumption that the same source spectrum is input along the entire profile is not correct. As discussed in Section 3.4.3, an attempt was made (unsuccessfully) to determine the input source spectrum by analysis of the sweep using downhole receivers along the profile. Such a procedure should be incorporated in any future investigations using Vibroseis sources. It would also be interesting to study the spectral content of the near-source traces from the shot-gathers of the field data in more detail.

References: Chapter 4

Aki, Keiiti, 1973. Scattering of P waves under the Montana Lasa, *J. Geophys. Res.*, **78**, 1334-1346.

Bott, Martin H. P., 1971. *The Interior of the Earth*, Edward Arnold, London.

Clowes, R. M. and E. R. Kanasewich, 1970. Seismic attenuation and the nature of reflecting horizons within the crust, *J. Geophys. Res.*, **75**, 6693-6705.

Dickinson, W. R., 1981. Plate tectonics and the continental margin of California, in *The Geotectonic Development of California*, W. G. Ernst, Editor, Prentice-Hall, New York, 1-28.

Feng, R. and T. V. McEvilly, 1983. Interpretation of seismic reflection data for the structure of the San Andreas fault zone, *Bull. Seism. Soc. Am.*, **73**, 1701-1720.

Futterman, Walter I., 1962. Dispersive body waves, *J. Geophys. Res.*, **67**, 5279-5291.

Ganley, D.C., 1981. A method for calculating synthetic seismograms which include the effects of absorption and dispersion, *Geophysics*, **46**, 1100-1107.

Gouppillaud, P. L., 1961. An approach to inverse filtering of near-surface layer effects from seismic records, *Geophysics*, **26**, 754-760.

Hale, L. D. and G. A. Thompson, 1982. The seismic reflection character of the continental Mohorovicic discontinuity, *J. Geophys. Res.*, **87**, 4625-4635.

Lerche, I., 1986. Stratigraphic filter theory: Combined effects of parallel bedding and rednom inhomogeneities, *Geophysics*, **51**, 1531-1537.

Lynn, Heloise B., Laura D. Hale and George A. Thompson, 1981. Seismic reflections from the basal contacts of batholiths, *J. Geophys. Res.*, **86**, 10633-10638.

McEvilly, T. V., 1976. Reflection seismic survey near the San Andreas fault, *U. S. Geol. Surv., Final Report, contract no. 14-08-0001-14845,*

McEvilly, T. V., 1980. Extended reflection survey of the San Andreas fault zone, *U. S. Geol. Surv., Final Report, contract no. 14-08-0001-16804,*

O'Doherty, R. F. and N. A. Anstey, 1971. Reflections on amplitudes, *Geophysical Prospecting*, **19**, 430-458.

Spencer, T. W., J. R. Sonnad, and T. M. Butler, 1982. Seismic Q--Stratigraphy or dissipation, *Geophysics*, **47**, 16-24.

Stewart, Samuel W., 1968. Preliminary comparison of seismic traveltimes and inferred crustal structure adjacent to the San Andreas fault in the Diablo and Gabilan Ranges of central California, *Proc. Conf. Geol. Problems of San Andreas Fault System, Stanford Univ. Publ. Geol. Sci.*, **11**, 218-230.

Walter, A. W. and W. D. Mooney, 1982. Crustal structure of the Diablo and Gabilan Ranges, central California: A reinterpretation, *Bull. Seism. Soc. Am.*, **72**, 1567-1590.

Chapter 5

Summary and Conclusions

Detailed analysis of an 18 km seismic reflection profile across a creeping segment of the San Andreas fault indicates that, consistent with the trend of numerous other studies of earthquake data, the fault zone may be represented as a low velocity zone situated between a largely granitic crustal block to the west and a crustal block composed predominately of Franciscan material to the east. Although the actual composition of these bounding crusts is not well-constrained by such field studies, comparison of these general results with those of laboratory investigations of the appropriate basement rocks exposed at the surface indicates that these exposed rocks probably represent the type of rocks that exist at depth. A rough outline of the granitic batholith of the Gabilan Range can be observed in the stacked seismic sections (e.g. Figures 3-6, 3-16 to 3-19); the base of the batholith is roughly at a depth of about 10 km, corresponding to a (two-way) reflection time of about 3.5 seconds. This basal contact appears at a somewhat shallower depth as one approaches the San Andreas fault zone (near CDP 540); it has been postulated that a low velocity wedge extends westward at or below this depth (Feng and McEvilly, 1983). Analysis of a gravity survey along the same profile as the reflection line suggests that such a low velocity wedge may be of the same clay-rich gouge constitution as the fault zone itself (Wang et al., 1986). Such a constitution is also consistent with the electrical resistivity results of Phillips and Kuckes (1983), which suggest that a low resistivity layer exists below the upper high resistivity Gabilan crust; Wang (1984) has analyzed samples of fault gouge that were obtained in this region and has shown that significantly low resistivities may be obtained by such samples when saturated with aqueous saline fluids. The conventional velocity analyses carried out with the aforementioned seismic reflection data did not allow for sufficient resolution to delineate such a low velocity wedge at or below this depth within the Gabilan crust; results of these velocity analyses are, however, not inconsistent with such a feature.

The constitution of the lower 'Gabilan' crust is not well-understood. Seismological arguments (Stewart, 1968) as well as geotectonic inferences (Dickinson, 1981) suggest that below this basal contact at about 10 km depth a somewhat lower velocity medium may be present which could consist of Franciscan material. The seismological inference of Stewart has been refuted by Walter and Mooney (1982) who have re-examined the relevant refraction data. They favor a gneissic composition for the lower Gabilan crust. In their final model the average P-wave velocity for the lower Gabilan crust ($10 < z < 24$ km) is 6.5 km/sec whereas that of the lower Diablo crust ($16 < z < 30$ km) is 6.9 km/sec. Given that their model of the Diablo crust is considerably thicker and that the differences in velocity below a depth of 18 km are actually only 0.2 km/sec it is not clear whether one can definitively conclude whether a transition occurs from a granitic (e.g. quartz monzonite) upper crust to a gneissic constitution or to one of a highly metamorphosed Franciscan material. This becomes especially difficult when one considers that the P-wave velocity of such a Franciscan material under the temperatures and pressures appropriate for these depths is noticeably less than that of the gabbroic material thought to characterize the lower Diablo crust (Stewart and Peselnick, 1978; Lin and Wang, 1980). On the other hand, observations of the spectral contrast manifested in various types of data suggests that significant differences in upper crustal composition between the two crustal blocks persist at depth; given the consistent observation involving both P and S-wave data (for either Vibroseis or microearthquake sources), that the high frequencies have been depleted in the Franciscan relative to waves propagating within the western crust, one is led to favor a gneissic composition in the lower Gabilan crust. This argument assumes that the depletion of the high frequencies in the eastern crust is due to the intrinsic *lossiness* and/or to the heterogeneity structure of the Franciscan material; conversely, the relative preservation of the high frequencies within the western crust is assumed to manifest the relative efficiency with which a granitic (i.e. gneissic) material propagates seismic waves.

The question of whether the observed reflection at about 3.5 seconds represents a transition from a granitic rock to a different petrological unit bears critically upon the question of

whether the large-scale lateral translation of the Salinian Block occurs over a mid-crustal slip plane or whether such motion occurs at or below the crust-mantle boundary. Hence there is some uncertainty as to the degree of coupling between the upper and lower 'Gabilan' crusts and to the consequent possibility of overthrusting of the Salinian Block above an older Franciscan formation. Given the importance of this question in understanding the development of the entire western margin of California, it is necessary to expand the scope of geophysical inquiry to include detailed studies of the shear wave profile for this region. It is hoped that such studies of the shear wave data from both earthquake and, possibly, (Vibroseis) reflection data may help to illuminate the structure of the lower Gabilan crust. The incorporation of shear wave information from field data must be accompanied by corresponding laboratory studies of the shear wave properties of the relevant rocks. In this way, the shear wave information will help to further constrain our understanding of the constitution of the crusts bounding the fault as well as that of the fault zone itself.

Although there is considerably less spatially coherent reflection detail east of the San Andreas fault on the stacked sections, the composition of the lower Diablo crust is generally thought to be composed of a different chemistry and petrology than that of the upper Diablo crust; on the basis of careful laboratory investigation of various rocks exposed at the surface Stewart and Peselnick (1978) and Lin and Wang (1980) have concluded that a gabbroic (olivine or hornblende) composition fits the seismic data whereas that of a highly metamorphosed Franciscan material (i.e. jadeitic metagreywacke) would have a lower P-wave velocity than has been observed in several field studies (see Walter and Mooney (1982) for a summary of the published field results). Unfortunately, such a conclusion cannot be definitively drawn from the velocity analyses of the Bickmore Canyon seismic reflection data set due to the relative lack of spatially coherent reflectivity there; both the constant velocity analysis (CVA) technique and the various coherency methods employed to determine the velocity structure were hampered by this lack of reflectivity east of the San Andreas fault (see Figures 3-6, 3-16 to 3-19). This lack of spatially coherent reflectivity within the eastern portion of the stacked sections is probably due to the

higher degree of crustal heterogeneity of the Franciscan medium relative to that of a granitic medium. Indeed, the marked contrast in crustal reflectivity between the Gabilan and Diablo crusts as observed in these studies of the reflection data motivated the study of the attenuation structure of the media using a scattering model of wave propagation.

One of the most striking features of these stacked sections is the series of reflections at about 7 to 8 seconds west of the San Andreas fault. This laminated and east-dipping feature corresponds to the crust-mantle contact. Its east-dipping nature is primarily a local 'push-down' effect of the strong lateral heterogeneity of the velocity structure, although there are indications that the Diablo crust is thicker than that of the Gabilan crust (i.e. 30 km and 24 km, respectively (Walter and Mooney, 1982)). What is particularly intriguing about the reflection signature of the Moho here is its laminated appearance. Such an appearance has been widely reported in many different tectonic regimes (Clowes and Kanasewich, 1970; Lynn et al., 1981; Hale and Thompson, 1982). In this data set the Moho appears over a depth range of two to three seconds (two-way time) and, as is shown in forward modeling studies, is probably due to a cyclic series of layers spanning at least 3 kilometers in thickness and having reflection coefficients as high as 0.067. The seismic signature of the Moho east of the fault is not well-known and is of great interest, especially in light of the aforementioned discussion of the lower Gabilan crust and the depth of coupling of the northwestward-migrating Salinian Block. Although the Moho reflection is not prominent within the Franciscan crust in this survey, a previous survey shot in 1974 wholly on the east side of the San Andreas fault, with 37-fold coverage did show a Moho reflection (McEvilly and Clymer, 1975). It may just be that the multiplicity in the 1978 data is insufficient to bring it out, in which case the signal enhancement process could be a trustworthy aid (see Figure 3-19). The 1978 data was not from exactly the same location as that of the 1974 data (e.g. the Bickmore line was about 25 km south of this latter profile), however there is no plausible argument to explain any lateral discontinuity of the crust-mantle contact over this length scale.

The marked contrast in spatially coherent reflectivity across the San Andreas fault suggests that significant differences in the characteristics of wave propagation exist between the two crustal blocks. Such a contrast in energy return between the two crusts is probably due to the differences in the heterogeneity and attenuation structures of the two bounding crusts. In this light two extreme scattering models of P-wave propagation were applied to the stacked reflection data; the attenuation was parameterized by an apparent Q operator which included both the effects of intrinsic absorption and elastic scattering losses. The resulting Q values correspond to an average over a mid-crustal depth range of approximately six to seventeen kilometers. The two models lead to essentially similar results: Both a diffusion approach and a weak scattering model show that, although the apparent scattering attenuation (Q^{-1}) is greater in the Franciscan portion of the section it is only slightly greater than that of the granitic crust. The apparent Qs average about 115 in the western crust and about 70 in the eastern crust with a Q of 40 in the fault zone. These values of Q for the unfiltered data are consistent with those of a similar analysis of S-wave coda from a microearthquake data set in the region; however, unlike the CDP data, the S-wave coda show a somewhat higher average Q for the Franciscan medium (e.g., Q = 114) than for the S-coda recorded in the Gabilan medium to the west (e.g., Q = 92). This difference in apparent attenuation is probably not due to differences in attenuation mechanisms, but rather to the fact that the precision of the coda method of determining apparent or scattering attenuation is insufficient to accurately delineate either the heterogeneity structure or the intrinsic *lossiness* of the medium using such a small data set. It has been shown in the investigation of the microearthquake data that significantly large spatial variations in the character of the coda exist over relatively small areas. In addition, the problem of contamination of the S-coda due to the presence of wave conversions and surface waves is unavoidably present in such data. In the case of the CDP reflection data there are contaminating problems owing to the potential inclusion within the given window of data of spatially coherent reflection energy from later arriving horizons of high impedance contrast. Although great care was employed to preclude arrivals from subsequent reflectors, there is no quantifiable way to

ensure that such contamination does not occur. The application of the coda decay technique to seismic reflection data is novel, but it assumes the existence of spatially coherent (*primary*) reflection energy in the presence of a moderate degree of scattering due to heterogeneities. Hence, the method cannot be applied to very regular or deterministic media in which little heterogeneity or coda generation exists. Conversely, the requirement that spatially coherent (*primary*) reflection energy exists precludes the application of the method to intensely fractured or otherwise strongly inhomogeneous media in which no discernible spatially coherent reflectors exist; in the absence of such *primary* energy a misleading and inaccurate value of high apparent Q will result. Finally, the application of the coda decay technique to stacked reflection data must be applied to data that have been migrated prior to stacking; in the application to stacked data the CDP seismogram is interpreted as an approximation to the impulse response of the medium directly beneath the source-receiver (coincident) point at the surface. Thus if the medium is laterally inhomogeneous this assumption will be strictly valid only if the data has been migrated prior to stacking. The coda decay technique may only be accurate in the determination of the apparent attenuation of the crustal medium if it involves a significant amount of averaging and thus a relatively large data set. It is interesting to note that, despite the limited nature of the data sets analyzed here, these results for both Q_P and Q_S are consistent with those obtained by Aki and Chouet (1975) in the same general region. (They did not attempt to differentiate in their data whether the propagation medium was primarily east or west of the San Andreas fault.) This consistency of absolute Q values is actually greater at the lower frequencies (the range of frequencies used in the study by Aki and Chouet ranged from about 1 to 25 Hz): while their values for the apparent Q range from a low of 70 at 1 Hz to almost 1000 at 20 Hz, those computed in this microearthquake study range from a low of 45 at 3 Hz to a high of 593 at 24 Hz.

In contrast to the ambiguity regarding the absolute values of the apparent Q parameter, analysis of the filtered data for each data set reveals a consistent difference in the degree of frequency dependence of the apparent Q between the bounding crusts of the fault. (Results within

the fault zone itself are poor due primarily to the lack of discernible structure as well as signal, in this portion of the stacked reflection section.) Consistent with numerous other studies of body waves at frequencies above about 0.5 Hz (see text–section 3.4.6 for a summary of published results), the apparent Qs were found in all cases to increase with frequency; of perhaps greater significance is the trend toward greater frequency dependence in the 'Franciscan' data relative to the 'granitic' data (P and S-waves). This may be part of an emerging pattern for body wave data; whereas several studies have detailed the relation between the degree of frequency dependence of Q and the degree of heterogeneity or tectonic activity, very few studies have sought to determine the fine structure associated with the comparison of this frequency dependence over a small regional area (Chen et al., 1984; Rhea, 1984). The results of these studies are consistent with this emerging pattern, suggesting that there is a greater degree of frequency dependence for heterogeneous and/or tectonically active regions than for more homogeneous and/or quiescent regions. In other words one may associate the degree of frequency dependence of the apparent Q with the *complexity* of the propagation medium.

Since it was not possible to determine the partitioning of the attenuation process according to its intrinsic and elastic scattering components, it remains unclear to what extent the observed frequency dependence is dominated by either process. Given that most laboratory measurements of attenuation suggest that the intrinsic Q is independent of frequency it seems reasonable that the observed frequency dependence is dominated by some scattering process. However this conclusion cannot be drawn definitively, especially considering the generally high (e.g. ultrasonic) frequencies over which these laboratory measurements are carried out relative to seismic frequencies. The partitioning of the apparent attenuation according to these basic processes is a significant problem that must be addressed, although no particular method is suggested by this study. The weak scattering model may be used for such a partitioning (see Section 3.4.3) however because of its inherent non-linearity, the solution to the problem involves *a priori* knowledge of both the overall level of apparent attenuation and the degree of partitioning of the two components. As such, this technique remains wholly inadequate to address the partitioning

problem. Although it was with some disappointment that the initial goal of decomposing the observed attenuation according to its elastic and anelastic components was not realized, it is believed that as much useful information as possible has been gleaned from these data.

Future investigations should include detailed analyses of the shear wave properties of this region at depth in an effort to constrain the composition of the fault and its bounding crusts. Such investigations should include both field studies, such as earthquake and microearthquake array analyses and reflection profiles, as well as laboratory analyses of the rocks exposed at the surface. These general types of seismological and laboratory analyses should also be conducted in other regions of the San Andreas fault zone in an effort to understand how these properties vary with other characteristics of the fault such as heat flow and fault width; the locked regions to the northwest and southeast of this creeping segment of the fault may be characterized by significantly different seismological and geophysical properties such that it may be possible to determine the exact relationship between these properties and the patterns of seismicity observed.

As discussed in Section 3.4.3 and Section 4.5, the assumption that the input source spectrum is invariant along the profile line is probably not correct. It is recommended that analysis of the source spectrum at shallow depth below the soil-baseplate coupling layer (e.g. $\approx$40meters) be conducted in any future investigations using Vibroseis sources.

LAWRENCE BERKELEY LABORATORY
UNIVERSITY OF CALIFORNIA
INFORMATION RESOURCES DEPARTMENT
BERKELEY, CALIFORNIA 94720